frontiers | Research Topics

Gastrointestinal and liver effects of fruits and their synergism with drug therapy: Exploring possible mechanisms of action

Edited by
Irwin Rose Alencar De Menezes, Jackson Almeida,
Henrique Melo Coutinho and Lucindo Quintans-Júnior

Published in
Frontiers in Pharmacology

ISSN 1664-8714
ISBN 978-2-8325-5242-1
DOI 10.3389/978-2-8325-5242-1

About Frontiers

Frontiers is more than just an open access publisher of scholarly articles: it is a pioneering approach to the world of academia, radically improving the way scholarly research is managed. The grand vision of Frontiers is a world where all people have an equal opportunity to seek, share and generate knowledge. Frontiers provides immediate and permanent online open access to all its publications, but this alone is not enough to realize our grand goals.

Frontiers journal series

The Frontiers journal series is a multi-tier and interdisciplinary set of open-access, online journals, promising a paradigm shift from the current review, selection and dissemination processes in academic publishing. All Frontiers journals are driven by researchers for researchers; therefore, they constitute a service to the scholarly community. At the same time, the *Frontiers journal series* operates on a revolutionary invention, the tiered publishing system, initially addressing specific communities of scholars, and gradually climbing up to broader public understanding, thus serving the interests of the lay society, too.

Dedication to quality

Each Frontiers article is a landmark of the highest quality, thanks to genuinely collaborative interactions between authors and review editors, who include some of the world's best academicians. Research must be certified by peers before entering a stream of knowledge that may eventually reach the public - and shape society; therefore, Frontiers only applies the most rigorous and unbiased reviews. Frontiers revolutionizes research publishing by freely delivering the most outstanding research, evaluated with no bias from both the academic and social point of view. By applying the most advanced information technologies, Frontiers is catapulting scholarly publishing into a new generation.

What are Frontiers Research Topics?

Frontiers Research Topics are very popular trademarks of the *Frontiers journals series*: they are collections of at least ten articles, all centered on a particular subject. With their unique mix of varied contributions from Original Research to Review Articles, Frontiers Research Topics unify the most influential researchers, the latest key findings and historical advances in a hot research area.

Find out more on how to host your own Frontiers Research Topic or contribute to one as an author by contacting the Frontiers editorial office: frontiersin.org/about/contact

Gastrointestinal and liver effects of fruits and their synergism with drug therapy: Exploring possible mechanisms of action

Topic editors

Irwin Rose Alencar De Menezes — Regional University of Cariri, Brazil
Jackson Almeida — Federal University of São Francisco Valley, Brazil
Henrique Melo Coutinho — Regional University of Cariri, Brazil
Lucindo Quintans-Júnior — Federal University of Sergipe, Brazil

Citation

De Menezes, I. R. A., Almeida, J., Melo Coutinho, H., Quintans-Júnior, L., eds. (2024). *Gastrointestinal and liver effects of fruits and their synergism with drug therapy: Exploring possible mechanisms of action*. Lausanne: Frontiers Media SA. doi: 10.3389/978-2-8325-5242-1

Table of contents

frontiers | Frontiers in Pharmacology

EDITORIAL
published: 01 July 2022
doi: 10.3389/fphar.2022.940668

Editorial: Gastrointestinal and Liver Effects of Fruits and Their Synergism With Drug Therapy: Exploring Possible Mechanisms of Action

Almir Gonçalves Wanderley[1]*, *Lucindo José Quintans Júnior*[2]*, *Henrique Douglas Melo Coutinho*[3], *Jackson Roberto Guedes da Silva Almeida*[4] and *Irwin Rose Alencar De Menezes*[3]*

[1]Department of Pharmaceutical Sciences, Institute of Environmental, Chemical and Pharmaceutical Sciences, Universidade Federal de São Paulo—UNIFESP, São Paulo, Brazil, [2]Department of Physiology, Federal University of Sergipe—UFS, Aracaju, Brazil, [3]Department of Chemical Biology, Regional University of Cariri—URCA, Crato, Brazil, [4]Department of Pharmacy, Federal University of Vale do São Francisco—UNIVASF, Petrolina, Brazil

Keywords: mechanisms of action, fruits, gastrointestinal tract, liver disease, gastrointestinal disease, synergism, biological activity

Editorial on the Research Topic

Gastrointestinal and Liver Effects of Fruits and their Synergism with Drug Therapy: Exploring Possible Mechanisms of Action

Historically, natural products have been rich sources of molecules that can be used in the prevention or treatment of different pathological conditions. With the advent of the second industrial revolution and the development of organic chemistry and pharmacology, drugs of synthetic origin started being produced and used on a large scale, and products of natural origin began to occupy a secondary role in the therapeutic arsenal. However, the increase in the incidence of adverse effects and the high cost of synthetic drugs are among the factors that contributed to the rediscovery of products from biodiversity.

This Research Topic aims to add contributions to the potential use of bioactive natural products or their association with synthetic drugs in the prevention and/or treatment of liver and gastrointestinal system disorders.

This Research Topic presented one systematic review with a meta-analysis dedicated to dyslipidemia (Carvalho et al.), two experimental studies (Zhang et al.; Cui et al.), and one review study (Yu et al.) addressing Nonalcoholic Fatty Liver Disease (NAFLD). Two experimental studies explored the theme of liver fibrosis (Zhao et al.; Zhang et al.) while studies also looked at severe acute pancreatitis (Yang et al.), hepatic ischemia/reperfusion (Chen et al.), and gastroprotection (Mahmoud et al.).

Rhein is an anthraquinone derivative found in some medicinal plants, such as Rhubarb, Polygonum multiflorum, Ruta graveolens, and Folium sennae, that has hepatoprotective, nephroprotective, anti-inflammatory, antioxidant, anticancer, and antimicrobial properties (Zhou et al., 2015). Yang et al. were able to show that Rhein was effective in protecting against the deleterious effects of Severe Acute Pancreatitis (SAP) in both *in vivo* and *in vitro* models, possibly via the JAK2/STAT3 signaling pathway.

According to Younossi et al. (2018), the global prevalence of NAFLD is increasing and is estimated to be ~25% in the general population. Yu et al. contributed to this Research Topic with a review of the underlying mechanisms of dietary fructose and its role in the development and progression of NAFLD, and they also proposed possible targets to prevent the pathogenic process.

OPEN ACCESS

Edited and reviewed by:
Angelo A. Izzo,
University of Naples Federico II, Italy

***Correspondence:**
Irwin Rose Alencar De Menezes
irwin.alencar@urca.br
Almir Gonçalves Wanderley
almir.wanderley@unifesp.br

Specialty section:
This article was submitted to Gastrointestinal and Hepatic Pharmacology, a section of the journal Frontiers in Pharmacology

Received: *10 May 2022*
Accepted: *20 May 2022*
Published: *01 July 2022*

Citation:
Wanderley AG, Quintans Júnior LJ, Melo Coutinho HD, Guedes da Silva Almeida JR and De Menezes IRA (2022) Editorial: Gastrointestinal and Liver Effects of Fruits and Their Synergism With Drug Therapy: Exploring Possible Mechanisms of Action. Front. Pharmacol. 13:940668. doi: 10.3389/fphar.2022.940668

Zhang et al. reported that Tiaoganquzhi Decoction, a traditional Chinese herbal formulation, has a protective action against NAFLD, whose mode of action is associated with the promotion of CGI-58 to inhibit the expression of ROS-induced NLRP3 inflammasome. Pogostemon cablin (Blanco) Benth/Huo Xiang (HX) is a species that has antioxidant and anti-inflammatory properties with used in traditional Chinese medicine. Cui et al. explored the potential mechanism of HX on NAFLD through network pharmacological and experimental studies. The data showed that HX can attenuate abnormal lipid metabolic responses and enhance antioxidant mechanisms through multiple pathways.

Dihydromyricetin (DHM), also known as ampelosin, is a natural compound with distinct pharmacological properties and has multiple hepatoprotective effects (Chen et al., 2021). Zhao et al. investigated the effect of DHM as a novel nutritional supplement in the thioacetamide (TAA)-induced liver fibrosis model. The results showed that DHM mitigated TAA-induced hepatic fibrosis through inhibition of NF-κB-mediated inflammation and the TGF-β1-regulated PI3K/Akt signaling pathway, indicating that the compound is a potential hepatoprotective factor with prospects to be used in the treatment of liver fibrosis.

Pentagalloyl glucose (PGG) is a polyphenolic compound with potent antioxidant action and antimicrobial, anti-viral, anti-diabetic, anti-inflammatory, and antitumor properties (Patnaik et al., 2019). Mahmoud et al. evaluated the gastroprotective potential of PGG against indomethacin-induced ulcers in rats and found that this polyphenol promoted an antiulcerogenic effect mediated by increasing mucus production, scavenging free radicals, decreasing inflammation, and attenuating the NO/NOS signaling in favor of eNOS.

Kaempferol (KAE) is a flavonoid present in several plant species, including Penthorum chinense, and is traditionally used in Chinese medicine for the treatment of liver diseases (Wang et al., 2020). Chen et al. confirmed the hepatoprotective effect of KAE in the hepatic ischemia/reperfusion injury model in mice whose mechanism is associated with inhibition of oxidative stress and inflammation by activating the Nrf2/HO-1 signaling pathway.

The beneficial effects of Bone Marrow Mesenchymal Stem Cells (BMSCs) (Watanabe et al., 2021) and ferulic acid (FA) (Mu et al., 2019) in the treatment of cystic fibrosis have been described in the literature. Considering this information, Zhang et al. have expertly demonstrated the beneficial and synergistic effect of the combined therapy BMSCs and FA in a CCL4-induced liver fibrosis rat model.

Carvalho et al. have suggested in a systematic review with meta-analysis that Citrus species extracts are potential candidates for dyslipidemia control; however, the high heterogeneity indicates that more studies are required to increase the strength of this occurrence.

In summary, the different herbal formulations or compounds obtained from the plant were potentially effective in the treatment of pathological conditions that affect the liver and gastrointestinal system. We hope that these contributions serve as a guide for new pre-clinical and clinical studies, expecting to find new drug/phytopharmaceutical candidates for therapeutic use in the future.

AUTHOR CONTRIBUTIONS

All authors listed have made a substantial, direct, and intellectual contribution to the work and approved it for publication.

ACKNOWLEDGMENTS

The editors acknowledge the contributions of all authors.

REFERENCES

Chen, J., Wang, X., Xia, T., Bi, Y., Liu, B., Fu, J., et al. (2021). Molecular Mechanisms and Therapeutic Implications of Dihydromyricetin in Liver Disease. *Biomed. Pharmacother.* 142, 111927. doi:10.1016/j.biopha.2021.111927

Mu, M., Zuo, S., Wu, R. M., Deng, K. S., Lu, S., Zhu, J. J., et al. (2019). Ferulic Acid Attenuates Liver Fibrosis and Hepatic Stellate Cell Activation via Inhibition of TGF-β/Smad Signaling Pathway. *Drug Des. devel. Ther.* 13, 1819. doi:10.2147/DDDT.S215949

Patnaik, S. S., Simionescu, D. T., Goergen, C. J., Hoyt, K., Sirsi, S., and Finol, E. A. (2019). Pentagalloyl Glucose and its Functional Role in Vascular Health: Biomechanics and Drug-Delivery Characteristics. *Ann. Biomed. Eng.* 47, 39–59. doi:10.1007/s10439-018-02145-5

Wang, A., Li, M., Huang, H., Xiao, Z., Shen, J., Zhao, Y., et al. (2020). A Review of Penthorum Chinense Pursh for Hepatoprotection: Traditional Use, Phytochemistry, Pharmacology, Toxicology and Clinical Trials. *J. Ethnopharmacol.* 251, 112569. doi:10.1016/j.jep.2020.112569

Watanabe, Y., Tsuchiya, A., and Terai, S. (2021). The Development of Mesenchymal Stem Cell Therapy in the Present, and the Perspective of Cell-free Therapy in the Future. *Clin. Mol. Hepatol.* 27, 70–80. doi:10.3350/cmh.2020.0194

Younossi, Z., Anstee, Q. M., Marietti, M., Hardy, T., Henry, L., Eslam, M., et al. (2018). Global Burden of NAFLD and NASH: Trends, Predictions, Risk Factors and Prevention. *Nat. Rev. Gastroenterol. Hepatol.* 15, 11–20. doi:10.1038/nrgastro.2017.109

Zhou, Y. X., Xia, W., Yue, W., Peng, C., Rahman, K., and Zhang, H. (2015). Rhein: A Review of Pharmacological Activities. *Evid. Based Complement. Altern. Med.* 2015, 578107. doi:10.1155/2015/578107

Conflict of Interest: The authors declare that the research was conducted in the absence of any commercial or financial relationships that could be construed as a potential conflict of interest.

frontiers in Pharmacology

ORIGINAL RESEARCH
published: 15 November 2021
doi: 10.3389/fphar.2021.783886

Dihydromyricetin Reverses Thioacetamide-Induced Liver Fibrosis Through Inhibiting NF-κB-Mediated Inflammation and TGF-β1-Regulated of PI3K/Akt Signaling Pathway

Yingchun Zhao[1†], *Xinglong Liu*[1†], *Chuanbo Ding*[1], *Yan Gu*[2*] and *Wencong Liu*[1,3*]

[1]College of Chinese Medicinal Materials, Jilin Agricultural University, Changchun, China, [2]College of Agriculture, Jilin Agricultural University, Changchun, China, [3]National and Local Joint Engineering Research Center for Ginseng Breeding and Development, Changchun, China

OPEN ACCESS

Edited by:
Irwin Rose Alencar De Menezes,
Regional University of Cariri, Brazil

Reviewed by:
Jaime Ribeiro-Filho,
Gonçalo Moniz Institute (FIOCRUZ), Brazil
Cícero Felipe,
Federal University of Paraíba, Brazil

***Correspondence:**
Yan Gu
guyan@jlau.edu.cn
Wencong Liu
jwlw6803@126.com

[†]These authors have contributed equally to this work and share first authorship

Specialty section:
This article was submitted to Gastrointestinal and Hepatic Pharmacology, a section of the journal Frontiers in Pharmacology

Received: 27 September 2021
Accepted: 27 October 2021
Published: 15 November 2021

Citation:
Zhao Y, Liu X, Ding C, Gu Y and Liu W (2021) Dihydromyricetin Reverses Thioacetamide-Induced Liver Fibrosis Through Inhibiting NF-κB-Mediated Inflammation and TGF-β1-Regulated of PI3K/Akt Signaling Pathway. Front. Pharmacol. 12:783886. doi: 10.3389/fphar.2021.783886

As a natural active substance, dihydromyricetin (DHM) has been proven to have good hepatoprotective activity. However, the therapeutic effect of DHM on liver fibrosis, which has become a liver disease threatening the health of people around the world, has not been studied to date. The purpose of this study was to investigate the effect of DHM as a new nutritional supplement on thioacetamide (TAA)-induced liver fibrosis. The liver fibrosis model was established by intraperitoneal injection of TAA (200 mg/kg, every 3 days) for 8 weeks, and oral administration of DHM (20 mg/kg and 40 mg/kg, daily) after 4 weeks of TAA-induced liver fibrosis. The results showed that DHM treatment significantly inhibited the activities of alanine aminotransferase (ALT) (37.81 ± 7.62 U/L) and aspartate aminotransferase (AST) (55.18 ± 10.94 U/L) in serum of liver fibrosis mice, and increased the levels of superoxide dismutase (SOD) and glutathione (GSH) while reversed the level of malondialdehyde (MDA). In addition, histopathological examination illustrated that TAA induced the inflammatory infiltration, apoptosis and fibroatherosclerotic deposition in liver, which was further confirmed by western-blot and immunofluorescence staining. Moreover, DHM inhibited hepatocyte apoptosis by regulating the phosphorylation level of phosphatidylinositol 3-kinase (PI3K), protein kinase-B (AKT) and its downstream apoptotic protein family. Interestingly, immunofluorescence staining showed that DHM treatment significantly inhibited alpha smooth muscle actin (α-SMA), which was a marker of hepatic stellate cell activation, and regulated the expression of transforming growth factor (TGF-β1). Importantly, supplementation with DHM significantly inhibited the release of nuclear factor kappa-B (NF-κB) signaling pathway and pro-inflammatory factors in liver tissue induced by TAA, and improved liver fiber diseases, such as tumor necrosis factor alpha (TNF-α) and recombinant rat IL-1β (IL-1β). In conclusion, the evidence of this study revealed that DHM is a potential hepatoprotective and health factor, and which also provides the possibility for the treatment of liver fibrosis.

Keywords: dihydromyricetin, liver fibrosis, NF-κB signaling pathway, inflammation, hepatic stellate cell activation, anti-apoptosis

INTRODUCTION

As an important immune and metabolic organ of the human body, liver is vulnerable to damage from various causes, including hepatitis virus infection, alcohol and drug injury, autoimmune response and metabolic diseases (Marrone et al., 2016). Chronic liver disease and liver fibrosis have always been the focus of contemporary medical research, and people have tried to establish a model of liver fibrosis to adapt to contemporary research needs in recent years (Sepanlou et al., 2020). As a potent hepatotoxin, TAA-induced liver fibrosis is a well-recognised model for the development of liver damage, regenerative nodules and fibrosis, similar to human liver fibrosis (Passos et al., 2010; Nascimento et al., 2018). Numerous experiments have shown that long-term administration of TAA leads to proliferative liver nodules, liver fibrosis, hepatocellular adenomas and hepatocellular carcinoma (Li et al., 2002; Yeh et al., 2004; Constantinou et al., 2007; Jantararussamee et al., 2021). The toxicity of TAA arises from its bioactivation of reactive metabolites, including TAA-sulfur oxides and reactive oxygen species (ROS) *via* the monooxygenases flavin adenine dinucleotide (FAD) and cytochrome P2E1 (CYP2E1) (Tunez et al., 2005). These metabolites bind to cellular macromolecules, induce oxidative stress through lipid peroxidation and increased free radical load, and participate in fibril formation (Chilakapati et al., 2005). More seriously, TAA attacks hepatocyte DNA, RNA and protein-related synthetic enzymes in the body, produces toxic effects, affects liver metabolism, causes metabolic disorders and leads to imbalance of antioxidant defense system, and aggravates chronic liver inflammation and even liver necrosis (Hessien et al., 2010; Kadir et al., 2011). Therefore, TAA induces a progressive liver disease characterised by inflammation, oxidative stress, apoptosis, extensive fibrosis and eventual development of hepatocellular carcinoma, thereby mimicking the progression of inflammation/fibrosis/malignancy in patients.

Studies have shown that the key to prevent liver fibrosis is to inhibit the activation of hepatic stellate cells (HSCs) or promote the apoptosis of HSCs (Zhang et al., 2017a). In addition, some profibrotic mediators are also involved in stimulating HSCs activation and myofibroblast transformation, such as TGF-β1, which is not only involved in the pleiotropic cytokine produced by extracellular matrix (ECM), but also regulated the signaling pathways related to cell proliferation, differentiation and apoptosis in the liver (Gressner and Weiskirchen, 2006; Vaidya and Kale, 2015; Zhang, 2017). Therefore, this may be an important way to study the mechanism and targeted therapy of liver fibrosis at the molecular level in the future by inhibiting the multi effect cytokine and its downstream apoptotic proteins, reducing collagen accumulation and ECM deposition (Bakin et al., 2000). NF-κB pathway participates in regulating a variety of inflammatory cell responses, and has been used for targeted therapy of many inflammatory diseases. Studies have shown that inflammatory cells can further activate HSCs, which may be the main source of myofibroblasts in the liver (Cubero, 2016). NF-κB is involved in the inhibition of apoptosis through the transcriptional induction of a variety of anti-apoptotic factors, including B cell-lymphoma-2 (Bcl-2) family proteins (Zheng et al., 2009). In addition, the expression of NF-κB-regulated gene products is also involved in the apoptotic Bcl-2 family (Bui et al., 2001; Gupta et al., 2002). Therefore, this may be a crucial way to improve TAA-induced liver fibrosis by reducing NF-κB-mediated inflammation and apoptotic signaling pathways.

Vine tea (*Ampelopsis grossedentata*) is a traditional medicinal plant widely used to improve health or suppressing disease in Chinese folk (Ye et al., 2015). In addition to being used as a tea drink, vine tea was traditionally used as a folk medicine according to ancient texts for the treatment of fever and cough, stab wounds, bruises, jaundiced hepatitis and sore throats (Gao et al., 2009). Moreover, extracts from vine tea have been proved to have significant anti-inflammatory properties *in vitro* and *in vivo*, and have been recommended as a potential therapeutic agent for inflammation-related diseases (Chen et al., 2015). Importantly, the leaves and stems of vine tea are rich in a large number of natural active substance dihydromyricetin, which has become an important plant resource for the development and research of functional products (Gao et al., 2009; Kou and Chen, 2012; Zhao et al., 2013; Zheng et al., 2014; Ye et al., 2015; Zhang et al., 2020; Carneiro et al., 2021). It is worth mentioning that as a natural active substance, dihydromyricetin from vine tea has been approved by the Food and Drug Administration (FDA) as a nutritional supplement and can be added in food industry.

The hepatoprotective effects of dihydromyricetin are now well recognized. zhuangwei Zhang et al. investigated the down-regulation of the Akt/Bad pathway in HepG2 cells to reduce apoptosis (Zhang et al., 2017b). Sijing Dong et al. used dihydromyricetin to counteract acetaminophen-induced liver injury by modulating lipid homeostasis, cell death and regenerative pathways (Dong et al., 2019). Yi Zeng et al. demonstrated a protective effect of dihydromyricetin in improving non-alcoholic steatohepatitis (Zeng et al., 2020). Xi Zhou et al. demonstrated that dihydromyricetin attenuated carbon tetrachloride-induced liver injury by modulating autophagy and inhibiting the activation of hepatic stellate cells (Zhou et al., 2021). Ping Qiu et al. also demonstrated the protective effect of dihydromyricetin against ethanol-induced liver injury (Qiu et al., 2017). However, dihydromyricetin has not been found to improve liver fibrosis. Based on this, the present study aimed to explore the improvement effect of dihydromyricetin on liver fibrosis by establishing a mouse model of TAA-induced liver fibrosis and further revealed its possible molecular mechanism, supplemented the relevant research and provided a potential clinical possibility for the treatment of liver disease.

MATERIALS AND METHODS

Chemicals and Reagents

DHM (purity ≥99.0%) and TAA (purity ≥99.0%) were purchased from Sigma. Hematoxylin-eosin (H and E), TUNEL and Masson

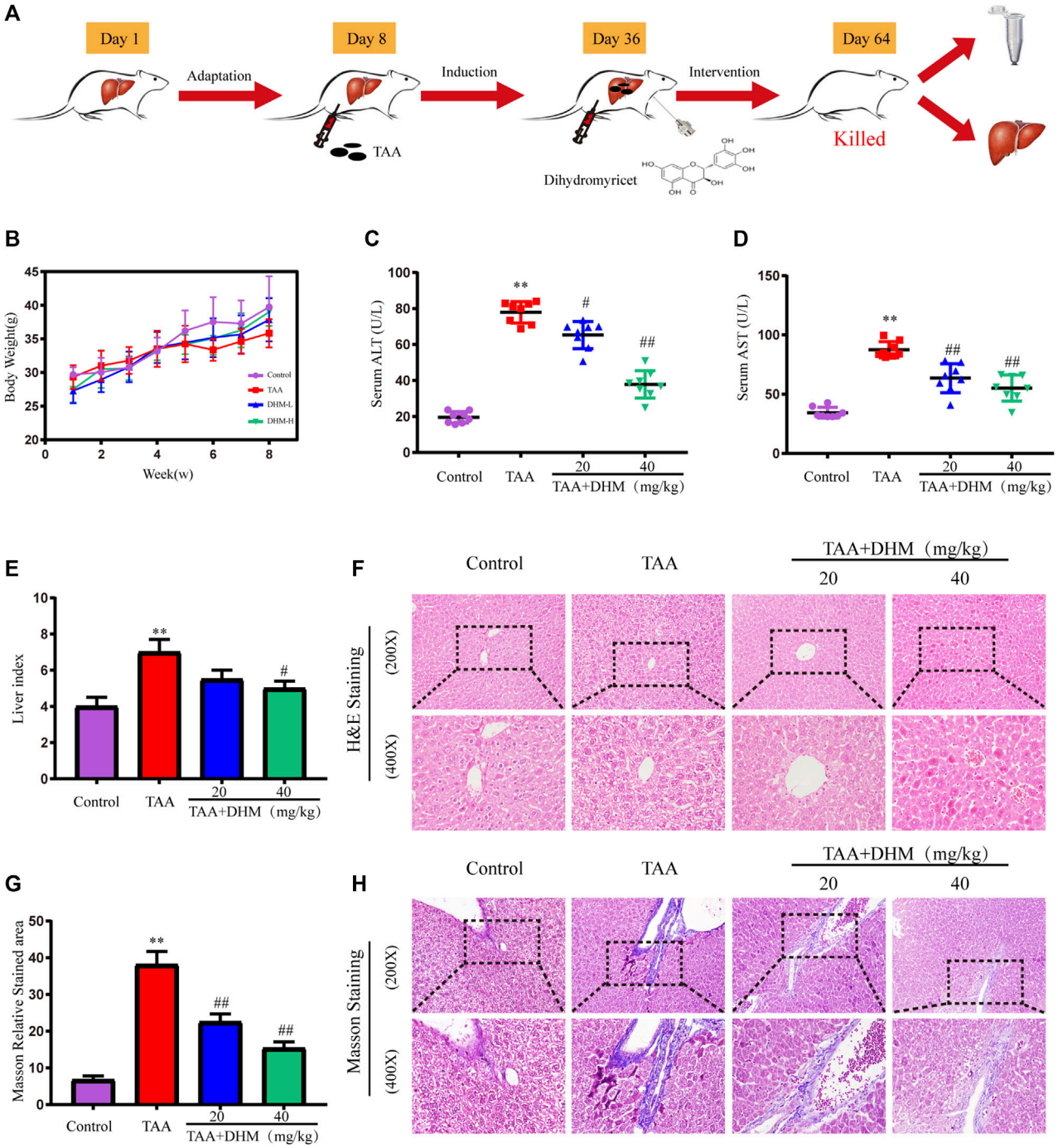

FIGURE 1 | DHM ameliorated TAA-induced hepatic injury in mice. The experimental design **(A)**; Body weight **(B)** and serum levels of ALT **(C)** and AST **(D)** (n = 8); liver index **(E)**, H&E staining **(F)**; Masson relative stained area **(G)** and Masson' strichrome staining **(H)**; Data was expressed as the mean ± SD. The differences between groups were analyzed by two tailed T-test or one-way analysis of variance (ANOVA). $^{**}p < 0.01$, $^{*}p < 0.05$ *versus* control group; $\#\#p < 0.01$, $\#p < 0.05$ *versus* TAA group.

stain kits, and commercial assay kits for ALT and AST, SOD, GSH, MDA were obtained from the Nanjing Jiancheng Bioengineering Research Institute (Nanjing, China). The immunofluorescent staining kits and the enhanced chemiluminescence (ECL) kit were purchased from Beyotime science and technology Co., Ltd. (Beijing, China). The antibody of rabbit monoclonal α-SMA, TGF-β1, CYP2E1, Cleaved Caspase-3, Caspase3, Cleaved Caspase-9, Caspase-9, IκB kinase α (IKK-α), IκB kinase β (IKK-β), *p*-IKKα, *p*-IKKβ, inhibitor of IκBα (IκBα), *p*-IκBα, NF-κB, p-NF-κB, PI3K, p-PI3K, Akt, *p*-Akt, B-associated

X (Bax), Bcl-2, β-actin and secondary antibodies for western blot were all obtained from Abcam (Cambridge, United Kingdom).

Animals and Drug Treatment

The forty fully-grown male ICR mice (4–6 weeks old, weight 20–25 g) were purchased from Changchun Yisi Experimental Animal Co., Ltd. (Changchun, China), and the certificate of quality was No. SCXK (JI)-2019–0,001. Mice were maintained under a professional animal breeding room with constant temperature and humidity and pathogen-free, and unlimited access to sufficient food and water. This study was approved by the animal research ethics committee of Jilin Agricultural University, ethics approval No.: 2019–08–28–002.

Forty mice were divided into four groups under 7 days adaptive feeding conditions (control, TAA group, TAA + DHM 20 mg/kg and 40 mg/kg groups, n = 10), and the detailed experimental design process was shown in **Figure 1A**. All mice (excluding the control group) were received TAA (200 mg/kg, every 3 days) from day 8 to day 64. Moreover, the TAA + DHM groups were received the treatment of DHM (20 mg/kg and 40 mg/kg, daily) from day 36 to day 64. At the completion of the last TAA injection, mice were treated with a 12-h fast. After anaesthetics treatment with 2% chloral hydrate intraperitoneally, blood samples were collected from the eyes of mice and serum was collected by centrifugation (4°C, 3,500 rmp, 10 min). After the mice were killed after cervical spondylectomy, the livers were collected immediately, measured and the liver index of the mice was obtained by the formula (liver weight/body weight) × 100. Some of them were soaked in 4% paraformaldehyde solution, and the others were stored at −80°C.

Determination of Biochemical Indicators

ALT and AST are involved in central metabolism in the body, and the level of ALT and AST transaminases are markers of liver injury. Therefore, we evaluated the degree of liver injury by detecting the levels of serum ALT and AST. Serum ALT and AST levels were measured using commercial kits purchased from Nanjing Jiancheng reagent company. Determine the absorbance according to the instructions and calculate the ALT and AST levels according to the formula.

Histopathological Staining

The liver tissue samples were stained by H&E routine staining, and evaluated by histopathological according to standard procedures. In order to evaluate the degree of fibrosis in liver samples, the connective tissue, muscle fibers and collagen fibers in liver tissues were stained with Masson trichrome staining kit. Observe pathological changes such as fatty degeneration, necrosis, and inflammatory cell infiltration of liver cells under an optical microscope.

Determination of Oxidative Stress Indicators

The levels of GSH, MDA, and SOD are important indicators reflecting oxidative stress damage (Ding et al., 2021). Therefore, the levels of GSH, MDA and SOD in liver tissue were detected. Take an appropriate amount of liver tissue and fully grind it with 9 times the volume of normal saline under low temperature to make 10% tissue homogenate. The operation was carried out according to the method of each kit and finally the absorbance was measured and calculated according to the formula.

Immunofluorescence Staining

In order to assess the expression of apoptosis and inflammation-related proteins in liver tissue induced by TAA, immunofluorescence staining was performed on liver tissue sections of each group (Hou et al., 2015). After the tissue sections were deparaffinized with xylene solution and hydrated in ethanol, the antigen was recovered by microwave in a citrate buffer solution (0.01 M, pH 6.0) for 20 min. After washing 3 times with PBS, the tissue was incubated with 1% bovine serum albumin (BSA) for 1 h, and then the primary antibody caspase 3 (1:200), CYP2E1 (1:200), TNF-α (1:400) was added dropwise, TGF-β1 (1:200) and α-SMA (1:200) were incubated overnight at 4°C. The next day, it was labeled with a fluorescent secondary antibody at 37°C for 30 min and then labeled with SABC-CY3 (1:100) again. The nucleus was stained with 4,6 diamidino-2-phenylindole (DAPI). The protein expression was observed with a fluorescence microscope, and the immunofluorescence intensity was analyzed with Image-Pro Plus 6.0 software.

Western Blot Analysis

RIPA lysate lyses liver tissue and extracts its protein. The extracted protein samples were separated by 10% SDS-PAGE gel electrophoresis, and then transferred to PVDF membrane. After blocking with skim milk for 1.5 h, then use primary antibodies (Bax, Bcl-2, recombinant human B-cell Leukemia/Lymphoma XL (Bcl-XL), cysteine proteases3 (Caspases3), cleaved caspase 3, cysteine proteases9 (caspase 9), cleaved caspase 9, PI3K, p-PI3K, AKT, *p*-AKT, IKKα/β, *p*-IKKα/β, IκBα, *p*-IκBα, NF-κB (p65), p-NF-κB (p-p65), TNF-α, IL-1β, β-actin at 4°C Incubate overnight. Then, the membrane was washed 3 times in Tris-buffered saline (TBS) containing 0.1% Tween-20, and then the membrane was incubated with the secondary antibody for 1 h at room temperature. After the band was detected by ECL luminescent solution, the protein expression was displayed by Bio-Lad Laboratories Segrate.

TUNEL Staining

TUNEL staining was used to analyze the extent of apoptosis in hepatocyte nuclei. Liver tissue antigen was extracted with 20 μg/ml proteinase K for 10 min, then TUNEL reaction mixture (TdT: dUTP, 1:9) was added for 1 h in the dark at 37°C. The cells were washed three times with PBS and then observed under a fluorescent microscope for apoptosis.

Statistical Analysis

Statistical analysis was carried out using SPSS statistical software. The differences between groups were analyzed by two tailed T-test or one-way analysis of variance (ANOVA). The results are shown as the mean ± SD, and the significance level is defined

as $p < 0.05$. Graphs were drawed with GraphPad Prism software (version 7).

RESULTS

Dihydromyricetin Alleviates Thioacetamide-Induced Chronic Hepatic Injury

During the experiment, the weight of mice in each group were recorded. Although there was no significant difference in body weight, the overall increase trend of body weight was lower than that of the control group in TAA-treated mice (**Figure 1B**). Besides, a significant increase in relative liver index was observed in the TAA model group compared to the control group (**Figure 1E**), with the increase in liver mass attributed to the accumulation of fat and breakdown of liver tissue. However, the DHM intervention resulted in a reduction in liver index. Furthermore, the appropriate commercial kits were used for serological examinations, and the levels of ALT and AST in serum were measured to determine the severity of liver injury. Compared with the control group, the levels of ALT and AST in the serum of mice were significantly increased by TAA-induced ($p < 0.01$, **Figures 1C,D**). Nevertheless, ALT and AST levels were reduced to varying degrees by DHM supplementation, with a particularly significant improvement in DHM (40 mg/kg), suggesting that DHM significantly improved TAA-induced hepatotoxicity.

Dihydromyricetin Improve Thioacetamide-Induced Liver Histopathological Damage

In order to evaluate the hepatoprotective effect of DHM, the improvement effect of DHM on TAA-induced liver dysfunction was examined by histopathology in this study. H and E staining showed that the hepatocytes in the control group were arranged regularly, with large round nucleoli and uniform cytoplasm, and there was no inflammatory cell infiltration in the portal area (**Figure 1F**). However, the liver structure treated with TAA was disordered, the liver lobule structure was destroyed or disappeared, the hepatocytes were arranged irregularly and had obvious apoptosis, and the fibrous deposition around the central vein gradually increased, and a large number of inflammatory cells and fibroblasts were infiltrated in the fibrous septum. In contrast, continuous treatment with DHM significantly alleviated pathological changes by TAA-induced, lipid degeneration and inflammatory injury in liver.

In addition, the results observed by Masson staining were basically consistent with the fibrosis in H and E staining (**Figure 1H**). The structure of central vein and catheter endothelial fibers in the control group was normal, and there was no abnormal fiber proliferation in other places, but there was slight inflammation. However, a large number of collagen fibers were observed in the portal area and central vein of the liver tissue treated with TAA, the hepatic lobules were divided by different fiber intervals, and there were obvious fiber adhesion and a large number of inflammatory cells between portal duct and central vein. Obviously, DHM treatment significantly inhibited the production of collagen fibers compared with the TAA group, there were a small amount of scattered proliferative fibers in hepatic lobules, and inflammatory cells were significantly reduced. In particular, the results of collagen area measurement by software also demonstrated that DHM treatment reduced collagen deposition and resulted in a reduction in collagen area (**Figure 1G**).

Dihydromyricetin Alleviated Thioacetamide-Induced Hepatotoxicity

Studies have shown that oxidative stress damage was related to TAA-induced liver toxicity (Chen et al., 2021). To evaluate the effect of DHM on TAA-induced oxidative stress in the liver, oxidative stress parameters were measured in the liver, such as SOD, GSH, and MDA. TAA induction significantly increased MDA levels but decreased SOD activity, accompanied by GSH depletion, compared to the control group ($p < 0.01$, **Figures 2A–C**). On the contrary, DHM-treated significantly increased the activities of GSH and SOD, while decreased the level of MDA in a dose-dependent manner ($p < 0.05$). The above results indicated that DHM significantly reduced TAA-induced oxidative stress damage.

Since the CYP-mediated biological activity plays an important role in TAA-induced hepatotoxicity, in order to further confirm the damage and hepatotoxicity caused by TAA to the liver, the expression of CYP2E1 protein was examined by immunofluorescence staining in liver tissue. The results showed that TAA caused the overexpression of CYP2E1 metabolic enzymes, while treatment with DHM significantly reduced the expression of CYP2E1 ($p < 0.01$, **Figures 2D,E**). These results also indicated to a certain extent that DHM improved TAA-induced oxidative stress damage and hepatotoxicity, especially in the DHM (40 mg/kg) group, which had a significant ameliorative effect and approached that of the control group.

The activation of HSCs is a key event leading to liver fibrosis, and the HSCs activation marker α-SMA and pro-fibrotic factor TGF-β1 in liver were analyzed by immunofluorescence staining in this study. The results demonstrated that the positive expression and fluorescence intensity of TGF-β1 and α- SMA were significantly improved by immunofluorescence staining compared with the control group after long-term TAA induction ($p < 0.01$, **Figures 3A–D**). On the contrary, the administration of DHM (20, 40 mg/kg) effectively reduced the secretion of TGF-β1 and the expression of α-SMA, which intuitively indicated that DHM inhibited the activation of HSCs and thus reversed the development of liver fibrosis by TAA-induced.

Dihydromyricetin Attenuates Liver Fibrosis by Inhibiting Thioacetamide-Induced Inflammatory Injury

In order to explore the anti-inflammatory and hepatoprotective functions of DHM, the expression of NF-κB-related proteins were

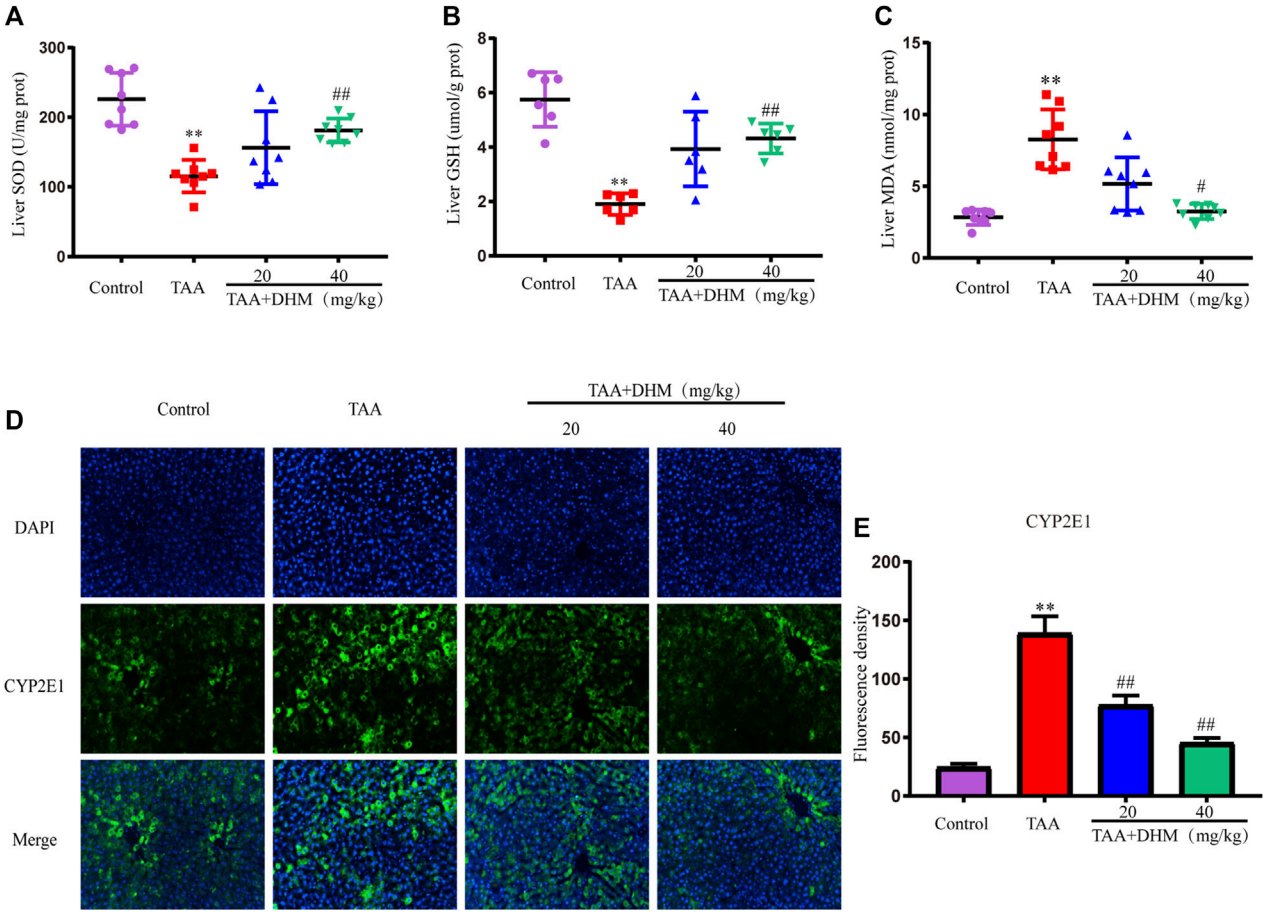

FIGURE 2 | DHM attenuates TAA-induced oxidative stress and hepatotoxicity. The hepatic levels of SOD **(E)**, GSH **(F)** and MDA **(G)** in TAA-induced liver fibrosis (n = 6–8); The protein expression levels of CYP2E1 **(E)** and Fluorescence density **(F)**; Data was expressed as the mean ± SD. The differences between groups were analyzed by two tailed T-test or one-way analysis of variance (ANOVA). $^{**}p < 0.01$, $^{*}p < 0.05$ *versus* control group; $\#\#p < 0.01$, $\#p < 0.05$ *versus* TAA group.

explored by western blotting in this study. Phosphorylated protein and its upstream inflammatory regulators p-IKKα/β and p-IκBα were significantly increased by TAA-induced (**Figures 4A–D**). Interestingly, the expression of NF-κB and its related proteins were significantly reduced after DHM treatment, especially DHM (40 mg/kg) had a significant ameliorating effect ($p < 0.05$). In addition, DHM inhibited the expression of pro-inflammatory factors TNF-α and IL-1β in the liver ($p < 0.01$), which was further confirmed by TNF-α immunofluorescence staining ($p < 0.01$, **Figures 4E,F**). These evidences suggested that DHM alleviated TAA-induced liver fibrosis by inhibiting the expression of NF-κB signaling pathway and other inflammatory factors.

Dihydromyricetin Decreases Hepatocyte Apoptosis by Regulating the PI3K/Akt Signaling Pathway

To further explore the molecular mechanism of DHM antagonizing TAA-induced liver fibrosis, western blotting and immunofluorescence staining were used to analyze the expression level of PI3K/Akt signaling pathway, including its downstream the expression levels of Bcl-2 family and caspase family proteins, which was also an important way to regulate the proliferation, apoptosis and differentiation of activated HSCs. The results observed that the expression of p-PI3K and p-AKT proteins were significantly down-regulated after TAA treatment ($p < 0.05$, **Figures 5A,B**). On the contrary, DHM increased the expression of PI3K/AKT proteins in liver tissue. Not only that, DHM pretreatment also significantly reduced the expression of caspase pathway related proteins. Apparently, the expression of the pro-apoptotic proteins Bax, cleaved Caspase-9 and cleaved Caspase-3 were increased significantly after TAA induction, while the expression of anti-apoptotic proteins Bcl-2 and Bcl-XL were significantly decreased in this study ($p < 0.01$, **Figures 5C,D**). However, these proteins were effectively reversed after DHM treatment. In addition, the immunofluorescence staining of Caspase 3 was analyzed, and Caspase 3 positive cells may be the key event of activated HSCs (Mi et al., 2019). Interestingly, the results of caspase 3 obtained by immunofluorescence analysis were consistent with western blot analysis, which showed that

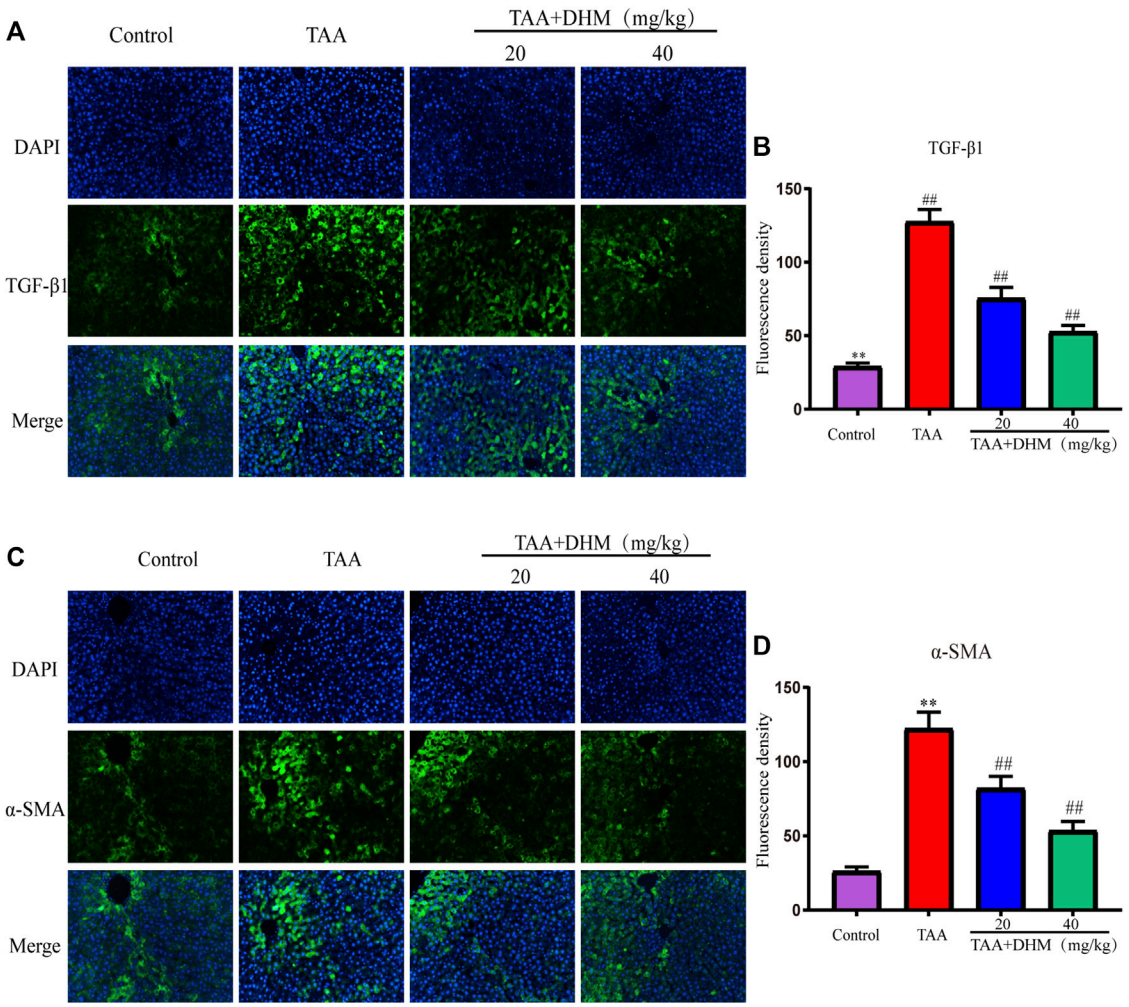

FIGURE 3 | DHM alleviated TAA-induced activation of hepatic stellate cells. The protein expression levels of TGF-β1 **(A)** and Fluorescence density **(B)**, The protein expression levels of α-SMA **(C)** and Fluorescence density **(D)**; Data was expressed as the mean ± SD. The differences between groups were analyzed by two tailed T-test or one-way analysis of variance (ANOVA). $^{**}p < 0.01$, $^{*}p < 0.05$ *versus* control group; $\#\#p < 0.01$, $\#p < 0.05$ *versus* TAA group.

DHM exhibited anti-apoptotic effects in TAA-induced chronic liver fibrosis and further promoted the apoptosis of activated HSCs (**Figures 6A,B**).

TUNEL staining was used to identify hepatocyte apoptosis and the number of green apoptotic nuclei was significantly increased after TAA establishment of the model compared to the control, indicating that TAA caused severe hepatocyte apoptosis. Specifically, DHM (40 mg/kg) administration reduced the amount of green fluorescence, resulting in reduced hepatic apoptosis ($p < 0.01$, **Figures 6C,D**). These results indicate that DHM has a significant anti-apoptotic effect and is directly proportional to the dose.

DISCUSSION

This study established the liver fibrosis model of mice by long-term intraperitoneal injection of TAA, and the ameliorative effect of dihydromyricetin on TAA-induced liver fibrosis was observed. In liver disease, transaminase levels in serum are elevated due to damage to liver cells (Williams and Hoofnagle, 1988; Nascimento et al., 2018). Elevated serum aminotransferase levels are a marker of liver injury, therefore we measured ALT and AST in mouse serum to assess the extent of liver injury. Interestingly, the results showed that TAA significantly increased serum ALT and AST concentrations, which was consistent with the results of some researchers (Tsai et al., 2021), while that DHM was able to modify this phenomenon (Salama et al., 2013; Abood et al., 2020; Elnfarawy et al., 2020). In addition, liver indices were measured in mice and the results represent the effect of DHM with hepatoprotective activity on the liver weight/body weight ratio, which was consistent with previous studies (Salama et al., 2013; Abood et al., 2020; Elnfarawy et al., 2020). Under TAA induction, liver tissue is usually fibrotic, leading to an increase in the liver weight ratio, which subsequently decreased after administration of DHM.

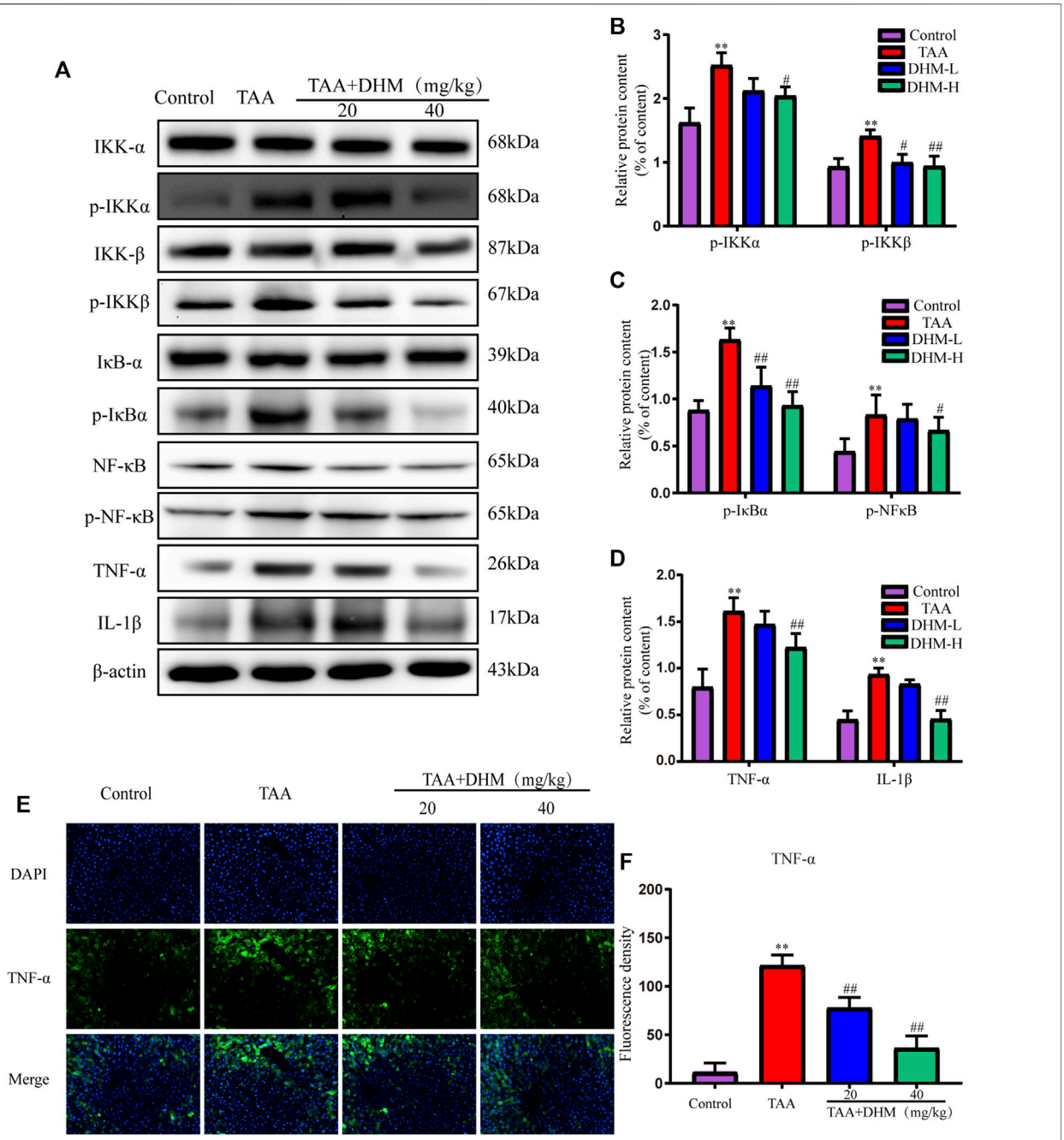

FIGURE 4 | DHM inhibits NF-κB-mediated inflammatory infiltration to reverse TAA-induced liver fibrosis. The protein expression levels of *p*-IKKα, IKKα, IKKβ, p-IKKβ, IκBα, p- IκBα, NFκB, p- NFκB, TNF-α and IL-1β in liver tissues were examined by western blot **(A)**, The protein expression levels of *p*-IKKα, IKKβ **(B)**, The protein expression levels of p- IκBα, p- NFκB **(C)**, The protein expression levels of TNF-α and IL-1β **(D)**, The protein expression levels of TNF-α **(E)** and Fluorescence density **(F)**; Column charts showed relative expression levels of target protein, and protein expression levels were performed by quantification of relative protein expression analysis in each group. Data was expressed as the mean ± SD. The differences between groups were analyzed by two tailed T-test or one-way analysis of variance (ANOVA). $^{**}p < 0.01$, $^{*}p < 0.05$ *versus* control group; $\#\#p < 0.01$, $\#p < 0.05$ *versus* TAA group.

Current research generally believes that the activation of HSCs is considered to be a key event in the development of liver fibrosis (Kisseleva and Brenner, 2006; Tsuchida and Friedman, 2017). α-SMA is a marker of HSCs activation, and TGF-β1 is generally considered to be the main hepatic fibrosis-promoting cytokine, and many factors leading to liver disease are related to TGF-β1 in varying degrees (Dewidar et al., 2015). In this study, immunofluorescence staining demonstrated that the positive expression of a-SMA and TGF-β1 were significantly increased in liver tissue by TAA-induced, which was consistent with previous studies (Mi et al., 2019; Zhou et al., 2021). The increase in α-SMA and TGF-β1 in turn induced the synthesis

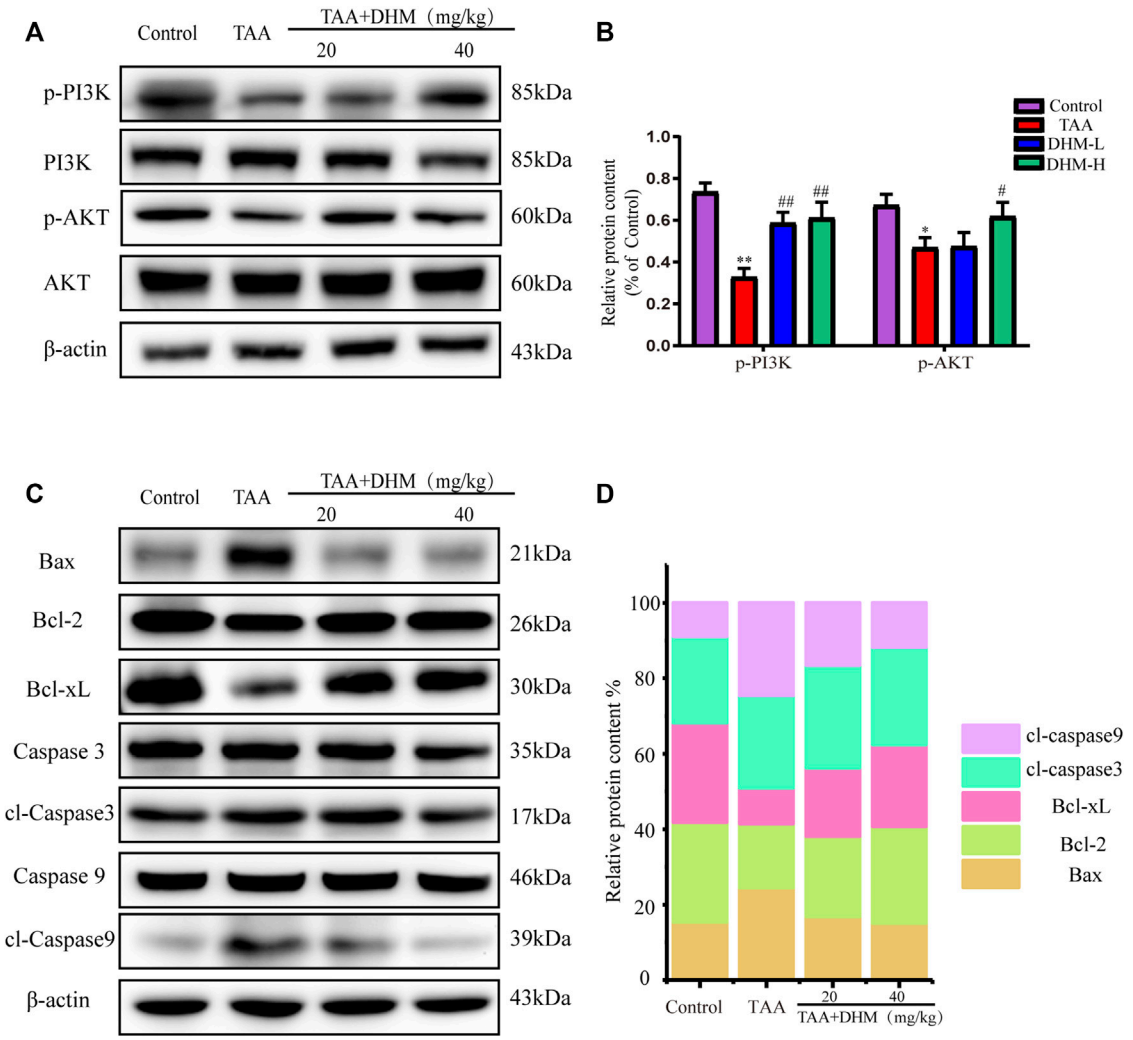

FIGURE 5 | DHM ameliorates PI3K/Akt-mediated apoptosis to reverse TAA-induced hepatic fibrosis. The protein expression levels of p-PI3K, PI3K, AKT, *p*-AKT in liver tissues were examined by western blot. **(A)** and the protein expression levels of p-PI3K and *p*-AKT protein **(B)**; The protein expression levels of Bax, Bcl-2, Bcl-xL, *p*-Caspase 3, Caspase 3, *p*-Caspase 9, Caspase 9 in liver tissues were examined by western blot **(C)** and the protein expression levels of Bax, Bcl-2, Bcl-xL, *p*-Caspase 3 and *p*-Caspase 9 protein **(D)**; β-actin protein was used as a loading control. Column charts showed relative expression levels of target protein, and protein expression levels were performed by quantification of relative protein expression analysis in each group. Data was expressed as the mean ± SD. The differences between groups were analyzed by two tailed T-test or one-way analysis of variance (ANOVA). $^{**}p < 0.01$, $^{*}p < 0.05$ *versus* control group; $\#\#p < 0.01$, $\#p < 0.05$ *versus* TAA group.

and secretion of ECM by HSC, thus aggravating liver fibrosis (Crosas-Molist et al., 2015). When there is an imbalance between the production and degradation of ECM, it will cause accumulation and scar reaction, and eventually lead to liver collagen deposition and fibrosis (El Taghdouini and van Grunsven, 2016). Furthermore, the histopathological examination of H&E and Masson found that TAA caused a large number of macrophage inflammatory infiltration and liver tissue structural disorders, which speculated that the inflammatory infiltration caused a large number of hepatocyte apoptosis, resulting in the expansion of hepatic veins and sinuses. Besides, the staining results showed that the massive deposition of collagen fibers and portal vein bridging led to the appearance of long fibrous septum, suggesting that long-term TAA induced severe liver fibrosis, while DHM treatment significantly reversed these changes, this was consistent with previous studies (Park et al., 2015; Zeng et al., 2020).

There was a view that many chronic liver diseases were accompanied by the certain degree of oxidative stress, and the extent of hepatic oxidative stress represented the level of liver injury (Uchida et al., 2020). Studies have shown that lipid peroxide products in liver fibrosis may play an important role in the activation of HSCs, especially in the early stage of liver fibrosis (Poli, 2000). Particularly, the excessive accumulation of typical liver lipid peroxidation product reactive oxygen species (ROS) may destroy the intracellular balance, lead to oxidative stress and mitochondrial dysfunction, and further cause the damage of enzyme and non-enzyme defense systems, which in turn causes cell damage (Demarquoy and Borgne, 2015; Horn and Jaiswal, 2018). Among them, these enzymes can transfer

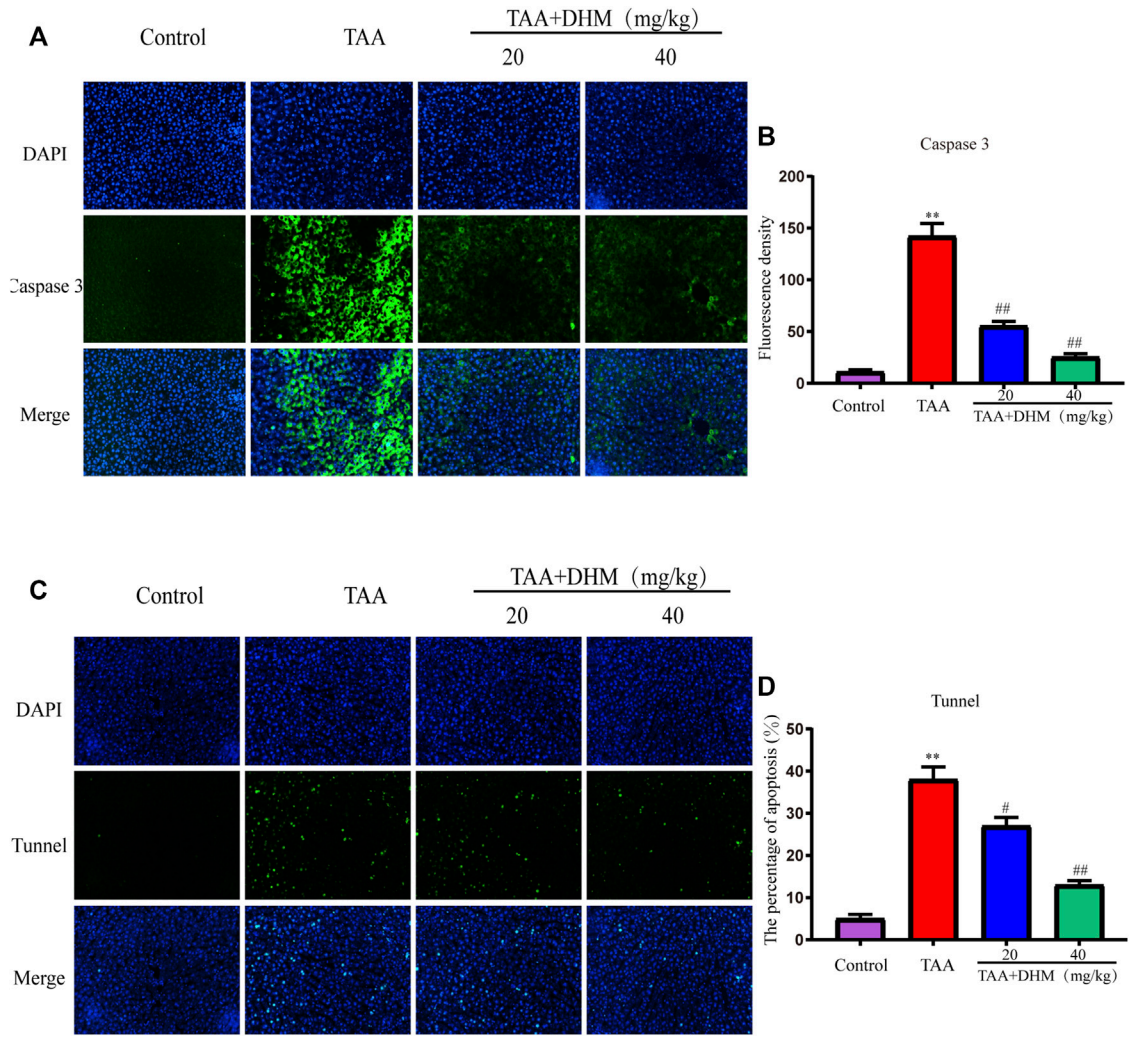

FIGURE 6 | DHM alleviated TAA-induced apoptosis of hepatocytes. The protein expression levels of caspase 3 **(A)** and Fluorescence density **(B)**, Fluorescence analysis of hepatocyte apoptosis **(C)** and Fluorescence density **(D)**; Data was expressed as the mean ± SD. The differences between groups were analyzed by two tailed T-test or one-way analysis of variance (ANOVA). $^{**}p < 0.01$, $^{*}p < 0.05$ *versus* control group; $\#\#p < 0.01$, $\#p < 0.05$ *versus* TAA group.

superoxide free radicals to other metabolites (Naqshbandi et al., 2013), including SOD and GSH. In this study, the activities of SOD and GSH were significantly reduced, while the level of MDA, as a marker of oxidative stress, was significantly increased by TAA-induced. On the contrary, DHM effectively inhibited the consumption of the above two enzymes and reduced the level of MDA, which was very important for maintaining cell function (Wright et al., 1981; Karadeniz et al., 2011). Consistent with the previous results, DHM had a significant regulatory effect on the decrease of GSH and SOD levels and the increase of MDA levels by TAA-induced.

In addition, studies have shown that inflammatory damage is an important factor leading to many chronic liver diseases, and which is usually accompanied by the development of liver fibrosis, cirrhosis and hepatocellular carcinoma (Koyama and Brenner, 2017). Among them, NF-κB induces the expression of pro-inflammatory cytokines, such as TNF-α and IL-1β, which produces the cytotoxic environment, thereby further triggering the development of chronic inflammation and progressive liver fibrosis (Wang et al., 2008). Therefore, this study detected the inflammation-related proteins in the liver tissue by TAA-induced, including IKKα/β, *p*-IKKα/β, IκBα, *p*-IκBα, NF-κB (p65), p-NF-κB (p-p65), TNF-α, IL-1β, which proved that DHM effectively inhibited the expression of these proteins, thereby reducing the inflammatory injury of liver fibrosis by TAA-induced.

Explicitly, chronic liver disease by TAA-induced causes severe cell injury and apoptosis. Some studies have shown that TAA attacks DNA, RNA and protein synthase in hepatocytes, produce toxic effects, which also induces liver metabolic disorder and even

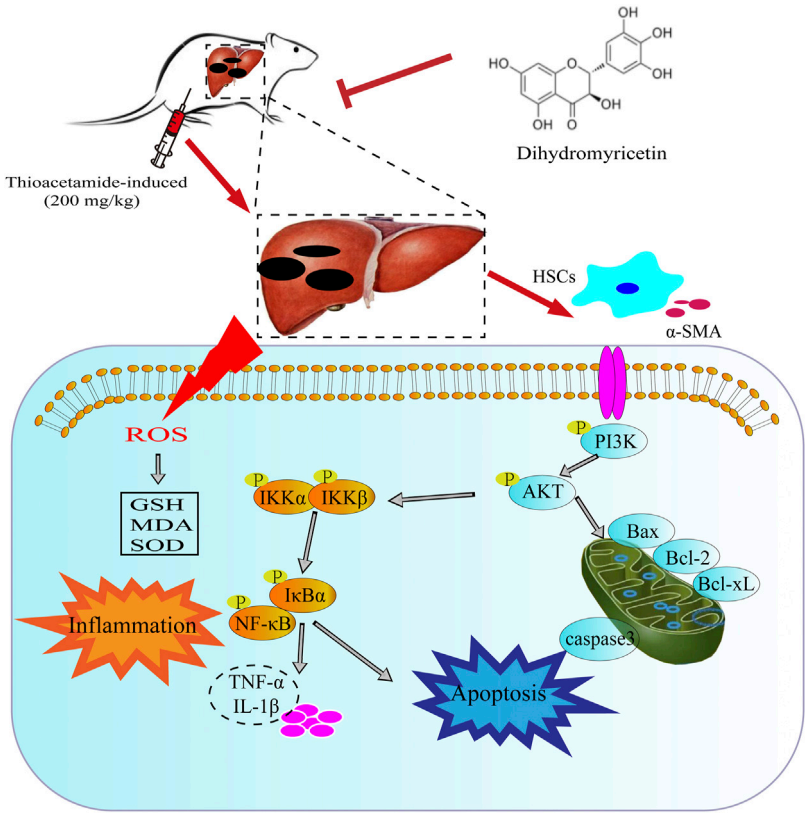

FIGURE 7 | The potential mechanism of DHM in alleviating TAA-induced liver fibrosis. DHM reverses TAA-induced liver fibrosis by inhibiting suppression of HSC activation, NF-κB-mediated inflammatory infiltration and improving PI3K/Akt-mediated apoptosis, which may be a potential mechanism for the hepatoprotective effects of DHM.

hepatocyte apoptosis. As one of the important signal transduction pathways in cells, PI3K/Akt signaling pathway plays a key role in inhibiting apoptosis and promoting proliferation by affecting a variety of downstream effector molecules related to apoptosis, which is closely related to the occurrence and development of liver diseases. When PI3K binds to growth factor receptors (such as EGFR), it can change the protein structure of AKT, which is a downstream protein of PI3K, and activates or inhibits a series of downstream substrates by phosphorylation, such as the apoptosis related proteins Bad and Caspase9, and further triggers apoptosis (Lin et al., 2015; Fang et al., 2019). Caspases are the key mediator of programmed cell death or apoptosis, and also the guide of the path of living cells to death (Singh et al., 2013). Therefore, the Caspases pathway, as a marker of apoptosis, plays an important role in mediating the process of cell apoptosis (Rehman et al., 2013; Prokhorova et al., 2018). In this study, immunofluorescence and western blot proved that DHM played an anti-apoptotic effect by regulating PI3K/AKT and its downstream pathway caspase-related proteins.

Indeed, the expression of Bcl-2 and Bax apoptotic molecules is also driven by nuclear NF-κB and oxidative stress in addition to PI3K/Akt (Zhang Q. et al., 2017; Sun et al., 2020). NF-κB, an important transcription factor in the nucleus, is not only involved in immunity, inflammation, tissue damage repair and embryonic development processes, but also upregulates the expression levels of inflammatory factors including TNF-α and IL-1β as well as apoptotic genes of the Bcl-2 family (Shou et al., 2002). Akt activates IκB kinase (IKKα/β), causes degradation of the NF-κB inhibitor IκB, results in the release of NF-κB from the cytoplasm for nuclear translocation, activates of its target genes and promotes of cell survival (Bava et al., 2011). In this study, DHM inhibited Bax expression while promoted Bcl-2 expression in TAA-induced liver fibrosis in mice. Bax and Bcl-2 apoptosis-related genes play an important role in the regulation of mitochondria-dependent pathways. In addition, Akt inhibited the activity of proteolytic enzyme caspase 9 and its downstream factor caspase 3 and reduced the activation of apoptosis cascade, which indicated that DHM improved hepatocyte metabolism by regulating hepatocyte proliferation and apoptosis.

In conclusion, the current study clearly demonstrated that TAA administration increased inflammation, oxidative stress, pro-fibrotic markers and hepatotoxic markers in mice and decreased liver function and abnormal liver histology. However, DHM treatment improved damaged liver structure, effectively reduced oxidative stress and hepatotoxic markers. More importantly, DHM reversed TAA-induced liver fibrosis by inhibiting NF-κB-mediated inflammation and TGF-β1-regulated apoptotic proteins downstream of the PI3K/Akt signalling pathway, which also indicated that DHM may be a potential active substance against chronic liver disease (**Figure 7**).

DATA AVAILABILITY STATEMENT

The original contributions presented in the study are included in the article/Supplementary Material, further inquiries can be directed to the corresponding authors.

ETHICS STATEMENT

The animal study was reviewed and approved by the Animal Investigational Morals Committee of Jilin Agricultural University 2020-08-28-001.

AUTHOR CONTRIBUTIONS

YG and WL perceived and planned the whole experiment. YZ and XL carried out the work, data analysis and drafted the manuscript. CD critically revised the manuscript.

FUNDING

This work was supported by the Innovation Capacity Building Project of Jilin Provincial Development and Reform Commission (2021C041-1).

REFERENCES

Abood, W. N., Bradosty, S. W., Shaikh, F. K., Salehen, N. A., Farghadani, R., Agha, N. F. S., et al. (2020). Garcinia Mangostana Peel Extracts Exhibit Hepatoprotective Activity against Thioacetamide-Induced Liver Cirrhosis in Rats. *J. Funct. Foods* 74, 104200. doi:10.1016/J.JFF.2020.104200

Bakin, A. V., Tomlinson, A. K., Bhowmick, N. A., Moses, H. L., and Arteaga, C. L. (2000). Phosphatidylinositol 3-Kinase Function Is Required for Transforming Growth Factor β-Mediated Epithelial to Mesenchymal Transition and Cell Migration. *J. Biol. Chem.* 275, 36803–36810. doi:10.1074/JBC.M005912200

Bava, S. V., Sreekanth, C. N., Thulasidasan, A. K. T., Anto, N. P., Cheriyan, V. T., Puliyappadamba, V. T., et al. (2011). Akt Is Upstream and MAPKs Are Downstream of NF-Kb in Paclitaxel-Induced Survival Signaling Events, Which Are Down-Regulated by Curcumin Contributing to Their Synergism. *Int. J. Biochem. Cel Biol.* 43, 331–341. doi:10.1016/J.BIOCEL.2010.09.011

Bui, N. T., Livolsi, A., Peyron, J.-F., and Prehn, J. H. M. (2001). Activation of Nuclear Factor κb and Bcl-X Survival Gene Expression by Nerve Growth Factor Requires Tyrosine Phosphorylation of IκBα. *J. Cel Biol.* 152, 753–764. doi:10.1083/JCB.152.4.753

Carneiro, R. C. V., Ye, L., Baek, N., Teixeira, G. H. A., and O'Keefe, S. F. (2021). Vine tea (Ampelopsis Grossedentata): A Review of Chemical Composition, Functional Properties, and Potential Food Applications. *J. Funct. Foods* 76, 104317. doi:10.1016/J.JFF.2020.104317

Chen, S., Zhao, X., Wan, J., Ran, L., Qin, Y., Wang, X., et al. (2015). Dihydromyricetin Improves Glucose and Lipid Metabolism and Exerts Anti-Inflammatory Effects in Nonalcoholic Fatty Liver Disease: A Randomized Controlled Trial. *Pharmacol. Res.* 99, 74–81. doi:10.1016/J.PHRS.2015.05.009

Chen, X., Ding, C., Liu, W., Liu, X., Zhao, Y., Zheng, Y., et al. (2021). Abscisic Acid Ameliorates Oxidative Stress, Inflammation, and Apoptosis in Thioacetamide-Induced Hepatic Fibrosis by Regulating the NF-Kb Signaling Pathway in Mice. *Eur. J. Pharmacol.* 891, 173652. doi:10.1016/J.EJPHAR.2020.173652

Chilakapati, J., Shankar, K., Korrapati, M. C., Hill, R. A., and Mehendale, H. M. (2005). Saturation Toxicokinetics of Thioacetamide: Role in Initiation of Liver Injury. *Drug Metab. Disposition* 33, 1877–1885. doi:10.1124/DMD.105.005520

Constantinou, M., Theocharis, S., and Mikros, E. (2007). Application of Metabonomics on an Experimental Model of Fibrosis and Cirrhosis Induced by Thioacetamide in Rats. *Toxicol. Appl. Pharmacol.* 218, 11–19. doi:10.1016/j.taap.2006.10.007

Crosas-Molist, E., Bertran, E., and Fabregat, I. (2015). Cross-Talk between TGF-β and NADPH Oxidases during Liver Fibrosis and Hepatocarcinogenesis. *Curr. Pharm. Des.* 21, 5964–5976. doi:10.2174/1381612821666151029112126

Cubero, F. J. (2016). Shutting off Inflammation: A Novel Switch on Hepatic Stellate Cells. *Hepatology* 63, 1086–1089. doi:10.1002/HEP.28442

Demarquoy, J., and Borgne, F. L. (2015). Crosstalk between Mitochondria and Peroxisomes. *World J. Biol. Chem.* 6, 301. doi:10.4331/WJBC.V6.I4.301

Dewidar, B., Soukupova, J., Fabregat, I., and Dooley, S. (2015). TGF-β in Hepatic Stellate Cell Activation and Liver Fibrogenesis: Updated. *Curr. Pathobiol. Rep.* 3, 291–305. doi:10.1007/S40139-015-0089-8

Ding, C., Zhao, Y., Chen, X., Zheng, Y., Liu, W., and Liu, X. (2021). Taxifolin, a Novel Food, Attenuates Acute Alcohol-Induced Liver Injury in Mice through Regulating the NF-Kb-Mediated Inflammation and PI3K/Akt Signalling Pathways. *Pharm. Biol.* 59, 868–879. doi:10.1080/13880209.2021.1942504

Dong, S., Ji, J., Hu, L., and Wang, H. (2019). Dihydromyricetin Alleviates Acetaminophen-Induced Liver Injury via the Regulation of Transformation, Lipid Homeostasis, Cell Death and Regeneration. *Life Sci.* 227, 20–29. doi:10.1016/J.LFS.2019.04.019

El Taghdouini, A., and van Grunsven, L. A. (2016). Epigenetic Regulation of Hepatic Stellate Cell Activation and Liver Fibrosis. *Expert Rev. Gastroenterol. Hepatol.* 10, 1397–1408. doi:10.1080/17474124.2016.1251309

Elnfarawy, A. A., Nashy, A. E., Abozaid, A. M., Komber, I. F., Elweshahy, R. H., and Abdelrahman, R. S. (2020). Vinpocetine Attenuates Thioacetamide-Induced Liver Fibrosis in Rats. *Hum. Exp. Toxicol.* 40, 355–368. doi:10.1177/0960327120947453

Fang, L., Zhang, Y., Wang, Q., Zang, Y., Li, Z., Duan, Z., et al. (2019). A Polysaccharide from Huaier Ameliorates Cisplatin Nephrotoxicity by Decreasing Oxidative Stress and Apoptosis via PI3K/AKT Signaling. *Int. J. Biol. Macromol.* 139, 932–943. doi:10.1016/J.IJBIOMAC.2019.07.219

Gao, J., Liu, B., Ning, Z., Zhao, R., Zhang, A., and Wu, Q. (2009). Characterization and Antioxidant Activity of Flavonoid-Rich Extracts from Leaves of Ampelopsis Grossedentata. *J. Food Biochem.* 33, 808–820. doi:10.1111/J.1745-4514.2009.00253.X

Gressner, A. M., and Weiskirchen, R. (2006). Modern Pathogenetic Concepts of Liver Fibrosis Suggest Stellate Cells and TGF-Beta as Major Players and Therapeutic Targets. *J. Cel. Mol. Med.* 10, 76–99. doi:10.1111/j.1582-4934.2006.tb00292.x

Gupta, S., Afaq, F., and Mukhtar, H. (2002). Involvement of Nuclear Factor-Kappa B, Bax and Bcl-2 in Induction of Cell Cycle Arrest and Apoptosis by Apigenin in Human Prostate Carcinoma Cells. *Oncogene* 21, 3727–3738. doi:10.1038/sj.onc.1205474

Hessien, M. H., El-Sharkawi, I. M., El-Barbary, A. A., El-Beltagy, D. M., and Snyder, N. (2010). Non-Invasive index of Liver Fibrosis Induced by Alcohol, Thioacetamide and Schistosomal Infection in Mice. *BMC Gastroenterol.* 10, 53. doi:10.1186/1471-230X-10-53

Horn, A., and Jaiswal, J. K. (2018). Cellular Mechanisms and Signals that Coordinate Plasma Membrane Repair. *Cell. Mol. Life Sci.* 75, 3751–3770. doi:10.1007/S00018-018-2888-7

Hou, X., Tong, Q., Wang, W., Xiong, W., Shi, C., and Fang, J. (2015). Dihydromyricetin Protects Endothelial Cells from Hydrogen Peroxide-Induced Oxidative Stress Damage by Regulating Mitochondrial Pathways. *Life Sci.* 130, 38–46. doi:10.1016/J.LFS.2015.03.007

Jantararussamee, C., Rodniem, S., Taweechotipatr, M., Showpittapornchai, U., and Pradidarcheep, W. (2021). Hepatoprotective Effect of Probiotic Lactic Acid Bacteria on Thioacetamide-Induced Liver Fibrosis in Rats. *Probiotics Antimicro. Prot.* 13, 40–50. doi:10.1007/S12602-020-09663-6

Kadir, F. A., Othman, F., Abdulla, M. A., Hussan, F., and Hassandarvish, P. (2011). Effect of Tinospora Crispa on Thioacetamide-Induced Liver Cirrhosis in Rats. *Indian J. Pharmacol.* 43, 64–68. doi:10.4103/0253-7613.75673

Karadeniz, A., Simsek, N., Karakus, E., Yildirim, S., Kara, A., Can, I., et al. (2011). Royal Jelly Modulates Oxidative Stress and Apoptosis in Liver and Kidneys of Rats Treated with Cisplatin. *Oxidative Med. Cell Longevity* 2011, 1–10. doi:10.1155/2011/981793

Kisseleva, T., and Brenner, D. A. (2006). Hepatic Stellate Cells and the Reversal of Fibrosis. *J. Gastroenterol. Hepatol.* 21 (Suppl. 3), S84–S87. doi:10.1111/J.1440-1746.2006.04584.X

Kou, X., and Chen, N. (2012). Pharmacological Potential of Ampelopsin in Rattan tea. *Food Sci. Hum. Wellness* 1, 14–18. doi:10.1016/J.FSHW.2012.08.001

Koyama, Y., and Brenner, D. A. (2017). Liver Inflammation and Fibrosis. *J. Clin. Invest.* 127, 55–64. doi:10.1172/JCI88881

Li, X., Benjamin, I. S., and Alexander, B. (2002). Reproducible Production of Thioacetamide-Induced Macronodular Cirrhosis in the Rat with No Mortality. *J. Hepatol.* 36, 488–493. doi:10.1016/S0168-8278(02)00011-9

Lin, M., Zhai, X., Wang, G., Tian, X., Gao, D., Shi, L., et al. (2015). Salvianolic Acid B Protects against Acetaminophen Hepatotoxicity by Inducing Nrf2 and Phase II Detoxification Gene Expression via Activation of the PI3K and PKC Signaling Pathways. *J. Pharmacol. Sci.* 127, 203–210. doi:10.1016/J.JPHS.2014.12.010

Marrone, G., Shah, V. H., and Gracia-Sancho, J. (2016). Sinusoidal Communication in Liver Fibrosis and Regeneration. *J. Hepatol.* 65, 608–617. doi:10.1016/j.jhep.2016.04.018

Mi, X. J., Hou, J. G., Jiang, S., Liu, Z., Tang, S., Liu, X. X., et al. (2019). Maltol Mitigates Thioacetamide-Induced Liver Fibrosis through TGF-B1-Mediated Activation of PI3K/Akt Signaling Pathway. *J. Agric. Food Chem.* 67, 1392–1401. doi:10.1021/ACS.JAFC.8B05943

Naqshbandi, A., Rizwan, S., Khan, M. W., and Khan, F. (2013). Dietary Flaxseed Oil Supplementation Ameliorates the Effect of Cisplatin on brush Border Membrane Enzymes and Antioxidant System in Rat Intestine. *Hum. Exp. Toxicol.* 32, 385–394. doi:10.1177/0960327112438929

Nascimento, M., Piran, R., Da Costa, R. M., Giordani, M. A., Carneiro, F. S., Aguiar, D. H., et al. (2018). Hepatic Injury Induced by Thioacetamide Causes Aortic Endothelial Dysfunction by a Cyclooxygenase-Dependent Mechanism. *Life Sci.* 212, 168–175. doi:10.1016/J.LFS.2018.09.051

Park, M., Kim, Y.-H., Woo, S.-Y., Lee, H. J., Yu, Y., Kim, H. S., et al. (2015). Tonsil-Derived Mesenchymal Stem Cells Ameliorate CCl4-Induced Liver Fibrosis in Mice via Autophagy Activation. *Sci. Rep.* 5, 8616. doi:10.1038/srep08616

Passos, C. C., Ferreira, A. O., Blazquez, F. J. H., and Guerra, R. R. (2010). Modelos experimentais para indução de cirrose hepática em animais: Revisão de literatura doi: 10.5007/2175-7925.2010v23n2p183. *Biotemas* 23, 183–190. doi:10.5007/2175-7925.2010V23N2P183

Poli, G. (2000). Pathogenesis of Liver Fibrosis: Role of Oxidative Stress. *Mol. Aspects Med.* 21, 49–98. doi:10.1016/S0098-2997(00)00004-2

Prokhorova, E. A., Kopeina, G. S., Lavrik, I. N., and Zhivotovsky, B. (2018). Apoptosis Regulation by Subcellular Relocation of Caspases. *Sci. Rep.* 8, 12199. doi:10.1038/s41598-018-30652-x

Qiu, P., Dong, Y., Li, B., Kang, X. J., Gu, C., Zhu, T., et al. (2017). Dihydromyricetin Modulates P62 and Autophagy Crosstalk with the Keap-1/Nrf2 Pathway to Alleviate Ethanol-Induced Hepatic Injury. *Toxicol. Lett.* 274, 31–41. doi:10.1016/J.TOXLET.2017.04.009

Rehman, M. U., Tahir, M., Quaiyoom Khan, A., Khan, R., Lateef, A., Hamiza, O. O., et al. (2013). Diosmin Protects against Trichloroethylene-Induced Renal Injury in Wistar Rats: Plausible Role of P53, Bax and Caspases. *Br. J. Nutr.* 110, 699–710. doi:10.1017/S0007114512005752

Salama, S. M., Abdulla, M. A., AlRashdi, A. S., Ismail, S., Alkiyumi, S. S., and Golbabapour, S. (2013). Hepatoprotective Effect of Ethanolic Extract of Curcuma Longa on Thioacetamide Induced Liver Cirrhosis in Rats. *BMC Complement. Altern. Med.* 13, 56. doi:10.1186/1472-6882-13-56

Sepanlou, S. G., Safiri, S., Bisignano, C., Ikuta, K. S., Merat, S., Saberifiroozi, M., et al. (2020). The Global, Regional, and National burden of Cirrhosis by Cause in 195 Countries and Territories, 1990-2017: A Systematic Analysis for the Global Burden of Disease Study 2017. *Lancet Gastroenterol. Hepatol.* 5, 245–266. doi:10.1016/S2468-1253(19)30349-8

Shou, Y., Li, N., Li, L., Borowitz, J. L., and Isom, G. E. (2002). NF-κB-mediated Up-Regulation of Bcl-XS and Bax Contributes to Cytochrome C Release in Cyanide-Induced Apoptosis. *J. Neurochem.* 81, 842–852. doi:10.1046/J.1471-4159.2002.00880.X

Singh, M., Chaudhry, P., Fabi, F., and Asselin, E. (2013). Cisplatin-Induced Caspase Activation Mediates PTEN Cleavage in Ovarian Cancer Cells: A Potential Mechanism of Chemoresistance. *BMC Cancer* 13, 233. doi:10.1186/1471-2407-13-233

Sun, K., Luo, J., Guo, J., Yao, X., jing, X., and Guo, F. (2020). The PI3K/AKT/mTOR Signaling Pathway in Osteoarthritis: A Narrative Review. *Osteoarthritis and Cartilage* 28, 400–409. doi:10.1016/J.JOCA.2020.02.027

Tsai, M.-Y., Yang, W.-C., Lin, C.-F., Wang, C.-M., Liu, H.-Y., Lin, C.-S., et al. (2021). The Ameliorative Effects of Fucoidan in Thioacetaide-Induced Liver Injury in Mice. *Molecules* 26, 1937. doi:10.3390/MOLECULES26071937

Tsuchida, T., and Friedman, S. L. (2017). Mechanisms of Hepatic Stellate Cell Activation. *Nat. Rev. Gastroenterol. Hepatol.* 14, 397–411. doi:10.1038/nrgastro.2017.38

Tunez, I., Munoz, M., Villavicencio, M., Medina, F., Deprado, E., Espejo, I., et al. (2005). Hepato- and Neurotoxicity Induced by Thioacetamide: Protective Effects of Melatonin and Dimethylsulfoxide. *Pharmacol. Res.* 52, 223–228. doi:10.1016/J.PHRS.2005.03.007

Uchida, D., Takaki, A., Oyama, A., Adachi, T., Wada, N., Onishi, H., et al. (2020). Oxidative Stress Management in Chronic Liver Diseases and Hepatocellular Carcinoma. *Nutrients* 12, 1576. doi:10.3390/NU12061576

Vaidya, A., and Kale, V. P. (2015). TGF-β Signaling and its Role in the Regulation of Hematopoietic Stem Cells. *Syst. Synth. Biol.* 9, 1–10. doi:10.1007/S11693-015-9161-2

Wang, J., Brymora, J., and George, J. (2008). Roles of Adipokines in Liver Injury and Fibrosis. *Expert Rev. Gastroenterol. Hepatol.* 2, 47–57. doi:10.1586/17474124.2.1.47

Williams, A. L., and Hoofnagle, J. H. (1988). Ratio of Serum Aspartate to Alanine Aminotransferase in Chronic Hepatitis. Relationship to Cirrhosis. *Gastroenterology* 95, 734–739. doi:10.1016/S0016-5085(88)80022-2

Wright, J. R., Colby, H. D., and Miles, P. R. (1981). Cytosolic Factors Which Affect Microsomal Lipid Peroxidation in Lung and Liver. *Arch. Biochem. Biophys.* 206, 296–304. doi:10.1016/0003-9861(81)90095-3

Ye, L., Wang, H., Duncan, S. E., Eigel, W. N., and O'Keefe, S. F. (2015). Antioxidant Activities of Vine Tea (Ampelopsis Grossedentata) Extract and its Major Component Dihydromyricetin in Soybean Oil and Cooked Ground Beef. *Food Chem.* 172, 416–422. doi:10.1016/J.FOODCHEM.2014.09.090

Yeh, C.-N., Maitra, A., Lee, K-F., Jan, Y-Y., and Chen, M-F. (2004). Thioacetamide-induced Intestinal-Type Cholangiocarcinoma in Rat: an Animal Model Recapitulating the Multi-Stage Progression of Human Cholangiocarcinoma. *Carcinogenesis* 25, 631–636. doi:10.1093/CARCIN/BGH037

Zeng, Y., Hua, Y. Q., Wang, W., Zhang, H., and Xu, X. L. (2020). Modulation of SIRT1-Mediated Signaling Cascades in the Liver Contributes to the Amelioration of Nonalcoholic Steatohepatitis in High Fat Fed Middle-Aged LDL Receptor Knockout Mice by Dihydromyricetin. *Biochem. Pharmacol.* 175, 113927. doi:10.1016/J.BCP.2020.113927

Zhang, Z., Yao, Z., Zhao, S., Shao, J., Chen, A., Zhang, F., et al. (2017a). Interaction between Autophagy and Senescence Is Required for Dihydroartemisinin to Alleviate Liver Fibrosis. *Cell Death Dis* 8, e2886. doi:10.1038/cddis.2017.255

Zhang, Z., Zhang, H., Chen, S., Xu, Y., Yao, A., Liao, Q., et al. (2017b). Dihydromyricetin Induces Mitochondria-Mediated Apoptosis in HepG2 Cells through Down-Regulation of the Akt/Bad Pathway. *Nutr. Res.* 38, 27–33. doi:10.1016/J.NUTRES.2017.01.003

Zhang, Q., Sun, J., Wang, Y., He, W., Wang, L., Zheng, Y., et al. (2017c). Antimycobacterial and Anti-Inflammatory Mechanisms of Baicalin via Induced Autophagy in Macrophages Infected with *Mycobacterium T*. *Front. Microbiol.* 8, 2142. doi:10.3389/FMICB.2017.02142

Zhang, Q., Zhao, Y., Zhang, M., Zhang, Y., Ji, H., and Shen, L. (2020). Recent Advances in Research on Vine tea, a Potential and Functional Herbal tea with Dihydromyricetin and Myricetin as Major Bioactive Compounds. *J. Pharm. Anal.* 11, 555–563. doi:10.1016/J.JPHA.2020.10.002

Zhang, Y. E. (2017). Non-Smad Signaling Pathways of the TGF-β Family. *Cold Spring Harb. Perspect. Biol.* 9, a022129. doi:10.1101/CSHPERSPECT.A022129

Zhao, J., Deng, J. W., Chen, Y. W., and Li, S. P. (2013). Advanced Phytochemical Analysis of Herbal tea in China. *J. Chromatogr. A.* 1313, 2–23. doi:10.1016/J.CHROMA.2013.07.039

Zheng, C., Ren, Z., Wang, H., Zhang, W., Kalvakolanu, D. V., Tian, Z., et al. (2009). E2F1 Induces Tumor Cell Survival via Nuclear Factor-kappaB-dependent

Induction of EGR1 Transcription in Prostate Cancer Cells. *Cancer Res.* 69, 2324–2331. doi:10.1158/0008-5472.CAN-08-4113

Zheng, X. J., Xiao, H., Zeng, Z., Sun, Z. W., Lei, C., Dong, J. Z., et al. (2014). Composition and Serum Antioxidation of the Main Flavonoids from Fermented Vine tea (Ampelopsis Grossedentata). *J. Funct. Foods* 9, 290–294. doi:10.1016/J.JFF.2014.04.028

Zhou, X., Yu, L., Zhou, M., Hou, P., Yi, L., and Mi, M. (2021). Dihydromyricetin Ameliorates Liver Fibrosis via Inhibition of Hepatic Stellate Cells by Inducing Autophagy and Natural Killer Cell-Mediated Killing Effect. *Nutr. Metab. (Lond)* 18, 64. doi:10.1186/S12986-021-00589-6

Conflict of Interest: The authors declare that the research was conducted in the absence of any commercial or financial relationships that could be construed as a potential conflict of interest.

Publisher's Note: All claims expressed in this article are solely those of the authors and do not necessarily represent those of their affiliated organizations, or those of the publisher, the editors, and the reviewers. Any product that may be evaluated in this article, or claim that may be made by its manufacturer, is not guaranteed or endorsed by the publisher.

GLOSSARY

DHM dihydromyricetin
TAA thioacetamide
ALT alanine aminotransferase
AST aspartate aminotransferase
SOD superoxide dismutase
GSH glutathione
MDA malondialdehyde
PI3K phosphatidylinositol 3-kinase
AKT protein kinase B
α-SMA α-smooth muscle actin
TGF-β1 transforming growth factor-β1
NF-κB nuclear factor kappa-B
TNF-α tumor necrosis factor alpha
IL-1β recombinant rat IL-1β
ROS reactive oxygen species
FAD flavin adenine dinucleotide
CYP2E1 cytochrome P2E1
HSCs hepatic stellate cells
ECM extracellular matrix
Bcl-2 B cell lymphoma/lewkmia-2
Bcl-XL recombinant Human B-Cell Leukemia/Lymphoma XL
Bax Bcl2-associated X
caspase 3 cysteine-dependent aspartate-specifc proteases
Caspases3 cysteine proteases3
caspase 9 cysteine proteases9
NAFLD non-alcoholic fatty liver disease
H and E hematoxylin-eosin
ECL enhanced chemiluminescence
IKK-α IκB kinase α
IKK-β IκB kinase β
IκBα inhibitor of IκBα
Bax B-associated X
BSA bovine serum albumin
DAPI 4,6 diamidino-2-phenylindole
TBS Tris-buffered saline
CCl4 carbon tetrachloride
IL-6 interleukin-6

frontiers in Pharmacology

MINI REVIEW
published: 18 November 2021
doi: 10.3389/fphar.2021.783393

The Contribution of Dietary Fructose to Non-alcoholic Fatty Liver Disease

Siyu Yu[†], *Chunlin Li*[†], *Guang Ji* * *and Li Zhang* *

Institute of Digestive Diseases, Longhua Hospital, Shanghai University of Traditional Chinese Medicine, Shanghai, China

Fructose, especially industrial fructose (sucrose and high fructose corn syrup) is commonly used in all kinds of beverages and processed foods. Liver is the primary organ for fructose metabolism, recent studies suggest that excessive fructose intake is a driving force in non-alcoholic fatty liver disease (NAFLD). Dietary fructose metabolism begins at the intestine, along with its metabolites, may influence gut barrier and microbiota community, and contribute to increased nutrient absorption and lipogenic substrates overflow to the liver. Overwhelming fructose and the gut microbiota-derived fructose metabolites (e.g., acetate, butyric acid, butyrate and propionate) trigger the *de novo* lipogenesis in the liver, and result in lipid accumulation and hepatic steatosis. Fructose also reprograms the metabolic phenotype of liver cells (hepatocytes, macrophages, NK cells, etc.), and induces the occurrence of inflammation in the liver. Besides, there is endogenous fructose production that expands the fructose pool. Considering the close association of fructose metabolism and NAFLD, the drug development that focuses on blocking the absorption and metabolism of fructose might be promising strategies for NAFLD. Here we provide a systematic discussion of the underlying mechanisms of dietary fructose in contributing to the development and progression of NAFLD, and suggest the possible targets to prevent the pathogenetic process.

Keywords: non-alcoholic fatty liver disease (NAFLD), fructose, intestinal environment, *de novo* lipogenesis, inflammation

OPEN ACCESS

Edited by:
Irwin Rose Alencar de Menezes, Regional University of Cariri, Brazil

Reviewed by:
Almir Gonçalves Wanderley, Federal University of São Paulo, Brazil
Radosław Kowalski, University of Life Sciences of Lublin, Poland

***Correspondence:**
Guang Ji
jg@shutcm.edu.cn
jiliver@vip.sina.com
Li Zhang
zhangli.hl@163.com

[†]*These authors have contributed equally to this work*

Specialty section:
This article was submitted to Gastrointestinal and Hepatic Pharmacology, a section of the journal Frontiers in Pharmacology

Received: *26 September 2021*
Accepted: *02 November 2021*
Published: *18 November 2021*

Citation:
Yu S, Li C, Ji G and Zhang L (2021) The Contribution of Dietary Fructose to Non-alcoholic Fatty Liver Disease. Front. Pharmacol. 12:783393. doi: 10.3389/fphar.2021.783393

INTRODUCTION

Nonalcoholic fatty liver disease (NAFLD) is characterized by an excessive fat build-up in the liver without clear other causes, e.g., alcohol addiction, virus infection, and drug induction. Epidemiology investigation reveals that NAFLD has affected more than one-quarter population around the world (Loomba and Sanyal, 2013; Softic et al., 2017). Recently, NAFLD is proposed to be named as metabolic (dysfunction) associated fatty liver disease (MAFLD) due to the heterogeneous etiology and metabolic risks (Eslam et al., 2020). NAFLD has a spectrum ranging from simple fatty liver (NAFL) to nonalcoholic steatohepatitis (NASH), related fibrosis, cirrhosis and even hepatocellular carcinoma (Williams et al., 2011). While NAFL is usually considered to be benign, patients with NASH often potentiate a high probability to further progression. Although NAFLD has been the focus of numerous studies, the pathological mechanisms are still unclear.

Fructose is a plant-derived monosaccharide, the natural form can be found in fruits, berries, and certain vegetables. The association of fructose with NAFLD can be derived from the ancient Egyptians, who fed ducks and geese-dried fruits to make foie gras. Industrial fructose, e.g., the high-fructose corn syrup, is widely used in almost all kinds of processed foods and beverages,

partially driven by the huge commercial profits (Moeller et al., 2009; Vos and Lavine, 2013). During food processing, fructose undergoes a series of reactions (e.g., polymerization, condensation, *etc.*) upon heating to produce aldehydes, reducing ketones, and heterocyclic compounds, thus enhancing the flavor and improving the palatability of food (Maillard reaction). In the past 200 years, per capita dietary fructose intake has increased more than 100-fold (Jang et al., 2018). The average daily consumption of added sugars currently is estimated at 15% of total energy intake all over the world, and almost half is fructose (Wittekind and Walton, 2014; Newens and Walton, 2016; Powell et al., 2016). The wide application of processed foods, such as various baked food and yogurt, further exaggerate the increase of "invisible sugar" intake. Although fructose intake has significantly increased, the early warning mechanisms for the harm in humans are still immature. When excess glucose consumption raises blood glucose, insulin will be secreted to reduce the overwhelmed blood glucose, and prevents the continuous hyperglycemia. The metabolic rate of fructose is much higher than that of glucose, but no immediate feedback mechanisms to suppress its absorption or transportation. Furthermore, the transcription of glucose transporter 5 (GLUT5) increases upon fructose stimulation, which, in turn, enhances fructose transportation and absorption (Gouyon et al., 2003). Simultaneously, fructose is continuously transformed into fructose-1-phosphate (F1P) in the liver, which is an unrestricted process. High fructose-contained diets also induce more caloric intake, thus exacerbating the metabolic disorders indirectly (Lustig, 2013).

Fructose consumption is found to be positively correlated with obesity, diabetes, cardiovascular disease, NAFLD, hypertension, and cancer (Ouyang et al., 2008; Shapiro et al., 2011; White, 2013; DiNicolantonio et al., 2018). Excessive fructose-contained drinks intake is strongly related to the childhood obesity and pediatric NAFLD (Forshee and Storey, 2003). In adults ≥48 years old, daily fructose consumption increases hepatic inflammation and hepatocyte ballooning (Abdelmalek et al., 2010). By producing toxic advanced glycation end-products, fructose is also a threat to the aging process, the occurrence of diabetic complications (e.g. vascular, renal, and ocular complications), and the development of atherosclerosis (Gaby, 2005). In a prospective study involving 77,797 subjects in Sweden, overconsumption of high-sugar-containing foods is found to be a great risk of pancreatic cancer (Larsson et al., 2006). In addition, fructose is also the main cause of symptoms associated with chronic diarrhea or functional bowel disturbances (Gaby, 2005). In animals, overconsumption of fructose can assemble most metabolic features that associated with NAFLD patients, such as insulin resistance, hyperlipidemia, visceral obesity and hyperuricemia (Sánchez-Lozada et al., 2008), suggesting that fructose is a noticeable factor that drives the process of NAFLD. Therefore, we will review the recent studies that focus on the contribution of dietary fructose to NAFLD development and progression, and highlight the metabolic risks and possible drug targets.

DIETARY FRUCTOSE AND INTESTINAL ENVIRONMENT

Fructose and Dysbiosis

Diet is the main source of fructose, and most fructose is absorbed in the small intestine, with 25 g being the upper limit for a healthy adult. Fructose transport proteins (GLUT2 and GLUT5) that locate in the enterocytes are accounting for sensing and passively transporting fructose (Ferraris et al., 2018). Studies showed that GLUT5 transcription is specifically stimulated by fructose *via* cyclic adenosine monophosphate (cAMP) and phosphatidylinositol 3-kinase/protein kinase B (PI3K/Akt) systems (Cui et al., 2004; Cui et al., 2005), whereas GLUT2 is modulated by fructose and glucose levels, as well as systemic factors that released during their absorption (Cui et al., 2003). Absorbed fructose enters the liver *via* the portal vein for further metabolism. When fructose intake exceeds the absorptive capacity of enterocytes, it can transport to the colon where settles more than 100 trillion bacteria (Boulangé et al., 2016). These microbiomes are able to hydrolyze and ferment dietary polysaccharides by producing glycoside hydrolase enzymes (Xu et al., 2003; Sonnenburg et al., 2005; Patterson et al., 2016). By the action of gut microbiomes, fructose can transform into glucose, glycerol, and various organic acids, including uric acids (UA), short-chain fatty acids (SCFA) (e.g., acetate, butyric acid, butyrate and propionate), and amino acids (e.g., glutamic acid, glutamine and alanine) (Jahn et al., 2019; Qi et al., 2020; Zhao et al., 2020). These fructose metabolites either transport to the liver and serve as lipogenic substrates, or interact with the intestinal environment locally. As a monosaccharide, fructose can be the energy source for certain gut microbiomes, for instance, fructose is the single energy source of *Anaerostipes caccae DSM 14662* and *Roseburia intestinalis DSM 14610*, the acetate-converting and butyrate-producing strains (Falony et al., 2006). High fructose diet (HFrD) is reported to affect the composition of gut microbiota characterized by decreased bacterial diversity, increased *Firmicutes*/*Bacteriodetes* ratio in Sprague-Dawley rats (Sen et al., 2017), and reduced protective commensal and bile salt hydrolase-expressing microorganisms in dextran sodium sulfate (DSS)-induced colitis mice (Montrose et al., 2021). HFrD decreases the abundance of *Firmicutes* phylum (*Lactobacillus*) and *Verrucomicrobia* phylum (*Akkermansia*), while increases the abundance of *Bacteroidetes* phylum (*Bacteroides fragilis*) and *Proteobacteria* phylum (*Sutterella*, *Bilophila*, and *Escherichia*) in rodents (Sen et al., 2017; Zubiría et al., 2017; Do et al., 2018; Cho et al., 2021). And the alteration of these gut microbiomes might contribute to the dysbiosis and possibly the impairment of gut barrier (**Figure 1**). Luminal fructose at the physiological level stimulates the release of glucagon-like peptide 1 (GLP-1) from L-subtype EECs in humans and animals, however, the type 2 diabetic mice are GLP-1 resistant due to gut dysbiosis (Kuhre et al., 2014; Seino et al., 2015; Grasset et al., 2017).

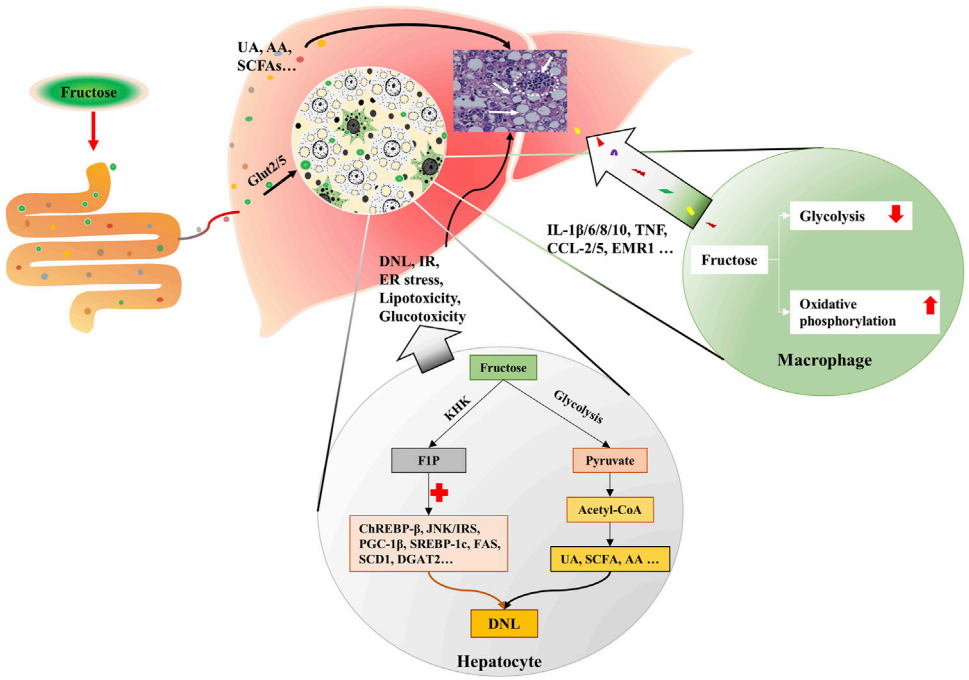

FIGURE 1 | Excessive fructose intake leads to dysbiosis and gut barrier impairment. Fructose is absorbed in the small intestine, and transforms into glycerol, organic acids, and glucose, *etc.* by the action of resident microbiota. Fructose and fructose-derived metabolites may trigger dysbiosis characterized by decreased bacterial diversity and increased *Firmicutes/Bacteriodetes* ratio. Fructose over-intake also impairs gut barrier by decreasing protein expression of the tight junction (zonula occludens 1, occludin, claudin-1, and claudin-4) and adherent junction (β-catenin and E-cadherin) proteins, desmosome plakoglobin, and α-tubulin of enterocytes.

Fructose and Gut Barrier

When high-dose fructose saturates fructose clearance capacity in the ileum, the excessive fructose can enter the colon, and influence the gut barrier. Evidence implied that fructose acts on the intestinal barrier by regulating the transcriptional and post-translational modification of related proteins. In mammals, HFrD decreases protein expression of the tight junction (zonula occludens 1, occludin, claudin-1, and claudin-4) and adherent junction (β-catenin and E-cadherin) proteins, desmosome plakoglobin, and α-tubulin, and increases apoptotic proteins (p-JNK, Bax, cleaved caspase-3, and caspase-3 activity) of enterocytes (Cho et al., 2021). At the transcriptional level, prolonged HFrD feeding reduces genes encoding tight-junction protein-2, occluding, and different claudins in the intestine (Todoric et al., 2020) (**Figure 1**). In addition, HFrD feeding is reported to cause colon shortening possibly through endoplasmic reticulum (ER) stress and inflammatory reaction (Todoric et al., 2020). Recently, fructose is found to improve the survival of intestinal villus under hypoxia, resulting in the expanded nutrient absorption of the gut, thus contributing to increased body weight gain and fat accumulation in mice (Taylor et al., 2021). Nonetheless, it is still unclear whether there is an association between the extension of intestinal villi and disordered gut barrier.

Fructose also influences the intestinal barrier by regulating ethanol metabolism (Bradford et al., 1991; Uzuegbu and Onyesom, 2009; Villalobos-García et al., 2021). In alcohol-fed mice that lack alcohol dehydrogenase (ADH), fructose administration decreases the rates of ethanol metabolism by about 60% *via* diminishing H_2O_2 generation (Bradford et al., 1991). In light alcohol drinkers (<20 g/day) between 25 and 35 years old, however, fructose reduced the duration of alcohol intoxication by 30.7% through facilitating its clearance (Uzuegbu and Onyesom, 2009). At the same time, dysbiosis in fructose-exposed rodents may contribute to the endogenous ethanol production. Additionally, excess fructose intake may lead to fructose malabsorption, and unabsorbed fructose has been found to draw fluid into the intestinal lumen, resulting in abdominal pain, flatulence, diarrhea, and other digestive dysfunctions (Beyer et al., 2005; Gaby, 2005). The organic acids and gas that are produced during fructose metabolism also contribute to the aforementioned gastrointestinal symptoms (Southgate, 1995; Beyer et al., 2005).

FRUCTOSE METABOLISM IN THE DEVELOPMENT OF NASH

Fructose Metabolism and Hepatic Lipogenesis

Fructose dose as low as 0.33 g·kgBM^{-1} is sufficient to stimulate *de novo* lipogenesis (DNL) in mice (Tran et al., 2010), while fructose <0.35 g·kgBM^{-1} would not appear in the portal blood as a prototype (Jang et al., 2018), implicating that gut-derived

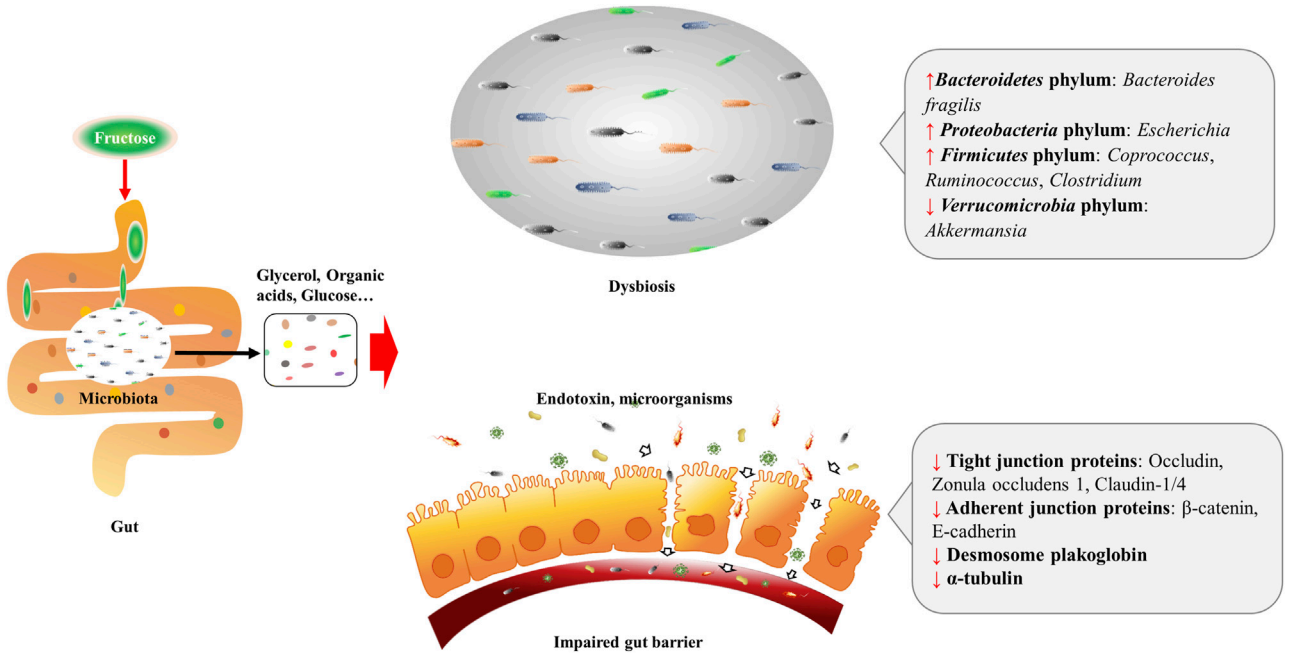

FIGURE 2 | Fructose metabolism in the liver. Fructose is mainly catabolized by hepatocytes. Fructose is absorbed by hepatocytes *via* Glut2/5. Intracellular fructose transforms into F1P by the action of KHK. Then, F1P is metabolized into pyruvate and acetyl-CoA for tricarboxylic acid cycle. During this process, fructose, F1P, as well as their intermediates can activate ChREBP-β, JNK/IRS, and PGC-1β/ SREBP-1/ACC1, which results in DNL. Gut-derived fructose metabolites enter the liver through portal vein, and contribute to DNL in the liver. In addition, UA, SCFA and AA produced in this process also trigger DNL. Simultaneously, fructose exposure alters the energy supply mode of macrophages, which induces oxidative stress and secretion of inflammatory cytokines. KHK, fructokinase; F1P, fructose-1-phosphate; ChREBP-β, carbohydrate-responsive element-binding protein β; JNK, c-Jun N-terminal kinase; IRS, insulin receptor substrates; PGC-1β, peroxisome proliferator-activated receptor gamma co-activator-1β; SREBP-1, sterol regulatory element-binding protein-1; ACC1, acetyl-CoA carboxylase 1; DNL, *de novo* lipogenesis; UA, uric acid; SCFA, short chain fatty acid; AA, amino acid.

fructose metabolites, e.g., acetate, amino acid, endotoxins, SCFA, and ethanol can enter the liver and stimulate lipogenesis physiologically. The saturation of intestinal fructose catabolism would occur at about 5 g sugar intake (e.g., one-fourth of a banana) (Ferraris et al., 2018; Gonzalez and Betts, 2018). And the hepatocellular metabolism of fructose (which bypasses the rate-limiting step of glycolysis at the level of phosphofructokinase) is responsible for most of the metabolic disorders (Andres-Hernando et al., 2020). Fructose at the physiological level can be completely metabolized by the liver, overwhelming fructose consumption, however, leads to steatosis *via* promoting lipogenesis, dyslipidemia, visceral adiposity, and insulin resistance (Jin and Vos, 2015). In addition, fructose metabolism lacks hormonal regulation (Douard and Ferraris, 2008; Douard et al., 2013), which may explain the significant variation in peripheral fructose levels (from 0.008 to 16 mM) (Kawasaki et al., 2002; Hui et al., 2009). On the contrary, fructose malabsorption is negatively correlated to hepatic steatosis (Walker et al., 2012), suggesting that fructose is an environmental factor that favors the development of NAFLD.

More than a quarter of the intrahepatic lipid is generated by DNL in obese and NAFLD individuals (Donnelly et al., 2005; Lim et al., 2010). Fructose enters hepatocytes in a GLUT5-mediated process, intracellular fructose transforms into Fructose-1-phosphate (F1P) by the action of fructokinase (KHK) (Mirtschink et al., 2018). Then, F1P is metabolized into pyruvate and acetyl-CoA for the tricarboxylic acid cycle (Lustig, 2013). During this process, fructose, F1P, as well as their intermediates can activate carbohydrate-responsive element-binding protein (ChREBP)-β, c-Jun N-terminal kinase/insulin receptor substrates, and peroxisome proliferator-activated receptor gamma co-activator-1β/sterol regulatory element-binding protein-1(SREBP-1)/acetyl-CoA carboxylase 1 (ACC1) and downstream DNL pathways (Lustig, 2013; Premachandran et al., 2017; Softic et al., 2017; Gonzalez and Betts, 2018; Pan et al., 2018). Concurrently, genes that encode fatty acid oxidizing enzymes are down-regulated upon fructose exposure, which further exacerbate the hepatic lipid accumulation (Premachandran et al., 2017; Pan et al., 2018). The metabolites of fructose in the intestine, such as SCFA, and amino acid also provide substrates for hepatic DNL, leading to the lipid accumulation in hepatocytes and the increase of circulating fatty acids (Jang et al., 2018; Jahn et al., 2019; Zhao et al., 2020) (**Figure 2**). Besides, fructolysis provides a carbon backbone for the synthesis of nucleotides, triglyceride-glycerol (glycerol-3-phosphate), and amino acids (serine, glutamate, glutamine, aspartate, and asparagine) (Liu et al., 2020).

Fructose in the liver can be transformed into glycogen (Davies et al., 1990; Warner et al., 2021), and hepatic glycogen storage also stimulates DNL (Hengist et al., 2019). In humans, fructose intake

rapidly increases post-exercise liver glycogen synthesis (Décombaz et al., 2011). In rats, administration of fructose causes an immediate increase of glycogen synthase (GS) activity and initiates a fast accumulation of glycogen in the liver (Bezborodkina et al., 2014). Actually, glucose is usually used in food processing in a ratio of nearly 1:1 with fructose, high levels of glucose in the portal vein can induce the expression of hepatic aldose reductase (AR), resulting in the conversion of glucose into sorbitol, which is then metabolized to fructose by sorbitol dehydrogenase (Lanaspa et al., 2013). The production of endogenous fructose may further increase the total fructose content. Fructose contributes to hepatic lipid accumulation also by blocking fatty acid oxidation (FAO) (Lanaspa et al., 2012a; Lanaspa et al., 2012b). In high-fat high-fructose-fed mice, the activity of CTP1a (the rate-limiting enzyme of FAO) and its acylcarnitine products are decreased, and the mitochondrial fission and mitochondrial integrity are damaged (Softic et al., 2019), suggesting the blockage of FAO.

Fructose and Liver Inflammation

Fructose is believed to be an inflammatory mediator that promotes the progression of NAFLD to NASH (Jegatheesan and De Bandt, 2017). HFrD has been proven to induce insulin resistance, hepatic steatosis, ballooning degeneration and fibrosis in transgenic (Tg) MUP-uPA mice, and significantly increased the tumor necrosis factor (*Tnf*), interleukin (*Il*)-*6*, *Il1β*, *Ccl2*, *Ccl5* and *Emr1* (Todoric et al., 2020). Moreover, HFrD enhances diethyl nitrosamine-induced hepatocellular carcinoma in BL6 mice (Todoric et al., 2020).

Macrophage plays an important role in the hepatic inflammatory response. Fructose is thought to influence the metabolic phenotype of macrophages, which is a decisive factor for cellular function. Stressed macrophages present increased glycolysis, whereas oxidative metabolism primed macrophages for a less inflammatory mode (Vats et al., 2006). 2-deoxy-glucose (2-DG), an inhibitor of glycolysis, also blocks TNF-α and IL-6 production in macrophages (Wang et al., 2014). In lipopolysaccharide (LPS)-stressed macrophages, high concentrations of fructose alter the mode of energy supply, with impaired glycolysis and enhanced oxidative phosphorylation, along with glutaminolysis and oxidative stress, which result in the secretion of inflammatory cytokines, such as interleukin-1β (IL-1β), IL-6, IL-8, IL-10, and TNF (Jones et al., 2021) (**Figure 2**). Considering the fact that increased glycolysis favors cell proliferation in cancer while enhanced oxidative phosphorylation supplies sufficient amounts of energy for inflammatory macrophages, the different effects of fructose on cells may be derived from cell demands in different situations. And glycolysis-produced intermediates may contribute to both cell proliferation and activation.

And fructose overconsumption is shown to induce local macrophage infiltration in the liver (Hotamisligil et al., 1993; Glushakova et al., 2008; DiNicolantonio et al., 2018). Studies also show that fructose promotes monocyte recruitment *via* monocyte chemoattractant protein 1 and intracellular adhesion molecule 1 (Fantuzzi and Faggioni, 2000; Shapiro et al., 2011; DiNicolantonio et al., 2018). Besides, fructose exposure in LPS-stimulated human dendritic cells provokes the secretion of pro-inflammatory cytokines from T cells (Jaiswal et al., 2019). And mice deficient in T or NK cells are prevented from developing fructose-induced NAFLD (Bhattacharjee et al., 2014). Moreover, fructose treatment influences the viability of stressed immune cells (Jones et al., 2021).

Fructose overconsumption also increases visceral adipose tissue mass and intracellular cortisol concentration (Targher et al., 2006; Kovačević et al., 2014). Adipocyte hypertrophy may trigger ER stress, disturb adipokines (leptin and adiponectin) release, and increase pro-inflammatory cytokine secretion (de Heredia et al., 2012; DiNicolantonio et al., 2018). Fructose-induced increase of intracellular cortisol level *via* 11beta-hydroxysteroid dehydrogenase type1 (11β-HSD1) leads to a raise of fatty acid flux out of the subcutaneous adipocytes, thus providing more substrates for visceral fat accumulation (de Heredia et al., 2012; DiNicolantonio et al., 2018). Plasminogen activator inhibitor 1 (PAI-1) is an acute-phase protein that participates in hepatic lipid transport and provokes inflammation in the liver (Bergheim et al., 2006). It is reported that fructose content is positively correlated to PAI-1 concentration, and PAI-1 knock-out mice are protected from fructose-induced steatosis and inflammation (Castrogiovanni et al., 2012).

DIETARY FRUCTOSE AND UA METABOLISM

Dietary fructose increases both serum and intrahepatic UA levels (Lanaspa et al., 2012b). UA is primarily produced in hepatocytes, and the process of fructose metabolization to F1P consumes a large amount of intracellular ATP and phosphate, the decrease of phosphate activates adenosine monophosphate (AMP) deaminase that converts AMP to inosine monophosphate, which results in UA production (Van den Berghe, 1986). Simultaneously, fructose-derived amino acids also increase UA excretion and decrease plasma uridine (Yamamoto et al., 1999). UA is known to promote hepatic fat accumulation, and provokes mitochondrial oxidative stress by increasing superoxide generation and mitochondrial NOX4 expression, and decreasing manganese superoxide dismutase in NASH mice (Lanaspa et al., 2012b; Ishimoto et al., 2012). Meanwhile, UA can activate nuclear factor-κB and Nod-like receptor protein 3 inflammasomes (Wan et al., 2016). In patients with NAFLD/NASH, the serum UA level is positively correlated to the extent of the lobular inflammation and steatosis (Sertoglu et al., 2014). Additionally, UA may increase endogenous fructose production in a feedback way (Jensen et al., 2018). Inhibition of UA formation has been proven to be beneficial for metabolic diseases (Lanaspa et al., 2012c; Lanaspa et al., 2013; Nakatsu et al., 2015).

Fructose metabolites are found to induce renal damage (Ramezani and Raj, 2014; Tang et al., 2015). In healthy male adults, daily ingestion of 200 g fructose for 2 weeks appears to increase urinary stone formation partly *via* regulating urate metabolism, urinary pH, and increasing oxalate (Johnson

et al., 2018). Fructose-contained beverage intake in infancy has been reported to be associated with worse outcomes in a later event of acute kidney injury and kidney damage during adolescence (García-Arroyo et al., 2020). In experimental hamsters, monosodium glutamate plus a high-fat and high-fructose (HFF) diet increases the risk of kidney injury, induces gut dysbiosis, and an increase in the amount of p-cresol sulfate (Pongking et al., 2020). At the same time, HFF can induce dyslipidemia and lipid accumulation in the kidney (Thongnak et al., 2020). Besides, fructose increases segmental artery vascular resistance by increasing serum UA and copeptin (Chapman et al., 2020), enhances angiotensin II-stimulated Na transport *via* activation of protein kinase C α1 in renal proximal tubules (Yang et al., 2020). Renal DNL stimulated by high-fructose supplementation may also contribute to the increase of intrahepatic triglycerides (Milutinović et al., 2020).

POSSIBLE DRUG TARGETS IN FRUCTOSE METABOLISM

Glucose Transporter Family Members (GLUTs)

Glucose transporter family members (GLUTs) belong to the major facilitator superfamily, which are encoded by the SLC2 genes (Mueckler and Thorens, 2013; Nomura et al., 2015). In humans, 14 GLUTs are found to mediate the facilitative diffusion of sugar along the concentration gradient (Schmidl et al., 2020). Dietary fructose absorption is very efficient in the small intestine mediated by GLUTs transporters.

The transport of fructose across the intestinal basolateral membrane is mediated by one or more sodium-independent routes. GLUT2 is responsible for moving both fructose in and glucose out of the enterocyte across the basolateral membrane under basal conditions (Cheeseman, 1993). The malfunction or dysregulation of GLUT2 is associated with diabetes, metabolic syndrome, and cancer (Schmidl et al., 2020). GLUT2 variants increase the risks of fasting hyperglycemia, type 2 diabetes, hypercholesterolemia and cardiovascular diseases. Besides, individuals with a missense mutation in GLUT2 show a preference for sugar-containing foods (Thorens, 2015). GLUT2 inhibition is desirable for patients with fructose-induced metabolic disorders, but it may lead to insulin insensitivity (Ferraris et al., 2018), suggesting that specific inhibition of GLUT2 is necessary. GLUT5 level is increased in patients with acute myeloid leukemia and prostate cancer, and is reported to be negatively related to the prognosis of patients (Carreno et al., 2021; Jeong et al., 2021). In rodents, increased GLUT5 is associated with enhanced steatosis and pancreatic inflammation (Roncal-Jimenez et al., 2011). GLUT5 deletion could reduce fructose absorption by approximately 75% in the jejunum and decrease the concentration of serum fructose by approximately 90% in comparison to wild-type mice on excess fructose intake, suggesting that GLUT5 is required for fructose transportation, and the function cannot be compensated by GLUT2 (Barone et al., 2009; Patel et al., 2015). GLUT5 is also highly expressed in many cancers, thus promoting the proliferation of cancer cells (Su et al., 2018; Jin et al., 2019; Chen et al., 2020). Inhibiting GLUT5 is expected to be a promising strategy for fructose-associated diseases. Lately, several drugs are found to inhibit GLUT2/5. *i.e.*, Chamomile and green tea display acute inhibition on GLUT2/5 and thus decrease fructose and glucose transportation in human Caco-2 cells and Xenopus oocytes (Villa-Rodriguez et al., 2017). Kefir, a fermented drink, is found to decrease GLUT2/5 in the liver of HFrD fed rats (Akar et al., 2021).

Fructokinase (KHK)

KHK is an essential fructose-metabolizing enzyme in the liver, which specifically catalyzes the transfer of a phosphate group from adenosine triphosphate to fructose. KHK-C, the principal isoform of KHK in the liver, is increased in NAFLD patients that consume excessive fructose-contained beverages (Ouyang et al., 2008; Ishimoto et al., 2012). Pharmacological inhibition of KHK activity with PF-06835919 is reported to prevent patients from hepatic steatosis, lipogenic, and fibrosis (Shepherd et al., 2021). KHK deficiency or inhibition (PF-06835919) protects animals from fructose-induced obesity, insulin resistance, hypertriglyceridemia, and NAFLD (Lanaspa et al., 2013; Futatsugi et al., 2020; Gutierrez et al., 2021). Knockout KHK could also decrease fructose-derived UA production and attenuate mitochondrial oxidative stress in mice (Ishimoto et al., 2012). Besides, Extracts of Angelica archangelica, Garcinia mangostana, Petroselinum crispum, and Scutellaria baicalensis are identified with inhibitory activity against ketohexokinase-C (Le et al., 2016). Interestingly, fructokinase A (KHK-A), another isoform of KHK, protects against C-mediated metabolic diseases, but its activity is relatively low due to a low fructose affinity (Ishimoto et al., 2012). Drugs such as that targeting reshaping the balance between the two types of KHK is an attractive strategy.

Triokinase (TK)

TK is a rate-limiting enzyme in fructolysis, and is essential for the induction of the lipogenic program under physiological conditions (Liu et al., 2020). TK knockdown abrogates the expression of lipogenic enzymes and results in a significant reduction in HFrD-induced hepatic steatosis, as well as liver size and plasma glucose levels (Liu et al., 2020). Meanwhile, TK is necessary for maintaining mitochondrial respiration. It is found that 5 mM fructose is sufficient to have a significant decapacitating effect on mitochondrial respiration in the TK-deficient cells, an overnight culture of mutant cells with 15 mM fructose obliterates their respiration capacity (Liu et al., 2020). Liver TK deficiency results in a more than 2-fold sensitization of hepatocytes to fructose toxicity, indicating TK might be a promising target to block fructose toxicity. Although ADP is reported to be a potent inhibitor of TK, agents that target TK inhibition are not available yet.

Aldose Reductase (AR)

AR is the key enzyme in stimulating endogenous fructose production. It can be activated under pathological conditions, including ischemia, heart failure, inflammation, and

hyperuricemia (Huang et al., 2017; Nakagawa et al., 2020). Increased AR results in the conversion of blood glucose into sorbitol, which is further metabolized into endogenous fructose by sorbitol dehydrogenase (Lanaspa et al., 2013). Liver AR knockdown, or AR inhibitors can attenuate hepatic steatosis and related metabolic disorders in mice (Lanaspa et al., 2013; Nakagawa et al., 2020). Furthermore, the addition of salt to fructose in the drinking water significantly accelerates the development of NAFLD, the high-salt diet activates the AR-fructokinase pathway in the liver and hypothalamus, resulting in endogenous fructose production (Lanaspa et al., 2018). These results suggest that AR is the target of blocking endogenous fructose production. Actually, a series of extracts from natural products such as Luteolin, quercetin, apigenin, fisetin, and myricitrin are potential AR inhibitors, and found to be beneficial for NAFLD/NASH (Grewal et al., 2016). And AR inhibitors Sorbinil and Ranirestat, are under clinical trials.

CONCLUSIONS AND PERSPECTIVES

The liver is the critical organ to metabolize fructose, the increasing consumption of fructose in various forms specially exaggerates liver burden and contributes to NAFLD/NASH. The rapidly metabolized fructose in the liver promotes lipogenesis, lipotoxicity, as well as the inflammatory reaction of immune cells. Meanwhile, the interaction of fructose and gut microbiota results in dysbiosis, impaired intestinal mucosa barrier, production of toxins and microbial metabolites that may further serve as substrates for liver lipogenesis, and pathogens for liver inflammation. In addition, fructose metabolism lacks hormonal regulation, making excessive fructose consumption thus a more dangerous factor to NAFLD patients.

Even so, patients with obesity, hypertension, and diabetes are encouraged to intake certain fructose contained in vegetables and specific fruits, such as blueberries, grapes, and apples (Bazzano et al., 2008; Muraki et al., 2013; Sundborn et al., 2019). The possible explanation might be that most fruits contain modest amounts of fructose (3–8 g per fruit), and the fiber, vitamin, and other constituents (flavonols, epicatechin, ascorbate, and other antioxidants) in it carries substantial metabolic benefits (Vasdev et al., 2002; Sundborn et al., 2019). Restriction of calorie intake when supplying high fructose failed to induce obesity but still triggered steatosis in rats (Roncal-Jimenez et al., 2011). Even supplement with high palm oil in high fructose diet, the rats tend to become non-obese NAFLD model (Abdelmoneim et al., 2021), suggested fructose induction may account for lean NAFLD. Lean NAFLD makes up about one-third of the NAFLD population, according to recent studies, lean NAFLD may potentiate higher metabolic risks than obese NAFLD. Thus, the association of fructose intake and lean NAFLD deserve to be systematically explored. Also, the fructose-associated NAFLD in children and adolescents needs to be highlighted. Considering the global epidemic of metabolic syndrome especially NAFLD, it is extremely important to provide alarming in controlling daily fructose intake for people, especially children and teenagers, in prevention and management of NAFLD.

AUTHOR CONTRIBUTIONS

LZ and GJ conceptualized the manuscript, SY and CL retrieved the literature, SY and CL drafted the manuscript, GJ and LZ revised the manuscript. All authors edited, revised, and approved the final version of this review.

FUNDING

This work is supported by the grant from Shanghai Shenkang Hospital Development Center (No. SHDC2020CR4044). The funding resources have no involvement in conceptualization, the literature collection, the writing of the review, and the decision to submit the article for publication. The fund and our institution all acknowledge open access publication fees.

REFERENCES

Abdelmalek, M. F., Suzuki, A., Guy, C., Unalp-Arida, A., Colvin, R., Johnson, R. J., et al. (2010). Increased Fructose Consumption Is Associated with Fibrosis Severity in Patients with Nonalcoholic Fatty Liver Disease. *Hepatology* 51 (6), 1961–1971. doi:10.1002/hep.23535

Abdelmoneim, D., El-Adl, M., El-Sayed, G., and El-Sherbini, E. S. (2021). Protective Effect of Fenofibrate Against High-Fat-High-Fructose Diet Induced Non-obese NAFLD in Rats. *Fundam. Clin. Pharmacol.* 35 (2), 379–388. doi:10.1111/fcp.12597

Akar, F., Sumlu, E., Alçığır, M. E., Bostancı, A., and Sadi, G. (2021). Potential Mechanistic Pathways Underlying Intestinal and Hepatic Effects of Kefir in High-Fructose-Fed Rats. *Food Res. Int.* 143, 110287. doi:10.1016/j.foodres.2021.110287

Andres-Hernando, A., Orlicky, D. J., Kuwabara, M., Ishimoto, T., Nakagawa, T., Johnson, R. J., et al. (2020). Deletion of Fructokinase in the Liver or in the Intestine Reveals Differential Effects on Sugar-Induced Metabolic Dysfunction. *Cell Metab* 32 (1), 117–127.e3. doi:10.1016/j.cmet.2020.05.012

Barone, S., Fussell, S. L., Singh, A. K., Lucas, F., Xu, J., Kim, C., et al. (2009). Slc2a5 (Glut5) Is Essential for the Absorption of Fructose in the Intestine and Generation of Fructose-Induced Hypertension. *J. Biol. Chem.* 284 (8), 5056–5066. doi:10.1074/jbc.M808128200

Bazzano, L. A., Li, T. Y., Joshipura, K. J., and Hu, F. B. (2008). Intake of Fruit, Vegetables, and Fruit Juices and Risk of Diabetes in Women. *Diabetes Care* 31 (7), 1311–1317. doi:10.2337/dc08-0080

Bergheim, I., Guo, L., Davis, M. A., Lambert, J. C., Beier, J. I., Duveau, I., et al. (2006). Metformin Prevents Alcohol-Induced Liver Injury in the Mouse: Critical Role of Plasminogen Activator Inhibitor-1. *Gastroenterology* 130 (7), 2099–2112. doi:10.1053/j.gastro.2006.03.020

Beyer, P. L., Caviar, E. M., and McCallum, R. W. (2005). Fructose Intake at Current Levels in the United States May Cause Gastrointestinal Distress in Normal Adults. *J. Am. Diet. Assoc.* 105 (10), 1559–1566. doi:10.1016/j.jada.2005.07.002

Bezborodkina, N. N., Chestnova, A. Y., Okovity, S. V., and Kudryavtsev, B. N. (2014). Activity of Glycogen Synthase and Glycogen Phosphorylase in Normal and Cirrhotic Rat Liver During Glycogen Synthesis from Glucose or Fructose. *Exp. Toxicol. Pathol.* 66 (2-3), 147–154. doi:10.1016/j.etp.2013.12.001

Bhattacharjee, J., Kumar, J. M., Arindkar, S., Das, B., Pramod, U., Juyal, R. C., et al. (2014). Role of Immunodeficient Animal Models in the Development of

Fructose Induced NAFLD. *J. Nutr. Biochem.* 25 (2), 219–226. doi:10.1016/j.jnutbio.2013.10.010

Boulangé, C. L., Neves, A. L., Chilloux, J., Nicholson, J. K., and Dumas, M. E. (2016). Impact of the Gut Microbiota on Inflammation, Obesity, and Metabolic Disease. *Genome Med.* 8 (1), 42. doi:10.1186/s13073-016-0303-2

Bradford, B. U., Handler, J. A., Seed, C. B., Forman, D. T., and Thurman, R. G. (1991). Inhibition of Ethanol Metabolism by Fructose in Alcohol Dehydrogenase-Deficient Deer Mice In Vivo. *Arch. Biochem. Biophys.* 288 (2), 435–439. doi:10.1016/0003-9861(91)90217-7

Carreño, D. V., Corro, N. B., Cerda-Infante, J. F., Echeverría, C. E., Asencio-Barría, C. A., Torres-Estay, V. A., et al. (2021). Dietary Fructose Promotes Prostate Cancer Growth. *Cancer Res.* 81 (11), 2824–2832. doi:10.1158/0008-5472.CAN-19-0456

Castrogiovanni, D., Alzamendi, A., Ongaro, L., Giovambattista, A., Gaillard, R. C., and Spinedi, E. (2012). Fructose Rich Diet-Induced High Plasminogen Activator Inhibitor-1 (PAI-1) Production in the Adult Female Rat: Protective Effect of Progesterone. *Nutrients* 4 (8), 1137–1150. doi:10.3390/nu4081137

Chapman, C. L., Grigoryan, T., Vargas, N. T., Reed, E. L., Kueck, P. J., Pietrafesa, L. D., et al. (2020). High-fructose Corn Syrup-Sweetened Soft Drink Consumption Increases Vascular Resistance in the Kidneys at Rest and During Sympathetic Activation. *Am. J. Physiol. Ren. Physiol* 318 (4), F1053–f1065. doi:10.1152/ajprenal.00374.2019

Cheeseman, C. I. (1993). GLUT2 Is the Transporter for Fructose Across the Rat Intestinal Basolateral Membrane. *Gastroenterology* 105 (4), 1050–1056. doi:10.1016/0016-5085(93)90948-c

Chen, W. L., Jin, X., Wang, M., Liu, D., Luo, Q., Tian, H., et al. (2020). GLUT5-mediated Fructose Utilization Drives Lung Cancer Growth by Stimulating Fatty Acid Synthesis and AMPK/mTORC1 Signaling. *JCI Insight* 5 (3), e131596. doi:10.1172/jci.insight.131596

Cho, Y. E., Kim, D. K., Seo, W., Gao, B., Yoo, S. H., and Song, B. J. (2021). Fructose Promotes Leaky Gut, Endotoxemia, and Liver Fibrosis Through Ethanol-Inducible Cytochrome P450-2e1-Mediated Oxidative and Nitrative Stress. *Hepatology* 73 (6), 2180–2195. doi:10.1002/hep.30652

Cui, X. L., Jiang, L., and Ferraris, R. P. (2003). Regulation of Rat Intestinal GLUT2 mRNA Abundance by Luminal and Systemic Factors. *Biochim. Biophys. Acta* 1612 (2), 178–185. doi:10.1016/s0005-2736(03)00129-9

Cui, X. L., Soteropoulos, P., Tolias, P., and Ferraris, R. P. (2004). Fructose-Responsive Genes in the Small Intestine of Neonatal Rats. *Physiol. Genomics* 18 (2), 206–217. doi:10.1152/physiolgenomics.00056.2004

Cui, X. L., Schlesier, A. M., Fisher, E. L., Cerqueira, C., and Ferraris, R. P. (2005). Fructose-induced Increases in Neonatal Rat Intestinal Fructose Transport Involve the PI3-kinase/Akt Signaling Pathway. *Am. J. Physiol. Gastrointest. Liver Physiol.* 288 (6), G1310–G1320. doi:10.1152/ajpgi.00550.2004

Davies, D. R., Detheux, M., and Van Schaftingen, E. (1990). Fructose 1-Phosphate and the Regulation of Glucokinase Activity in Isolated Hepatocytes. *Eur. J. Biochem.* 192 (2), 283–289. doi:10.1111/j.1432-1033.1990.tb19225.x

Décombaz, J., Jentjens, R., Ith, M., Scheurer, E., Buehler, T., Jeukendrup, A., et al. (2011). Fructose and Galactose Enhance Postexercise Human Liver Glycogen Synthesis. *Med. Sci. Sports Exerc.* 43 (10), 1964–1971. doi:10.1249/MSS.0b013e318218ca5a

de Heredia, F. P., Gómez-Martínez, S., and Marcos, A. (2012). Obesity, Inflammation and the Immune System. *Proc. Nutr. Soc.* 71 (2), 332–338. doi:10.1017/s0029665112000092

DiNicolantonio, J. J., Mehta, V., Onkaramurthy, N., and O'Keefe, J. H. (2018). Fructose-induced Inflammation and Increased Cortisol: A New Mechanism for How Sugar Induces Visceral Adiposity. *Prog. Cardiovasc. Dis.* 61 (1), 3–9. doi:10.1016/j.pcad.2017.12.001

Do, M. H., Lee, E., Oh, M. J., Kim, Y., and Park, H. Y. (2018). High-Glucose or -Fructose Diet Cause Changes of the Gut Microbiota and Metabolic Disorders in Mice Without Body Weight Change. *Nutrients* 10 (6), 761. doi:10.3390/nu10060761

Donnelly, K. L., Smith, C. I., Schwarzenberg, S. J., Jessurun, J., Boldt, M. D., and Parks, E. J. (2005). Sources of Fatty Acids Stored in Liver and Secreted via Lipoproteins in Patients with Nonalcoholic Fatty Liver Disease. *J. Clin. Invest.* 115 (5), 1343–1351. doi:10.1172/jci23621

Douard, V., and Ferraris, R. P. (2008). Regulation of the Fructose Transporter GLUT5 in Health and Disease. *Am. J. Physiol. Endocrinol. Metab.* 295 (2), E227–E237. doi:10.1152/ajpendo.90245.2008

Douard, V., Sabbagh, Y., Lee, J., Patel, C., Kemp, F. W., Bogden, J. D., et al. (2013). Excessive Fructose Intake Causes 1,25-(OH)(2)D(3)-Dependent Inhibition of Intestinal and Renal Calcium Transport in Growing Rats. *Am. J. Physiol. Endocrinol. Metab.* 304 (12), E1303–E1313. doi:10.1152/ajpendo.00582.2012

Eslam, M., Sanyal, A. J., and George, J. (2020). MAFLD: A Consensus-Driven Proposed Nomenclature for Metabolic Associated Fatty Liver Disease. *Gastroenterology* 158 (7), 1999–2014.e1. doi:10.1053/j.gastro.2019.11.312

Falony, G., Vlachou, A., Verbrugghe, K., and De Vuyst, L. (2006). Cross-feeding BBetween Bifidobacterium Longum BB536 and Acetate-Converting, Butyrate-Producing Colon Bacteria During Growth on Oligofructose. *Appl. Environ. Microbiol.* 72 (12), 7835–7841. doi:10.1128/aem.01296-06

Fantuzzi, G., and Faggioni, R. (2000). Leptin in the Regulation of Immunity, Inflammation, and Hematopoiesis. *J. Leukoc. Biol.* 68 (4), 437–446.

Ferraris, R. P., Choe, J. Y., and Patel, C. R. (2018). Intestinal Absorption of Fructose. *Annu. Rev. Nutr.* 38, 41–67. doi:10.1146/annurev-nutr-082117-051707

Forshee, R. A., and Storey, M. L. (2003). Total Beverage Consumption and Beverage Choices Among Children and Adolescents. *Int. J. Food Sci. Nutr.* 54 (4), 297–307. doi:10.1080/09637480120092143

Futatsugi, K., Smith, A. C., Tu, M., Raymer, B., Ahn, K., Coffey, S. B., et al. (2020). Discovery of PF-06835919: A Potent Inhibitor of Ketohexokinase (KHK) for the Treatment of Metabolic Disorders Driven by the Overconsumption of Fructose. *J. Med. Chem.* 63 (22), 13546–13560. doi:10.1021/acs.jmedchem.0c00944

Gaby, A. R. (2005). Adverse Effects of Dietary Fructose. *Altern. Med. Rev.* 10 (4), 294–306.

García-Arroyo, F. E., Pérez-Estévez, H. E., Tapia, E., Gonzaga, G., Muñoz-Jiménez, I., Soto, V., et al. (2020). Restricted Water Intake and Hydration with Fructose-Containing Beverages During Infancy Predispose to Aggravate an Acute Renal Ischemic Insult in Adolescent Rats. *Biomed. Res. Int.* 2020, 4281802. doi:10.1155/2020/4281802

Glushakova, O., Kosugi, T., Roncal, C., Mu, W., Heinig, M., Cirillo, P., et al. (2008). Fructose Induces the Inflammatory Molecule ICAM-1 in Endothelial Cells. *J. Am. Soc. Nephrol.* 19 (9), 1712–1720. doi:10.1681/asn.2007121304

Gonzalez, J. T., and Betts, J. A. (2018). Dietary Fructose Metabolism by Splanchnic Organs: Size Matters. *Cel Metab* 27 (3), 483–485. doi:10.1016/j.cmet.2018.02.013

Gouyon, F., Onesto, C., Dalet, V., Pages, G., Leturque, A., and Brot-Laroche, E. (2003). Fructose Modulates GLUT5 mRNA Stability in Differentiated Caco-2 Cells: Role of cAMP-Signalling Pathway and PABP (Polyadenylated-Binding Protein)-Interacting Protein (Paip) 2. *Biochem. J.* 375 (Pt 1), 167–174. doi:10.1042/bj20030661

Grasset, E., Puel, A., Charpentier, J., Collet, X., Christensen, J. E., Tercé, F., et al. (2017). A Specific Gut Microbiota Dysbiosis of Type 2 Diabetic Mice Induces GLP-1 Resistance Through an Enteric NO-Dependent and Gut-Brain Axis Mechanism. *Cel Metab* 25 (5), 1075–1090.e5. doi:10.1016/j.cmet.2017.04.013

Grewal, A. S., Bhardwaj, S., Pandita, D., Lather, V., and Sekhon, B. S. (2016). Updates on Aldose Reductase Inhibitors for Management of Diabetic Complications and Non-Diabetic Diseases. *Mini Rev. Med. Chem.* 16 (2), 120–162. doi:10.2174/1389557515666150909143737

Gutierrez, J. A., Liu, W., Perez, S., Xing, G., Sonnenberg, G., Kou, K., et al. (2021). Pharmacologic Inhibition of Ketohexokinase Prevents Fructose-Induced Metabolic Dysfunction. *Mol. Metab.* 48, 101196. doi:10.1016/j.molmet.2021.101196

Hengist, A., Koumanov, F., and Gonzalez, J. T. (2019). Fructose and Metabolic Health: Governed by Hepatic Glycogen Status. *J. Physiol.* 597 (14), 3573–3585. doi:10.1113/jp277767

Hotamisligil, G. S., Shargill, N. S., and Spiegelman, B. M. (1993). Adipose Expression of Tumor Necrosis Factor-Alpha: Direct Role in Obesity-Linked Insulin Resistance. *Science* 259 (5091), 87–91. doi:10.1126/science.7678183

Huang, Z., Hong, Q., Zhang, X., Xiao, W., Wang, L., Cui, S., et al. (2017). Aldose Reductase Mediates Endothelial Cell Dysfunction Induced by High Uric Acid Concentrations. *Cell Commun. Signal.* 15 (1), 3. doi:10.1186/s12964-016-0158-6

Hui, H., Huang, D., McArthur, D., Nissen, N., Boros, L. G., and Heaney, A. P. (2009). Direct Spectrophotometric Determination of Serum Fructose in Pancreatic Cancer Patients. *Pancreas* 38 (6), 706–712. doi:10.1097/MPA.0b013e3181a7c6e5

Ishimoto, T., Lanaspa, M. A., Le, M. T., Garcia, G. E., Diggle, C. P., Maclean, P. S., et al. (2012). Opposing Effects of Fructokinase C and A Isoforms on Fructose-Induced Metabolic Syndrome in Mice. *Proc. Natl. Acad. Sci. U S A.* 109 (11), 4320–4325. doi:10.1073/pnas.1119908109

Jahn, D., Kircher, S., Hermanns, H. M., and Geier, A. (2019). Animal Models of NAFLD from a Hepatologist's Point of View. *Biochim. Biophys. Acta Mol. Basis Dis.* 1865 (5), 943–953. doi:10.1016/j.bbadis.2018.06.023

Jaiswal, N., Agrawal, S., and Agrawal, A. (2019). High Fructose-Induced Metabolic Changes Enhance Inflammation in Human Dendritic Cells. *Clin. Exp. Immunol.* 197 (2), 237–249. doi:10.1111/cei.13299

Jang, C., Hui, S., Lu, W., Cowan, A. J., Morscher, R. J., Lee, G., et al. (2018). The Small Intestine Converts Dietary Fructose into Glucose and Organic Acids. *Cel Metab* 27 (2), 351–361.e3. doi:10.1016/j.cmet.2017.12.016

Jegatheesan, P., and De Bandt, J. P. (2017). Fructose and NAFLD: The Multifaceted Aspects of Fructose Metabolism. *Nutrients* 9 (3), 230. doi:10.3390/nu9030230

Jensen, T., Abdelmalek, M. F., Sullivan, S., Nadeau, K. J., Green, M., Roncal, C., et al. (2018). Fructose and Sugar: A Major Mediator of Non-Alcoholic Fatty Liver Disease. *J. Hepatol.* 68 (5), 1063–1075. doi:10.1016/j.jhep.2018.01.019

Jeong, S., Savino, A. M., Chirayil, R., Barin, E., Cheng, Y., Park, S. M., et al. (2021). High Fructose Drives the Serine Synthesis Pathway in Acute Myeloid Leukemic Cells. *Cel Metab* 33 (1), 145–159.e6. doi:10.1016/j.cmet.2020.12.005

Jin, R., and Vos, M. B. (2015). Fructose and Liver Function-Iis This Behind Nonalcoholic Liver Disease? *Curr. Opin. Clin. Nutr. Metab. Care* 18 (5), 490–495. doi:10.1097/mco.0000000000000203

Jin, C., Gong, X., and Shang, Y. (2019). GLUT5 Increases Fructose Utilization in Ovarian Cancer. *Onco Targets Ther.* 12, 5425–5436. doi:10.2147/ott.S205522

Johnson, R. J., Perez-Pozo, S. E., Lillo, J. L., Grases, F., Schold, J. D., Kuwabara, M., et al. (2018). Fructose Increases Risk for Kidney Stones: Potential Role in Metabolic Syndrome and Heat Stress. *BMC Nephrol.* 19 (1), 315. doi:10.1186/s12882-018-1105-0

Jones, N., Blagih, J., Zani, F., Rees, A., Hill, D. G., Jenkins, B. J., et al. (2021). Fructose Reprogrammes Glutamine-dependent Oxidative Metabolism to Support LPS-Induced Inflammation. *Nat. Commun.* 12 (1), 1209. doi:10.1038/s41467-021-21461-4

Kawasaki, T., Akanuma, H., and Yamanouchi, T. (2002). Increased Fructose Concentrations in Blood and Urine in Patients with Diabetes. *Diabetes Care* 25 (2), 353–357. doi:10.2337/diacare.25.2.353

Kovačević, S., Nestorov, J., Matić, G., and Elaković, I. (2014). Dietary Fructose-Related Adiposity and Glucocorticoid Receptor Function in Visceral Adipose Tissue of Female Rats. *Eur. J. Nutr.* 53 (6), 1409–1420. doi:10.1007/s00394-013-0644-1

Kuhre, R. E., Gribble, F. M., Hartmann, B., Reimann, F., Windeløv, J. A., Rehfeld, J. F., et al. (2014). Fructose Stimulates GLP-1 but Not GIP Secretion in Mice, Rats, and Humans. *Am. J. Physiol. Gastrointest. Liver Physiol.* 306 (7), G622–G630. doi:10.1152/ajpgi.00372.2013

Lanaspa, M. A., Cicerchi, C., Garcia, G., Li, N., Roncal-Jimenez, C. A., Rivard, C. J., et al. (2012a). Counteracting Roles of AMP Deaminase and AMP Kinase in the Development of Fatty Liver. *PLoS One* 7 (11), e48801. doi:10.1371/journal.pone.0048801

Lanaspa, M. A., Sanchez-Lozada, L. G., Choi, Y. J., Cicerchi, C., Kanbay, M., Roncal-Jimenez, C. A., et al. (2012b). Uric Acid Induces Hepatic Steatosis by Generation of Mitochondrial Oxidative Stress: Potential Role in Fructose-dependent and -independent Fatty Liver. *J. Biol. Chem.* 287 (48), 40732–40744. doi:10.1074/jbc.M112.399899

Lanaspa, M. A., Sanchez-Lozada, L. G., Cicerchi, C., Li, N., Roncal-Jimenez, C. A., Ishimoto, T., et al. (2012c). Uric Acid Stimulates Fructokinase and Accelerates Fructose Metabolism in the Development of Fatty Liver. *PLoS One* 7 (10), e47948. doi:10.1371/journal.pone.0047948

Lanaspa, M. A., Ishimoto, T., Li, N., Cicerchi, C., Orlicky, D. J., Ruzycki, P., et al. (2013). Endogenous Fructose Production and Metabolism in the Liver Contributes to the Development of Metabolic Syndrome. *Nat. Commun.* 4, 2434. doi:10.1038/ncomms3434

Lanaspa, M. A., Kuwabara, M., Andres-Hernando, A., Li, N., Cicerchi, C., Jensen, T., et al. (2018). High Salt Intake Causes Leptin Resistance and Obesity in Mice by Stimulating Endogenous Fructose Production and Metabolism. *Proc. Natl. Acad. Sci. U S A.* 115 (12), 3138–3143. doi:10.1073/pnas.1713837115

Larsson, S. C., Bergkvist, L., and Wolk, A. (2006). Consumption of Sugar and Sugar-Sweetened Foods and the Risk of Pancreatic Cancer in a Prospective Study. *Am. J. Clin. Nutr.* 84 (5), 1171–1176. doi:10.1093/ajcn/84.5.1171

Le, M. T., Lanaspa, M. A., Cicerchi, C. M., Rana, J., Scholten, J. D., Hunter, B. L., et al. (2016). Bioactivity-Guided Identification of Botanical Inhibitors of Ketohexokinase. *PLoS One* 11 (6), e0157458. doi:10.1371/journal.pone.0157458

Lim, J. S., Mietus-Snyder, M., Valente, A., Schwarz, J. M., and Lustig, R. H. (2010). The Role of Fructose in the Pathogenesis of NAFLD and the Metabolic Syndrome. *Nat. Rev. Gastroenterol. Hepatol.* 7 (5), 251–264. doi:10.1038/nrgastro.2010.41

Liu, L., Li, T., Liao, Y., Wang, Y., Gao, Y., Hu, H., et al. (2020). Triose Kinase Controls the Lipogenic Potential of Fructose and Dietary Tolerance. *Cel Metab* 32 (4), 605–618.e7. doi:10.1016/j.cmet.2020.07.018

Loomba, R., and Sanyal, A. J. (2013). The Global NAFLD Epidemic. *Nat. Rev. Gastroenterol. Hepatol.* 10 (11), 686–690. doi:10.1038/nrgastro.2013.171

Lustig, R. H. (2013). Fructose: It's "Alcohol without the Buzz". *Adv. Nutr.* 4 (2), 226–235. doi:10.3945/an.112.002998

Milutinović, D. V., Brkljačić, J., Teofilović, A., Bursać, B., Nikolić, M., Gligorovska, L., et al. (2020). Chronic Stress Potentiates High Fructose-Induced Lipogenesis in Rat Liver and Kidney. *Mol. Nutr. Food Res.* 64 (13), 1901141. doi:10.1002/mnfr.201901141

Mirtschink, P., Jang, C., Arany, Z., and Krek, W. (2018). Fructose Metabolism, Cardiometabolic Risk, and the Epidemic of Coronary Artery Disease. *Eur. Heart J.* 39 (26), 2497–2505. doi:10.1093/eurheartj/ehx518

Moeller, S. M., Fryhofer, S. A., Osbahr, A. J., 3rd, and Robinowitz, C. B. (2009). The Effects of High Fructose Syrup. *J. Am. Coll. Nutr.* 28 (6), 619–626. doi:10.1080/07315724.2009.10719794

Montrose, D. C., Nishiguchi, R., Basu, S., Staab, H. A., Zhou, X. K., Wang, H., et al. (2021). Dietary Fructose Alters the Composition, Localization, and Metabolism of Gut Microbiota in Association with Worsening Colitis. *Cell Mol Gastroenterol Hepatol* 11 (2), 525–550. doi:10.1016/j.jcmgh.2020.09.008

Mueckler, M., and Thorens, B. (2013). The SLC2 (GLUT) Family of Membrane Transporters. *Mol. Aspects Med.* 34 (2-3), 121–138. doi:10.1016/j.mam.2012.07.001

Muraki, I., Imamura, F., Manson, J. E., Hu, F. B., Willett, W. C., van Dam, R. M., et al. (2013). Fruit Consumption and Risk of Type 2 Diabetes: Results from Three Prospective Longitudinal Cohort Studies. *Bmj* 347, f5001. doi:10.1136/bmj.f5001

Nakagawa, T., Lanaspa, M. A., Millan, I. S., Fini, M., Rivard, C. J., Sanchez-Lozada, L. G., et al. (2020). Fructose Contributes to the Warburg Effect for Cancer Growth. *Cancer Metab.* 8, 16. doi:10.1186/s40170-020-00222-9

Nakatsu, Y., Seno, Y., Kushiyama, A., Sakoda, H., Fujishiro, M., Katasako, A., et al. (2015). The Xanthine Oxidase Inhibitor Febuxostat Suppresses Development of Nonalcoholic Steatohepatitis in a Rodent Model. *Am. J. Physiol. Gastrointest. Liver Physiol.* 309 (1), G42–G51. doi:10.1152/ajpgi.00443.2014

Newens, K. J., and Walton, J. (2016). A Review of Sugar Consumption from Nationally Representative Dietary Surveys Across the World. *J. Hum. Nutr. Diet.* 29 (2), 225–240. doi:10.1111/jhn.12338

Nomura, N., Verdon, G., Kang, H. J., Shimamura, T., Nomura, Y., Sonoda, Y., et al. (2015). Structure and Mechanism of the Mammalian Fructose Transporter GLUT5. *Nature* 526 (7573), 397–401. doi:10.1038/nature14909

Ouyang, X., Cirillo, P., Sautin, Y., McCall, S., Bruchette, J. L., Diehl, A. M., et al. (2008). Fructose Consumption as a Risk Factor for Non-alcoholic Fatty Liver Disease. *J. Hepatol.* 48 (6), 993–999. doi:10.1016/j.jhep.2008.02.011

Pan, J. H., Kim, H. S., Beane, K. E., Montalbano, A. M., Lee, J. H., Kim, Y. J., et al. (2018). IDH2 Deficiency Aggravates Fructose-Induced NAFLD by Modulating Hepatic Fatty Acid Metabolism and Activating Inflammatory Signaling in Female Mice. *Nutrients* 10 (6), 679. doi:10.3390/nu10060679

Patel, C., Douard, V., Yu, S., Gao, N., and Ferraris, R. P. (2015). Transport, Metabolism, and Endosomal Trafficking-dependent Regulation of Intestinal Fructose Absorption. *Faseb j* 29 (9), 4046–4058. doi:10.1096/fj.15-272195

Patterson, E., Ryan, P. M., Cryan, J. F., Dinan, T. G., Ross, R. P., Fitzgerald, G. F., et al. (2016). Gut Microbiota, Obesity and Diabetes. *Postgrad. Med. J.* 92 (1087), 286–300. doi:10.1136/postgradmedj-2015-133285

Pongking, T., Haonon, O., Dangtakot, R., Onsurathum, S., Jusakul, A., Intuyod, K., et al. (2020). A Combination of Monosodium Glutamate and High-Fat and High-Fructose Diets Increases the Risk of Kidney Injury, Gut Dysbiosis and

Host-Microbial Co-metabolism. *PLoS One* 15 (4), e0231237. doi:10.1371/journal.pone.0231237

Powell, E. S., Smith-Taillie, L. P., and Popkin, B. M. (2016). Added Sugars Intake across the Distribution of US Children and Adult Consumers: 1977-2012. *J. Acad. Nutr. Diet.* 116 (10), 1543–1550.e1. doi:10.1016/j.jand.2016.06.003

Premachandran, V., Tarlow, D., Yuille, A. L., and Batra, D. (2017). Empirical Minimum Bayes Risk Prediction. *IEEE Trans. Pattern Anal. Mach Intell.* 39 (1), 75–86. doi:10.1109/tpami.2016.2537807

Qi, Y., Wan, M., Abd El-Aty, A. M., Li, H., Cao, L., She, Y., et al. (2020). A "half" Core-Shell Magnetic Nanohybrid Composed of Zeolitic Imidazolate Framework and Graphitic Carbon Nitride for Magnetic Solid-phase Extraction of Sulfonylurea Herbicides from Water Samples Followed by LC-MS/MS Detection. *Mikrochim Acta* 187 (5), 279. doi:10.1007/s00604-020-04243-5

Ramezani, A., and Raj, D. S. (2014). The Gut Microbiome, Kidney Disease, and Targeted Interventions. *J. Am. Soc. Nephrol.* 25 (4), 657–670. doi:10.1681/asn.2013080905

Roncal-Jimenez, C. A., Lanaspa, M. A., Rivard, C. J., Nakagawa, T., Sanchez-Lozada, L. G., Jalal, D., et al. (2011). Sucrose Induces Fatty Liver and Pancreatic Inflammation in Male Breeder Rats Independent of Excess Energy Intake. *Metabolism* 60 (9), 1259–1270. doi:10.1016/j.metabol.2011.01.008

Sánchez-Lozada, L. G., Le, M., Segal, M., and Johnson, R. J. (2008). How Safe Is Fructose for Persons With or Without Diabetes. *Am. J. Clin. Nutr.* 88 (5), 1189–1190. doi:10.3945/ajcn.2008.26812

Schmidl, S., Tamayo Rojas, S. A., Iancu, C. V., Choe, J. Y., and Oreb, M. (2020). Functional Expression of the Human Glucose Transporters GLUT2 and GLUT3 in Yeast Offers Novel Screening Systems for GLUT-Targeting Drugs. *Front. Mol. Biosci.* 7, 598419. doi:10.3389/fmolb.2020.598419

Seino, Y., Ogata, H., Maekawa, R., Izumoto, T., Iida, A., Harada, N., et al. (2015). Fructose Induces Glucose-dependent Insulinotropic Polypeptide, Glucagon-like Peptide-1 and Insulin Secretion: Role of Adenosine Triphosphate-Sensitive K(+) Channels. *J. Diabetes Investig.* 6 (5), 522–526. doi:10.1111/jdi.12356

Sen, T., Cawthon, C. R., Ihde, B. T., Hajnal, A., DiLorenzo, P. M., de La Serre, C. B., et al. (2017). Diet-driven Microbiota Dysbiosis Is Associated with Vagal Remodeling and Obesity. *Physiol. Behav.* 173, 305–317. doi:10.1016/j.physbeh.2017.02.027

Sertoglu, E., Ercin, C. N., Celebi, G., Gurel, H., Kayadibi, H., Genc, H., et al. (2014). The Relationship of Serum Uric Acid with Non-alcoholic Fatty Liver Disease. *Clin. Biochem.* 47 (6), 383–388. doi:10.1016/j.clinbiochem.2014.01.029

Shapiro, A., Tümer, N., Gao, Y., Cheng, K. Y., and Scarpace, P. J. (2011). Prevention and Reversal of Diet-Induced Leptin Resistance with a Sugar-free Diet Despite High Fat Content. *Br. J. Nutr.* 106 (3), 390–397. doi:10.1017/s000711451100033x

Shepherd, E. L., Saborano, R., Northall, E., Matsuda, K., Ogino, H., Yashiro, H., et al. (2021). Ketohexokinase Inhibition Improves NASH by Reducing Fructose-Induced Steatosis and Fibrogenesis. *JHEP Rep.* 3 (2), 100217. doi:10.1016/j.jhepr.2020.100217

Softic, S., Gupta, M. K., Wang, G. X., Fujisaka, S., O'Neill, B. T., Rao, T. N., et al. (2017). Divergent Effects of Glucose and Fructose on Hepatic Lipogenesis and Insulin Signaling. *J. Clin. Invest.* 127 (11), 4059–4074. doi:10.1172/jci94585

Softic, S., Meyer, J. G., Wang, G. X., Gupta, M. K., Batista, T. M., Lauritzen, H. P. M. M., et al. (2019). Dietary Sugars Alter Hepatic Fatty Acid Oxidation via Transcriptional and Post-translational Modifications of Mitochondrial Proteins. *Cel Metab.* 30 (4), 735–753.e4. doi:10.1016/j.cmet.2019.09.003

Sonnenburg, J. L., Xu, J., Leip, D. D., Chen, C. H., Westover, B. P., Weatherford, J., et al. (2005). Glycan Foraging In Vivo by an Intestine-Adapted Bacterial Symbiont. *Science* 307 (5717), 1955–1959. doi:10.1126/science.1109051

Southgate, D. A. (1995). Digestion and Metabolism of Sugars. *Am. J. Clin. Nutr.* 62 (1), 203S–210S. doi:10.1093/ajcn/62.1.203S

Su, C., Li, H., and Gao, W. (2018). GLUT5 Increases Fructose Utilization and Promotes Tumor Progression in Glioma. *Biochem. Biophys. Res. Commun.* 500 (2), 462–469. doi:10.1016/j.bbrc.2018.04.103

Sundborn, G., Thornley, S., Merriman, T. R., Lang, B., King, C., Lanaspa, M. A., et al. (2019). Are Liquid Sugars Different from Solid Sugar in Their Ability to Cause Metabolic Syndrome? *Obesity (Silver Spring)* 27 (6), 879–887. doi:10.1002/oby.22472

Tang, W. H., Wang, Z., Kennedy, D. J., Wu, Y., Buffa, J. A., Agatisa-Boyle, B., et al. (2015). Gut Microbiota-Dependent Trimethylamine N-Oxide (TMAO) Pathway Contributes to Both Development of Renal Insufficiency and Mortality Risk in Chronic Kidney Disease. *Circ. Res.* 116 (3), 448–455. doi:10.1161/circresaha.116.305360

Targher, G., Bertolini, L., Rodella, S., Zoppini, G., Zenari, L., and Falezza, G. (2006). Associations Between Liver Histology and Cortisol Secretion in Subjects with Nonalcoholic Fatty Liver Disease. *Clin. Endocrinol. (Oxf)* 64 (3), 337–341. doi:10.1111/j.1365-2265.2006.02466.x

Taylor, S. R., Ramsamooj, S., Liang, R. J., Katti, A., Pozovskiy, R., Vasan, N., et al. (2021). Dietary Fructose Improves Intestinal Cell Survival and Nutrient Absorption. *Nature* 597, 263–267. doi:10.1038/s41586-021-03827-2

Thongnak, L., Chatsudthipong, V., Kongkaew, A., and Lungkaphin, A. (2020). Effects of Dapagliflozin and Statins Attenuate Renal Injury and Liver Steatosis in High-Fat/high-Fructose Diet-Induced Insulin Resistant Rats. *Toxicol. Appl. Pharmacol.* 396, 114997. doi:10.1016/j.taap.2020.114997

Thorens, B. (2015). GLUT2, Glucose Sensing and Glucose Homeostasis. *Diabetologia* 58 (2), 221–232. doi:10.1007/s00125-014-3451-1

Todoric, J., Di Caro, G., Reibe, S., Henstridge, D. C., Green, C. R., Vrbanac, A., et al. (2020). Fructose Stimulated De Novo Lipogenesis Is Promoted by Inflammation. *Nat. Metab.* 2 (10), 1034–1045. doi:10.1038/s42255-020-0261-2

Tran, C., Jacot-Descombes, D., Lecoultre, V., Fielding, B. A., Carrel, G., Lê, K. A., et al. (2010). Sex Differences in Lipid and Glucose Kinetics After Ingestion of an Acute Oral Fructose Load. *Br. J. Nutr.* 104 (8), 1139–1147. doi:10.1017/s000711451000190x

Uzuegbu, U. E., and Onyesom, I. (2009). Fructose-induced Increase in Ethanol Metabolism and the Risk of Syndrome X in Man. *C R. Biol.* 332 (6), 534–538. doi:10.1016/j.crvi.2009.01.007

Van den Berghe, G. (1986). Fructose: Metabolism and Short-Term Effects on Carbohydrate and Purine Metabolic Pathways. *Prog. Biochem. Pharmacol.* 21, 1–32.

Vasdev, S., Gill, V., Parai, S., Longerich, L., and Gadag, V. (2002). Dietary Vitamin E and C Supplementation Prevents Fructose Induced Hypertension in Rats. *Mol. Cel Biochem* 241 (1-2), 107–114. doi:10.1023/a:1020835229591

Vats, D., Mukundan, L., Odegaard, J. I., Zhang, L., Smith, K. L., Morel, C. R., et al. (2006). Oxidative Metabolism and PGC-1beta Attenuate Macrophage-Mediated Inflammation. *Cel Metab* 4 (1), 13–24. doi:10.1016/j.cmet.2006.05.011

Villalobos-García, D., Ayhllon-Osorio, C. A., and Hernández-Muñoz, R. (2021). The Fructose-dependent Acceleration of Ethanol Metabolism. *Biochem. Pharmacol.* 188, 114498. doi:10.1016/j.bcp.2021.114498

Villa-Rodriguez, J. A., Aydin, E., Gauer, J. S., Pyner, A., Williamson, G., and Kerimi, A. (2017). Green and Chamomile Teas, but Not Acarbose, Attenuate Glucose and Fructose Transport via Inhibition of GLUT2 and GLUT5. *Mol. Nutr. Food Res.* 61 (12), 1700566. doi:10.1002/mnfr.201700566

Vos, M. B., and Lavine, J. E. (2013). Dietary Fructose in Nonalcoholic Fatty Liver Disease. *Hepatology* 57 (6), 2525–2531. doi:10.1002/hep.26299

Walker, R. W., Lê, K. A., Davis, J., Alderete, T. L., Cherry, R., Lebel, S., et al. (2012). High Rates of Fructose Malabsorption Are Associated with Reduced Liver Fat in Obese African Americans. *J. Am. Coll. Nutr.* 31 (5), 369–374. doi:10.1080/07315724.2012.10720445

Wan, X., Xu, C., Lin, Y., Lu, C., Li, D., Sang, J., et al. (2016). Uric Acid Regulates Hepatic Steatosis and Insulin Resistance Through the NLRP3 Inflammasome-dependent Mechanism. *J. Hepatol.* 64 (4), 925–932. doi:10.1016/j.jhep.2015.11.022

Wang, Q., Zhao, Y., Sun, M., Liu, S., Li, B., Zhang, L., et al. (2014). 2-Deoxy-d-glucose Attenuates Sevoflurane-Induced Neuroinflammation Through Nuclear Factor-Kappa B Pathway In Vitro. *Toxicol. Vitro* 28 (7), 1183–1189. doi:10.1016/j.tiv.2014.05.006

Warner, S. O., Wadian, A. M., Smith, M., Farmer, B., Dai, Y., Sheanon, N., et al. (2021). Liver Glycogen-Induced Enhancements in Hypoglycemic Counterregulation Require Neuroglucopenia. *Am. J. Physiol. Endocrinol. Metab.* 320 (5), E914–e924. doi:10.1152/ajpendo.00501.2020

White, J. S. (2013). Challenging the Fructose Hypothesis: New Perspectives on Fructose Consumption and Metabolism. *Adv. Nutr.* 4 (2), 246–256. doi:10.3945/an.112.003137

Williams, C. D., Stengel, J., Asike, M. I., Torres, D. M., Shaw, J., Contreras, M., et al. (2011). Prevalence of Nonalcoholic Fatty Liver Disease and Nonalcoholic Steatohepatitis Among a Largely Middle-Aged Population Utilizing Ultrasound and Liver Biopsy: A Prospective Study. *Gastroenterology* 140 (1), 124–131. doi:10.1053/j.gastro.2010.09.038

Wittekind, A., and Walton, J. (2014). Worldwide Trends in Dietary Sugars Intake. *Nutr. Res. Rev.* 27 (2), 330–345. doi:10.1017/s0954422414000237

Xu, J., Bjursell, M. K., Himrod, J., Deng, S., Carmichael, L. K., Chiang, H. C., et al. (2003). A Genomic View of the Human-Bacteroides Thetaiotaomicron Symbiosis. *Science* 299 (5615), 2074–2076. doi:10.1126/science.1080029

Yamamoto, T., Moriwaki, Y., Takahashi, S., Tsutsumi, Z., Ohata, H., Yamakita, J., et al. (1999). Effect of Amino Acids on the Plasma Concentration and Urinary Excretion of Uric Acid and Uridine. *Metabolism* 48 (8), 1023–1027. doi:10.1016/s0026-0495(99)90200-7

Yang, N., Hong, N. J., and Garvin, J. L. (2020). Dietary Fructose Enhances Angiotensin II-Stimulated Na+ Transport via Activation of PKC-α in Renal Proximal Tubules. *Am. J. Physiol. Ren. Physiol* 318 (6), F1513–f1519. doi:10.1152/ajprenal.00543.2019

Zhao, S., Jang, C., Liu, J., Uehara, K., Gilbert, M., Izzo, L., et al. (2020). Dietary Fructose Feeds Hepatic Lipogenesis via Microbiota-Derived Acetate. *Nature* 579 (7800), 586–591. doi:10.1038/s41586-020-2101-7

Zubiría, M. G., Gambaro, S. E., Rey, M. A., Carasi, P., Serradell, M. L. Á., and Giovambattista, A. (2017). Deleterious Metabolic Effects of High Fructose Intake: The Preventive Effect of Lactobacillus Kefiri Administration. *Nutrients* 9 (5), 470. doi:10.3390/nu9050470

Conflict of Interest: The authors declare that the research was conducted in the absence of any commercial or financial relationships that could be construed as a potential conflict of interest.

Publisher's Note: All claims expressed in this article are solely those of the authors and do not necessarily represent those of their affiliated organizations, or those of the publisher, the editors and the reviewers. Any product that may be evaluated in this article, or claim that may be made by its manufacturer, is not guaranteed or endorsed by the publisher.

frontiers in Pharmacology

ORIGINAL RESEARCH
published: 24 November 2021
doi: 10.3389/fphar.2021.789430

Network Pharmacology-Based Analysis of *Pogostemon cablin* (Blanco) Benth Beneficial Effects to Alleviate Nonalcoholic Fatty Liver Disease in Mice

Yizhe Cui[1,2†], *Qiuju Wang*[1†], *Renxu Chang*[1†], *Ahmad Aboragah*[3], *Juan J. Loor*[3] *and Chuang Xu*[1,2*]

[1]College of Animal Science and Technology, Heilongjiang Bayi Agricultural University, Daqing, China, [2]Heilongjiang Provincial Key Laboratory of Prevention and Control of Bovine Diseases, Heilongjiang Bayi Agricultural University, Daqing, China, [3]Department of Animal Sciences, Division of Nutritional Sciences, University of Illinois, Urbana, IL, United States

Nonalcoholic fatty liver disease (NAFLD) is the most common cause of chronic liver disease and is associated with high morbidity and mortality. *Pogostemon cablin* (Blanco) Benth/Huo Xiang (HX) is a perennial herb with unique anti-oxidant and anti-inflammatory properties, and thus, can positively affect liver function. In this study, we used network pharmacology to predict the potential mechanism of HX on NAFLD. Pharmacological experiments were used to verify the effect of HX on the functions of NAFLD. Network pharmacology identified nine components that interacted with 82 NAFLD-related targets, revealing four target genes: *TNF*, *IL6*, *TP53*, and *AKT1*. HX prevents the development and progression of NAFLD through different pathways and targets with quercetin-regulated lipid metabolism, anti-inflammatory, and anti-oxidant pathways playing an essential role in the treatment of NAFLD. Compared with feeding HFD, HX significantly attenuated lipid accumulation *in vivo* with mice and also *in vitro* with mouse liver cells. A high dose of HX decreased hepatocyte lipid accumulation and the abundance of SREBF1 and FASN. Validation experiments revealed that HX inhibited the activation of NF-κB/IκB signaling and decreased the release and levels of pro-inflammatory factors (TNF-α and IL-6). These data suggest that HX can attenuate abnormal lipid metabolic responses and enhance antioxidant mechanisms. Thus, the pharmacological effects from plants used in traditional Chinese medicine are achievde through a multi-level response.

Keywords: network pharmacology, *Pogostemon cablin* (Blanco) Benth, mice, AML12 cells, multi-targets, NAFLD

OPEN ACCESS

Edited by:
Irwin Rose Alencar De Menezes, Regional University of Cariri, Brazil

Reviewed by:
Radosław Kowalski, University of Life Sciences of Lublin, Poland
Fu Peng, Sichuan University, China
Natália Cruz-Martins, Faculdade de Medicina da Universidade do Porto, Portugal

***Correspondence:**
Chuang Xu
xuchuang7175@163.com

†These authors have contributed equally to this work

Specialty section:
This article was submitted to Gastrointestinal and Hepatic Pharmacology, a section of the journal Frontiers in Pharmacology

Received: *04 October 2021*
Accepted: *08 November 2021*
Published: *24 November 2021*

Citation:
Cui Y, Wang Q, Chang R, Aboragah A, Loor JJ and Xu C (2021) Network Pharmacology-Based Analysis of Pogostemon cablin *(Blanco) Benth Beneficial Effects to Alleviate Nonalcoholic Fatty Liver Disease in Mice. Front. Pharmacol. 12:789430. doi: 10.3389/fphar.2021.789430*

Abbreviations: ACACA, acetyl-CoA carboxylase-alpha; ALT, alanine aminotransferase; AML12, alpha mouse liver 12; AST, aspartate aminotransferase; ATF6, activating transcription factor 6; FASN, fatty acid synthase; FFA, free fatty acid; HX, Huo Xiang; LC/MS, liquid chromatography-electrospray ionization/mass spectrometry; H&E, hematoxylin and eosin; HFD, high-fat diet; IL-6, interleukin-6; IKK, inhibitor of κB kinase; IκB, inhibitor of NF-κB; IR, insulin resistance; IRE1, inositol-requiring enzyme-1; MDA, malondialdehyde; MTT, 3-(4,5-dimethyl-2-thiazolyl)-2,5-diphenyl-2-H-tetrazolium bromide; NAFLD, Nonalcoholic fatty liver disease; NF-κB, nuclear factor-κB; PERK, protein kinase (PKR)-like endoplasmic reticulum kinase; SOD, superoxide dismutase; SREBF1, sterol regulatory element binding transcription factor 1; TC, total cholesterol; TCM, traditional Chinese medicine; TG, triglyceride; TNF-α, tumor necrosis factor-α.

INTRODUCTION

Nonalcoholic fatty liver disease (NAFLD) is a crucial component of the metabolic syndrome when obesity and insulin resistance (IR) are present (Danford and Lai, 2019). Inflammatory reactions induced by reactive oxygen species (ROS) in liver parenchymal cells during NAFLD characterize the so-called "first hit" (Buzzetti et al., 2016). Dysregulation of adipocyte metabolism in the metabolic syndrome is an independent risk factor for developing NAFLD (Eslam and George, 2019). Natural substances are not the only effective treatment for obesity, diabetes, insulin resistance (IR), and other metabolic diseases, but they are relatively safe to consume (Li et al., 2016). Traditional Chinese medicine (TCM) formulas based on plant extracts contain substances capable of eliciting the so-called "multiple organ-multiple hit" effect (Yan et al., 2020). Various TCMs and supplements offer suitable therapeutic options for the treatment and prevention of NAFLD (Perumpail et al., 2018).

Patchouli (*Pogostemon cablin* (Blanco) Benth./Huo Xiang (HX)), from the Labiatae family, has been used by humans for the treatment of anorexia, vomiting, hepatic injury (Cui BW. et al., 2019), and other intestinal disorders (Tuan et al., 2012; Li HQ. et al., 2013). Compilation of Materia Medica ("Ben Cao Gang Mu" in pinyin) also contains information indicating that HX can be used to treat dampness obstruction, abdominal distension, vomiting, and heat dampness syndrome. Previous studies indicated that HX exerts anticarcinogenic (Lu et al., 2016) and protective effects against lung (Su et al., 2016) and brain injury (Wei et al., 2018). Extracts of HX are also uesed to treat inflammatory (Li et al., 2011) and oxidative stress-induced disorders (Lian et al., 2018). In addition, HX reduces toll-like receptor (TLR) 4 and glycosylation end product (receptor for advanced glycation end products [RAGE]) protein signaling contributing to lipopolysaccharide-induced liver injury (Cho et al., 2015). Despite the substantial amount of information available, the main pharmacodynamic components contained in HX and the molecular mechanism of its protective effect on acute alcoholic liver injury are still unclear.

Network pharmacology is an emerging discipline based on systems biology theory, i.e. combining multiple disciplines to design multi-target drugs, analyze the interactions between biological networks, and identify desired targets (Hao and Xiao, 2014). It provides a scientific channel for mechanistic research focused on TCM prescriptions and how they may be successfully applied to various diseases (Luo et al., 2020). The framework of system biology is consistent with the characteristics of multi-component, multi-target, and multi-channel interactions of a given compound. The systems approach is compatible with the holistic view to differentiate various syndromes, but alos their treatment using TCM.

Therefore, our goal was to apply a network pharmacology–based approach to investigate the relationship between HX compounds and potential targets in NAFLD. Our specific objectives were to induce NAFLD *in vivo* and *in vitro* to study the underlying mechanisms whereby HX could positively affect the disease, focusing on the use of network pharmacology and experimental validation.

MATERIALS AND METHODS

Network Pharmacology Study

Collection of Potential Targets of HX

A search was performed for the active components of HX in the TCM system pharmacology technology platform (TCMIP, http://www.tcmip.cn/TCMIP/index.php/Home/) databases with "*Pogostemon cablin* (Blanco) Benth" as the keyword. The bioactive compounds were screened further using oral bioavailability (OB) criteria of ≥30% and drug-likeness (DL) of ≥0.18 (Xu et al., 2019). Potential bioactive compounds of HX were submitted to the DrugBank (https://www.drugbank.ca/) server. Then, potential targets (proteins) from DrugBank and the Traditional Chinese Medicine Systems Pharmacology (TCMSP) database were translated into genes using STRING 11.5 (https://string-db.org/). The UniProt (https://www.uniprot.org/) database was used to standardize the results. An interaction network of component targets was constructed and visualized via Cytoscape software.

Nonalcoholic fatty liver–related targets were mined from DisGeNET (https://www.disgenet.org/) (Piñero et al., 2021). We used "nonalcoholic fatty liver disease" as index words and limited the species to "Homo sapiens" to collect therapeutic targets for NAFLD. Lastly, Cytoscape 3.8.2 was used to perform visual network analysis of the "disease-target."

Construction and Analysis of the Protein-Protein Interaction Network

To explain the interactions between putative targets, the target information between HX and NAFLD obtained above was imported into the STRING platform (https://string-db.org) to generate relationships between these potential targets. High-confidence data >0.4 were included to ensure reliability of the analysis. Subsequently, the protein–protein interaction network was constructed and visualized.

Functional Enrichment and Pathways Analysis

The potential targets for the active ingredients of HX in NAFLD were annotated using the biomolecular function of Metascape (https://metascape.org/gp/index.html#/main/step1). A heatmap was plotted using http://www.bioinformatics.com.cn, a free online platform for data analysis and visualization. Gene Ontology (GO) enrichment analyses included biological process (BP), cellular component (CC), and molecular function (MF). In addition, Kyoto Encyclopedia of Gene and Genome (KEGG) pathway enrichment analyses were performed. Lastly, $p < 0.01$ was set as the threshold value to identify biological processes and signaling pathways that were significantly different. Enrichment analyses of the KEGG for the ingredients of HX in NAFLD were analyzed using ClueGO.

Herbal Plant Extract

The HX used in this study (Origin: Guangxi, China; Batch No.: 20170601; Quality standard: Chinese Pharmacopoeia 2015) was purchased from Fu Rui Bang Chinese Medicine Co., Ltd. (Daqing, China). Raw herbs were soaked in distilled water overnight, followed by decoction twice in boiling water (60 min each

time). The combined aqueous extract was filtered through gauze and then heated until evaporation (Gou et al., 2017). Low-speed centrifugation was used to remove insoluble particles, and the concentration of the HX residue was at 1 g/ml. The supernatant was sterilized by filtration through a 0.22-μm Millipore filter (Millex, GP) and stored at 4°C until use. The main components of HX were analyzed by high-performance liquid chromatography-electrospray ionization/mass spectrometry (HPLC-ESI/MS Qingdao Kechuang Quality Inspection Co., Ltd. Qingdao, China) (Application No. PDFD-16-01 D/0). All samples were extracted with 300 μl methanol and 10 μl of internal standard was added. Samples were then sonicated in an ice bath. Two-hundred μl supernatant was transferred to vials for LC-MS analysis. The data were extracted and preprocessed using compound discovery software (Thermo), and then normalized and edited into a two-dimensional data matrix using Excel 2010 software, including retention time (RT), compound molecular weight (COMP MW), observed value (sample), and peak strength (Cui et al., 2019c).

Animals and Treatment

Male ICR mice (20–22 g; 8 weeks) were obtained from Harbin Medical University (Daqing, China). The mice were housed in cages with a 12-h light/dark cycle in a temperature-controlled environment and were acclimatized to laboratory conditions for 1 week before the study. Subsequently, mice were randomly divided into five groups of six animals each: 1) a control (Con) group and 2) a NAFLD group fed a high-fat diet (HFD), 3) a low-dose group fed HFD +1.8 g/kg HX (HFD+1.8HX) given orally (0.1 ml per 10 g body weight), 4) a medium-dose group (HFD+4.5HX), and a high-dose group (HFD+9.0HX). The dosage of HX was chosen based on recommendations from the Chinese Pharmacopoeia (Chinese Pharmacopoeia Commission, 2015). According to the literature, HX does not cause any behavioral changes or mortality (Li CW. et al., 2013). The Con diet was prepared by following the AIN-93M formula with adjustments (Reeves et al., 1993, 93), and the HFD was formulated by modifying the AIN-93M diet according to Chen et al. (Chen et al., 2016) (**Supplementary Table S1**). HFD feeding was initiated at 8 weeks of age and continued for an additional 8 weeks, at which point the mice were fasted for 12 h euthanasia with ether. Blood was collected for serum biochemical analysis. The liver was quickly excised, entirely cleaned with ice-cold phosphate-buffered saline (PBS), weighed, and preserved in liquid nitrogen until use. The Ethics Committee approved all animal studies of Heilongjiang Bayi Agricultural University following the Chinese Guidelines for the Care and Use of Laboratory Animals.

Histological Examination

A portion of liver tissue was fixed with 4% paraformaldehyde and embedded in paraffin. Rehydration was performed in a decreasing ethanol series, followed by staining with hematoxylin and eosin (H&E) (Ohtani et al., 2007). Frozen sections were prepared and stained with Oil Red O to determine hepatic lipid accumulation. The most severe hepatic inflammation in the representative histology sections was photographed using a microscope. Cells were fixed with 4% paraformaldehyde and stained with freshly diluted Oil Red O solution. Representative photomicrographs were captured using a system incorporated into the microscope.

ELISA Assays

The tissues were placed in pre-cooled PBS and homogenized. Then the supernatant was recovered by centrifugation for analysis. The following substances were quantified by ELISA kits (Shanghai Lington Biotechnology Co., Ltd.). Liver injury was evaluated via concentrations of alanine aminotransferase (ALT) (Catalog No. BPE20168), aspartate aminotransferase (AST) (Catalog No. BPE20184); inflammation was assessed via concentrations of tumor necrosis factor-α (TNF-α) (Catalog No. BPE20220), interleukin-6 (IL-6) (Catalog No. BPE20012); oxidative stress was evaluated via malondialdehyde (MDA) (Catalog No. BPE20347), superoxide dismutase (SOD) (Catalog No. BPE20348); and lipid metabolism was determined via triglyceride (TG) (Catalog No. BPE20754), and total cholesterol (TC) (Catalog No. BPE20095). All assays were performed according to the manufacturers' instructions.

Cell Culture

Alpha mouse liver 12 (AML12) cells, a hepatocyte cell line from a mouse transgene for human transforming growth factor α, were kindly provided by the Stem Cell Bank, Chinese Academy of Sciences. The cells were cultured in the manufacturer's recommended medium which was DMEM/F-12 (Dulbecco's modified Eagle's medium/Nutrient Mixture F-12, Gibco, 12400-024) medium containing 10% fetal bovine serum (FBS, CLARK, FB25015), 1% streptomycin (100 μg/ml) and penicillin-streptomycin (100 U/ml) (Solarbio, P1400), 1% transferrin (Gibco, 41400-045), and 40 ng/ml dexamethasone (Sigma, D4902-25MG). Cells were incubated with fresh medium at 37°C in 95% air and 5% CO_2 and used in each experiment after 3 days.

Cell Viability Analysis

The compound 3-(4,5-dimethyl-2-thiazolyl)-2,5-diphenyl-2-H-tetrazolium bromide (MTT) (Solarbio, M8180) was used to analyze cell viability. Cells were treated with different concentrations of HX for 20 h, and then 10 μl MTT was added for another 4 h. The culture medium was then completely removed, and dimethyl sulfoxide (DMSO) was added, followed by measurement of absorbance using a microplate reader. All MTT assays were performed at least three times in each group. Subsequently, results of the MTT assay were used to select five different concentrations of HX to add to the cell culture media. Real-time cell growth curves were measured using a real-time label-free cell analysis system (ACEA Biosciences).

Cell Treatment

AML12 cells were seeded in 6-well plates. Hepatic steatosis *in vitro* was induced according to previously-established methods (Zhang et al., 2010). The AML12 cells were treated for 24 h with a mixture of free fatty acids (FFA) containing a 2:1 ratio of oleate (Sigma, O1383-5G) and palmitate (Sigma, P5585-10G), at a final FFA concentration of 1 mM. For the HX

supplementation experiment, herbal extracts were added to the aforementioned medium containing 1 mM FFA for 24 h at high (25 mg/ml), medium (12.5 mg/ml), and low (6.25 mg/ml) concentrations.

Protein Extraction and Western Blotting

Lysates of liver or AML12 cell samples containing protease inhibitors were prepared by adding frozen radioimmunoprecipitation assay (RIPA) buffer before determining the protein concentration with a bicinchoninic acid (BCA) kit (Beyotime, P0010). Protein samples (25 μg) were separated on 10% sodium dodecyl sulfate-polyacrylamide gel electrophoresis (SDS-PAGE) gels and then transferred onto polyvinylidene difluoride (PVDF) membranes. After blocking for 1 h in Tris-buffered saline (TBS) containing (0.1% Tween 20, pH 7.4 (TBST) with 5% nonfat milk, the membranes were incubated overnight with the indicated primary antibodies. After dilution with TBST (1:1,000 dilution), ACACA (Abcam, ab45174), FASN (CST, 3180S), SREBF1 (Novusbio, NB100-2215), NF-κB (CST, 6956S), p-NF-κB (CST, 3033S), IκBα (CST, 4814S), p-IκBα (CST, 2859S), IKKα (CST, 2682S), ATF6 (Abcam, ab203119), PERK (CST, 3192S), and IRE1 (Abcam, ab37073) monoclonal antibodies were used to detect the protein expression levels in the samples. Membranes were washed three times with TBST, followed by room temperature incubation for 30 min with horseradish peroxidase (HRP)-labeled goat anti-mouse or goat anti-rabbit (3:5,000; Beyotime, A0208, A0216) IgG secondary antibody in TBST plus 5% milk. The membranes were washed with PBS, developed using a HaiGene (M2301) detection kit, and then imaged with the AI600 imaging system. ImageJ software was used for protein quantitation.

Confocal Laser Fluorescence Imaging

Cells were plated on coverslips at a density of 0.5×10^5 cells per well, followed by treatment, and then fixed with 4% paraformaldehyde for 30 min (Kim et al., 2018). After incubation in blocking solution (3% bovine serum albumin (BSA), 5% goat serum, 0.5% Triton X-100 in PBS, pH 7.4) for 30 min, the cells were incubated overnight at 4°C with NF-κB (1: 800) antibody. They were then washed with PBS five times and incubated with fluorescein isothiocyanate (FITC)-conjugated goat anti-mouse IgG (E1216, Santa Cruz Biotechnology) for 1 h. Hoechst 33342 (C1026, Beyotime) was used for nuclear staining. Fluorescence images were observed and photographed using an immunofluorescence microscope (Leica Microsystems).

Flow Cytometry

An ROS Assay Kit (APPLYGEN, C1300) was used to measure ROS production according to the manufacturer's instructions. Results were then analyzed by fluorescent microscopy and a flow cytometer (BD Biosciences, USA) (Cui et al., 2019b).

Statistical Analysis

All analyses were performed using SPSS 22.0 (SPSS, Inc., Chicago, IL, USA) statistical software.

In vivo experiments, 6 mice were treated in each group, one-way ANOVA analyzed data, and multiple comparisons were employed, and results are expressed as the mean ± SEM (n = 6 per group). $p < 0.05$ was considered significant between any two groups by analysis of variance (ANOVA) followed by Tukey's post hoc test.

In vitro experiments, three concentrations of HX were added to cell culture, statistical analyses were performed using Student's t-test, and continuous data are presented as the mean with S.E.M. Multiple comparisons were performed using one-way analysis of variance (ANOVA) followed by Tukey's post hoc test. All tests were two-sided, and $p < 0.05$ was considered significant.

RESULTS

Composition of Compounds in HX

The chemical composition of HX (peak MS spectra) is reported in **Figure 1**. Feature extraction was performed on the data and preprocessed with XCMS in R software. Data were then normalized and edited into a two-dimensional data matrix in Excel 2010 software, including retention time (RT), mass-to-charge ratio (MZ), observations (samples), and peak intensity. Concentrations of identified substances are reported in **Supplementary Tables S2, S3**. Ninety-nine compounds were identified, with 33% of those classified as flavonoids. The full spectrum of constituents was identified based on the METLIN database (https://metlin.scripps.edu).

Active Ingredient Targets and Disease Targets

Evaluation of the Drugbank and TCMSP databases revealed 164 potential targets from 9 bioactive compounds. **Figure 2A** depicts 174 nodes (9 bioactive compounds and 164 potential targets) and 239 edges. The red triangles denote HX, the green hexagons denote bioactive compounds, the blue rectangles denote potential targets, and each edge indicates an interaction among them. Green nodes represent compounds, and the degree value determines the size of the nodes. The potential active compounds were 5-hydroxy-7,4′-dimethoxyflavanon, quercetin 7-O-β-D-glucoside, quercetin, diop, acanthoside B, phenanthrone, irisolidone, genkwanin, and 3,23-dihydroxy-12-oleanen-28-oic acid (**Supplementary Table S4**). After translation, 964 target genes of disease were retrieved from potential targets in the protein. Targets associated with NAFLD were identified in the DisGeNET databases.

Target Network Analysis

All active compound target proteins and disease-associated proteins were divided into two independent groups. The sets and their relationships were represented in a closed format with fixed positions, yielding a Venn diagram and 82 interacting proteins (**Figure 2B**). The Cytoscape plug-in generated protein-protein interaction (PPI) networks based on the STRING database and topological data analysis to obtain a PPI network of 82 essential targets in **Figure 3**. Through

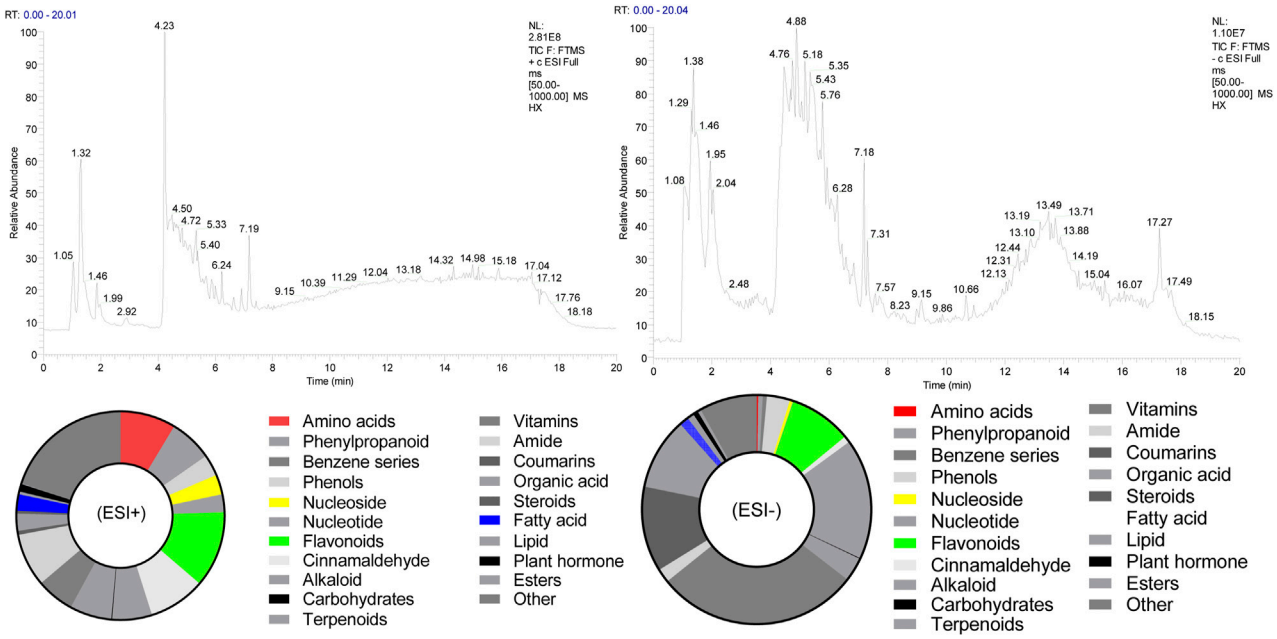

FIGURE 1 | Total ion chromatogram of HX. (ESI+) represents the positive ion detection mode, in which the mass analyzer scans only positively charged ions and filters out negatively charged ions. This allows us to obtain positively charged ion information during the detection process; (ESI-) denotes the negative ion detection mode, in which the mass analyzer scans only negatively charged ions and filters out positively charged ions, thus obtaining information regarding negatively charged ions.

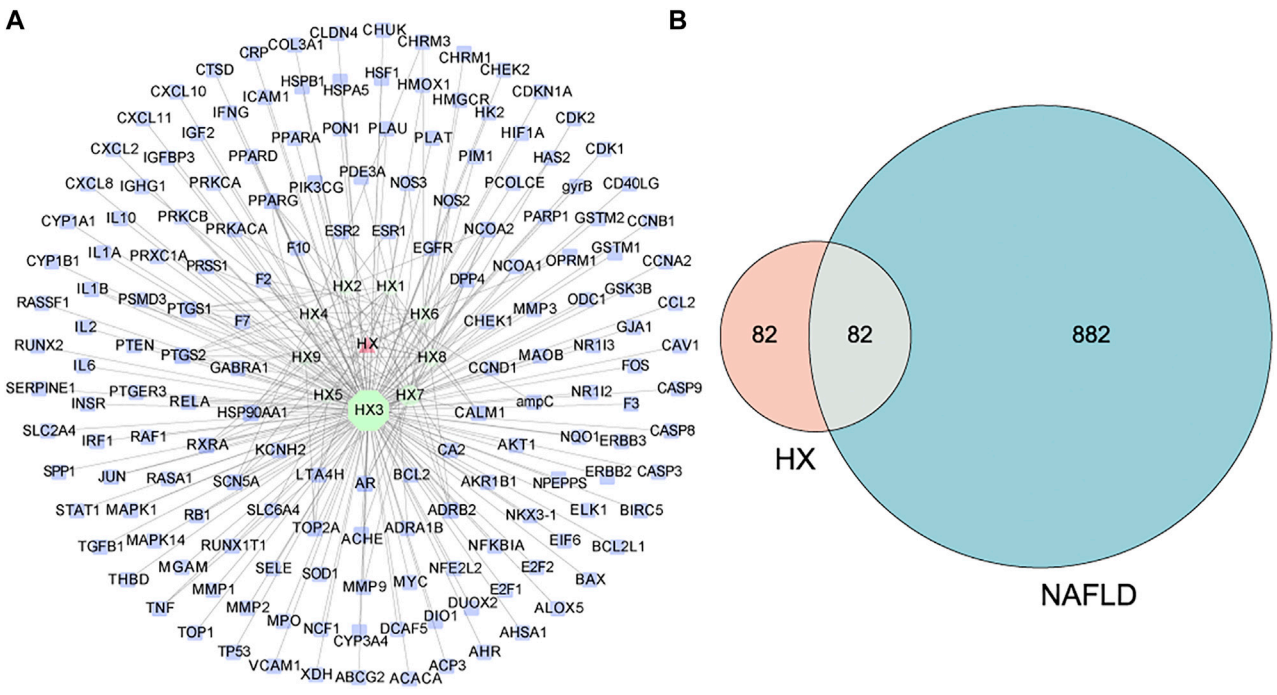

FIGURE 2 | Predicted effects of HX against NAFLD. **(A)** The compound target network of HX, which consists of 164 compound target nodes, 174 compound nodes, and 239 edges. The hexagons in green represent compounds, while the squares in blue denote potential targets. The node size of gene targets is proportional to the number of degrees. Lines represent the relationship between compounds and target nodes. **(B)** Venn diagram of active ingredient targets and disease proteins.

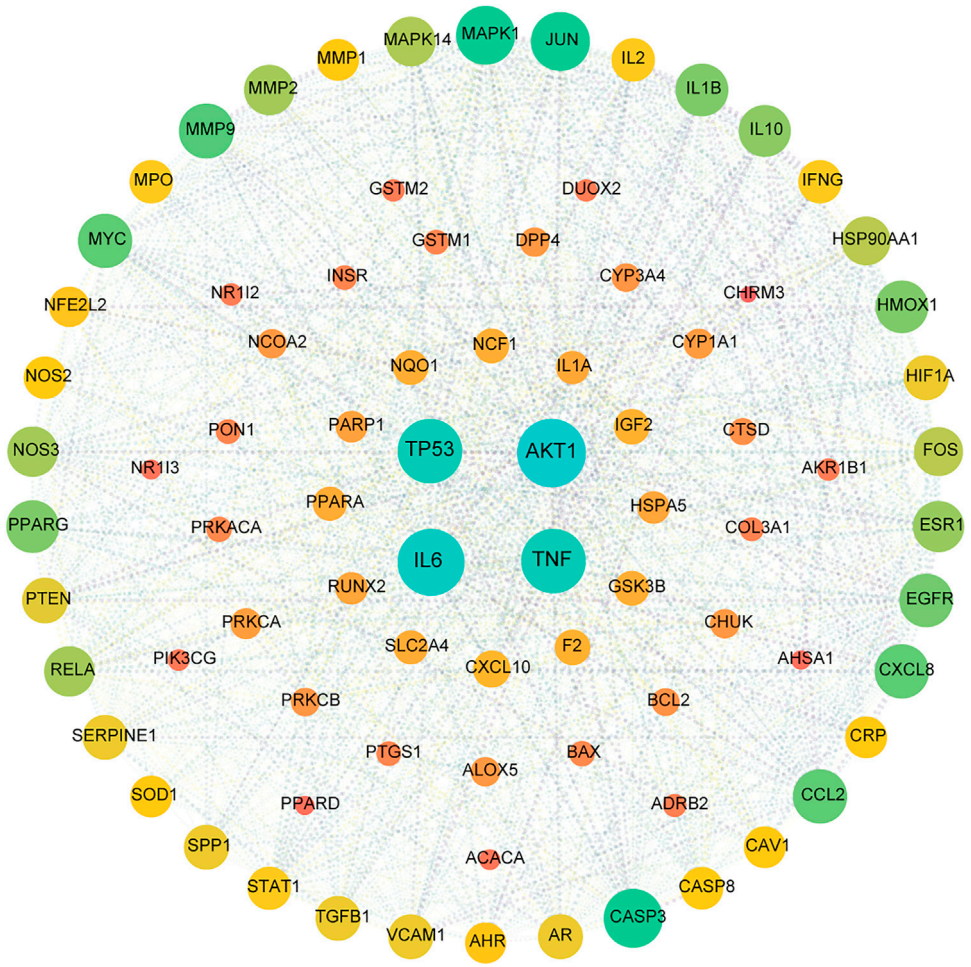

FIGURE 3 | PPI network for HX acting on NAFLD. This target network was composed of 82 nodes and 1,246 edges. A node represents one target, the degree value determines the node's size, and the edges represent protein–protein relationships. The 82 nodes represent therapeutic targets for HX acting on NAFLD, and the lines denote the relationship of 1,246 targets. The nodes (TP53, AKT1, IL6, and TNF) have higher degrees.

network prediction, it was revealed that *Tnf, Il6, Tp53, and Akt1* were essential target genes in the first few degrees.

Pathway Enrichment Analysis of HX Target Proteins

Eighty-two common targets were studied using GO and pathway enrichment analysis functions of the Metascape platform; an advanced bubble chart was generated with the top 20 results selected according to *p*-value ($p < 0.01$). The analysis included BP, CC, and MF (**Figures 4A–C**). BP analysis showed that HX acts mainly through cellular responses to chemical stress and lipopolysaccharide. The CC was mostly composed by vesicle lumen, perinuclear region of the cytoplasm, and transferase complex. Results of the MF analysis showed that HX exerted its function mainly through interactions with DNA-binding transcription factor binding, cytokine receptor binding, oxidoreductase activity, and antioxidant activity. On these basis, KEGG analyses were performed to elucidate potential targets in NAFLD of the components that make up HX. As shown in **Figure 4D**, HX mainly functioned in Fluid shear stress and atherosclerosis, Hepatocellular carcinoma, and Diabetic cardiomyopathy (ClueGo analysis). The common parts of the KEGG enrichment pathways were further extracted, and Lipid and atherosclerosis, Nonalcoholic fatty liver disease, TNF signaling pathway, and MAPK signaling pathway were the main common factors (**Supplementary Table S5**).

HX Alleviated Liver Lesions Induced by High-Fat Diet

To exclude the effect of HX on cell viability, tests were carried out 20 h after treatment of AML12 cells with different concentrations of HX. When cells were treated with 30, 60, and 90 mg/ml HX for 20 h, the inhibitory rate on cell viability was 110.1, 97.9, and 92.9%, respectively, and the IC_{50} value for AML12 cells was 199.3 mg/ml (**Supplementary Figure S1**). According to the experimental results, a concentration of HX was selected from

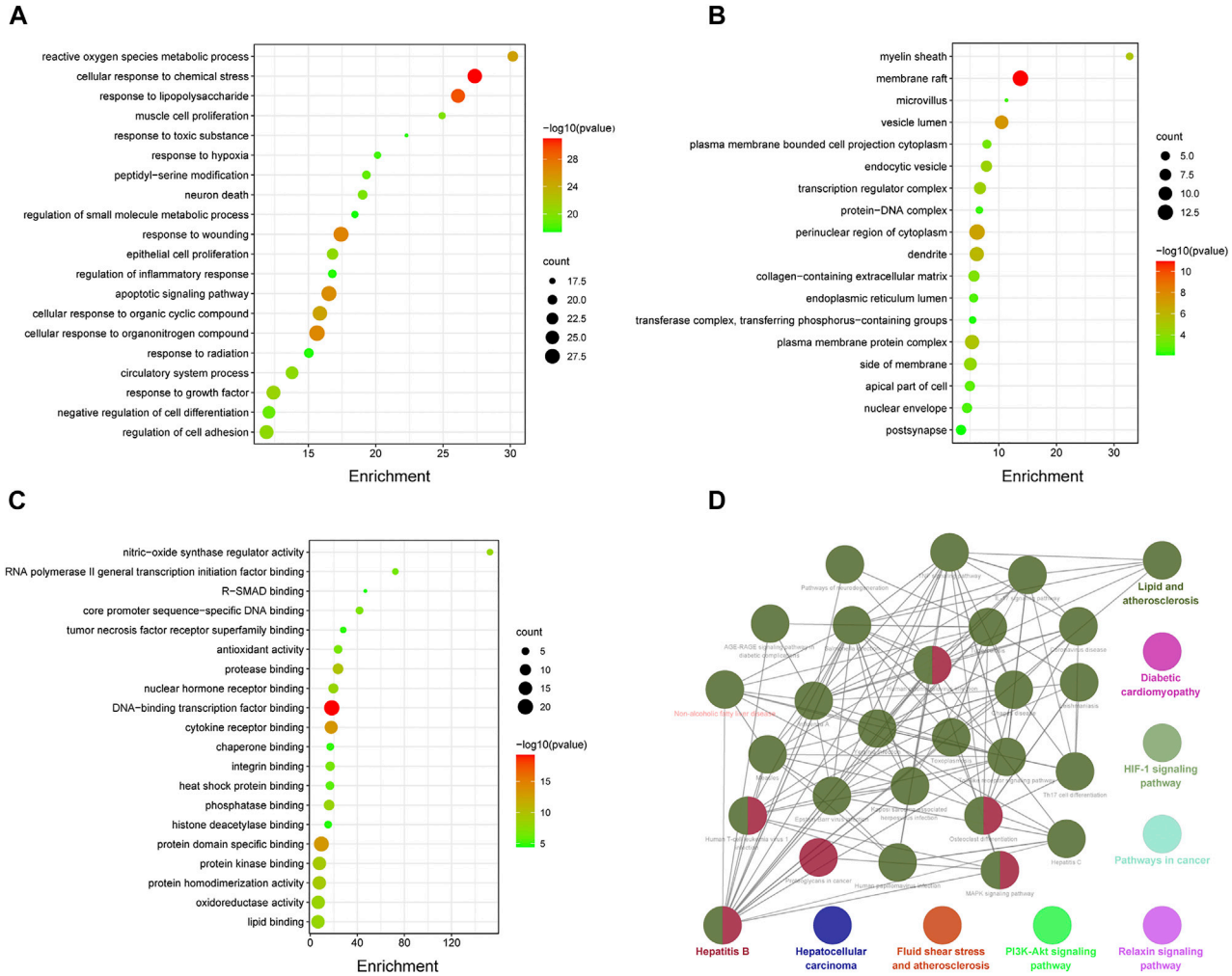

FIGURE 4 | Enrichment analysis of potential genes involved in the anti-NAFLD effects of HX. **(A)** Part of a GO functional analysis—biological process. **(B)** Part of a GO functional analysis—cellular components. **(C)** Part of a GO functional analysis—molecular functions. **(D)** Enriched KEGG pathways of potential targets of HX.

the cell experiments for use in the follow-up experiment because it would provide sufficient safety.

Compared with the Con group, the content of ALT and AST in the liver homogenate of the HFD group were significantly greater ($p < 0.01$). Compared with the HFD group, the amounts of ALT and AST in the HX groups were lower with increasing concentrations of HX in the diet (**Figure 5A**).

Hepatocytes were structurally intact in the Con group, with polygonal shape, clear borders, red cytoplasm, no vacuoles, centered nuclei, clear outlines of the hepatic lobules, and stable structure. The hepatic cords were radially arranged with the central vein as the axis. However, the HFD group exhibited diffuse vacuoles around the central vein and portal vein, unclear borders between cells in the visual field, and swollen or inflated hepatocytes. Numerous sub-circular vacuoles were visible inside the cells. The vacuoles squeezed the nuclei of hepatocytes to one side, compressed and narrowed the hepatic sinusoids, and the structures of hepatic sinusoids and hepatic cords were unclear.

Compared with the HFD group, there was greater normality in liver tissue from the HX groups in terms of sinuses, the structural arrangement of hepatic cords, the morphology of liver cells and fat globules, and balloon-like changes (**Figure 5B**).

Oil Red O staining of the liver tissue showed that the nuclei in the Con group were blue, there were no apparent orange lipid droplets, the space between liver cells was clear, and the structure of the liver sinuses was typical. In the HFD group, however, hepatocytes were enlarged, with diffused lipid droplets in the field of vision. In the HX groups, decreasing amounts of orange lipid droplets were evident, denoting decreased lipid accumulation (**Figure 5C**).

Oil Red O staining revealed many lipid droplets in the AML12 cells in the FFA group, and there were chain and mass changes in some of the fusions. In the low-, medium-, and high-dose HX groups, the number of orange lipid droplets in the hepatocytes decreased as the HX dose increased, and the degree of lipid accumulation was reduced, which was

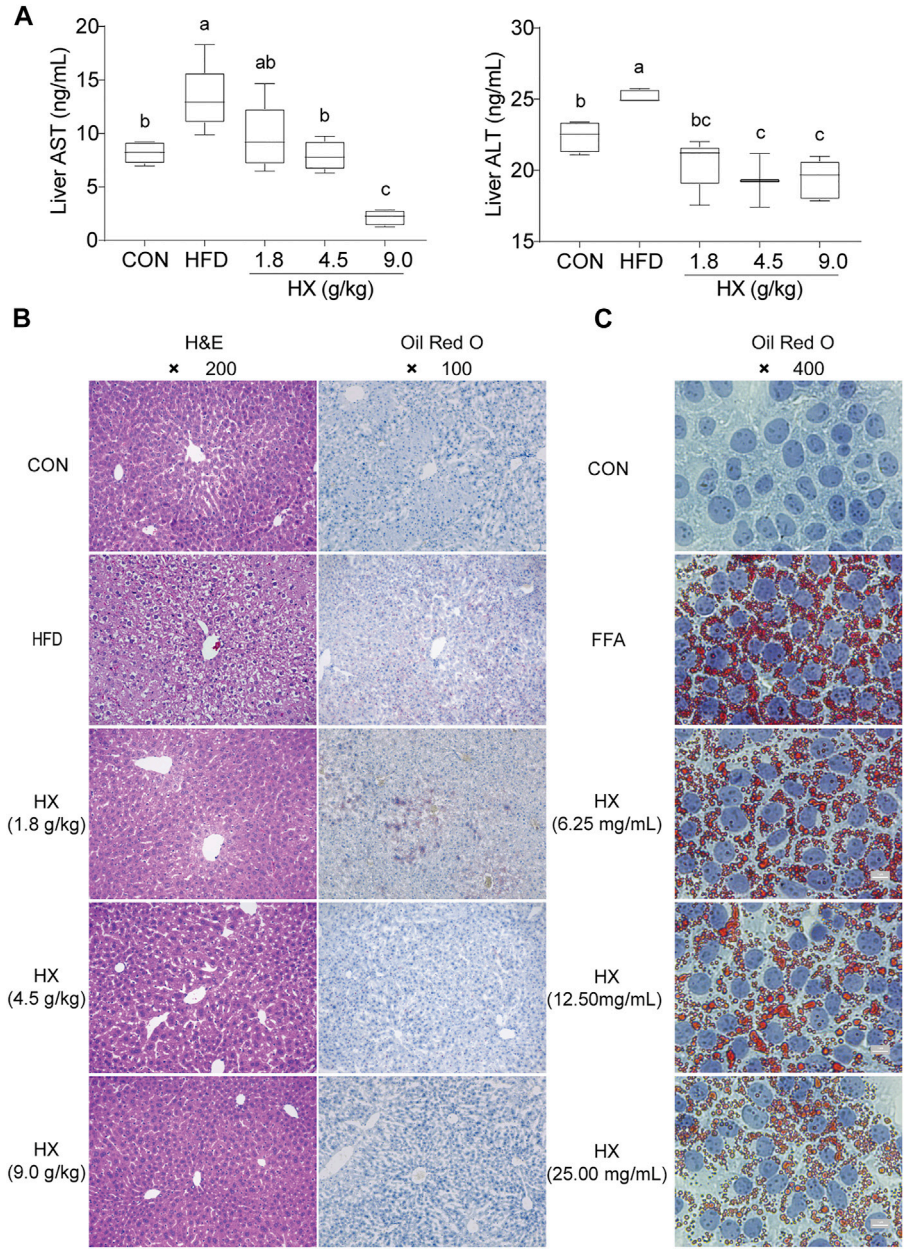

FIGURE 5 | (A) Concentrations of ALT and AST **(B)** H&E and Oil-Red-O staining in the liver tissue of mice after 8 weeks of HFD feeding, and **(C)** Oil-Red-O staining in AML12 cells incubated without or with FFA and different concentrations of HX (6.25, 12.50, and 25.00 mg/ml). A one-way ANOVA was used to analyze data, and multiple comparisons were employed, and the results are expressed as the mean ± SEM (n = 6 per group). Statistical analyses were performed using Student's t-test. Different lowercase letters a, b and c denote significant differences between any two groups ($p < 0.05$), but with the same lowercase letters, like bc and c, ab and a or b means no differences between the two groups ($p > 0.05$). ALT, alanine aminotransferase; AST, aspartate aminotransferase; CON, control; HFD, high-fat diet; FFA, free fatty acid; HX, Huo Xiang.

consistent with the changes observed in the liver tissue (**Figure 5C**).

HX Increased the Liver Antioxidant Capacity During Nonalcoholic Fatty Liver Disease Induced by High-Fat Diet

Compared with the Con group, the activity of SOD in the liver of the HFD group was significantly lower ($p < 0.01$), while the concentration of MDA was significantly greater ($p < 0.01$). Furthermore, HX significantly decreased the MDA level ($p < 0.01$) in a dose-dependent manner (**Figure 6A**). In AML12 cells, the amount of ROS in the FFA group was significantly greater ($p < 0.01$) compared with the Con group, while the amount of ROS in the HX groups was significantly lower ($p < 0.01$) compared with the Con group (**Figure 6B**).

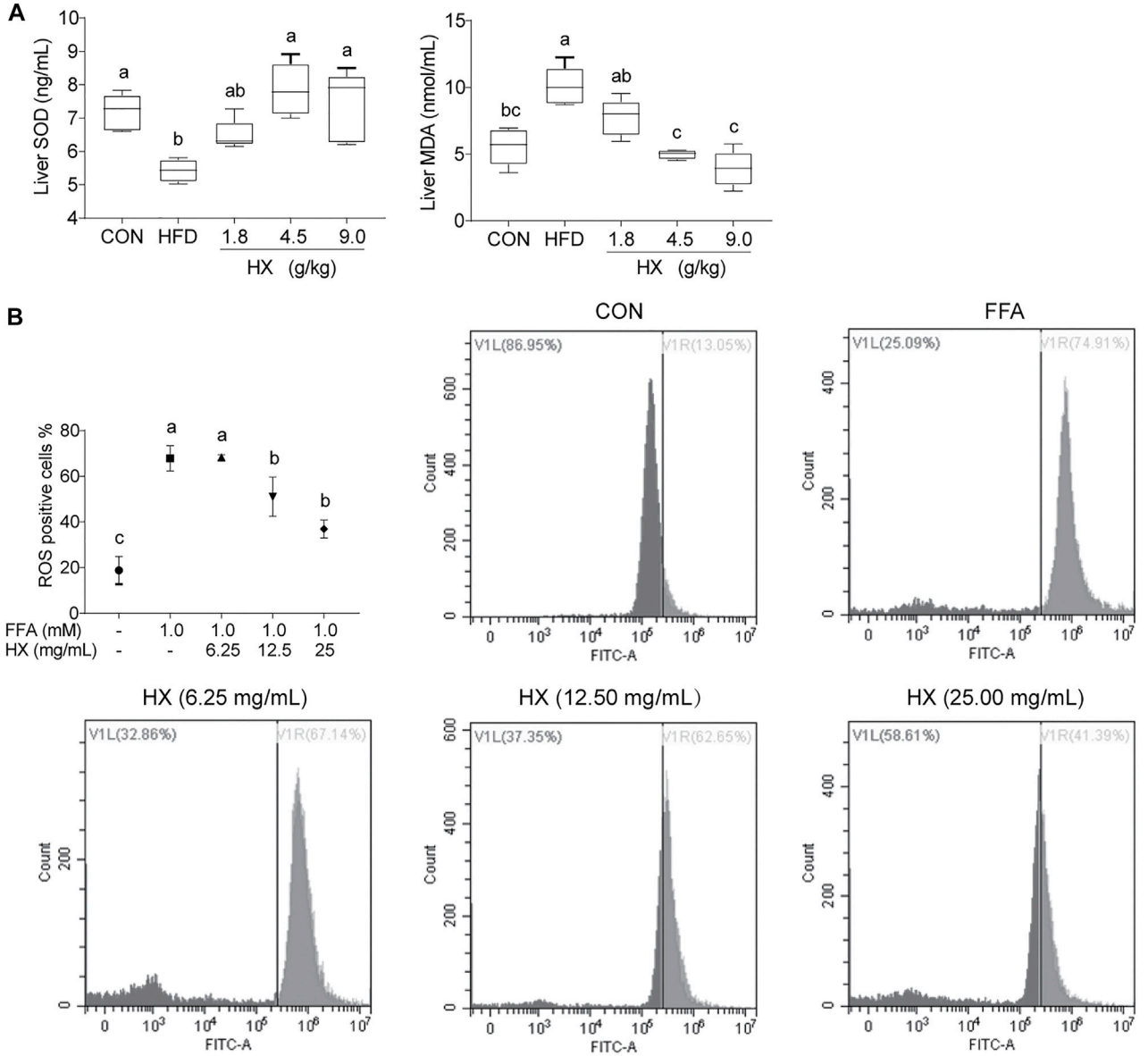

FIGURE 6 | (A) Concentrations of SOD and MDA in liver tissue of mice after 8 weeks of HFD feeding and **(B)** ROS percentage in AML12 cells incubated without or with FFA and different concentrations of HX (6.25, 12.50, and 25.00 mg/ml). "Count": cell counts; VL: Visible left of ROS negative percentage dye in cells; VR: Visible right of ROS positive percentage dye in cells. A one-way ANOVA was used to analyze the data for A, and multiple comparisons were employed, and the results are expressed as the mean ± SEM (n = 6 per group). Statistical analyses were performed using Student's t test. Different lowercase letters a, b and c denote significant differences between any two groups ($p < 0.05$), but with the same lowercase letters, like bc and c, ab and a or b means no differences between the two groups ($p > 0.05$). SOD, superoxide dismutase; MDA, malondialdehyde. CON, control; FFA, free fatty acid; HX, Huo Xiang.

HX Suppressed Inflammation in the Liver and AML12 Cells

Compared with the Con group, the levels of TNF-α and IL-6 (**Figure 7A**) and abundance of IKK, p-NF-κB/NF-κB, and p-IκB/IκB protein in the liver of the HFD group were significantly increased ($p < 0.01$), and were significantly lower ($p < 0.01$) in the 9.0 g/kg HX groups (**Figure 7B**). Furthermore, HX significantly decreased p-NF-κB/NF-κB and p-IκB/IκB abundance in the AML12 cells ($p < 0.01$) (**Figure 7C**). In AML12 cells, compared with the Con group, NF-κB protein was mainly distributed in the nucleus of the FFA group, while the abundance of NF-κB protein was more significant in the cytoplasm of the high-dose HX groups (**Figure 8**).

HX Reduced Fat Deposition During NAFLD Induced by a High-Fat Diet

Compared with the Con group, the amounts of TC and TG in the liver homogenate of the HFD group were significantly greater

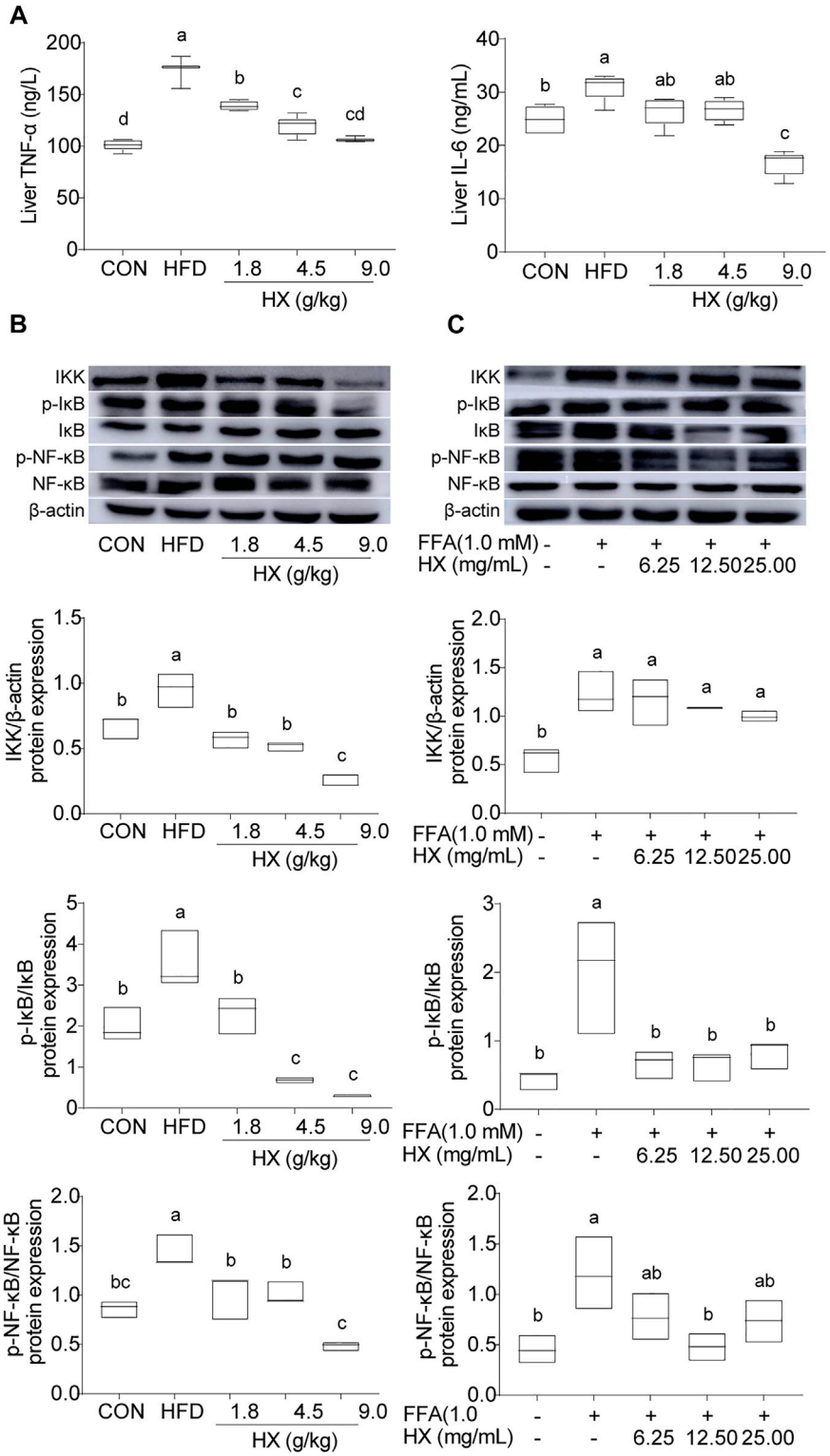

FIGURE 7 | (A) Concentrations of TNF-α and IL-6 and **(B)** components of the inflammatory pathway in the liver tissue of mice after 8 weeks of HFD feeding, **(C)** and in AML12 cells incubated without or with FFA and different concentrations of HX (6.25, 12.50, and 25.00 mg/ml). A one-way ANOVA was used, and multiple comparisons were employed, and the results are expressed as the mean ± SEM ($n = 6$ per group). Statistical analyses were performed using Student's *t* test. Different lowercase letters denote significant differences among groups ($p < 0.05$). TNF-α, tumor necrosis factor-α; IL-6, interleukin-6; IKK, inhibitor of κB kinase; NF-κB, nuclear factor-κB; IκB, inhibitor of NF-κB; p-IκB, phosphorylation inhibitor of NF-κB; p-NF-κB, phosphorylation nuclear factor-κB; CON, control; HFD, high-fat diet; HX, Huo Xiang.

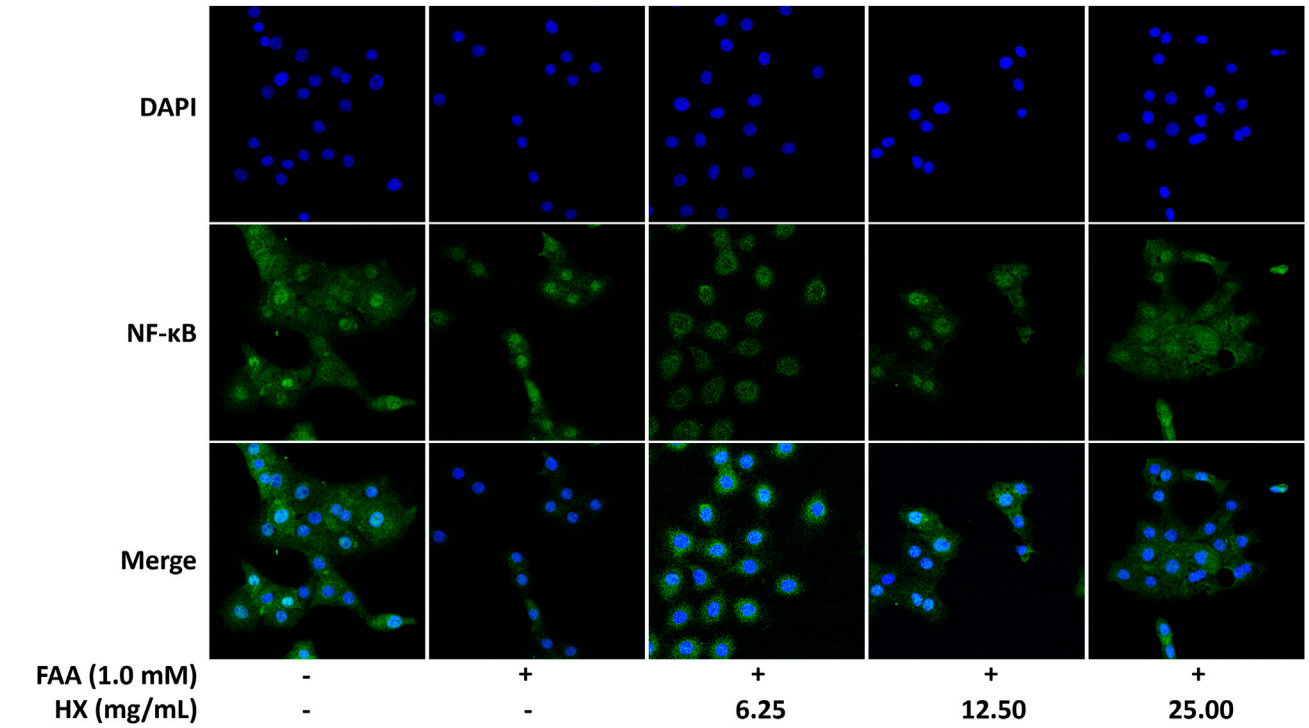

FIGURE 8 | Immunofluorescence images demonstrating nuclear staining **(DAPI, blue; top images)**, NF-κB droplet staining **(green; middle images)**, and an overlay of both **(merge, bottom images)** in AML12 cells incubated without or with FFA and different concentrations of HX (6.25, 12.50, and 25.00 mg/ml). FFA, free fatty acid; HX, Huo Xiang.

($p < 0.01$). Compared with that of the HFD group, the amounts of TC and TG in the liver homogenate of the HX groups were significantly lower ($p < 0.01$) (**Supplementary Figure S2A**). Compared with the Con group, the abundance of SREBF1, ACACA, and FASN was significantly upregulated in the HFD group. Compared with the HFD group, there was a significantly lower abundance of SREBF1, ACACA, and FASN in the HX groups (**Supplementary Figure S2B**). In addition, the protein abundance of SREBF1 and FASN decreased in a dose-dependent manner in the HX groups. Furthermore, the abundance trends of SREBF1, ACACA, and FASN in AML12 cells were consistent with those in liver tissue (**Supplementary Figure S2C**).

HX Alleviated Endoplasmic Reticulum Stress During Nonalcoholic Fatty Liver Disease Induced by a High-Fat Diet

Compared with the standard group, protein abundance of PERK, IRE1, and ATF6 in the livers of the HFD group was significantly increased ($p < 0.05$), although no difference was observed in the groups with different HX dosage ($p > 0.05$). In contrast, marked decreases in the abundance of PERK, IRE1, and ATF6 were observed in the HX groups compared with the HFD group ($p < 0.05$) (**Supplementary Figure S3A**). Compared with the Con cells, cells treated with FFA exhibited significantly greater amounts of PERK and IRE1 ($p < 0.05$). Compared with the FFA-treated cells, there was a considerably lowered abundance of PERK and IRE1 proteins ($p < 0.05$) in a dose-dependent manner in cells pretreated with HX (**Supplementary Figure S3B**).

DISCUSSION

Based on traditional studies following the "one drug for one target" concept, in 2007 Hopkins proposed the idea of network pharmacology (Hopkins, 2007), which is a comprehensive discipline integrating systems biology, information networks, computer science, and pharmacology. Specifically, a single drug regulates multiple proteins simultaneously, or multiple drugs act together on one protein to produce better therapeutic effects on diseases.

Network pharmacology has become a popular tool for research on the traditional Chinese medicines' pharmacological basis and mechanisms of action (TCM). This approach allows for modeling and studying biological systems using complex networks. It is widely used in the screening of active components in Chinese medicines, repositioning of drugs, exploration of the mechanism of compatibility of Chinese medicines, and explanation of the mechanism across multiple components, targets and pathways (Zheng et al., 2020; Zhou et al., 2021). According to literature reports, we predicted the relationship between the effective target of HX and NAFLD disease-related proteins through network pharmacology, which allowed us to speculate about the mechanism of HX action on

NAFLD. The effect of HX on NAFLD was further verified through *in vivo* and *in vitro* experiments.

In this study, we used network pharmacological tool and discovered that HX has the ability to regulate molecules. These molecules are targets for the treatment of NAFLD, and are found in the signaling pathway for NAFLD (Chyau et al., 2020). The main compounds contained in HX that are effective for the treatment of NAFLD are flavonoids. The results of the topological analysis showed that quercetin attained the most targets, and these components were highly correlated with the core targets predicted by NAFLD. Quercetin can reduce hepatic stellate cell activation and prevent hepatic fibrosis by inhibiting the TGF-β1/Smads signaling pathway, with activation of PI3K/Akt signaling inhibiting autophagy caused by liver fibrosis and reduce liver injury (Wu et al., 2017). PPI network topology analysis showed that the inflammation related key targets, TNF, and IL-6 were essential components for the effect of HX on NAFLD. Hepatic steatosis and inflammation pathogenesis accour through the secretion of cytokines such as TNF- α and IL-6 (Zhang et al., 2019), which are critical pro-inflammatory factors in the development of steatohepatitis (Jing et al., 2015, 3). Pathway and function enrichment analysis also showed that HX mainly regulates metabolism-related pathways. Hepatic accumulation of lipids is the hallmark of NAFLD and subsequently leads to cellular stress, inflammation, and hepatic injury, eventually resulting in chronic liver disease (Spahis et al., 2017; Dalekos et al., 2020). Abnormal lipid accumulation is associated with perturbed hepatocyte endoplasmic reticulum (ER) proteostasis in steatotic livers (Kitade et al., 2017).

In addition to flavonoids, the other main components of HX are terpenoids, ketones, alcohols, and aldehydes (Yamani et al., 2014). According to the mass value in the detected data, the entire spectrum identification was carried out based on the network database Metlin. The identified substances mainly included flavonoids, caffeic acid, ellagic acid, and other phenolic substances. Fatty acids such as stearic acid and palmitic acid, organic acids such as fumaric acid, and NADH, coenzyme Q, and other coenzymes were identified by the full spectrum. (see **Supplementary Tables S2, S3**). Pengran (Cao et al., 2017) and He Qin (Li HQ. et al., 2013) also analyzed the chemical composition of HX and reported that its main components acacetin and tilianin exhibited significant anticoagulant activity. However, it is well known that flavonoids elicit many pharmacological effects, including antioxidant, anti-inflammatory, analgesic, immunomodulatory, antiaging, hypolipidemic, and anti-tumor effects (Lei et al., 2019). Although the present study did not attempt to isolate a unique compound in HX, but instead used an extract of the whole plant, the results demonstrated that the mixture of compounds had the capability to reduce lipid accumulation, enhance antioxidant capacity, and reduce inflammation.

Oxidative stress is a critical factor of the "second hit" theory during NAFLD (Borrelli et al., 2018). Accumulation of lipid in hepatocytes leads to acceleration of mitochondrial β-oxidation capacity, which enhances the production of ROS that often exceeds the antioxidant capacity of the liver and causes oxidative stress (Hwang et al., 2020). Previous results showed that the activity of SOD in serum decreased and MDA significantly increased in patients with NAFLD. (Świderska et al., 2019). The antioxidant effect of HX is dose-dependent, leads to increased HO-1 protein and enzymatic activity, and protects cells from H_2O_2-induced cytotoxicity (Oh et al., 2006). This response also attenuates UVB-induced photoaging by upregulating antioxidant enzymes (Oh et al., 2016) and reducing ROS production (Shin et al., 2018). Our results showed that compared with the HFD group, the activity of SOD in the livers of the HX groups significantly increased, while activity of MDA and ROS in hepatocytes decreased. Thus, we speculate that HX directly decreases lipid peroxidation by increasing antioxidant enzymatic activity.

An increase in mitochondrial β-oxidation induced by feeding HFD can cause oxidative stress, and an increase in ROS production can activate the inflammatory pathway regulated by IKK/NF-κB (de Meneses Fujii et al., 2014). As an inflammatory signaling pathway component, NF-κB induces the transcription of numerous pro-inflammatory cytokines (TNF-α and IL-6) (Cortez et al., 2013, 6). In terms of anti-inflammatory effects, the essential oils in HX suppressed nitric oxide (NO) production by inhibiting NF-κB in lipopolysaccharide (LPS)-stimulated RAW264.7 cells (Lee et al., 2012, 3). Supplemental HX prevented NF-κB's activation and translocation to the nucleus (Hong et al., 2001; Oh et al., 2005). In the present study, feeding HX decreased the NF-κB-induced transcription of inflammatory cytokines in HFD-induced NAFLD and inhibited the protein abundance of IKK-NF-κB signaling pathway components. These results suggest that HX might inhibit activation of IKK/IKB/NF-κB signaling to interrupt the inflammatory cascade and thereby reduce the "second hit" of inflammatory factors on the liver.

Serum enzymology and blood lipids are stock indices used for the clinical diagnosis of NAFLD, but liver histology remains the "gold standard" (Castera et al., 2019). Our results showed that compared with the HFD group, there were decreased amounts of TC and TG and lipid accumulation in the hepatocytes of the HX groups. HFDs can lead to hyperlipidemia and disorders of liver lipid metabolism, including accumulation of TG and liver cell degeneration. According to the pathogenesis of HFD-induced NAFLD, many natural products can regulate hepatic lipogenesis and esterification of fatty acids into TG (Yh et al., 2020). SREBF1 is a crucial regulator of lipogenesis, and overactivation of this regulatory process is one characteristic of NAFLD (Khaleel et al., 2018). Hence, the downregulation of ACACA and FASN could prevent NAFLD (Cui et al., 2017). Recent studies have reported that ethanol extracts from HX conferred anti-adipogenicity effects in 3T3-L1 adipocytes (Park et al., 2016). Pogostone from HX reduced serum TNF-α and IL-6, increased IL-10, and increased the level of nonprotein sulfhydryl in gastric tissue to strengthen the inflammatory response (Chen et al., 2015). An anti-atherogenic effect was observed when HX was administered to low-density lipoprotein receptor$^{-/-}$ mice. Tilianin, a major component of HX, inhibits the TNF-α-induced expression of VCAM1 in cultured human umbilical vein endothelial cells (HUVECs) (Hong et al., 2001). Thus, our finding that HX decreased the abundance of SREBF1, ACACA, and FASN to modulate lipid accumulation and attenuate NAFLD induced by a HFD suggests a potent anti-lipogenic effect.

ER stress is a crucial feature of NAFLD (Ding et al., 2017). The ER is the central organelle where protein folding and post-

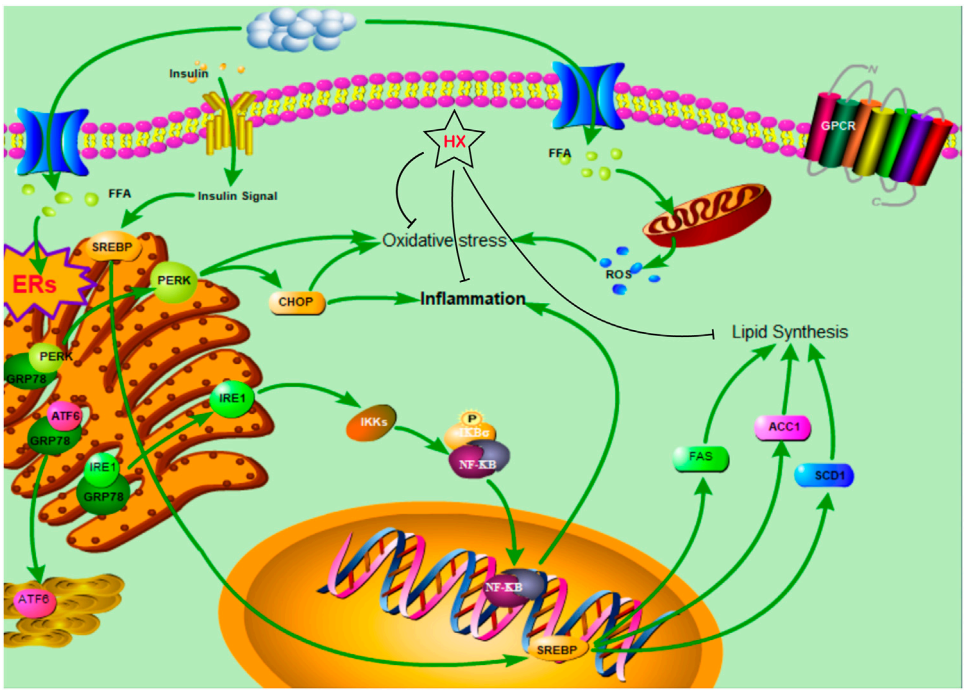

FIGURE 9 | The protective mechanism of a water extract of Huo Xiang (HX) on free fatty acid (FFA)-induced nonalcoholic fatty liver disease (NAFLD).

translational modifications of proteins occur, and it acts as a significant intracellular calcium reservoir in the cell. A HFD activates ER stress in the liver, with PERK, IRE1, and ATF6 also being involved in the development of NAFLD (Cao et al., 2012). The unfolded protein response acts as a complementary adaptive machinery against ER stress. Three ER transmembrane receptor proteins coordinate it: inositol-requiring kinase 1 (IRE1), double-stranded RNA-activated protein kinase (PKR)-like endoplasmic reticulum kinase (PERK), and activating transcription factor 6 (ATF6) (Wang et al., 2018). We observed that HX alleviated hepatic steatosis by decreasing ER stress-related protein expression *in vivo* and *in vitro*, which confirmed the results of Sandoval and Carrasco (Sandoval and Carrasco, 1997), who concluded that HX could successfully prevent ER stress.

HX treatment significantly reduced FFA-induced disruption of lipid metabolism, oxidative stress, and inflammatory responses in AML12 cells and inhibited lipid synthesis in the SREBF1/FASN/ACACA pathway, thereby ameliorating NAFLD symptoms and protecting the liver (**Figure 9**). These results are consistent with our predicted targets and signaling network analysis.

CONCLUSION

A preliminary prediction of the potential active compounds, core targets and possible mechanisms of HX action for the treatment of NAFLD were generated. The network pharmacological method provided new avenues for future development and research of HX in the context of health disorders. HX inhibits oxidative stress and inflammatory responses through various signaling pathways and reduces lipid metabolism disorders. Among the components in HX, quercetin may be particularly beneficial for treatment of NAFLD, which is a multifactorial and complex condition including lipid accumulation in hepatocytes. Further studies are needed to determine the regulatory role and mechanisms whereby HX elicits beneficial effects in animal models of NAFLD.

DATA AVAILABILITY STATEMENT

The datasets presented in this study can be found in online repositories. The names of the repository/repositories and accession number(s) can be found below: https://www.jianguoyun.com/p/DauG-wcQoOvyCRiZpJEE.

ETHICS STATEMENT

The animal study was reviewed and approved by the Ethics Committee approved all animal studies of Heilongjiang Bayi Agricultural University following the Chinese Guidelines for the Care and Use of Laboratory Animals.

AUTHOR CONTRIBUTIONS

YC and RC designed the experiment and performed sample preparation and data analysis. YC wrote the manuscript. QW

participated in method development and validation. AA, JL, and CX participated in study design and coordination and helped draft the manuscript. All authors read and approved the final manuscript.

FUNDING

This study was supported in part by the Provincial Institute Cooperation Project of Heilongjiang Science and Technology Plan (YS20B04); Talent Support Program of Heilongjiang Bayi Agricultural University (ZRCLG201904, ZRCQC201803), and the Postdoctoral scientific research developmental fund of Heilongjiang Province (LBH-Q20161).

SUPPLEMENTARY MATERIAL

The Supplementary Material for this article can be found online at: https://www.frontiersin.org/articles/10.3389/fphar.2021.789430/full#supplementary-material

REFERENCES

Borrelli, A., Bonelli, P., Tuccillo, F. M., Goldfine, I. D., Evans, J. L., Buonaguro, F. M., et al. (2018). Role of Gut Microbiota and Oxidative Stress in the Progression of Non-alcoholic Fatty Liver Disease to Hepatocarcinoma: Current and Innovative Therapeutic Approaches. *Redox Biol.* 15, 467–479. doi:10.1016/j.redox.2018.01.009

Buzzetti, E., Pinzani, M., and Tsochatzis, E. A. (2016). The Multiple-Hit Pathogenesis of Non-alcoholic Fatty Liver Disease (NAFLD). *Metabolism* 65, 1038–1048. doi:10.1016/j.metabol.2015.12.012

Cao, J., Dai, D. L., Yao, L., Yu, H. H., Ning, B., Zhang, Q., et al. (2012). Saturated Fatty Acid Induction of Endoplasmic Reticulum Stress and Apoptosis in Human Liver Cells via the PERK/ATF4/CHOP Signaling Pathway. *Mol. Cel. Biochem.* 364, 115–129. doi:10.1007/s11010-011-1211-9

Cao, P., Xie, P., Wang, X., Wang, J., Wei, J., and Kang, W. Y. (2017). Chemical Constituents and Coagulation Activity of Agastache Rugosa. *BMC Complement. Altern. Med.* 17, 93. doi:10.1186/s12906-017-1592-8

Castera, L., Friedrich-Rust, M., and Loomba, R. (2019). Noninvasive Assessment of Liver Disease in Patients with Nonalcoholic Fatty Liver Disease. *Gastroenterology* 156, 1264–e4. doi:10.1053/j.gastro.2018.12.036

Chen, H., Liao, H., Liu, Y., Zheng, Y., Wu, X., Su, Z., et al. (2015). Protective Effects of Pogostone from Pogostemonis Herba against Ethanol-Induced Gastric Ulcer in Rats. *Fitoterapia* 100, 110–117. doi:10.1016/j.fitote.2014.11.017

Chen, Y. J., Wallig, M. A., and Jeffery, E. H. (2016). Dietary Broccoli Lessens Development of Fatty Liver and Liver Cancer in Mice Given Diethylnitrosamine and Fed a Western or Control Diet. *J. Nutr.* 146, 542–550. doi:10.3945/jn.115.228148

Chinese Pharmacopoeia Commission (2015). *Pharmacopoeia of the People's Republic of China*. Beijing: The Medicine Science and Technology Press of China [S].

Cho, H. I., Hong, J. M., Choi, J. W., Choi, H. S., Hwan Kwak, J., Lee, D. U., et al. (2015). β-Caryophyllene Alleviates D-Galactosamine and Lipopolysaccharide-Induced Hepatic Injury through Suppression of the TLR4 and RAGE Signaling Pathways. *Eur. J. Pharmacol.* 764, 613–621. doi:10.1016/j.ejphar.2015.08.001

Chyau, C. C., Wang, H. F., Zhang, W. J., Chen, C. C., Huang, S. H., Chang, C. C., et al. (2020). Antrodan Alleviates High-Fat and High-Fructose Diet-Induced Fatty Liver Disease in C57BL/6 Mice Model via AMPK/Sirt1/SREBP-1c/PPARγ Pathway. *Int. J. Mol. Sci.* 21, 360. doi:10.3390/ijms21010360

Cortez, M., Carmo, L. S., Rogero, M. M., Borelli, P., and Fock, R. A. (2013). A High-Fat Diet Increases IL-1, IL-6, and TNF-α Production by Increasing NF-Kb and Attenuating PPAR-γ Expression in Bone Marrow Mesenchymal Stem Cells. *Inflammation* 36, 379–386. doi:10.1007/s10753-012-9557-z

Cui, B. W., Bai, T., Yang, Y., Zhang, Y., Jiang, M., Yang, H. X., et al. (2019a). Thymoquinone Attenuates Acetaminophen Overdose-Induced Acute Liver Injury and Inflammation via Regulation of JNK and AMPK Signaling Pathway. *Am. J. Chin. Med.* 47, 577–594. doi:10.1142/S0192415X19500307

Cui, C. X., Deng, J. N., Yan, L., Liu, Y. Y., Fan, J. Y., Mu, H. N., et al. (2017). Silibinin Capsules Improves High Fat Diet-Induced Nonalcoholic Fatty Liver Disease in Hamsters through Modifying Hepatic De Novo Lipogenesis and Fatty Acid Oxidation. *J. Ethnopharmacol.* 208, 24–35. doi:10.1016/j.jep.2017.06.030

Cui, Y., Chang, R., Zhang, T., Zhou, X., Wang, Q., Gao, H., et al. (2019b). Chinese Herbal Formula (CHF03) Attenuates Non-alcoholic Fatty Liver Disease (NAFLD) through Inhibiting Lipogenesis and Anti-oxidation Mechanisms. *Front. Pharmacol.* 10, 1190. doi:10.3389/fphar.2019.01190

Cui, Y., Wang, Q., Wang, M., Jia, J., and Wu, R. (2019c). Gardenia Decoction Prevent Intestinal Mucosal Injury by Inhibiting Pro-inflammatory Cytokines and NF-Kb Signaling. *Front. Pharmacol.* 10, 180. doi:10.3389/fphar.2019.00180

Dalekos, G. N., Gatselis, N. K., Zachou, K., and Koukoulis, G. K. (2020). NAFLD and Autoimmune Hepatitis: Do Not Judge a Book by its Cover. *Eur. J. Intern. Med.* 75, 1–9. doi:10.1016/j.ejim.2020.02.001

Danford, C. J., and Lai, M. (2019). NAFLD: a Multisystem Disease that Requires a Multidisciplinary Approach. *Frontline Gastroenterol.* 10, 328–329. doi:10.1136/flgastro-2019-101235

de Meneses Fujii, T. M., Jacob, P. S., Yamada, M., Borges, M. C., Norde, M. M., Pantaleão, L. C., et al. (2014). Yerba Mate (Ilex Paraguariensis) Modulates NF-kappaB Pathway and AKT Expression in the Liver of Rats Fed on a High-Fat Diet. *Int. J. Food Sci. Nutr.* 65, 967–976. doi:10.3109/09637486.2014.945153

Ding, S., Jiang, J., Zhang, G., Bu, Y., Zhang, G., and Zhao, X. (2017). Resveratrol and Caloric Restriction Prevent Hepatic Steatosis by Regulating SIRT1-Autophagy Pathway and Alleviating Endoplasmic Reticulum Stress in High-Fat Diet-Fed Rats. *PLoS One* 12, e0183541. doi:10.1371/journal.pone.0183541

Eslam, M., and George, J. (2019). Refining the Role of Epicardial Adipose Tissue in Non-alcoholic Fatty Liver Disease. *Hepatol. Int.* 13, 662–664. doi:10.1007/s12072-019-09990-z

Gou, X. J., Feng, Q., Fan, L. L., Zhu, J., and Hu, Y. Y. (2017). Serum and Liver Tissue Metabonomic Study on Fatty Liver in Rats Induced by High-Fat Diet and Intervention Effects of Traditional Chinese Medicine Qushi Huayu Decoction. *Evid. Based Complement. Alternat Med.* 2017, 6242697. doi:10.1155/2017/6242697

Hao, da. C., and Xiao, P. G. (2014). Network Pharmacology: a Rosetta Stone for Traditional Chinese Medicine. *Drug Dev. Res.* 75, 299–312. doi:10.1002/ddr.21214

Hong, J. J., Choi, J. H., Oh, S. R., Lee, H. K., Park, J. H., Lee, K. Y., et al. (2001). Inhibition of Cytokine-Induced Vascular Cell Adhesion Molecule-1 Expression; Possible Mechanism for Anti-atherogenic Effect of Agastache Rugosa. *FEBS Lett.* 495, 142–147. doi:10.1016/s0014-5793(01)02379-1

Hopkins, A. L. (2007). Network Pharmacology. *Nat. Biotechnol.* 25, 1110–1111. doi:10.1038/nbt1007-1110

Hwang, I., Uddin, M. J., Pak, E. S., Kang, H., Jin, E. J., Jo, S., et al. (2020). The Impaired Redox Balance in Peroxisomes of Catalase Knockout Mice Accelerates Nonalcoholic Fatty Liver Disease through Endoplasmic Reticulum Stress. *Free Radic. Biol. Med.* 148, 22–32. doi:10.1016/j.freeradbiomed.2019.12.025

Jing, Y., Liu, W., Cao, H., Zhang, D., Yao, X., Zhang, S., et al. (2015). Hepatic P38α Regulates Gluconeogenesis by Suppressing AMPK. *J. Hepatol.* 62, 1319–1327. doi:10.1016/j.jhep.2014.12.032

Khaleel, E. F., Abdel-Aleem, G. A., and Mostafa, D. G. (2018). Resveratrol Improves High-Fat Diet Induced Fatty Liver and Insulin Resistance by Concomitantly Inhibiting Proteolytic Cleavage of Sterol Regulatory Element-Binding Proteins, Free Fatty Acid Oxidation, and Intestinal Triglyceride Absorption. *Can. J. Physiol. Pharmacol.* 96, 145–157. doi:10.1139/cjpp-2017-0001

Kim, J. Y., Garcia-Carbonell, R., Yamachika, S., Zhao, P., Dhar, D., Loomba, R., et al. (2018). ER Stress Drives Lipogenesis and Steatohepatitis via Caspase-2 Activation of S1P. *Cell* 175, 133–e15. doi:10.1016/j.cell.2018.08.020

Kitade, H., Chen, G., Ni, Y., and Ota, T. (2017). Nonalcoholic Fatty Liver Disease and Insulin Resistance: New Insights and Potential New Treatments. *Nutrients* 9, 387. doi:10.3390/nu9040387

Lee, S. M., Park, K. H., Kim, S. S., Kwon, D. W., and Hong, S. C. (2012). Effect of the Mn Oxidation State and Lattice Oxygen in Mn-Based TiO2 Catalysts on the Low-Temperature Selective Catalytic Reduction of NO by NH3. *J. Air Waste Manag. Assoc.* 62, 1085–1092. doi:10.1080/10962247.2012.696532

Lei, Z., Sumner, B. W., Bhatia, A., Sarma, S. J., and Sumner, L. W. (2019). UHPLC-MS Analyses of Plant Flavonoids. *Curr. Protoc. Plant Biol.* 4, e20085. doi:10.1002/cppb.20085

Li, C. W., Wu, X. L., Zhao, X. N., Su, Z. Q., Chen, H. M., Wang, X. F., et al. (2013a). Anti-inflammatory Property of the Ethanol Extract of the Root and Rhizome of Pogostemon Cablin (Blanco) Benth. *ScientificWorldJournal* 2013, 434151. doi:10.1155/2013/434151

Li, H. Q., Liu, Q. Z., Liu, Z. L., Du, S. S., and Deng, Z. W. (2013b). Chemical Composition and Nematicidal Activity of Essential Oil of Agastache Rugosa against Meloidogyne incognita. *Molecules* 18, 4170–4180. doi:10.3390/molecules18044170

Li, J., Ding, L., Song, B., Xiao, X., Qi, M., Yang, Q., et al. (2016). Emodin Improves Lipid and Glucose Metabolism in High Fat Diet-Induced Obese Mice through Regulating SREBP Pathway. *Eur. J. Pharmacol.* 770, 99–109. doi:10.1016/j.ejphar.2015.11.045

Li, Y. C., Xian, Y. F., Ip, S. P., Su, Z. R., Su, J. Y., He, J. J., et al. (2011). Anti-inflammatory Activity of Patchouli Alcohol Isolated from Pogostemonis Herba in Animal Models. *Fitoterapia* 82, 1295–1301. doi:10.1016/j.fitote.2011.09.003

Lian, D. W., Xu, Y. F., Ren, W. K., Fu, L. J., Chen, F. J., Tang, L. Y., et al. (2018). Unraveling the Novel Protective Effect of Patchouli Alcohol against Helicobacter Pylori-Induced Gastritis: Insights into the Molecular Mechanism *In Vitro* and *In Vivo*. *Front. Pharmacol.* 9, 1347. doi:10.3389/fphar.2018.01347

Lu, X., Yang, L., Lu, C., Xu, Z., Qiu, H., Wu, J., et al. (2016). Molecular Role of EGFR-MAPK Pathway in Patchouli Alcohol-Induced Apoptosis and Cell Cycle Arrest on A549 CellsIn VitroandIn Vivo. *Biomed. Res. Int.* 2016, 1–12. doi:10.1155/2016/4567580

Luo, T. T., Lu, Y., Yan, S. K., Xiao, X., Rong, X. L., and Guo, J. (2020). Network Pharmacology in Research of Chinese Medicine Formula: Methodology, Application and Prospective. *Chin. J. Integr. Med.* 26, 72–80. doi:10.1007/s11655-019-3064-0

Oh, H. M., Kang, Y. J., Kim, S. H., Lee, Y. S., Park, M. K., Heo, J. M., et al. (2005). Agastache Rugosa Leaf Extract Inhibits the iNOS Expression in ROS 17/2.8 Cells Activated with TNF-Alpha and IL-1beta. *Arch. Pharm. Res.* 28, 305–310. doi:10.1007/BF02977797

Oh, H. M., Kang, Y. J., Lee, Y. S., Park, M. K., Kim, S. H., Kim, H. J., et al. (2006). Protein Kinase G-dependent Heme Oxygenase-1 Induction by Agastache Rugosa Leaf Extract Protects RAW264.7 Cells from Hydrogen Peroxide-Induced Injury. *J. Ethnopharmacol.* 103, 229–235. doi:10.1016/j.jep.2005.08.030

Oh, Y., Lim, H. W., Huang, Y. H., Kwon, H. S., Jin, C. D., Kim, K., et al. (2016). Attenuating Properties of Agastache Rugosa Leaf Extract against Ultraviolet-B-Induced Photoaging via Up-Regulating Glutathione and Superoxide Dismutase in a Human Keratinocyte Cell Line. *J. Photochem. Photobiol. B* 163, 170–176. doi:10.1016/j.jphotobiol.2016.08.026

Ohtani, N., Imamura, Y., Yamakoshi, K., Hirota, F., Nakayama, R., Kubo, Y., et al. (2007). Visualizing the Dynamics of p21(Waf1/Cip1) Cyclin-dependent Kinase Inhibitor Expression in Living Animals. *Proc. Natl. Acad. Sci. U. S. A.* 104, 15034–15039. doi:10.1073/pnas.0706949104

Park, M. J., Song, J. H., Shon, M. S., Kim, H. O., Kwon, O. J., Roh, S. S., et al. (2016). Anti-Adipogenic Effects of Ethanol Extracts Prepared from Selected Medicinal Herbs in 3T3-L1 Cells. *Prev. Nutr. Food Sci.* 21, 227–235. doi:10.3746/pnf.2016.21.3.227

Park, Y.-H., Lee, J.-J., Son, H.-K., Kim, B.-H., Byun, J., and Ha, J.-H. (2020). Antiobesity Effects of Extract from Spergularia marina Griseb in Adipocytes and High-Fat Diet-Induced Obese Rats. *Nutrients* 12, 336. doi:10.3390/nu12020336

Perumpail, B. J., Li, A. A., Iqbal, U., Sallam, S., Shah, N. D., Kwong, W., et al. (2018). Potential Therapeutic Benefits of Herbs and Supplements in Patients with NAFLD. *Diseases* 6, 80. doi:10.3390/diseases6030080

Piñero, J., Saüch, J., Sanz, F., and Furlong, L. I. (2021). The DisGeNET Cytoscape App: Exploring and Visualizing Disease Genomics Data. *Comput. Struct. Biotechnol. J.* 19, 2960–2967. doi:10.1016/j.csbj.2021.05.015

Reeves, P. G., Nielsen, F. H., and Fahey, G. C. (1993). AIN-93 Purified Diets for Laboratory Rodents: Final Report of the American Institute of Nutrition Ad Hoc Writing Committee on the Reformulation of the AIN-76A Rodent Diet. *J. Nutr.* 123, 1939–1951. doi:10.1093/jn/123.11.1939

Sandoval, I. V., and Carrasco, L. (1997). Poliovirus Infection and Expression of the Poliovirus Protein 2B Provoke the Disassembly of the Golgi Complex, the Organelle Target for the Antipoliovirus Drug Ro-090179. *J. Virol.* 71, 4679–4693. doi:10.1128/JVI.71.6.4679-4693.1997

Shin, D., Lee, Y., Huang, Y. H., Lim, H. W., Jang, K., Kim, D. D., et al. (2018). Probiotic Fermentation Augments the Skin Anti-photoaging Properties of Agastache Rugosa through Up-Regulating Antioxidant Components in UV-B-Irradiated HaCaT Keratinocytes. *BMC Complement. Altern. Med.* 18, 196. doi:10.1186/s12906-018-2194-9

Spahis, S., Delvin, E., Borys, J. M., and Levy, E. (2017). Oxidative Stress as a Critical Factor in Nonalcoholic Fatty Liver Disease Pathogenesis. *Antioxid. Redox Signal.* 26, 519–541. doi:10.1089/ars.2016.6776

Su, Z., Liao, J., Liu, Y., Liang, Y., Chen, H., Chen, X., et al. (2016). Protective Effects of Patchouli Alcohol Isolated from Pogostemon Cablin on Lipopolysaccharide-Induced Acute Lung Injury in Mice. *Exp. Ther. Med.* 11, 674–682. doi:10.3892/etm.2015.2918

Świderska, M., Maciejczyk, M., Zalewska, A., Pogorzelska, J., Flisiak, R., and Chabowski, A. (2019). Oxidative Stress Biomarkers in the Serum and Plasma of Patients with Non-alcoholic Fatty Liver Disease (NAFLD). Can Plasma AGE Be a Marker of NAFLD? Oxidative Stress Biomarkers in NAFLD Patients. *Free Radic. Res.* 53, 841–850. doi:10.1080/10715762.2019.1635691

Tuan, P. A., Park, W. T., Xu, H., Park, N. I., and Park, S. U. (2012). Accumulation of Tilianin and Rosmarinic Acid and Expression of Phenylpropanoid Biosynthetic Genes in Agastache Rugosa. *J. Agric. Food Chem.* 60, 5945–5951. doi:10.1021/jf300833m

Wang, L., Chen, J., Ning, C., Lei, D., and Ren, J. (2018). Endoplasmic Reticulum Stress Related Molecular Mechanisms in Nonalcoholic Fatty Liver Disease (NAFLD). *Curr. Drug Targets* 19, 1087–1094. doi:10.2174/1389450118666180516122517

Wei, L. L., Chen, Y., Yu, Q. Y., Wang, Y., and Liu, G. (2018). Patchouli Alcohol Protects against Ischemia/reperfusion-Induced Brain Injury via Inhibiting Neuroinflammation in normal and Obese Mice. *Brain Res.* 1682, 61–70. doi:10.1016/j.brainres.2017.12.039

Wu, L., Zhang, Q., Mo, W., Feng, J., Li, S., Li, J., et al. (2017). Quercetin Prevents Hepatic Fibrosis by Inhibiting Hepatic Stellate Cell Activation and Reducing Autophagy via the TGF-β1/Smads and PI3K/Akt Pathways. *Sci. Rep.* 7, 9289. doi:10.1038/s41598-017-09673-5

Xu, H. Y., Zhang, Y. Q., Liu, Z. M., Chen, T., Lv, C. Y., Tang, S. H., et al. (2019). ETCM: An Encyclopaedia of Traditional Chinese Medicine. *Nucleic Acids Res.* 41 (D1), D976–D982. doi:10.1093/nar/gky987

Yamani, H., Mantri, N., Morrison, P. D., and Pang, E. (2014). Analysis of the Volatile Organic Compounds from Leaves, Flower Spikes, and Nectar of Australian Grown Agastache Rugosa. *BMC Complement. Altern. Med.* 14, 495. doi:10.1186/1472-6882-14-495

Yan, T., Yan, N., Wang, P., Xia, Y., Hao, H., Wang, G., et al. (2020). Herbal Drug Discovery for the Treatment of Nonalcoholic Fatty Liver Disease. *Acta Pharm. Sin. B* 10, 3–18. doi:10.1016/j.apsb.2019.11.017

Zhang, X., Yang, J., Guo, Y., Ye, H., Yu, C., Xu, C., et al. (2010). Functional Proteomic Analysis of Nonalcoholic Fatty Liver Disease in Rat Models: Enoyl-Coenzyme a Hydratase Down-Regulation Exacerbates Hepatic Steatosis. *Hepatology* 51, 1190–1199. doi:10.1002/hep.23486

Zhang, X., Fan, L., Wu, J., Xu, H., Leung, W. Y., Fu, K., et al. (2019). Macrophage P38α Promotes Nutritional Steatohepatitis through M1 Polarization. *J. Hepatol.* 71, 163–174. doi:10.1016/j.jhep.2019.03.014

Zheng, S., Baak, J. P., Li, S., Xiao, W., Ren, H., Yang, H., et al. (2020). Network Pharmacology Analysis of the Therapeutic Mechanisms of the Traditional Chinese Herbal Formula Lian Hua Qing Wen in Corona Virus Disease 2019 (COVID-19), Gives Fundamental Support to the Clinical Use of LHQW. *Phytomedicine* 79, 153336. doi:10.1016/j.phymed.2020.153336

Zhou, Y., Wang, C., Kou, J., Wang, M., Rong, X., Pu, X., et al. (2021). Chrysanthemi Flos Extract Alleviated Acetaminophen-Induced Rat Liver Injury via Inhibiting Oxidative Stress and Apoptosis Based on Network Pharmacology Analysis. *Pharm. Biol.* 59, 1378–1387. doi:10.1080/13880209.2021.1986077

Conflict of Interest: The authors declare that the research was conducted in the absence of any commercial or financial relationships that could be construed as a potential conflict of interest.

Publisher's Note: All claims expressed in this article are solely those of the authors and do not necessarily represent those of their affiliated organizations, or those of the publisher, the editors and the reviewers. Any product that may be evaluated in this article, or claim that may be made by its manufacturer, is not guaranteed or endorsed by the publisher.

frontiers in Pharmacology

ORIGINAL RESEARCH
published: 04 February 2022
doi: 10.3389/fphar.2022.800986

Pentagalloyl Glucose, a Major Compound in Mango Seed Kernel, Exhibits Distinct Gastroprotective Effects in Indomethacin-Induced Gastropathy in Rats *via* Modulating the NO/eNOS/iNOS Signaling Pathway

Mona F. Mahmoud[1], Mohamed Nabil[2,3], Rehab A. Hasan[4], Assem M. El-Shazly[5], Mohamed A. El-Ansari[6] and Mansour Sobeh[7]**

[1]Department of Pharmacology and Toxicology, Faculty of Pharmacy, Zagazig University, Zagazig, Egypt, [2]Pharmaceutical and Fermentation Industries Development Center (PFIDC), City of Scientific Research and Technological Applications (SRTA-City), New Borg El-Arab, Alexandria, Egypt, [3]Pharmacology Department, Faculty of Pharmacy, Deraya University, New Mina, Egypt, [4]Department of Histology, Faculty of Medicine for Girls, Al Azhar University, Cairo, Egypt, [5]Department of Pharmacognosy, Faculty of Pharmacy, Zagazig University, Zagazig, Egypt, [6]Phytochemistry and Plant Systematics Department, National Research Centre, Cairo, Egypt, [7]AgroBioSciences, Mohammed VI Polytechnic University, Ben-Guerir, Morocco

Gastric ulcers are a common health disorder that affect up to 10% of the world's population. The gastroprotective potential of pentagalloyl glucose (PGG) against indomethacin-induced ulcer in rats and the possible underlying mechanisms were investigated. Gastric ulceration was induced by indomethacin (single dose, 60 mg/kg). Pretreatment with PGG (100 or 200 mg/kg, orally) for 8 days prior to the administration of indomethacin furnished significant reductions in gastric mucosal lesions as well as a significant increase in mucus concentration. Also, PGG significantly declined the elevations in gastric mucosal MDA, TNF-α, IL-6, PECAM-1, VEGF, and iNOS expression. It also mitigated the decrease in GSH and GPx and eNOS expression observed with indomethacin. The protective effects furnished by PGG were comparable to that of famotidine. The obtained results suggested that the anti-ulcer effects of PGG are mediated by increasing mucus production, scavenging free radicals, decreasing inflammation, and attenuating the NO/NOS signaling in favor of eNOS. To sum up, PGG could provide a potential therapy for gastric ulcer after evaluating its efficacy and effectiveness.

Keywords: indomethacin, pentagalloyl glucose, gastric ulcer, iNOS, eNOS, PECAM-1, VEGF

Abbreviations: eNOS: endothelial nitric oxide synthase; GPx: glutathione peroxidase; GRO: growth-regulated oncogene; GSH: reduced glutathione; IL-6: interleukin 6; iNOS: inducible nitric oxide synthase; MAPK1: mitogen-activated protein kinase 1; MDA: malondialdehyde; NMR: nuclear magnetic resonance; NSAIDs: non-steroidal anti-inflammatory drugs; PECAM-1: platelet endothelial cell adhesion molecule-1; PGG: pentagalloyl glucose; SDS-PAGE: sodium dodecyl sulfate-polyacrylamide gel electrophoresis; SOD: superoxide dismutase; TNF-α: tumor necrosis factor; VEGF: vascular endothelial growth factor.

OPEN ACCESS

Edited by:
Irwin Rose Alencar de Menezes, Regional University of Cariri, Brazil

Reviewed by:
Alaaeldin Ahmed Hamza, National Organization for Drug Control and Research (NODCAR), Egypt
Gomathi Rajkumar, Sri Sarada College for Women, India
Rajeev K. Singla, Sichuan University, China

***Correspondence:**
Mansour Sobeh
mansour.sobeh@um6p.ma
Mona F. Mahmoud
mona_pharmacology@yahoo.com;

Specialty section:
This article was submitted to Gastrointestinal and Hepatic Pharmacology, a section of the journal Frontiers in Pharmacology

Received: 24 October 2021
Accepted: 10 January 2022
Published: 04 February 2022

Citation:
Mahmoud MF, Nabil M, Hasan RA, El-Shazly AM, El-Ansari MA and Sobeh M (2022) Pentagalloyl Glucose, a Major Compound in Mango Seed Kernel, Exhibits Distinct Gastroprotective Effects in Indomethacin-Induced Gastropathy in Rats via Modulating the NO/eNOS/iNOS Signaling Pathway. Front. Pharmacol. 13:800986. doi: 10.3389/fphar.2022.800986

1 INTRODUCTION

Gastric ulcers, also known as peptic ulcers, are painful sores that develop in the stomach lining when the mucus layer is reduced or damaged. Gastric ulcer etiology includes several factors, such as excessive reactive oxygen/nitrogen species production, alcohol and spicy food intake, tobacco, radiation therapy, excessive use of NSAIDs, bile reflux, and *Helicobacter pylori* infection. The treatment of ulcer could be complicated because the pathology is multifactorial and includes antioxidant activity, inflammation, and angiogenesis, among others. Medications such as histamine H2-receptor antagonists and proton pump inhibitors are effectively used to treat gastric ulcers; however, they are associated with severe side effects. Therefore, there is a need to develop safe, natural, and multitarget agents (Ramakrishnan and Salinas, 2007; Lau et al., 2008; Mahmoud et al., 2021).

Medicinal plants that shape a major segment of flora have been used over centuries by mankind owing to their beneficial curing properties against diverse diseases and pathological conditions. These plants have been providing indigenous precursors and raw materials for medicine and drug industry all over the world. Natural polyphenols are the most abundant antioxidants present in a large number of foods of plant origin, such as fruits, vegetables, cereals, dry legumes, and beverages. Polyphenols exhibit a wide spectrum of biological activities and diverse chemical structures starting from simple phenolic compounds, such as phenolic acids and flavonoids, to oligomer tannins (Van Wyk and Wink, 2015; Ardalani et al., 2020). Mangiferin, a xanthonoid from *Mangifera indica* as well as from polyphenol-rich extract from leaf extracts of mango, exhibited gastroprotective activities highlighting the therapeutic activities of the plant (Carvalho et al., 2007; Severi et al., 2009).

The polyphenolic compound pentagalloyl glucose (PGG), found in numerous herbs, fruits, and by-products, among them mango seed kernel, is a potent antioxidant belongs to tannins. PGG demonstrated robust anti-inflammatory, antiviral, antimicrobial, antidiabetic, and antitumor activities (Patnaik et al., 2019). A recent study highlighted the ability of PGG to inhibit cell viability and cell growth in triple-negative breast cancer through the inhibition of MAPK1 and ƙBKE genes and the protein expression of MAPK and IƙBKE. PGG also reduced the expression of human proinflammatory cytokines GRO and GRO-α/CXCL1 (Mendonca et al., 2021). We previously isolated PGG (1,2,3,4,6-penta-*O*-*β*-D-galloyl glucose) from *Mangifera indica* L. seed kernels and comprehensively characterized its structure using mass spectrometry and NMR techniques and highlighted its promising larvicidal activities against the deadliest insect *Culex pipiens* (Emam et al., 2022). Furthermore, a recent study highlighted the potential antiviral activities of PGG against COVID-19 *via* blocking the fusion of SARS-CoV-2 spike-RBD to hACE2 receptors (Chen et al., 2021).

Herein, we investigated the protective effects of PGG on indomethacin-induced gastric ulcer in rats. We also explored a wide array of biochemical markers, including inflammatory cytokines, nitrosative stress, and oxidative stress. Additionally, we researched the interactions of PGG, through molecular docking, with two prostaglandin receptors, namely, EP3 and EP4 that are crucially involved in PGE2 gastroprotective action.

2 MATERIAL AND METHODS

2.1 Compound Isolation and Characterization

Mangifera indica L. seed kernels were crushed into small pieces and macerated with distilled water for 24 h and filtered, and the combined extract was reduced under pressure till dryness using Rotavapor® (Heizbad Hei-VAP, Heidolph, Germany). The combined extract was fractionated using ethyl acetate, and the obtained fraction was thoroughly cleaned using petroleum ether yielding gallotannin fraction. The latter was chromatographed over Sephadex LH-20 column (Pharmacia Co., Uppsala, Sweden) using methanol and prep-PC (Whatman 3 MM 46 × 57 cm) yielding PGG as a major compound. PGG identification was performed as previously described (Emam et al., 2022).

2.2 Animals

Male Wistar rats (200–250 g) had been purchased from the Faculty of Veterinary Medicine, Zagazig, Egypt. These rats were acclimatized to the animal house conditions (temperature of 25°C ± 2°C, with a light/dark cycle of 12 h/12 h) for 1 week before the study. Prior to administration of indomethacin, animals had free access to chow and tap water.

2.3 Experimental Design

The rats were randomly assigned into five groups (n = 6) as follows. Group 1 (control group) and group 2 received 2 ml/kg/day vehicle (5% Tween 80) for 8 days. Group 2 (ulcer group) was orally gavaged with a single dose of indomethacin (60 mg/kg, b.w.) (Nile Company for Pharmaceutical and Chemical Industries, Cairo, Egypt) 60 mg/kg after 24 h fasting (Slomiany and Slomiany, 2005). Groups 3–5 received 100 and 200 mg/kg of PGG (PGG 100, PGG 200), and 10 mg/kg famotidine (Amoun pharmaceutical company, Cairo, Egypt) suspended in 2 ml of 5% Tween 80, respectively, for 8 consecutive days followed by single oral dose of indomethacin (60 mg/kg, b.w.) at the eighth day. Six h after the last treatment, the rats were killed by decapitation. The stomachs were excised out of each rat, opened, and washed with normal saline for estimating ulcer indices. The stomachs were divided into two parts: one part was fixed in 10% neutral buffered formalin and coated in paraffin for the histological examinations and the other part was frozen in liquid nitrogen and kept at −80°C for biochemical measurements. The doses of PGG were chosen based on a previous study of Moharram et al. (2017). Famotidine dose was selected based on a previous study of Campos-Vidal et al. (2021).

2.4 Determination of Gastric Ulcer Index

The stomachs from different groups were opened along their greater curvature, cleaned with cold normal saline, blotted between two filter papers to dry them, and placed on a cardboard for gross examination of ulcers. Digital images of the stomachs were taken. The photomacrographs were

analyzed using ImageJ software (Wayne Rasband, MA, United States) to assess ulceration area according to Szabo and Hollander (Szabo and Hollander, 1989). The ulcer index was estimated using the following formula: ulcer index = [ulcerated area/total stomach area] × 100.

2.5 Determination of Gastric Mucosal Glycoproteins

For histochemical studies of gastric mucosal glycoprotein content, the tissues were stained with the Periodic acid–Schiff (PAS) technique with hematoxylin counterstaining (McManus, 1948; Al Batran et al., 2013). The slides were examined under a light microscope (Primo star, ZEISS, China). The photomicrographs were captured using a camera (Axiocam ERc 5s, ZEISS, China) at the Histology Department, Faculty of Medicine for Girls, Al Azhar University, Egypt.

2.6 Histological Examination of Gastric Lesions

For routine histological study, after proper fixation of the fundus of the stomach in 10% formaldehyde, it was dehydrated in an alcohol series of 100, 90, 70, and 50%, cleared in xylene, infiltrated, and embedded in paraffin and then sectioned (5 μm thick) using a rotary microtome (LEICA RM 2125, United Kingdom). They were further deparaffinized, stained with hematoxylin and eosin (H&E), and examined under a light microscope (Primo star, ZEISS, China) and photographed using a camera (Axiocam ERc 5s, ZEISS, China) (Bancroft and Gamble, 2008). The results were graded based on a scoring system (Sidahmed et al., 2019) as follows: epithelial cell loss (score 0–3), edema in submucosa (score: 0–4), hemorrhagic damage (score: 0–4), and the presence of inflammatory cells (score: 0–3). This scoring was performed using a light microscope (Primo star, ZEISS, China).

2.7 Immunohistochemical Studies

The stomach sections were processed and immune-stained using the peroxidase-labeled streptavidin–biotin method for iNOS and eNOS. The primary antibodies used in the present study were as follows: iNOS polyclonal antibodies (diluted 1:100; Abcam, Cat: ab15323, Cambridge, United Kingdom) and eNOS polyclonal antibodies (diluted 1:100; Abcam, Cat: ab5589, Cambridge, United Kingdom) (Wang et al., 2005). The secondary antibody used was anti-rabbit immunoglobulin (Ig, Santa Cruz Inc., Santa Cruz, CA, United States) conjugated with biotin. The positive slide was provided by the manufacturer. Negative control sections were prepared with omission of the primary antibody.

2.8 Morphometric Study

Morphometric study was performed using a Leica light microscope MDLSD coupled to a Leica digital camera transferred to the screen using a computerized image analyzer Leica Q500 MC program (Leica Microsystems Ltd., Cambridge, United Kingdom). The data were calibrated automatically to convert the measurement units (pixels) produced by the image analyzer program into actual micrometer units. Ten different non-overlapping randomly selected fields from a slide of each rat in all different experimental groups were examined to evaluate the following mean area percentage of PAS-positive histochemical reaction in PAS-stained sections at a magnification of 200; optical density of positive immunostaining for iNOS and eNOS was measured within and around the ulcer area at a magnification of 200 (Mahmoud et al., 2021).

2.9 Determination of Gastric Oxidative Stress

Gastric lipid peroxidation product, MDA, Gpx activity, and GSH were determined as reported previously (Mahmoud et al., 2021).

2.10 Determination of Gastric Inflammation

The levels of IL-6 and TNF-α in the gastric tissue lysate were determined using Sigma-Aldrich ELISA kits (Catalog numbers RAB0480 and RAB0311, respectively) according to the manufacturer's instructions.

2.11 Western Blot Analysis

The stomach tissues were dissected and crushed in ice-cold Nonidet-P40 (NP40) buffer with the addition of 1% protease inhibitor cocktail (Boster Biological Technology, Pleasanton, CA, United States, Catalog number: AR1182). The supernatants were recovered after centrifuging the samples. The Bradford technique was used to determine protein content. Ten percent SDS-PAGE was used to separate tissue proteins, which were then transferred to nitrocellulose membranes using the Trans-Blot® semi-dry transfer cell (Bio- Rad, Hercules, CA, United States) at 20 v for 15 min. After blocking with 1 × Tris-buffered saline/0.1% Tween 20 (TBST) with 5% non-fat dry milk for 1 h, rabbit polyclonal antibodies against VEGF (Catalog no: CAB12303; Assay genie, Dublin, Ireland; dilution, 1:500); primary rabbit polyclonal antibodies against PECAM-1 (Catalog no: PA5-96055; Invitrogen, Thermo Fisher Scientific corporation, Massachusetts, United States; dilution, 1:1,000); and primary rabbit monoclonal antibodies against β-actin (Catalog no: M01263; Boster Biological Technology, Pleasanton, CA, United States; diluted at 1:1,000) were all identified by the antibodies used (Sigma-Aldrich, United States). The membranes were subjected to goat anti-rabbit secondary antibodies (Catalog no: 5,220–0,308; SeraCare Life Sciences Inc., Massachusetts, United States; dilution, 1:3,000) for 2 h after being washed with 1 × TBST. Densitometrical analysis of protein bands was operated using Image Studio Lite software (LI-COR Biosciences, Nebraska, United States), and the protein expression was detected in consideration to its β-actin normalization.

2.12 Statistical Analysis

The data are presented as a mean standard error of the mean (S.E.M.). Student's t-test and one-way ANOVA were used to perform statistical comparisons, which were then followed by Tukey's multiple comparisons test. The severity scores of gastric

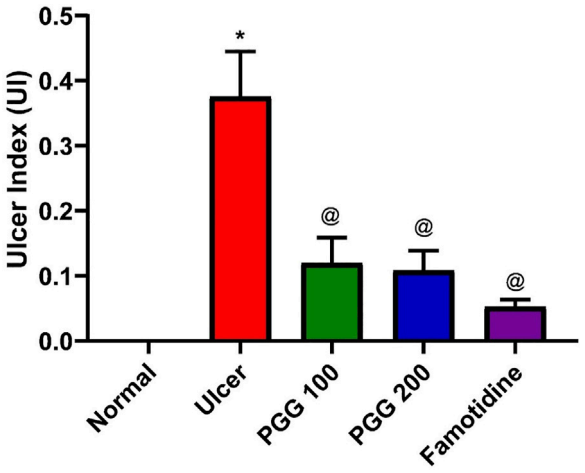

FIGURE 1 | Effect of pentagalloyl glucose (PGG) and famotidine on the ulcer index in indomethacin-induced ulcer in rats. Values are means of six rats ± S.E.M; as compared with normal (*) and indomethacin-treated (@) groups (one-way ANOVA followed by Tukey's multiple comparison tests), $p < 0.05$.

injuries among different groups were performed by one-way analysis of variance (ANOVA), followed by Dunnett's test. To illustrate statistical significance, a p value less than 0.05 was used. GraphPad Prism, version 8, was used to perform statistical calculations (GraphPad software Inc., La Jolla, CA, United States).

3 RESULTS AND DISCUSSION

3.1 Effect of PGG on Indomethacin-Induced Ulcer Index

Peptic ulcer is a debilitating global health problem. It develops when the usual balance between the aggressive factors (acid and pepsin) and the defensive processes, such as mucus production, bicarbonate, mucosal turnover, and blood flow (mucosal barrier), is disrupted (Piper and Stiel, 1986). When compared to other NSAIDs, indomethacin is a potent NSAID widely used in clinical practice. Because it has a higher ulcerogenic potency than other NSAIDs, it is commonly utilized for the induction of gastric ulcer in experimental animals (Suleyman et al., 2010). Similar to previous studies, the current study also found that indomethacin induced gastric ulceration and mucosal damage as it increased the ulcer index (Mahmoud et al., 2021; Ahmed et al., 2021; Nabil et al., 2021). PGG inhibited the indomethacin-induced gastric injury as presented by low values of ulcer index, and the effect of PGG was comparable to that shown by famotidine (**Figure 1**). This study confirmed the previous study findings that PGG and famotidine suppressed gastric ulceration induced by aspirin in rats by increasing PGE2 expression, antioxidant, anti-inflammatory, and antisecretory effects (Moharram et al., 2017).

3.2 Effect of PGG on Gastric Mucosal Glycoprotein Content

Mucous secretion is thought to be an important protective mechanism for the stomach mucosa against lesions (Mahmoud et al., 2021). One of the most important mechanisms of local stomach mucosal protection is mucus formation. To investigate the mechanism of the anti-ulcer effect of PGG, gastric mucosal glycoproteins, an indicator of gastric mucous secretion, was detected using PAS staining. Both control or famotidine-treated groups showed strong PAS positive reaction on the mucosal surface down to the pits, isthmus, neck, and body regions of the gastric glands, indicating normal glycoprotein content of the gastric mucosa (**Figures 2A,E**). Indomethacin caused depletion of gastric mucosal glycoprotein content where complete loss of PAS reaction at the ulcerated region was observed, but some positive reaction in the remaining part of the gastric glands can be noticed (**Figure 2B**). PGG at both dose levels restored glycoprotein content of the gastric mucosa where both groups showed strong PAS positive reaction on the mucosal surface down to the pits, isthmus, neck, and body regions of the gastric glands (**Figures 2C,D**).

The increased mucin content by PGG is crucial for cytoprotective and ulcer healing effect of PGG. It was reported that indomethacin-induced delay in the healing of chronic gastric ulcers is reversed by 11-deoxy-PGE1 (EP3/EP4 agonist) (Hatazawa et al., 2007). Therefore, we virtually explored the interaction of PGG with two prostaglandin receptors, EP3 (PDB id: 6AK3) and EP4 (PDB id: 5YWY), following the procedure adopted for the molecular docking in our previous study (Mahmoud et al., 2021). PGG displayed low binding energy compared to the reference drug famotidine when docked into the active side of EP3 and EP4. It showed four crucial interactions with Met 137, Me58, Arg 333, and Phe 209 for EP3, while furnishing a special H-bonding interaction with Thr 168 in the case of EP4 along with four other interactions, **Table 1** and **Figure 3**. Restoration of mucin content of gastric mucosa by PGG may be mediated by increasing PGE2 synthesis or activation of prostaglandin receptors, EP3 and EP4, as indicated by docking studies. Similar results were observed from other tannins, such as tellimagrandin II (score functions (kcal/mol) are -31.31 and -26.88 for EP3 and EP4, respectively) and casuarinin (score functions (kcal/mol) are −25.47 and −25.96 for EP3 and EP4, respectively) (Mahmoud et al., 2021).

3.3 Effect of PGG on Gastric Histological Changes

To reveal whether PGG was able to reverse indomethacin-induced gastric structural alteration, a histopathological study was performed. This study showed that both normal control and indomethacin group pretreated with famotidine demonstrated normal histology of gastric tissue with gastric mucosa containing closely packed fundic glands that open in the luminal surface by gastric pits. These fundic glands occupy the whole thickness of the fundic mucosa extending from the gastric pits. Each gland is formed of the isthmus, neck, body, and base. The upper part of

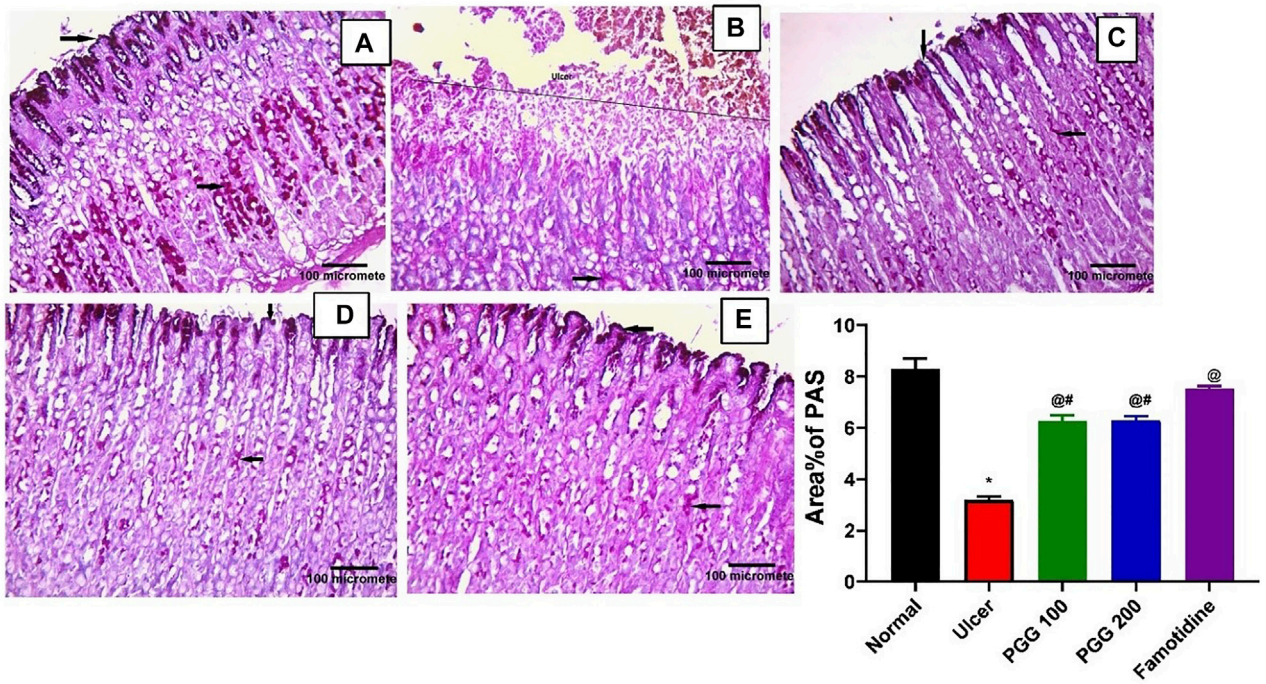

FIGURE 2 | Pentagalloyl glucose (PGG) effects on the gastric glycoprotein content of the gastric mucosa of ulcerative rats. Photomicrographs of gastric sections stained by Periodic acid–Schiff stain (PAS) collected from **(A)** normal control group, **(B)** ulcerative animals (indomethacin group, 60 mg/kg), **(C,D)** indomethacin + PGG-treated groups (100 mg/kg, and 200 mg/kg, respectively), and **(E)** indomethacin + famotidine-treated group (10 mg/kg). [PAS × 200]. The bar graph showed quantitative analysis of area percentage of PAS staining. Results are expressed as mean ± SEM, $n = 10$. $^{*, @, \#}$significantly different compared to the control group and indomethacin and famotidine groups, respectively at $p < 0.05$ by one-way ANOVA followed by Tukey's post hoc test.

TABLE 1 | Scoring functions (kcal/mol) and amino acid interactions for PGG and famotidine docked to two receptors (EP4 and EP3).

Compound	EP4		EP3	
	Score	Interactions	Score	Interactions
PGG	–25.34	Thr 168 (H bonding) Ser 319 (H bonding) Ser 95 (H bonding) ARG 316 (H bonding) Thr 76 (H bonding)	–28.42	Met 137 (H bonding) Asp 99 (H bonding) Met 58 (H bonding) Phe 140 (H bonding) Met 137 (H bonding) Arg 333 (H bonding) Phe 209 (H-pi and H bonding)
Famotidine	–11.35	Cys 170 (H bonding) Arg 316 (H bonding) Ser 95 (H bonding) Val 72 (H bonding)	–14.05	Met 137 (H bonding) Tyr 114 (H bonding) Phe 140 (H-pi)

the fundic glands is lined with surface columnar epithelial cells with basal oval nuclei. Mucous neck cells have flat basal nuclei. Pyramidal oxyntic cells have central rounded nuclei and deep acidophilic cytoplasm. Peptic cells have basal oval nuclei and basophilic cytoplasm (**Figures 4A,E**). The indomethacin only–treated group showed a large mucosal ulcer affecting the upper half of the fundic glands. Tissue erosion and degeneration can be seen; the fundic glands lose their orientation and arrangement. Exfoliated cells appear in the lumen. Extravasated blood can be seen within the fundic glands. Some fundic gland cells appear. Inflammatory cellular infiltration was also observed (Total score: 8.50 ± 0.85) (**Figure 4B**). Indomethacin groups treated with 100 mg/kg or 200 mg/kg PGG showed dose-dependent, marked improvement of gastric mucosa with no ulcer. Some vacuolations and congested blood vessels may be seen (Total score: 2.67 ± 0.67 and 1.50 ± 0.56 respectively) (**Figures 4C,D**). These findings are in accordance with those of a previous study that showed that PGG at 100 and 200 mg mitigated aspirin-induced gastric histological changes in rats (Moharram et al., 2017).

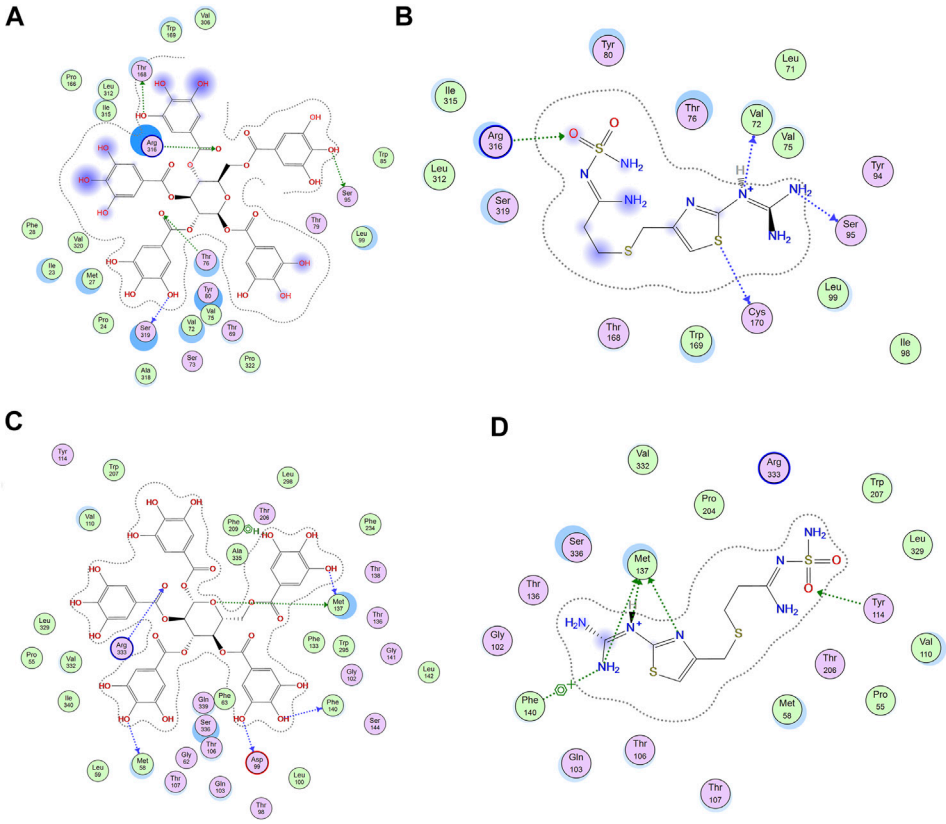

FIGURE 3 | 2D-interactions of **(A)** pentagalloyl glucose (PGG) and **(B)** famotidine with amino acid residues on EP4 and **(C)** PGG and **(D)** famotidine with amino acid residue EP3 receptor.

3.4 Effect of PGG on Immunoexpression of Endothelial Nitric Oxide Synthase

The action of nitric oxide in the stomach mucosa is paradoxical. Nitric oxide is made from L-arginine in a chemical reaction mediated by either cytotoxic-inducible nitric oxide synthase (iNOS) or cytoprotective constitutive eNOS (Abdel-Raheem, 2010). In this study, we investigated the effect of PGG on the nitric oxide signaling pathway and its contribution in the gastroprotective effect of PGG. As illustrated in **Figure 5**, indomethacin-treated rats exhibited a 6-fold dramatic decrease in eNOS level when related to the control group. Pretreatment with the reference drug famotidine or the tested compound PGG at doses (100 and 200 mg/kg) markedly increased eNOS levels by 4.4, 3.9, and 4.7 folds, respectively, when related to the ulcerative animals (indomethacin-treated group). The increased expression of eNOS by PGG may be responsible for the observed gastroprotective effects of PGG in the present study. NO produced by eNOS improves ulcer healing by increasing vasodilation, inducing angiogenesis, scavenging the toxic-free radicals, and reducing leukocyte infiltration, resulting in epithelial tissue integrity restoration and enhanced mucous secretion (Khattab et al., 2001; Abd El-Rady et al., 2021), as observed in our study.

3.5 Effect of PGG on Immunoexpression of Inducible Nitric Oxide Synthase

Nitric oxide produced by iNOS plays a role in ulcer formation through the production of cytotoxic peroxide–free radicals (Pan et al., 2005). We showed previously that indomethacin administration is associated with increased expression of gastric iNOS, and its inhibition promotes ulcer healing effects (Nabil et al., 2021). In this study, control and famotidine-pretreated ulcer group sections displayed a lower positive cytoplasmic immunoreactivity to iNOS in the gastric mucosal cells (**Figures 6A,E**). On the other hand, indomethacin-induced ulcer group sections demonstrated an intense and significant positive immune reaction to iNOS in the gastric mucosal cells when related to the control group ($p < 0.05$) (**Figure 6B**). The PGG-treated groups at both dose levels revealed a significant reduction in iNOS immunoreactivity when compared to the ulcerative animals, indomethacin group ($p < 0.05$) (**Figures 6C,D**, respectively). Moreover, famotidine exerted more potent effects than PGG in decreasing iNOS expression, $p < 0.05$, (**Figure 6F**). It was observed that PGG lowered the expression levels of iNOS in LPS-stimulated macrophages (Zhang et al., 2021); this confirms its anti-inflammatory and cytoprotective effects observed in the current study.

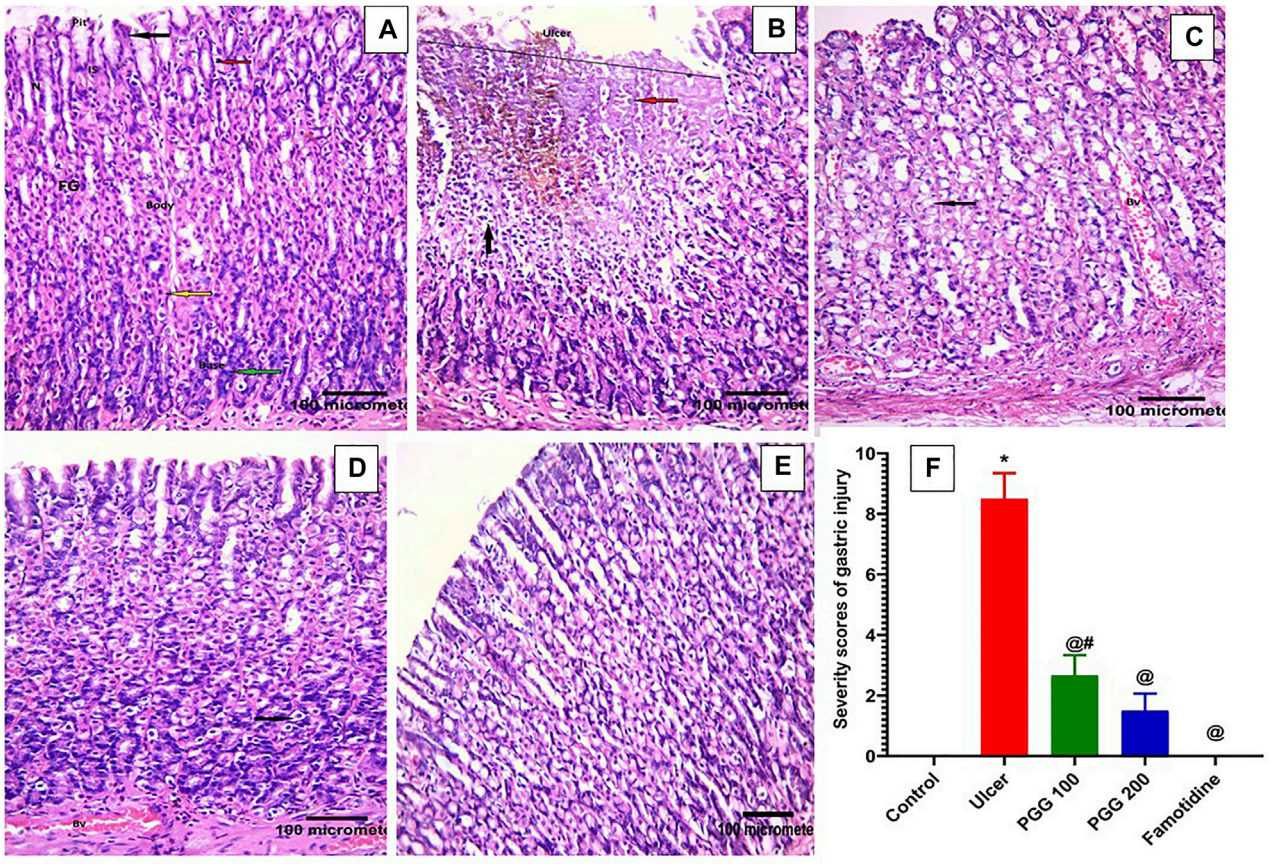

FIGURE 4 | Histopathological effects of pentagalloyl glucose (PGG) effects on the stomach mucosal tissues of animals. Representative gastric sections from **(A)** normal control group, **(B)** ulcerative animals (indomethacin alone, 60 mg/kg), **(C)** indomethacin + PGG-treated groups (100 mg/kg), **(D)** indomethacin + PGG-treated groups (200 mg/kg), and **(E)** indomethacin + famotidine-treated group (10 mg/kg). **(F)** Column graph illustrates the severity scores of gastric injuries among groups, Data are presented as mean ± SEM, $^{*,@,\#}p < 0.05$ vs. control, ulcer, and famotidine groups, respectively, by ANOVA followed by Dunnett's test. Fundic glands (FGs), gastric pits (Pits), isthmus (IS), neck (N), columnar epithelial cells (black arrow), mucous neck cells (red arrow), pyramidal oxyntic cells (yellow arrow), peptic cells or vacuolation (green arrow), tissue erosion and degeneration (black arrow), exfoliated cells (red arrow), extravasated blood (orang arrow), cellular infiltration (circle), and congested blood vessels (BV), [H&E × 200].

3.6 Effect of PGG on Oxidative Stress

In animal studies, reactive oxygen species, ROS, produced by activated neutrophils in gastric tissues are linked to the etiology and delayed stomach ulcer repair caused by indomethacin (Wang et al., 2014). Intracellular antioxidant systems, such as GPx, GSH, SOD, and catalase, can neutralize the produced ROS (Antonisamy et al., 2016). To further investigate the mechanism of action of PGG to prevent indomethacin-induced gastric injury, the endogenous antioxidants, such as GPx activity and GSH content, were examined in gastric tissues. Furthermore, malondialdehyde (MDA), a lipid peroxidation product resulted from increased cellular oxidative stress, was also measured. **Figure 7** shows that MDA content was elevated in indomethacin group administration ($p < 0.05$, **Figure 7A**), while GPX activity and GSH content were decreased ($p < 0.05$, **Figures 7B,C**, respectively) compared with the control group. PGG at both doses or famotidine pretreatment exerted protective effects, in which MDA content was decreased and GPX activity and GSH content were elevated in gastric tissues. Both PGG at the two dose levels and famotidine exerted similar protective effects on MDA, while the effect of PGG at 200-mg/kg level was stronger than that of famotidine on gastric GPX activity. Both 200 mg/kg PGG and famotidine had more potent effect on gastric GSH than PGG 100 mg/kg. These data indicated that PGG improved antioxidant capacity in the gastric injury model.

3.7 Effect of PGG on Gastric Inflammation

The induction and healing of gastric ulcers are influenced by a variety of inflammatory variables (Miyata et al., 1997; Mahmoud et al., 2021). As shown in the current study, indomethacin caused infiltration of inflammatory cells to the gastric tissues with subsequent release of ROS and inflammatory mediators. We previously reported that both TNF-α and IL-6 were elevated in gastric tissues following indomethacin administration (Mahmoud et al., 2021; Nabil et al., 2021). TNF-α and IL-6 are proinflammatory cytokines that play a role in the development of stomach ulcers and inflammation (Aziz et al., 2019). TNF-α induces the subsequent production of additional inflammatory factors, such as IL-2 and IL-6, that could activate neutrophils and release oxygen-free radicals,

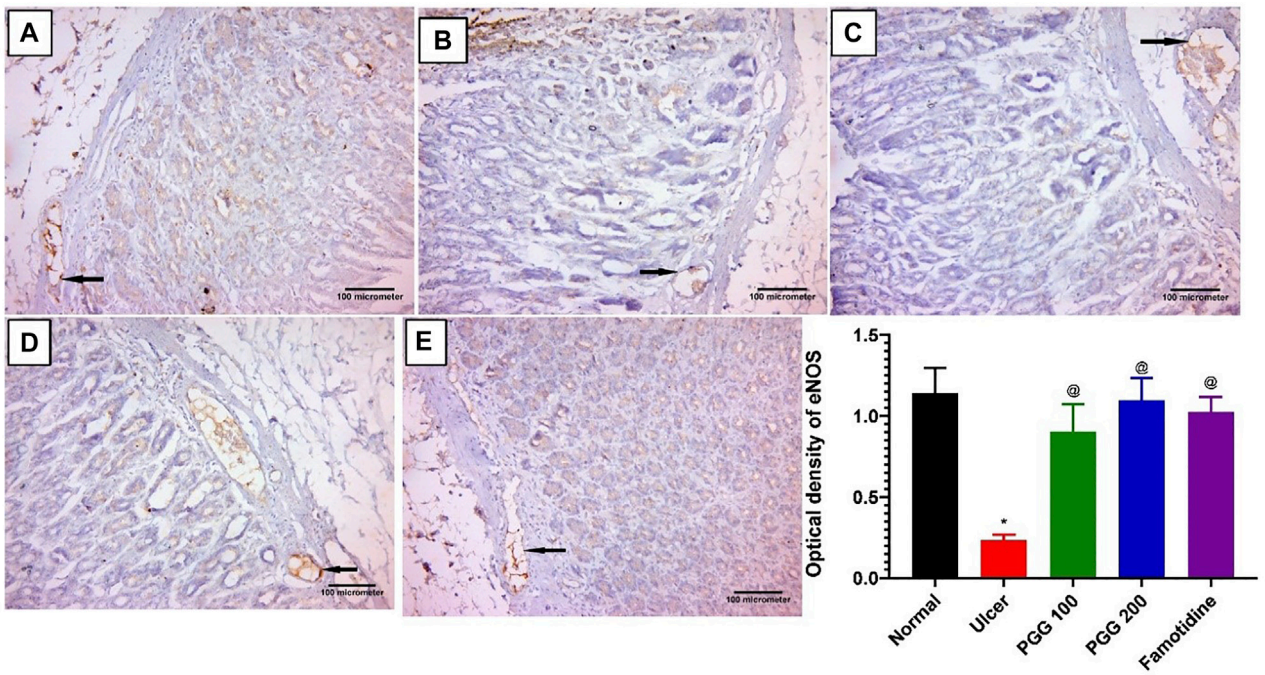

FIGURE 5 | Immunohistochemical staining of endothelial nitric oxide synthase (eNOS) in gastric mucosal tissues. Representative gastric mucosal sections from **(A)** normal control animals, **(B)** ulcerative animals treated with indomethacin alone (60 mg/kg), **(C,D)** ulcerative rats treated with indomethacin + PGG at two doses: 100 and 200 mg/kg, respectively, and **(E)** ulcerative animals treated with indomethacin + famotidine-treated group (10 mg/kg). Brown and blue indicate positive and negative staining of eNOS, respectively. Avidine biotin peroxidase stained with Hx counter stain x200. Data are expressed as mean ± S.E, $n = 10$. $^{*,@}$significantly different from corresponding control group of rats and indomethacin group, respectively, at $p < 0.05$ by one-way ANOVA was used for statistical analysis followed by Tukey's post hoc test.

generate acute phase proteins, obstruct gastric mucosal blood microcirculation, and increase gastric mucosal injury (Su et al., 2017; Lian et al., 2020). In the current study, the levels of inflammatory factors TNF-α and IL-6 were also significantly elevated in gastric injury rats induced by indomethacin ($p < 0.05$; **Figure 8**). In rats pretreated with either PGG (100, 200 mg/kg) or famotidine, a decrease in inflammatory factors was observed, indicating that PGG efficiently relieved inflammation. The decrease was clearer in the famotidine group. In this context, PGG was able to suppress the expression of proinflammatory cytokines, including IL-1β and TNF-α, and inflammatory enzyme, COX-2, in advanced glycation end product (AGE)–treated renal mesangial cells (Tong et al., 2021). Moreover, in LPS-stimulated RAW 264.7 cells, PGG dramatically reduced secretions of TNF-α, IL-1, IL-6, and NO (Zhang et al., 2021). Furthermore, in accordance with the present study, *in vivo* studies on the animal model of aortic aneurysm showed that PGG nanoparticles suppressed inflammatory cell infiltration and systemic inflammation (Wang et al., 2021).

3.8 Effect of PGG on Platelet Endothelial Cell Adhesion Molecule-1

PECAM-1 (platelet endothelial cell adhesion molecule-1 or cluster of differentiation 31, CD31) is a 130-kDa Ig superfamily member that is expressed on platelets and leukocytes and is particularly concentrated at endothelial cell–cell junctions (Newman, 1999). It was reported that increased expression of PECAM-1 is associated with increased leukocyte trans-endothelial migration and subsequent inflammation (Schenkel et al., 2004). PECAM-1 is engaged in the trans-endothelial migratory process in both leukocytes and endothelial cells (Muller et al., 1993). It was reported that PECAM-1 antibody administration attenuated lung inflammation and minimized tissue necrosis and leukocyte infiltration in a model of myocardial infarction (Vaporciyan et al., 1993; Gumina et al., 1996). PECAM-1's role, however, has not been explored in any experimental model of indomethacin-induced gastric ulcer. As shown in **Figure 9**, indomethacin administration was associated with increased expression of PECAM-1 by 8.4 fold, which explains the increased leukocyte infiltration observed in the histopathological study and the increased levels of proinflammatory cytokines, TNF- and IL-6, in the gastric tissues of the ulcer group. This finding is in accordance with that of a previous study by Konturek et al. (2004), who showed that PECAM-1 is overexpressed in vehicle-treated gastric mucosa at the ulcer margin, and capsaicin attenuated this effect in acetic acid–induced gastric ulcer. However, a previous study of Alese et al. (2017) showed that PECAM-1 is decreased in aspirin-

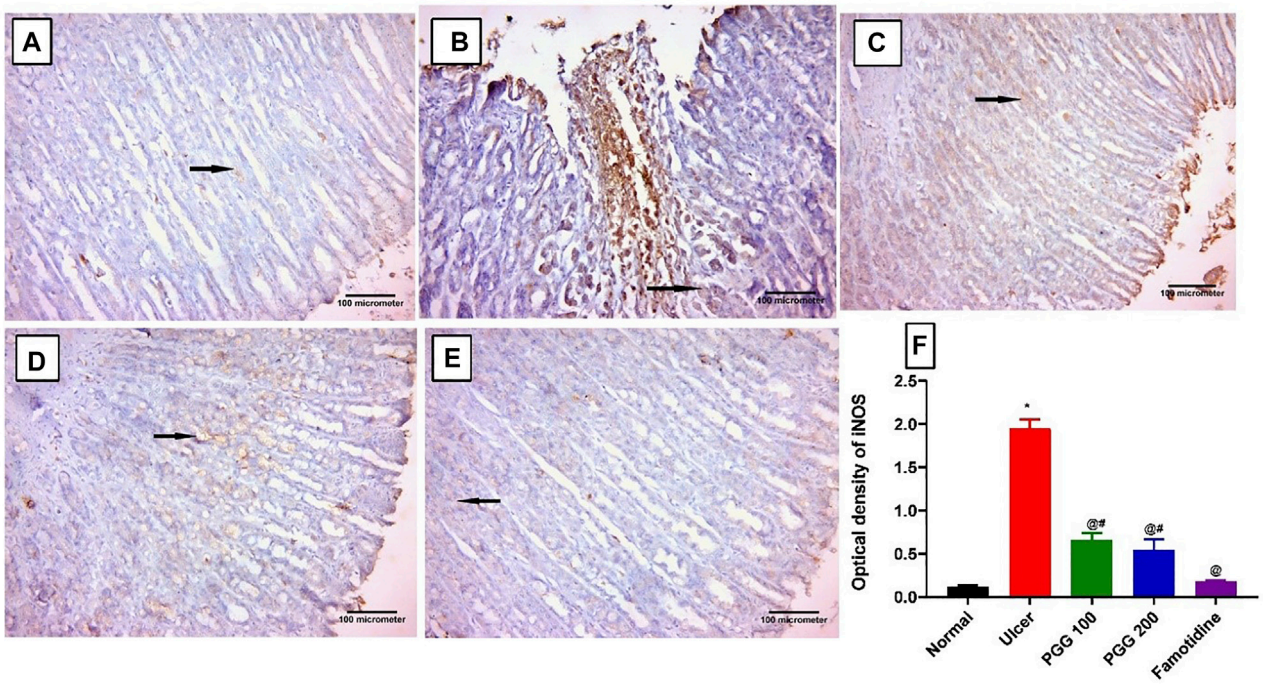

FIGURE 6 | Immunohistochemical staining of inducible nitric oxide synthase (iNOS) in gastric mucosal tissues. **(A)** Control and **(E)** famotidine-pretreated ulcer groups furnished a minimal positive cytoplasmic immunoreactivity to iNOS in the gastric mucosal cells (arrows). **(B)** Ulcerative animals (indomethacin group) displayed an intense positive immune reaction to iNOS in the gastric mucosal cells (arrows). **(C,D)** PGG -pretreated ulcer groups (100 or 200 mg/kg) showed a reduction in iNOS immunoreactivity (arrows). iNOS immunostaining (avidine biotin peroxidase stained with Hx counter stain X 200, scale bar = 100 μm). **(F)** Quantitative analysis of immunoreactivity intensity of iNOS. Results are shown as mean ± SEM, $n = 10$. $^{*\ @,\ \#}$significantly different compared the control group, indomethacin, and famotidine groups, respectively, at $p < 0.05$ by one-way ANOVA followed by Tukey's post hoc test.

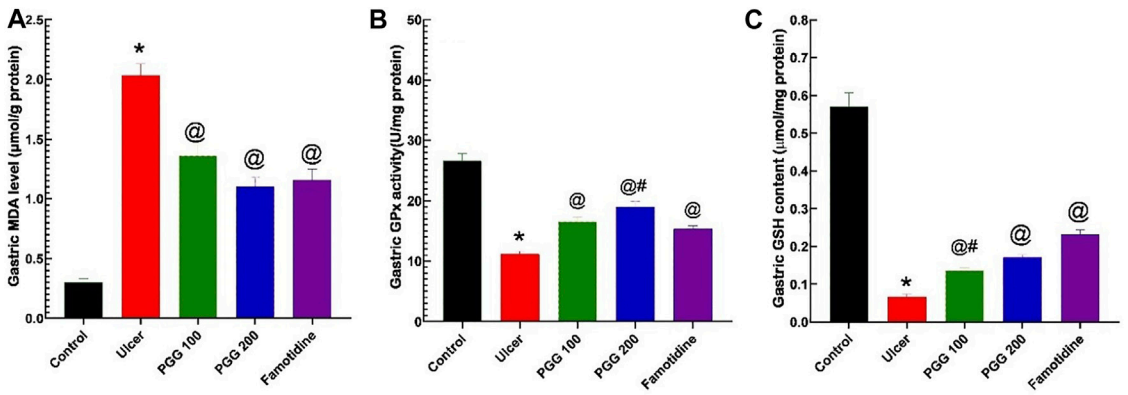

FIGURE 7 | Results from the malondialdehyde (MDA) level **(A)**, glutathione peroxidase activity (GPx), **(B)** and reduced glutathione content (GSH) **(C)** in gastric tissues. The data are shown as the mean ± SEM ($n = 6$). $^{*,\ @,\ \#}$Mean values with different symbols are significantly different ($p < 0.05$) according to one-way ANOVA followed by Tukey's post hoc test vs. control, indomethacin ulcer, or famotidine groups, respectively.

induced gastric ulcer, and flavonoid fraction of *Musa paradisiaca* increased its level. The difference in results may be attributed to the difference in the experimental design. As shown in **Figure 9**, the present study revealed that both PGG (100 & 200 mg/kg) and famotidine administration attenuated increased PECAM expression (6.4, 6.7, and 8.3 folds, respectively) compared to the ulcer group. The present study confirmed that PECAM-1 plays an important role in the ulcerogenic effect of indomethacin, and inhibition of its expression by PGG and famotidine may mediate their antiulcerogenic effects. Further studies using antibodies against PECAM-1 are required to confirm its role in indomethacin-induced ulcers.

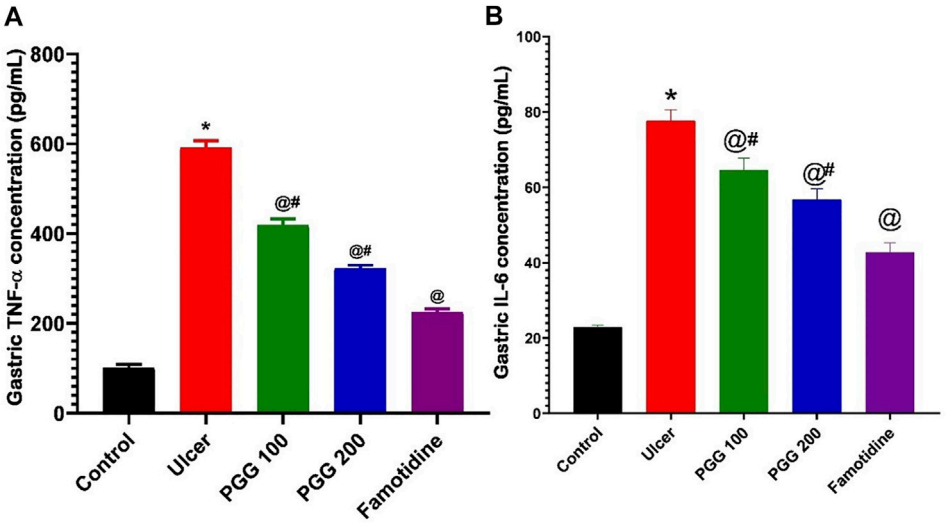

FIGURE 8 | Effect of pretreatment with either pentagalloyl glucose (PGG) (100 or 200 mg/kg) or famotidine on gastric TNF-α levels **(A)** and IL-6 **(B)** of indomethacin-induced gastric injury. Data are expressed as mean ± SEM, $n = 4$. *, $^{@}$ and $^{\#}$statistically significant from control, indomethacin group, or famotidine groups of rats, respectively, at $p < 0.05$ by one-way ANOVA was used for statistical analysis followed by Tukey's post hoc test.

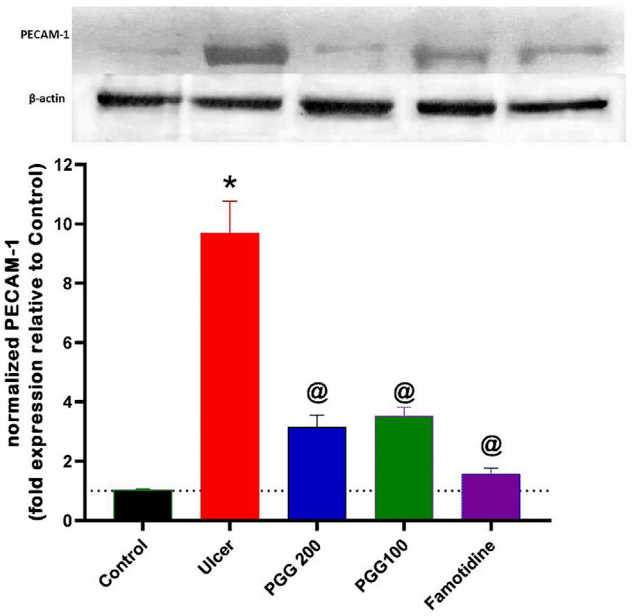

FIGURE 9 | Upper panel represents the effect of pretreatment with either pentagalloyl glucose (PGG) (100 or 200 mg/kg) or famotidine on gastric PECAM-1 level of indomethacin-induced gastric injury. The lower panel represents densitometry analysis of the ratio of PECAM-1 protein over β-actin protein. Data are expressed as mean ± SEM, $n = 3$. *, $^{@}$ Statistically significant from control and indomethacin groups of rats, respectively, at $p < 0.05$ by one-way ANOVA was used for statistical analysis followed by Tukey's post hoc test.

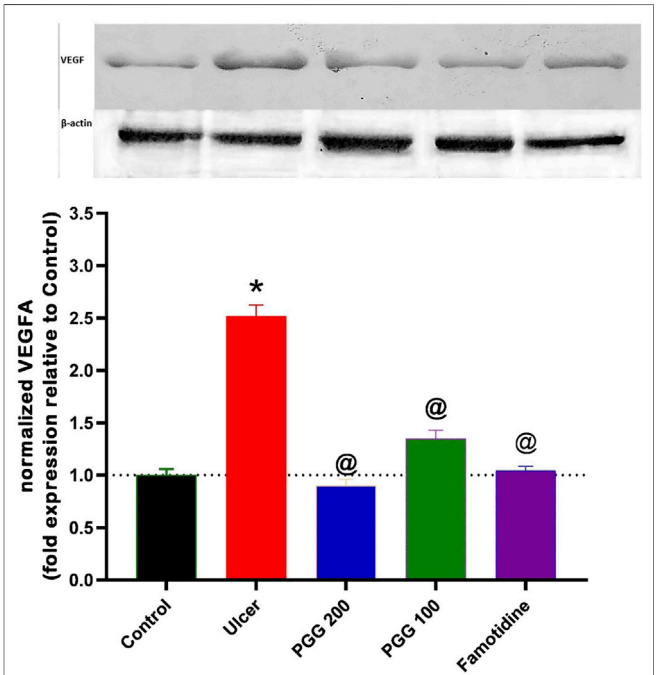

FIGURE 10 | Upper panel represents the effect of pretreatment with either pentagalloyl glucose (PGG) (100 or 200 mg/kg) or famotidine on gastric VEGF level of indomethacin-induced gastric injury. The lower panel represents densitometry analysis of the ratio of VEGF protein over β-actin protein. Data are expressed as mean ± SEM, $n = 3$. * and @ Statistically significant from control or indomethacin groups of rats, respectively, at $p < 0.05$ by one-way ANOVA was used for statistical analysis followed by Tukey's post hoc test.

3.9 Effect of PGG on Vascular Endothelial Growth Factor

As shown in **Figure 10**, indomethacin-induced ulcer was associated with increased expression of VEGF by 150% when compared to the control group. Administration of either PGG (100 and 200 mg/kg) or famotidine decreased VEGF expression by 46, 64, and 58.4% when compared to the ulcer group. Vascular endothelial factor is an important growth factor that is involved in angiogenesis and ulcer healing processes. Our results indicate that indomethacin increased VEGF in gastric tissues in an attempt to start ulcer healing following gastric mucosal damage. As a result of PGG and famotidine, there may be less injury to the gastric mucosa, resulting in VEGF synthesis not being stimulated. These findings are confirmed by the previous study in which 50% ethanol administration caused deep necrosis in the gastric mucosa and increased VEGF expression after 3 h of ethanol administration, and *Punica granatum* peel extract administration attenuated this increase (Jones et al., 1999). On the contrary, other studies showed that indomethacin administration was associated with decreased expression of VEGF, and *Chasmanthera dependens* extract or cimetidine increased it (Tijani et al., 2021). However, the experimental design is different where drugs are used for 14 days following ulcer induction. In our study, drugs were used 8 days before indomethacin administration, and VEGF expression was measured 6 h after indomethacin administration, not after 14 days as in the previous study.

4 CONCLUSION

This study is the first to show that pentagalloyl glucose (PGG) has a protective effect in a rat model of indomethacin-induced gastric ulcer. PGG's cytoprotective effect could be linked to an increase of gastric mucosal mucopolysaccharides, reduction of oxidative stress, triggered inflammatory response, and modulating NO/eNOS/iNOS signaling. The proven therapeutic benefits of PGG in the present study suggest that it could be effective in the treatment or prevention of gastric ulcers. However, further experiments are recommended to confirm the obtained results in other ulcer models and to evaluate the safety of PGG and determine the therapeutic doses and time.

DATA AVAILABILITY STATEMENT

The original contributions presented in the study are included in the article, further inquiries can be directed to the corresponding author.

ETHICS STATEMENT

The animal study was reviewed and approved and the experiments were carried out in accordance with the international ethical standards for the use and care of laboratory animals and were approved by the Ethics Committee of Zagazig University (No. ZU-IACUC/3/F/73/2020).

AUTHOR CONTRIBUTIONS

MM, MN, and RH performed the biological activities, MS performed the docking analysis, AE-S commented on the manuscript, ME-A performed extraction and compound isolation, and MM and MS wrote the manuscript and designed and conceived the study.

REFERENCES

Abd El-Rady, N. M., Dahpy, M. A., Ahmed, A., Elgamal, D. A., Hadiya, S., Ahmed, M. A. M., et al. (2021). Interplay of Biochemical, Genetic, and Immunohistochemical Factors in the Etio-Pathogenesis of Gastric Ulcer in Rats: A Comparative Study of the Effect of Pomegranate Loaded Nanoparticles versus Pomegranate Peel Extract. *Front. Physiol.* 12, 335. doi:10.3389/fphys.2021.649462

Abdel-Raheem, I. T. (2010). Gastroprotective Effect of Rutin against Indomethacin-induced Ulcers in Rats. *Basic Clin. Pharmacol. Toxicol.* 107 (3), 742–750. doi:10.1111/j.1742-7843.2010.00568.x

Ahmed, M. A. E., Mohanad, M., Ahmed, A. A. E., Aboulhoda, B. E., and El-Awdan, S. A. (2021). Mechanistic Insights into the Protective Effects of Chlorogenic Acid against Indomethacin-Induced Gastric Ulcer in Rats: Modulation of the Cross Talk between Autophagy and Apoptosis Signaling. *Life Sci.* 275, 119370. doi:10.1016/j.lfs.2021.119370

Al Batran, R., Al-Bayaty, F., Abdulla, M. A., Al-Obaidi, M. M., Hajrezaei, M., Hassandarvish, P., et al. (2013). Gastroprotective Effects of Corchorus Olitorius Leaf Extract against Ethanol-Induced Gastric Mucosal Hemorrhagic Lesions in Rats. *J. Gastroenterol. Hepatol.* 28 (8), 1321–1329. doi:10.1111/jgh.12229

Alese, M. O., Adewole, S. O., Akinwunmi, K. F., Omonisi, A. E., and Alese, O. O. (2017). Aspirin-Induced Gastric Lesions Alters EGFR and PECAM-1 Immunoreactivity in Wistar Rats: Modulatory Action of Flavonoid Fraction of Musa Paradisiaca. *Open Access Maced J. Med. Sci.* 5 (5), 569–577. doi:10.3889/oamjms.2017.058

Antonisamy, P., Arasu, M. V., Dhanasekaran, M., Choi, K. C., Aravinthan, A., Kim, N. S., et al. (2016). Protective Effects of Trigonelline against Indomethacin-Induced Gastric Ulcer in Rats and Potential Underlying Mechanisms. *Food Funct.* 7 (1), 398–408. doi:10.1039/c5fo00403a

Ardalani, H., Hadipanah, A., and Sahebkar, A. (2020). Medicinal Plants in the Treatment of Peptic Ulcer Disease: A Review. *Mini Rev. Med. Chem.* 20 (8), 662–702. doi:10.2174/1389557520666191227151939

Aziz, R. S., Siddiqua, A., Shahzad, M., Shabbir, A., and Naseem, N. (2019). Oxyresveratrol Ameliorates Ethanol-Induced Gastric Ulcer via Downregulation of IL-6, TNF-α, NF-κb, and COX-2 Levels, and Upregulation of TFF-2 Levels. *Biomed. Pharmacother.* 110, 554–560. doi:10.1016/j.biopha.2018.12.002

Bancroft, J. D., and Gamble, M. (2008). *Theory and Practice of Histological Techniques*. London: Elsevier Health Sciences.

Campos-Vidal, Y., Herrera-Ruiz, M., Trejo-Tapia, G., Gonzalez-Cortazar, M., Aparicio, A. J., and Zamilpa, A. (2021). Gastroprotective Activity of Kaempferol Glycosides from Malvaviscus Arboreus Cav. *J. Ethnopharmacol.* 268 (March), 113633. doi:10.1016/j.jep.2020.113633

Carvalho, A. C., Guedes, M. M., de Souza, A. L., Trevisan, M. T., Lima, A. F., Santos, F. A., et al. (2007). Gastroprotective Effect of Mangiferin, a Xanthonoid from Mangifera Indica, against Gastric Injury Induced by Ethanol and Indomethacin in Rodents. *Planta Med.* 73 (13), 1372–1376. doi:10.1055/s-2007-990231

Chen, R. H., Yang, L. J., Hamdoun, S., Chung, S. K., Lam, C. W., Zhang, K. X., et al. (2021). 1, 2, 3, 4, 6-Pentagalloyl Glucose, a RBD-ACE2 Binding Inhibitor to Prevent SARS-CoV-2 Infection. *Front. Pharmacol.* 12, 150. doi:10.3389/fphar.2021.634176

Emam, M., Abdel-Haleem, D. R., Farag, S. M., El-Ansari, M. A., and Sobeh, M. (2022). Larvicidal Activity of Pentagalloyl Glucose and Mangiferin Isolated

from the Waste of Mango Kernel against Culex Pipiens L. *Waste Biomass Valor* 13, 83–93. doi:10.1007/s12649-021-01532-9

Gumina, R. J., El Schultz, J., Yao, Z., Kenny, D., Warltier, D. C., Newman, P. J., et al. (1996). Antibody to Platelet/Endothelial Cell Adhesion Molecule-1 Reduces Myocardial Infarct Size in a Rat Model of Ischemia-Reperfusion Injury. *Circulation* 94 (12), 3327–3333. doi:10.1161/01.cir.94.12.3327

Hatazawa, R., Tanaka, A., Tanigami, M., Amagase, K., Kato, S., Ashida, Y., et al. (2007). Cyclooxygenase-2/Prostaglandin E2 Accelerates the Healing of Gastric Ulcers via EP4 Receptors. *Am. J. Physiol. Gastrointest. Liver Physiol.* 293 (4), G788–G797. doi:10.1152/ajpgi.00131.2007

Jones, M. K., Itani, R. M., Wang, H., Tomikawa, M., Sarfeh, I. J., Szabo, S., et al. (1999). Activation of VEGF and Ras Genes in Gastric Mucosa during Angiogenic Response to Ethanol Injury. *Am. J. Physiol.* 276 (6), G1345–G1355. doi:10.1152/ajpgi.1999.276.6.G1345

Khattab, M. M., Gad, M. Z., and Abdallah, D. (2001). Protective Role of Nitric Oxide in Indomethacin-Induced Gastric Ulceration by a Mechanism Independent of Gastric Acid Secretion. *Pharmacol. Res.* 43 (5), 463–467. doi:10.1006/phrs.2001.0801

Konturek, P. C., Brzozowski, T., Burnat, G., Kwiecien, S., Pawlik, T., Hahn, E. G., et al. (2004). Role of Brain-Gut Axis in Healing of Gastric Ulcers. *J. Physiol. Pharmacol.* 55 (2), 179–192.

Lau, J. Y., Sung, J. J., Metz, D. C., and Howden, C. W. (2008). 187 Systematic Review of the Epidemiology of Complicated Peptic Ulcer: Incidence, Recurrence, Risk Factors and Mortality. *Gastroenterology* 134 (4), A32. doi:10.1016/s0016-5085(08)60156-0

Lian, Y. Z., Lin, I. H., Yang, Y. C., and Chao, J. C. (2020). Gastroprotective Effect of Lycium Barbarum Polysaccharides and C-Phycocyanin in Rats with Ethanol-Induced Gastric Ulcer. *Int. J. Biol. Macromol.* 165, 1519–1528. doi:10.1016/j.ijbiomac.2020.10.037

Mahmoud, M. F., Nabil, M., Abdo, W., Abdelfattah, M. A. O., El-Shazly, A. M., El Kharrassi, Y., et al. (2021). Syzygium Samarangense Leaf Extract Mitigates Indomethacin-Induced Gastropathy via the NF-κB Signaling Pathway in Rats. *Biomed. Pharmacother.* 139, 111675. doi:10.1016/j.biopha.2021.111675

McManus, J. F. (1948). Histological and Histochemical Uses of Periodic Acid. *Stain Technol.* 23 (3), 99–108. doi:10.3109/10520294809106232

Mendonca, P., Alghamdi, S., Messeha, S., and Soliman, K. F. A. (2021). Pentagalloyl Glucose Inhibits TNF-α-Activated CXCL1/GRO-α Expression and Induces Apoptosis-Related Genes in Triple-Negative Breast Cancer Cells. *Sci. Rep.* 11 (1), 5649–5713. doi:10.1038/s41598-021-85090-z

Miyata, A., Goto, H., Niwa, Y., Hayakawa, T., Nagasaka, T., and Nakashima, N. (1997). Histological Evaluation of Connective Tissue Components in the Healing Process of Human Gastric Ulcer. *Clin. Exp. Pharmacol. Physiol.* 24 (9–10), 714–719. doi:10.1111/j.1440-1681.1997.tb02118.x

Moharram, F. A., El Dib, R. A., Wahman, L., El-Shenawy, S., and El-Awdan, S. (2017). Gastro Protective Effect of Pentagalloyl Glucose on Aspirin Induced Gastric Mucosal Ulcer in Comparison with Omeprazole, Famotidine and Melatonin. *J. Pharm. Sci. Res.* 9 (6), 785.

Muller, W. A., Weigl, S. A., Deng, X., and Phillips, D. M. (1993). PECAM-1 Is Required for Transendothelial Migration of Leukocytes. *J. Exp. Med.* 178 (2), 449–460. doi:10.1084/jem.178.2.449

Nabil, M., El Raey, M. A., Abdo, W., Abdelfattah, M. A. O., El-Shazly, A. M., Sobeh, M., et al. (2021). Gastro-Protective Effects of Albizia Anthelmintica Leaf Extract on Indomethacin-Induced Gastric Ulcer in Wistar Rats: In Silico and *In Vivo* Studies. *Antioxidants (Basel)* 10 (2), 176. doi:10.3390/antiox10020176

Newman, P. J. (1999). Switched at Birth: A New Family for PECAM-1. *J. Clin. Invest.* 103 (1), 5–9. doi:10.1172/JCI5928

Pan, L. R., Tang, Q., Fu, Q., Hu, B. R., Xiang, J. Z., and Qian, J. Q. (2005). Roles of Nitric Oxide in Protective Effect of Berberine in Ethanol-Induced Gastric Ulcer Mice. *Acta Pharmacol. Sin.* 26 (11), 1334–1338. doi:10.1111/j.1745-7254.2005.00186.x

Patnaik, S. S., Simionescu, D. T., Goergen, C. J., Hoyt, K., Sirsi, S., and Finol, E. A. (2019). Pentagalloyl Glucose and its Functional Role in Vascular Health: Biomechanics and Drug-Delivery Characteristics. *Ann. Biomed. Eng.* 47 (1), 39–59. doi:10.1007/s10439-018-02145-5

Piper, D. W., and Stiel, D. D. (1986). Pathogenesis of Chronic Peptic Ulcer, Current Thinking and Clinical Implications. *Med. Prog.* 2 (1), 7–10.

Ramakrishnan, K., and Salinas, R. C. (2007). Peptic Ulcer Disease. *Am. Fam. Phys.* 76 (7), 1005–1012.

Schenkel, A. R., Chew, T. W., and Muller, W. A. (2004). Platelet Endothelial Cell Adhesion Molecule Deficiency or Blockade Significantly Reduces Leukocyte Emigration in a Majority of Mouse Strains. *J. Immunol.* 173 (10), 6403–6408. doi:10.4049/jimmunol.173.10.6403

Severi, J. A., Lima, Z. P., Kushima, H., Brito, A. R., Santos, L. C., Vilegas, W., et al. (2009). Polyphenols with Antiulcerogenic Action from Aqueous Decoction of Mango Leaves (Mangifera Indica L). *Molecules* 14 (3), 1098–1110. doi:10.3390/molecules14031098

Sidahmed, H. M. A., Vadivelu, J., Loke, M. F., Arbab, I. A., Abdul, B., Sukari, M. A., et al. (2019). Anti-ulcerogenic Activity of Dentatin from Clausena Excavata Burm.F. Against Ethanol-Induced Gastric Ulcer in Rats: Possible Role of Mucus and Anti-oxidant Effect. *Phytomedicine* 55, 31–39. doi:10.1016/j.phymed.2018.06.036

Slomiany, B. L., and Slomiany, A. (2005). Endothelin-1-Dependent Up-Regulation of Leptin Production in Gastric Mucosal Injury by Indomethacin. *InflammoPharmacology* 13 (5–6), 455–466. doi:10.1163/156856005774649331

Su, M., Li, C.-y., Zhou, L., Yan, Y.-y., Ao, L.-y., Wang, G.-j., et al. (2017). Anti-ulcerogenic Effect of KFP-H008 against Ethanol-Induced Gastric Ulcer via P38 MAPK/NF-κB Pathway. *RSC Adv.* 7 (78), 49423–49435. doi:10.1039/c7ra08879e

Suleyman, H., Albayrak, A., Bilici, M., Cadirci, E., and Halici, Z. (2010). Different Mechanisms in Formation and Prevention of Indomethacin-Induced Gastric Ulcers. *Inflammation* 33 (4), 224–234. doi:10.1007/s10753-009-9176-5

Szabo, S., and Hollander, D. (1989). Pathways of Gastrointestinal Protection and Repair: Mechanisms of Action of Sucralfate. *Am. J. Med.* 86 (6), 23–31. doi:10.1016/0002-9343(89)90153-8

Tijani, A. S., Farombi, E. O., and Olaleye, S. B. (2021). Mechanisms Underlying the Healing Potentials of the Methanol Extract of Chasmanthera Dependens Stem on Indomethacin-Induced Gastric Ulcer. *Egypt. J. Basic Appl. Sci.* 8 (1), 17–31. doi:10.1080/2314808x.2021.1881746

Tong, J., Fang, J., Zhu, T., Pan, X., Shang, J., Chen, L., et al. (2021). Pentagalloylglucose Reduces AGE-Induced Inflammation by Activating Nrf2/HO-1 and Inhibiting the JAK2/STAT3 Pathway in Mesangial Cells. *J. Pharmacol. Sci.* 147, 305. doi:10.1016/j.jphs.2021.08.006

Van Wyk, B. E., and Wink, M. (2015). *Phytomedicines, Herbal Drugs, and Poisons*. Chicago: Royal Botanic Gardens, Kew: The University of Chicago Press, Kew Publishing.

Vaporciyan, A. A., DeLisser, H. M., Yan, H. C., Mendiguren, I. I., Thom, S. R., Jones, M. L., et al. (1993). Involvement of Platelet-Endothelial Cell Adhesion Molecule-1 in Neutrophil Recruitment *In Vivo*. *Science* 262 (5139), 1580–1582. doi:10.1126/science.8248808

Wang, Y. Z., Cao, Y. Q., Wu, J. N., Chen, M., and Cha, X. Y. (2005). Expression of Nitric Oxide Synthase in Human Gastric Carcinoma and its Relation to P53, PCNA. *World J. Gastroenterol.* 11 (1), 46–50. doi:10.3748/wjg.v11.i1.46

Wang, T., Zhao, S., Wang, Y., Yang, Y., Yao, L., Chu, L., et al. (2014). Protective Effects of Escin against Indomethacin-Induced Gastric Ulcer in Mice. *Toxicol. Mech. Methods* 24 (8), 560–566. doi:10.3109/15376516.2014.951815

Wang, X., Parasaram, V., Dhital, S., Nosoudi, N., Hasanain, S., Lane, B. A., et al. (2021). Systemic Delivery of Targeted Nanotherapeutic Reverses Angiotensin II-Induced Abdominal Aortic Aneurysms in Mice. *Sci. Rep.* 11 (1), 8584. doi:10.1038/s41598-021-88017-w

Zhang, X., Li, W., Feng, K., Xiao, J., Du, J., Cao, Y., et al. (2021). Immunomodulatory Effect of Pentagalloyl Glucose in LPS-Stimulated RAW264.7 Macrophages and PAO1-Induced *Caenorhabditis elegans*. *Exp. Gerontol.* 150, 111388. doi:10.1016/j.exger.2021.111388

Conflict of Interest: The authors declare that the research was conducted in the absence of any commercial or financial relationships that could be construed as a potential conflict of interest.

Publisher's Note: All claims expressed in this article are solely those of the authors and do not necessarily represent those of their affiliated organizations, or those of the publisher, the editors, and the reviewers. Any product that may be evaluated in this article, or claim that may be made by its manufacturer, is not guaranteed or endorsed by the publisher.

frontiers in Pharmacology

SYSTEMATIC REVIEW
published: 14 February 2022
doi: 10.3389/fphar.2022.822678

Citrus Extract as a Perspective for the Control of Dyslipidemia: A Systematic Review With Meta-Analysis From Animal Models to Human Studies

Betina M. R. Carvalho[1], *Laranda C. Nascimento*[1], *Jessica C. Nascimento*[1], *Vitória S. dos S. Gonçalves*[2], *Patricia K. Ziegelmann*[3], *Débora S. Tavares*[4] and *Adriana G. Guimarães*[5]*

[1]Programa de Pós-Graduação em Ciências Aplicadas à Saúde, Universidade Federal de Sergipe, Lagarto, Brazil, [2]Departamento de Química, Universidade Federal de Sergipe, São Cristóvão, Brazil, [3]Departamento de Estatística, Programa de Pós-graduação em Epidemiologia, Universidade Federal do Rio Grande do Sul, Porto Alegre, Brazil, [4]Departamento de Educação em Saúde, Universidade Federal de Sergipe, Lagarto, Brazil, [5]Departamento de Farmácia, Universidade Federal de Sergipe, São Cristóvão, Brazil

OPEN ACCESS

Edited by:
Irwin Rose Alencar de Menezes, Regional University of Cariri, Brazil

Reviewed by:
Amir Hadi, Isfahan University of Medical Sciences, Iran
Praveen Kumar M, Nference, India

***Correspondence:**
Adriana G. Guimarães
adrianagibara@hotmail.com
adrianagibara@pq.cnpq.br

Specialty section:
This article was submitted to Gastrointestinal and Hepatic Pharmacology, a section of the journal Frontiers in Pharmacology

Received: *26 November 2021*
Accepted: *10 January 2022*
Published: *14 February 2022*

Citation:
Carvalho BMR, Nascimento LC, Nascimento JC, Gonçalves VSS, Ziegelmann PK, Tavares DS and Guimarães AG (2022) Citrus *Extract as a Perspective for the Control of Dyslipidemia: A Systematic Review With Meta-Analysis From Animal Models to Human Studies. Front. Pharmacol. 13:822678. doi: 10.3389/fphar.2022.822678*

This study aims to obtain scientific evidence on the use of *Citrus* to control dyslipidemia. The surveys were carried out in 2020 and updated in March 2021, in the PubMed, Scopus, LILACS, and SciELO databases, using the following descriptors: *Citrus*, dyslipidemias, hypercholesterolemia, hyperlipidemias, lipoproteins, and cholesterol. The risk of bias was assessed according to the Cochrane methodology for clinical trials and ARRIVE for preclinical trials. A meta-analysis was performed using the application of R software. A total of 958 articles were identified and 26 studies demonstrating the effectiveness of the *Citrus* genus in controlling dyslipidemia were selected, of which 25 were included in the meta-analysis. The effects of *Citrus* products on dyslipidemia appear consistently robust, acting to reduce total cholesterol, LDL, and triglycerides, in addition to increasing HDL. These effects are associated with the composition of the extracts, extremely rich in antioxidant, as flavonoids, and that act on biochemical targets involved in lipogenesis and beta-oxidation. The risk of bias over all of the included studies was considered critically low to moderate. The meta-analysis demonstrated results favorable to control dyslipidemia by *Citrus* products. On the other hand, high heterogeneity values were identified, weakening the evidence presented. From this study, one can suggest that *Citrus* species extracts are potential candidates for dyslipidemia control, but more studies are needed to increase the strength of this occurrence.

Keywords: dyslipidemia, citrus, hyperlipidemia, flavonoids, cholesterol

Systematic Review Registration: [https://www.crd.york.ac.uk/prospero/display_record.php?ID=CRD42019121238], identifier [PROSPERO 2019 CRD42019121238].

INTRODUCTION

Dyslipidemia has high rates of occurrence in the world population (Pirillo et al., 2021), being closely related to obesity, metabolic syndrome (Mach et al., 2020), atherosclerosis (Wiggins et al., 2019),

coronary heart disease (Zhao et al., 2021), increased susceptibility to cancer (Khan et al., 2021), and more recently increased mortality and severity of COVID-19 (Atmosudigdo et al., 2021). This disorder is characterized by changes in the lipid profile, including an increase in total serum cholesterol, low-density lipoprotein (LDL-c), and triglycerides, as well as a decrease in high-density lipoprotein (HDL-c) rates in the blood (Fruchart et al., 2008). The relationships between these markers have been used as indicators of insulin resistance and metabolic disorders (Sowndarya et al., 2021), in addition to atherosclerosis and coronary heart disease (Abid et al., 2021). However, inflammation markers such as us-CRP (high serum sensitivity C-reactive protein) can also be considered important indicators to estimate the severity and risk of coronary artery disease (Patil et al., 2020). Although there are therapeutic options for the treatment of dyslipidemias, these are not fully effective, due to non-adherence to treatment by various factors such as adverse effects, intolerance, regimen complexity, and imperceptible benefits, besides the need to combine drugs to improve the clinical condition (Schulz, 2006; Ingersgaard et al., 2020). On the other hand, lipid-lowering drugs are still inaccessible to the majority of the population in low-income countries (Pirillo et al., 2021), making the search for new strategies to control dyslipidemia necessary.

In this sense, searching for new treatment strategies for this important health problem is necessary. In this perspective, several plants and natural products have been studied regarding their effects on dyslipidemia control (Ballard et al., 2019; Adel Mehraban et al., 2021); among them, the species of the genus *Citrus* (Lamiquiz-Moneo et al., 2020) stand out. Belonging to the Rutaceae family, the genus *Citrus* is widely distributed in tropical and subtropical regions (Manuel et al., 2020) and contains several substances with biological and nutritional potential, such as fibers (e.g., pectin), vitamins, and bioactive compounds, with emphasis on the flavonoids (Alam et al., 2013; Rafiq et al., 2018). Naringin, naringenin, nobiletin, narirutin, and hesperidin correspond to the most frequently found flavonoids. They have pronounced antioxidant and anti-inflammatory activities (Tripoli et al., 2007; Craft et al., 2012), in addition to being effective in controlling metabolic syndromes, lipid changes, and obesity (Geleijnse et al., 1999; Lee et al., 2001; Gattuso et al., 2007; Alam et al., 2013; Sahebkar, 2017; Ballard et al., 2019).

Thus, this review sought to compile the scientific findings that demonstrate the effect of *Citrus* extracts on the control of serum lipid levels, measuring the size of the effect through meta-analysis.

MATERIAL AND METHODS

Focused Question

The question to be answered was established from the bibliographic survey "Are species of the genus *Citrus* effective in reducing dyslipidemia?" conducted through four steps: (Pirillo et al., 2021) identification of the use of the *Citrus* species, (Mach et al., 2020) identification of the pathology to be applied (dyslipidemia), (Wiggins et al., 2019) definition of the types of studies included (preclinical and clinical), and (Zhao et al., 2021) definition of the target outcome to be analyzed, which is the lipid profile, building the PICOS strategy (patient or pathology, intervention, control, other outcomes, and the type of study). PICOS is highlighted as follows: P: dyslipidemia; I: species of the genera *Citrus* (extract); C: untreated or placebo-treated and hyperlipidemia-induced group; O: blood lipid levels; and S: preclinical or clinical studies.

Review Writing and Registration of Protocols

The writing of this systematic review was based on the recommendations of the Preferred Reporting Items for Systematic Reviews and Meta-Analyses (PRISMA) (Page et al., 2021) tool. In addition, the instrument that guides how the experimental studies should be analyzed was ARRIVE (Animal Research: Reporting of *In Vivo* Experiments) guidelines (Kilkenny et al., 2010). The protocol for this review was registered in the International Prospective Register of Systematic Reviews (Prospero) database and registered on the website https://www.crd.york.ac.uk/prospero/, through approved registry No. CRD42019121238.

Literature Search

The search was carried out through search strategies in the LILACS, PubMed, SciELO, and Scopus databases in 2019 and updated in March 2021. The terms used to compose the search in the databases were defined from consultations with MeSH and DeCS descriptors. Thus, the following search strategy was structured: "*CITRUS*" AND "Lipoproteins" OR "Cholesterol" OR "Epicholesterol" OR "Dyslipidemias" OR "Dyslipoproteinemia" OR "Hypercholesterolemia" OR "High Cholesterol Levels" OR "Hyperlipidemias" OR "Lipidemia," described in detail in **Supplementary Table S1**.

Study Selection and Eligibility Criteria

After excluding duplicate records, titles, abstracts, and full texts were independently analyzed by two researchers in order to determine the study's eligibility for inclusion in the review. The inclusion criteria were preclinical studies or randomized clinical trials that include the use of *Citrus* species to assess the effect on the lipid profile. In this review, were excluded reviews, case studies, case reports, and studies that did not assess the action on the lipid profile, which included the use of juices from *Citrus* species and their action on the lipid profile, or the association of *Citrus* species with another compound that could modify the lipid profile, as well as studies that used compounds isolated from *Citrus* species to target hyperlipidemia. To assess the agreement among researchers, the statistical test of the Kappa coefficient (K) was applied.

Data Extraction and Risk of Bias Assessment

Two independent reviewers extracted data from the included studies. The data from preclinical studies were as follows: *Citrus* species, type of extract and part of the plant, composition,

hyperlipidemia induction model, evaluation methods, treatment, animal species, and results (all results that were in mg/dL were converted to mmol/L using the OnlineConversion.com electronic calculator according to the type of cholesterol). The data from clinical studies were as follows: *Citrus* species, type of extract and part of the plant, composition, study design/location, sample, criteria for inclusion and exclusion of participants, pathologies, treatment, and results (all results that were in mmol/L were converted to mg/dL using the OnlineConversion.com electronic calculator according to the type of cholesterol). All the outcomes of the experiments carried out in the articles were extracted for descriptive and inferential analyses.

Through ARRIVE, we apply the following: precise and concise description of the content of the article in the title, abstract, explanation of the methodological approach of the introduction, general and specific objectives, ethical nature of care and use of animals, study design regarding the number of animals per group, experimental procedures, information about animals such as sex, size, weight, and age, housing and breeding, sample size, statistical methods, description of results and their interpretation, and study funding.

All clinical studies included in this research were approved for methodological quality in the risk checklist of Cochrane randomized for controlled trials (Cochrane Training, 2019). Items such as generation of random sequence, concealment of allocation, certification of participants and professionals, as well as of evaluators, incomplete and selective outcomes, or whether the study presents any other problem or fraud were used. The studies considered as having the highest methodological quality were those related to randomization, blinding, and complete outcomes.

Meta-Analysis

The studies selected for the meta-analysis had the following outcomes analyzed: total cholesterol, LDL, HDL, and triglyceride levels, including the baseline and post-treatment data from both the control and treatment groups for both preclinical and clinical studies. In addition to the primary outcomes, to improve the understanding of the effects observed in preclinical studies, the studies were separated into the following subgroups: route of administration of the extract, type of animal, type of extract, and parts of the plant used.

For the quantitative analysis of the articles, the studies selected presented the value of the sample n, mean, deviation, or standard error for the serum levels of total cholesterol, LDL, HDL, and/or triglycerides of the treatment and control groups. All data were tabulated in Excel and later analyzed using the application of R software. The heterogeneity of the studies was measured using Cochran's Q test, using the I^2 statistic, which was considered as heterogeneous when the p value was less than 0.05. The heterogeneity between the studies was defined using the I^2 statistic, which was considered with an unimportant (I^2 < 25%), moderate (25% < I^2 < 75%), or high degree of heterogeneity (I^2 > 75%) (Higgins and Thompson, 2002). For heterogeneous studies (I^2 > 75%), the following subgroup analyses were performed: route of administration, type of animal, parts of the plant used in the extract, type of fruit, and type of extract. In addition, we performed a sensitivity analysis, sequentially removing the individual studies to determine whether any single study affected the overall effect estimate.

RESULTS

Study Selection and Study Characteristics

During the search process, 958 articles were obtained: 169 from PubMed, 762 from SciVerse Scopus, 12 from SciELO, and 15 from LILACS. After analyzing the titles, 598 duplicate articles were removed. After excluding the repeated articles, 360 titles were screened for analysis according to the inclusion criteria, from which 329 studies were excluded for not inducing hyperlipidemia in an animal model or for not having dyslipidemia installed in the case of clinical studies. In addition, studies with isolated compounds of the *Citrus* species or without evaluation of total cholesterol, LDL-C, HDL-C, or triglycerides were also excluded.

After this design, 31 articles remained, the full texts of which were analyzed, thus yielding 27 articles that were finally included in the qualitative synthesis (**Figure 1**; **Tables 1–3**). Of these, 22 studies were preclinical trials (Vinson et al., 1998; Bok et al., 1999; Terpstra et al., 2002; Zulkhairi et al., 2010; Ding et al., 2012; Kang et al., 2012; Raasmaja et al., 2013; Lu et al., 2013; Kim et al., 2013; Muhtadi et al., 2015; Dinesh and Hegde, 2016; Shin et al., 2016; Ashraf et al., 2017; Fayek et al., 2017; Chou et al., 2018; Feksa et al., 2018; Mir et al., 2019; Sato et al., 2019; Hase-Tamaru et al., 2019; Ling et al., 2020; Ke et al., 2020; Lee et al., 2020), 3 were exclusively clinical studies (Gorinstein et al., 2007; Toth et al., 2015; Cai et al., 2017) and 1 study contained preclinical and clinical protocols (Mollace et al., 2011) (**Figure 1**). For the quantitative synthesis, 25 articles (Vinson et al., 1998; Bok et al., 1999; Gorinstein et al., 2007; Zulkhairi et al., 2010; Mollace et al., 2011; Ding et al., 2012; Kang et al., 2012; Terpstra et al., 2012; Kim et al., 2013; Lu et al., 2013; Raasmaja et al., 2013; Muhtadi et al., 2015; Dinesh and Hegde, 2016; Shin et al., 2016; Ashraf et al., 2017; Cai et al., 2017; Fayek et al., 2017; Chou et al., 2018; Feksa et al., 2018; Hase-Tamaru et al., 2019; Mir et al., 2019; Sato et al., 2019; Ke et al., 2020; Lee et al., 2020; Ling et al., 2020) were selected. The level of agreement among the reviewers was 0.470, being considered as moderate.

Tables 2 and **3** show the general characteristics and results of the preclinical studies, arranged in the chronological order of publication. **Table 4** present the experimental conditions and results of clinical trials also arranged in the chronological order.

The selected articles were published between 1998 and 2020, with a predominance of the number of publications in 2013 (n = 3), 2017 (n = 3), 2019 (n = 3), and 2020 (n = 3). These studies were conducted mainly in China (n = 6; 23.0%) and Korea (n = 5; 19.2%) followed by Italy (n = 2; 7.6%) and Japan (n = 2; 7.6%), in addition to other countries in which only 1 study was found as described in **Tables 1–3**.

In the 26 selected articles, 15 different species of *Citrus* were studied in a dyslipidemia model: *C. reticulata* (n = 4; 15.3%), *C. bergamia* (n = 3; 11.5%), *C. sinensis* (n = 3; 13.6%),

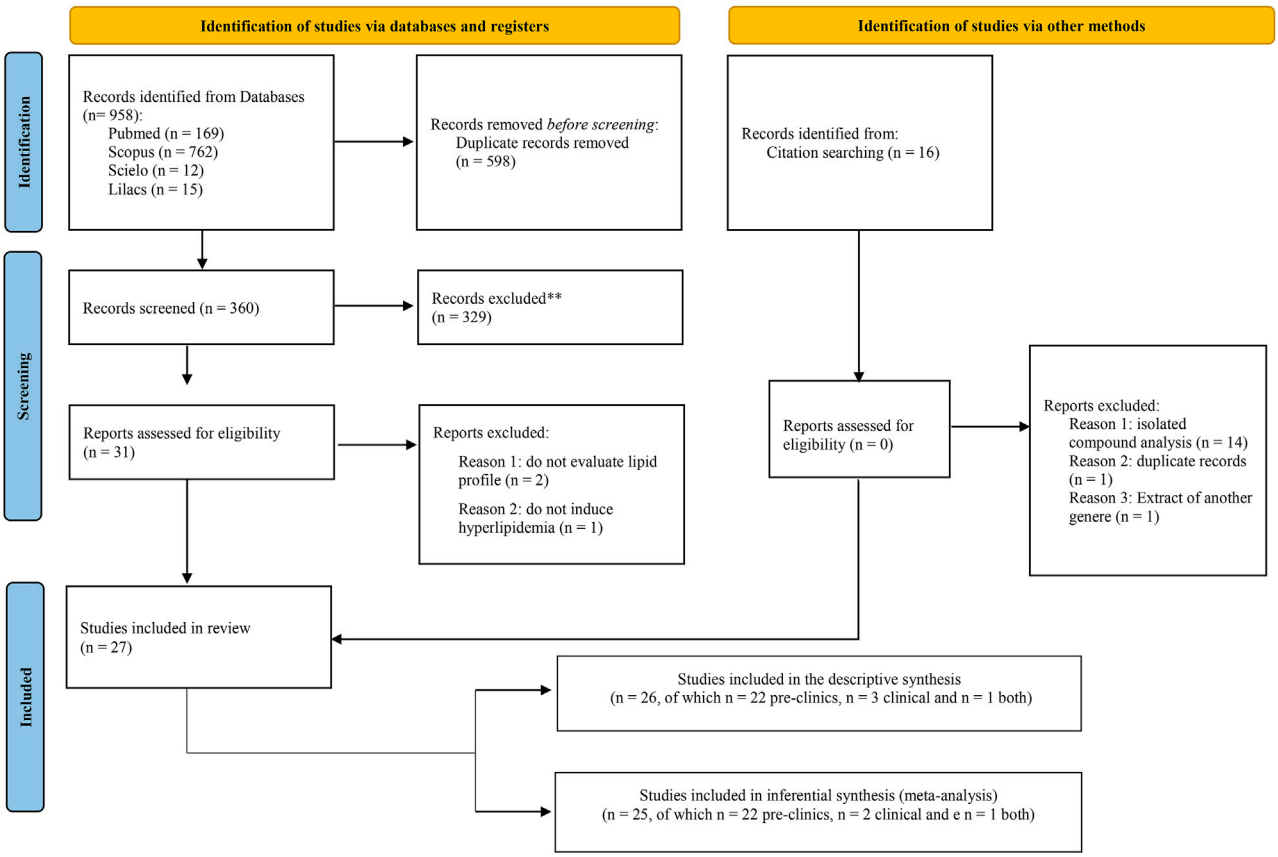

FIGURE 1 | Flowchart of the studies included in the qualitative and quantitative synthesis.

C. junos Tanaka (n = 2; 9.1%), *C. grandis* (L.) Osbeck also called *C. maxima* (n = 3; 11.5%), *C. paradise* also known as grapefruit (n = 2; 7.6%), *C. unshiu* (n = 2; 7.6%), *C. sunki* Hort. Ex Tanaka (n = 1; 3.8%), *C. aurantium* (n = 1; 3.8%), *C. mitis* (n = 1; 3.8%), *C. limon* (n = 1; 3.8%), *C. aurantiifolia* (n = 1; 3.8%), *C. ichangensis* (n = 1; 3.8%), *Poncirus trifoliata* x *Citrus sinensis* (n = 1; 3.8%), and *C. changshan-huyou* (n = 1; 3.8%). Among the *Citrus* species used in the preclinical studies, there was a predominance of six hybrid species in eight studies, followed by three orange species in eight studies and three types of lemons in four publications and tangerine species in four articles. In the clinical studies, on the other hand, there is a predominance of orange-based bergamot products (*C. bergamia*; n = 3 studies) and a study with supplements containing grapefruit (*C. paradise*).

\From these species, hydroalcoholic extracts or organic fractions (n = 20; 86.9%), aqueous extract (n = 1; 4.3%), and processed fruits (n = 3; 13.0%) were used, which were incorporated to the diet (n = 14; 60.8%) or administered orally by gavage (n = 9; 40.9%). In the clinical trials as a whole, supplementation with encapsulated dry extract was used or inclusion in the diet. In addition, 21 studies (80.7%) evaluated the chemical composition of the extracts, with a predominance of compounds belonging to the class of flavonoids, such as naringin, hesperidin, neoeriocitrin, neohesperidin, nobiletin, tangeretin, and naringenin (**Figure 2**).

As observed in **Table 1**, the method of inducing hyperlipidemia in the preclinical studies was by cholesterol-rich diet or cafeteria-type diet, conducted with rats (n = 12; 52.1%), mice (n = 8; 34.7%), and hamsters (n = 3; 13.0%). Among the randomized clinical trials (**Table 3**), the clinical conditions of the participants were in their entirety dyslipidemia (n = 4; 100%), associated or not with coronary disease (n = 1, 25%), and hypertension and glucose intolerance (n = 1; 25%). In the preclinical and clinical studies, the outcomes evaluated were the levels of total cholesterol (TC, n = 18; 100%), HDL (n = 14; 77.7%), LDL (n = 12; 66.7%), VLDL (n = 2; 13.3%), IDL (n = 1; 5.5%), and triglycerides (TG, n = 17; 94.4%).

From the analysis of the preclinical and clinical studies (**Tables 2–4**), it was found that the *Citrus* species were able to significantly alter the lipid profile in the 26 (100%) studies, decreasing serum total cholesterol (n = 25; 96.1%), LDL (n = 14; 53.8%), triglycerides (n = 17; 65.3%), and VLDL (n = 2; 7.6%) and increasing HDL (n = 4; 15.3%). In the liver, *Citrus* also reduced TC and TG (n = 6; 23.0%), lipid accumulation (n = 5; 19.2%), and weight (n = 2; 7.6%). These effects were accompanied by the maintenance (n = 1; 3.8%) of glutamic-oxaloacetic transaminase (GOT), glutamic-pyruvic transaminase (GPT), and alkaline phosphatase (ALP) serum levels or the

TABLE 1 | Detailed description of the preclinical studies of the effect of *Citrus* extract on hyperlipidemia included in the systematic review.

References, country	Extract, plant part, and species	Composition	Model	Evaluated parameters	Treatment protocol	Animal (n/group)
Vinson et al., 1998 (Vinson et al., 1998)	Hydroalcoholic extract of whole dried ripe fruits *C. aurantium*	25.7% ascorbic acid 9.9% flavonoids (quercetin, hesperidin, naringenin, and myricetin)	Hamster fed on a high-cholesterol diet	LDL, VLDL HDL, TC, TG, foam cell injury	Feed containing 3% of the extract or 4% of the extract associated with ascorbic acid	Male Golden Syrian
EUA		31.2% protein 3.2% ash 30% carbohydrates		in the aorta artery lipid peroxidation	(57 mmol/kg diet) daily, for 4 or 10 weeks	Hamsters (n = 10)
Bok et al., 1999 (Bok et al., 1999)	Hydroalcoholic extract of the peel *C. reticulata*	2.7 g of protein 1.8 g of fat	Rats fed on a high-cholesterol diet	Plasmatic and hepatic TC, TG, HDL, LDL AI[a], fecal neutral sterols, HMGR, and ACAT activities in liver tissue	16.7 g/100 g of diet for 6 weeks	Male Sprague Dawley rats (n = 10)
Korea		1.0 g of ash 20 g of fructose 16.5 g of glucose 8.6 g of sucrose 0.6 g of hesperidin 0.03 g of naringin and 9.67 g of other sugars				
Terpstra et al., 2002 (Terpstra et al., 2002)	Peels or waste stream material of *C. limon*	-	Hamster fed on a high-cholesterol diet	BW, FI, and liver weight	Diets containing 3% of cellulose or lemon peels or the waste stream of the lemon pectin extraction	Male hybrid
Netherlands				TC of plasma and liver Plasmatic TG, LDL, HDL, VLDL bile acids, and fecal sterols	for 8 weeks	F_1B Golden Syrian Hamster (n = 14)
Mollace et al., 2011 (Mollace et al., 2011)	Polyphenolic fraction of *C. bergamia* Risso & Poiteau peeled-off fruits	Neoeriocitrin (77,700 ppm), naringin (63,011 ppm), neohesperidin (72,056 ppm), melitidine (15,606 ppm), and brutieridine (33,202 ppm)	High-cholesterol diet-induced hyperlipemia	BW, TC, LDL, HDL	10 or 20 mg/kg daily (p.o.)	Male
Italy				TG and glucose Neutral sterols and fecal bile acids	for 30 days	Wistar Rats (n = 10)
Zulkhairi et al., (Zulkhairi et al., 2010)	Aqueous extract (5% and 10%) of dried whole fruits *C. mitis*	Phenolic compounds	Rats fed on a high-cholesterol diet	BW, TC, HDL, LDL, TG, AI[b], sdLDL[c]	5 mg/kg of extract at 5% and 10%	Male
Malaysia				Scavenging activity of DPPH radicals, reducing power, lipid peroxidation (*in vitro*)	daily (p.o.) for 10 weeks	Sprague Dawley rats (n = 6)
Ding et al., 2012 (Ding et al., 2012)	Hydroalcoholic extract of *C. ichangensis* peel	Naringin, hesperidin, poncirin, neoeriocitrin narirutin, neohesperidin, naringenin, nobiletin, and tangeretin	High-fat diet-induced Obese	BWG, FI TC, TG, LDL, HDL, and glucose	Diet supplemented with 1% of extract, for 8 weeks	Female C57BL/6 mice (n = 7)
China				Fecal and hepatic TC and TG; size of EWAT; mRNA expression of PPARγ, LXR, and them target genes in liver tissue		
Kang et al., 2012 (Kang et al., 2012)	Hydroalcoholic extract of *C sunki* peel	Tangeretin (55.13 mg/g) Nobiletin (38.83 mg/g)	High-fat diet-induced Obese	BWG, FI TC, TG, GPT, GOT, and LDH, EPAT weight, liver fat; p-AMPK, p-ACC, and adiponectin mRNA expression in EAT.	150 mg/kg/day of extract (p.o.) for 70 days	Male C57BL/6 mice (n = 10)

(Continued on following page)

TABLE 1 | (*Continued*) Detailed description of the preclinical studies of the effect of *Citrus* extract on hyperlipidemia included in the systematic review.

References, country	Extract, plant part, and species	Composition	Model	Evaluated parameters	Treatment protocol	Animal (n/group)
Korea		Hesperidin (17.11 mg/g)		In mature 3T3-L1 adipocytes: LKB1, AMPK, ACC, PKA, and HSL phosphorylation, CPT-1a gene expression, and glycerol release		
		Rutin (17.02 mg/g) Sinensetin (4.23 mg/g)				
Raasmaja et al., 2013 (Raasmaja et al., 2013)	Hydroalcoholic extract of *C. grandis* (L.) Osbeck whole fruits	Naringin at 19%	High-fat diet-induced	BWG, FI	300, 600, or 1,200 mg/kg (p.o.) daily	Female
Finland			Obese	TG, TC, HDL, glucose, insulin, ghrelin, GLP-1 PYY, leptin, and amylin in plasma	for 12 weeks	Zucker Rats (n = 10)
Lu et al.,	Hydroalcoholic extract of *Citrange* (*Poncirus trifoliata* x *C. sinensis*) peel or flesh and seed	Bark extract	High-fat diet-induced obese	BWG, FI, ipGTT, blood glucose, serum TG, TC, LDL and HDL, hepatic TG and TC	Diet supplemented with 1% w/w of peel extract	Female
2013 (Lu et al., 2013)		Neoeriocitrin (14.5 mg/g), naringin (8.12 mg/g), neohesperidin (21.1 mg/g), and poncirin (14.1 mg/g)		Fecal TC and TG, histological analysis	or 1% w/w of flesh and seed	C57BL/6 mice (n = 6)
China		Seed extract Poncirin (4.85 mg/g) Neohesperidin (1.87 mg/g) Naringin (0.87 mg/g)		of liver tissue mRNA levels of PPARγ, LXR, and their target genes in liver tissue	extract, daily for 8 weeks	
Kim et al.,	Hydroalcoholic extract of *C. junos* Tanaka peel	Hesperidin (36.3 mg/100 g)	High-fat diet-induced obese	BWG, FI	Diet supplemented with 1% and 5% of extract	Male
2013 (Kim et al., 2013)		Naringin (11.6 mg/100 g)		TC, TG, glucose, insulin, leptin, resistin, GOT, GPT, histological analysis of liver tissue	for 9 weeks	C57BL/6 J mice (n = 8)
Korea		Rutin (2.7 mg/100 g)		AMPK phosphorylation in muscle tissue		
		Quercetin (1.7 mg/100 g) and tangeretin (0.7 mg/100 g)		AMPK and PPARγ activation in C2C12 and HEK293 cells, respectively		
Muhtadi et al., 2015 (Muhtadi et al., 2015)	Hydroalcoholic extract of *C. sinensis* fruit peel	-	High-fat diet-induced hypercholesterolemia	TC; glucose in rats	125, 250, and 500 mg/kg (p.o.), daily for 2 weeks	Male
Indonesia				induced by alloxan monohydrate	After 4-week diet	Wistar rats (n = 5)
Dinesh and Hegde, 2016 (Dinesh and Hegde, 2016)	Hydroalcoholic extract of *C. maxim*a leaves	Flavonoids, alkaloids, carbohydrates, glycosides, saponins, and tannins	Cafeteria diet and Olanzapine-induced obesity	BWG, FI	200 and 400 mg/kg (p.o.), daily for 4 weeks	Female
India				TC, TG, HDL, LDL, VLDL, GOT, GPT, glucose Liver weight and TG		Wistar rats (n = 6)
Shin et al.,	Hydroalcoholic extract of *C. junos* Tanaka peel	-	Mice fed on a high-cholesterol diet	BWG, FI	Diet supplemented with 1% and 5% of the extract	Male
2016 (Shin et al., 2016)				TG, TC, HDL, GOT, GPT, ALP, histological analysis	for 10 weeks	C57BL/6 J mice (n = 8)
Korea				of liver tissue		

(Continued on following page)

TABLE 1 | (*Continued*) Detailed description of the preclinical studies of the effect of *Citrus* extract on hyperlipidemia included in the systematic review.

References, country	Extract, plant part, and species	Composition	Model	Evaluated parameters	Treatment protocol	Animal (n/group)
				Expression of PPARα, FAS, and HMGR in liver tissue Lipid accumulation and expression of p-AMPK, p-ACC, PPARα, CPT-1, and HMGR in HepG2 cells		
Ashraf et al., 2017 (Ashraf et al., 2017) Pakistan	Hydroalcoholic extract of *C. sinensis* peel	-	Rats fed on high-glucose or cholesterol-rich diet	BWG, FI TG, TC, LDL, HDL, glucose, insulin	Diet supplemented with 10% *Citrus* peel powder (functional) and 5% peel extract (nutraceutical), for 8 weeks	Male Sprague Dawley rats (n = 6)
Fayek et al., 2017 (Fayek et al., 2017) Egypt	Methanolic extract, hexanic extract, aqueous homogenate of *C. reticulata* (Mandarin), *C. sinensis* (sweet orange), *C. paradise* (white grapefruit), or *C. aurantiifolia* (lime) fruit peels	Nobiletin (%) in hexanic extracts Mandarin (10.14%) Sweet orange (3.6%) White grapefruit (0.9%) Lime (0.0045%) Pectin (%) in peel powder Sweet orange (21.33%) Lime (19.7%) While grapefruit (11.66%) Mandarin (9.14%)	Hypercholesterolemia induced by diet rich in cholesterol and bile salts	TC TG and glucose	0.1 ml of the corresponding extract (p.o.) for 8 weeks	Male Wistar rats (n = 6)
Chou et al., 2018 (Chou et al., 2018) China	Methanolic extract of *C. reticulata*	Narirutin (4.52 ± 0.31 mg/g), hesperidin (9.14 ± 0.32 mg/g), nobiletin (2.54 ± 0.07 mg/g) Tangeretin (1.67 ± 0.05 mg/g)	High-fat diet-induced obese	AST, ALT, triglyceride, total cholesterol, glucose, insulin, HOMA-IR	1% of the corresponding extract for 11 weeks	Male C57BL/6 J mice (n = 8)
Feksa et al., 2018 (Feksa et al., 2018) Brazil	Hydroalcoholic extract of leaves of *C. maxima*	Gallic acid, catechin, caffeic acid, epicatechin, rutin and isoquercetin, and the major compounds were caffeic acid (3.71 mg/g) and catechin (3.65 mg/g	High-fat diet and fructose	Blood count, AST, ALT, triglyceride, total cholesterol, LDL, HDL, glucose, urea, creatinine,	50 mg/kg	Male Wistar rats (n =
Mir et al., 2019 (Mir et al., 2019) Algeria	Hydroalcoholic extract of *C. latifolia*	-	Hypercholesterolemia induced by diet rich in cholesterol	triglyceride, and total cholesterol	1% of the corresponding extract for 4 weeks	Male Wistar rats (n = 10)
Sato et al., 2019 (Sato et al., 2019) Japan	*C. tumida* peel powder	Calorie (275 kcal), moisture (2.9 g), protein (7.4 g), fat (2.7 g), ash (4.9 g), carbohydrate (82.1 g), sugar (28.4 g), fiber (53.7 g), galacturonic acid (12.2 g), and sodium (4.3 mg)	High-fat diet	AST, ALT, triglyceride, total cholesterol, HDL-C, creatinine, albumin, calcium, and LDH	*C. tumida* peel powder 5% (w/w)	Male C57BL/6 J mice (n = 8)
Tamaru et al., 2019 (Hase-Tamaru et al., 2019) Japan	*C. unshiu* MARC lyophilized and powdered	76.1 g carbohydrate, 7.6 g crude protein, 0.7 g crude fat, 2.7 g ash, 12.9 g moisture, 40.9 g total fiber, 6.6 g total pectin, 14.4 g hesperidin, and 3.0 g narirutin	High-fat diet	Total cholesterol, triglycerides, free fatty acids, glucose, insulin, and leptin	2.5% 5.0%, or 10.0%	Sprague Dawley (SD) rats (n = 7)
Lee et al., 2020 (Lee et al., 2020) Korea	*C. unshiu*: dried extract (CPEW) and lyophilized (CPEF)	Hesperidin, narirutin, and synephrine	High-fat diet	AST, ALT, triglyceride, total cholesterol, and LDL-C	CPEW: 50 mg/kg; 100 mg/kg CPEF: 50 mg/kg; 100 mg/kg	Male SD rats (n = 8)
Ling et al., 2020 (Ling et al., 2020)	*C. changshan-huyou*	Naringin, narirutin, and neohesperidin	High-fat diet		PTFC: 25 mg/kg; 50 mg/kg; 100 mg/kg	

(Continued on following page)

TABLE 1 | (*Continued*) Detailed description of the preclinical studies of the effect of *Citrus* extract on hyperlipidemia included in the systematic review.

References, country	Extract, plant part, and species	Composition	Model	Evaluated parameters	Treatment protocol	Animal (n/group)
China				AST, ALT, triglyceride, total cholesterol, LDL-C, and HDL-C		Golden hamsters (n = 12)
Ke et al., 2020 (Ke et al., 2020) China	*C. reticulata* Blanco	Nobiletin (98.34 mg/g), heptamethoxyflavone (44.26 mg/g), tangeretin (26.20 mg/g), and isosinensetin (26.14 mg/g)	High-fat diet	Triglyceride, total cholesterol, LDL-C, and HDL-C	0.2 and 0.5% JZE	C57BL/6 J mice (n = 8)

glutamic p.o., intragastric gavage; TC, total cholesterol; TG, triglycerides; LDL, low-density lipoprotein; HDL, high-density lipoprotein; VLDL, very low-density lipoprotein; LDH, lactate dehydrogenase; GOT, -oxaloacetic transaminase; GPT, glutamic-pyruvic transaminase; EWAT, epididymal white adipose tissue; PPARγ, peroxisome proliferator-activated receptor γ; FAS, fatty acid synthase; ACO, acyl-CoA oxidase; LXRα, liver X receptor α; LXRβ, liver X receptor β; AMPK, AMP-activated protein kinase; ACC, acetyl-CoA carboxylase; PKA, cAMP-dependent protein kinase; HSL, hormone-sensitive lipase. GLP-1, glucagon-like peptide-1; PYY, pancreatic peptide YY; BWG, body weight gain; FI, food intake; ipGTT, intraperitoneal glucose tolerance test; ALP, alkaline phosphatase; FAS, fatty acid synthase receptor; CPT-1, carnitine palmitoyl transferase-1; HMGR, 3-hydroxy-3-methylglutaryl-coenzyme A reductase; EPAT, epididymal and perirenal adipose tissue; EAT, epididymal adipose tissue.

[a]*The duration of the experiment is not explicitly informed in the article. AI, atherogenic index.*

[b]*[(TC-HDL)/HDL].*

[c]*(LDL/HDL); sdLDL, small dense LDL, particle size.*

[d]*(TG/HDL).*

reduction of GOT, GPT (n = 2; 7.6%), and lactate dehydrogenase (LDH) (n = 1; 3.8%).

In addition, some *Citrus* products also reduced body weight gain (BWG; n = 7; 26.9%), food intake (FI; n = 1; 3.8%), and lipid accumulation in adipose tissue or cells (n = 3; 11.5%). In human, a study also demonstrated their effect on the reduction of waist circumference (WC), waist-to-hip ratio (WHR), and body mass index (BMI). Taken together, these effects can reduce the risk of atherosclerosis as shown in three studies (16.6%). However, its effects on the lipid excretion are still controversial, since two studies (11.0%) demonstrate increased excretion, two studies (11.0%) did not identify changes, and only one study (5.5%) found a reduction in excretion (**Table 3**). In parallel, some authors investigated the effect of *Citrus*-based products on glucose and their effects on blood glucose reduction (n = 8; 44.4%), insulin increase (n = 2; 11.0%), and glucose uptake in the cell (n = 1; 5.5%).

In addition, several targets involved in the energy and nutrient metabolism have been studied. As can be seen in **Table 3**, some species of *Citrus* demonstrated effects on peroxisome proliferator-activated receptor γ (PPARγ) and peroxisome proliferator-activated receptor α (PPARα), downmodulating fatty acid synthase (FAS), acyl-CoA oxidase (ACO), uncoupling protein 2 (UCP2), and adipocyte fatty-acid-binding protein (aP2), besides upregulating CD36 and acetyl-CoA carboxylase (ACC). They can also act on liver X receptor (LXR), reducing lipoprotein lipase (LPL), apolipoprotein E (ApoE), and cholesterol 7α-hydroxylase (CYP7A1) and increasing ATP-binding cassette transporter G1 (ABCG1) and ATP-binding cassette transporter A1 (ABCA1).

The adiponectin signaling pathway also can be involved in the lipid control. In fact, some *Citrus* products were able to increase adiponectin; stimulate the phosphorylation of LKB1, AMP-activated protein kinase (AMPK), ACC, and carnitine palmitoyl transferase-1 (CPT-1); and reduce HMGR and ACAT activities. Their effects on lipolysis were also observed by the upmodulation of cAMP-dependent protein kinase (PKA) and hormone-sensitive lipase (HSL), with increase in glycerol. Besides adiponectin, *Citrus* seems to act reducing other adipocytokines, as leptin and resistin, which regulate the appetite and glucose metabolism and have been associated with insulin resistance. Their effects were also observed in the hormones involved with satiety and hunger control, as leptin, glucagon-like peptide-1 (GLP-1), and ghrelin. Finally, the antioxidant potential of *Citrus* has also been demonstrated, which can offer benefits in reducing lipid oxidation and in the development of atheromatous plaques.

Methodological Quality/Risk of Bias

The 23 preclinical studies, using the criteria provided by the ARRIVE guidelines, were analyzed for methodological quality. The studies showed a percentage of adequacy varying between 50 and 92% (83.82 ± 10.77%), with a greater weakness in the quality of the methodological description of the studies (**Supplementary Table S2**).

As for the clinical studies included in this research and evaluated by the Cochrane list (**Figure 3**), all of them had blinding outcome evaluators and incomplete outcomes. In addition, 50% of the articles presented low risk of uncertain bias regarding the criteria of generating a random sequence, concealment of allocation, blinding of the participants, reporting of the selective outcome, and other sources of bias (conflict of interest, based on the source of funding for the study and method of determination of the sample size).

Meta-Analysis

For the meta-analysis, the preclinical studies measured the level of total cholesterol [n = 23; 100%; I^2 = 99.1% (98.9%; 99.2%)], triglycerides [n = 20; 87%; I^2 = 99.4% (99.3%; 99.5%)], LDL [n = 12; 52.2%; I^2 = 99.1% (98.9%; 99.3%)], and HDL [n = 14; 60.9%; I^2 = 93.4% (90.6%; 95.4%)]. As for the clinical studies, three clinical trials with 92, 98, and 237 participants were included in the

TABLE 2 | Outcomes of the preclinical studies included in this systematic review.

Reference	Experimental group (mmol/L)	Control group (mmol/L)	Summary of results
Vinson et al., (Vinson et al., 1998)	Baseline: TC: 5.84; HDL: 3.31; TG: 25.1	Baseline: TC: 10.3; HDL: 2.84; TG: 41.6	↓TC and TG
	10 weeks: TC: 6.88; HDL: 1.68; TG: 27.1	10 weeks: TC: 15.1; HDL: 1.48; TG: 55.9	↓ lipid peroxidation
			↓ atherosclerosis signals (↓ area and density of foam cells), without changing BW
Bok et al. (Bok et al., 1999)	Baseline	Baseline:	↓ plasma TC
	6 weeks: TC: 2.44; HDL: 0.61; TG: 1.22	6 weeks: TC: 3.8; HDL: 0.57; TG: 1.12	↓ hepatic TC and TG, without changing HDL, TG, and LDL plasmatic
			↓AI and cholesterol excretion
			↓ HMGR and ACAT activities
Terpstra et al. (Terpstra et al., 2002)	Baseline:	Baseline:	↓ plasma and liver TC, ↓ VLDL + LDL being more effective in ↓VLDL, without changing HDL, ↑ excretion of fecal neutral sterols and bile acids
	8 weeks (lemon peel): TC: 3.51	8 weeks (cellulose): TC: 4.21	without changing BW, FI, and liver weight
	8 weeks (waste stream): TC: 3.44		
Mollace et al. (Mollace et al., 2011)	Baseline:	Baseline:	↓TC, LDL, and TG, without changing BW, HDL and glucose
	30 days (10 mg): TC: 5.95; LDL: 4.49; HDL: 0.58; TG: 2.75	30 days: TC: 8.19; LDL: 6.04; HDL: 0.53; TG: 2.74	↑ fecal neutral sterols and bile acids
	30 days (20 mg): TC: 5.00; LDL: 3.90; HDL: 0.65; TG: 2.74		
Zulkhairi et al. (Zulkhairi et al., 2010)	Baseline (5%)	Baseline: TC: 1.75; LDL: 0.45; HDL: 0.85; TG: 0.54	↓ TC, LDL, TG
	TC: 1.73; LDL: 0.45; HDL: 1.34; TG: 0.76	4 weeks	↑ HDL
	Baseline (10%)	TC: 2.13; LDL: 0.93; HDL: 0.89; TG: 0.79	↓AI and sdLDL
	TC: 1.68; LDL: 0.49; HDL: 1.27; TG: 0.74		Antioxidant activity, without changing BW
	4 weeks (5%)		
	TC: 1.28; LDL: 0.27; HDL: 1.39; TG: 0.63		
	4 weeks (10%)		
	TC: 1.06; LDL: 0.23; HDL: 1.54; TG: 0.53		
Ding et al. (Ding et al., 2012)	Baseline:	Baseline:	↓ BWG
	8 weeks	8 weeks	↓TC and LDL plasmatic
	TC: 2.27; LDL: 0.35; HDL: 2.32; TG: 0.70	TC: 2.65; LDL: 0.46; HDL: 1.95; TG: 0.70	↓ hepatic TC, TG, glucose, and adipocyte size, without changing
			Plasmatic FI, HDL, and TG and
			fecal TC and TG
			↓ expression of PPARγ (↓FAS, ACO, and UCP2 and ↑ CD36) ↓ LXR α and β (↓ ApoE, CYP7A1, LPL, and ↑ABCA1)
Kang et al. (Kang et al., 2012)	Baseline:	Baseline:	↓ BWG without changing in FI
	70 days	70 days: TC: 4.63; TG: 1.56	↓ TC, TG, LDH, GOT, and GPT
	TC: 3.81; TG: 0.94		↓ weight and cell size of EPAT
			↓ liver fat
			↑ p-AMPK, p-ACC, p-LKB1, and adiponectin
			↑ glycerol release
			↑ p-PKA and p-HSL
Raasmaja et al. (Raasmaja et al., 2013)	Baseline (300 mg/kg)	Baseline	Tendency to ↓ TC, glucose, and TG and ↑ HDL
	TC: 3.72; HDL: 1.42; TG: 8.34	TC: 3.56; HDL: 1.67; TG: 7.31	↓ GLP-1 and reversing the ↓ of ghrelin, without changing BWG, FI
	Baseline (600 mg/kg)	12 weeks	PYY, leptin, insulin, and amylin
	TC: 3.13; HDL: 1.70; TG: 6.27	TC: 4.13; HDL: 0.52; TG: 15.76	
	Baseline (1,200 mg/kg)		
	TC: 3.59; HDL: 1.53; TG: 8.11		
	12 weeks (300 mg/kg)		
	TC: 4.23; HDL: 0.44; TG: 16.68		
	12 weeks (600 mg/kg)		
	TC: 3.62; HDL: 0.80; TG: 12.57		
	12 weeks (1,200 mg/kg)		
	TC: 4.36; HDL: 0.80; TG: 17.42		
Lu et al. (Lu et al., 2013)	Baseline	Baseline	↓ BWG

(Continued on following page)

TABLE 2 | (*Continued*) Outcomes of the preclinical studies included in this systematic review.

Reference	Experimental group (mmol/L)	Control group (mmol/L)	Summary of results
	8 weeks (peel) TC: 2.30; LDL: 0.36; HDL: 2.00; TG: 0.70 8 weeks (seed) TC: 2.43; LDL: 0.41; HDL: 1.87; TG: 0.74	8 weeks TC: 2.64; LDL: 0.41; HDL: 1.97; TG: 0.70	Improves glucose tolerance and insulin resistance ↓ serum glucose, TC, and LDL ↓ hepatic TC and TG, without changing FI, serum HDL, and fecal TC and TG ↓ PPARγ (↓ ap2, FAS); ↓ LXRβ (↓ LPL and ApoE and ↑ ABCG1) ↓ lipid accumulation in liver tissue
Kim et al. (Kim et al., 2013)	Baseline 9 weeks (1%) TC: 2.00; TG: 0.85 9 weeks (5%) TC: 1.91; TG: 0.76	Baseline: 9 weeks TC: 2.37; TG: 0.88	↓ BWG, glucose, TG, TC, insulin, leptin, and resistin ↑ glucose uptake ↓ liver tissue fat ↑ PPARγ and AMPK, without changing FI, GOT, and GPT
Muhtadi et al. (Muhtadi et al., 2015)	Baseline (125 mg/kg): TC: 4.31 Baseline (250 mg/kg): TC: 5.08 Baseline 500 (mg/kg): TC: 4.87 2 weeks (125 mg/kg): TC: 1.88 2 weeks (250 mg/kg): TC: 2.13 2 weeks (500 mg/kg): TC: 2.02	Baseline: TC: 3.77 2 weeks: TC: 3.27	↓ TC and glucose
Dinesh and Hegde (Dinesh and Hegde, 2016)	Baseline 4 weeks (200 mg/kg) TC: 79.76; LDL: 54.31; HDL: 40.68; TG: 104.3 4 weeks (400 mg/kg) TC: 75.77; LDL: 51.75; HDL: 43.22; TG: 98.05	Baseline: 4 weeks TC: 88.75; LDL: 74.71; HDL: 35.11; TG: 130.0	↓ BWG and FI ↓ TC, TG, LDL, and VLDL ↑ HDL ↓ GOT and GPT ↓ liver weight and TG ↓ glucose
Shin et al. (Shin et al., 2016)	Baseline: 10 weeks (1%) TC: 2.89; LDL: 1.81; HDL: 0.87 10 weeks (5%) TC: 2.96; LDL: 1.80; HDL: 0.80	Baseline: 10 weeks TC: 4.03; LDL: 3.03; HDL: 0.80	↓ BWG ↓ TC, LDL, GOT, GPT, ALP, without changing FI, HDL ↓ liver fat content and weight ↑ p-AMPK, p-ACC, PPARα, and CPT-1 expression ↓ FAS and HMGR expression ↓ lipid accumulation
Ashraf et al. (Ashraf et al., 2017)	Baseline (powder) TC: 3.34; HDL: 1.19; LDL: 1.67; TRI: 1.07 Baseline (extract) TC: 3.32; HDL: 1.21; LDL: 1.62; TRI: 1.05 8 weeks (powder) TC: 3.14; HDL: 1.21; LDL: 1.52; TRI: 1.01 8 weeks (extract) TC: 3.03; HDL: 1.24; LDL: 1.44; TRI: 0.97	Baseline TC: 3.30; HDL: 1.17; LDL: 1.63; TRI: 1.04 8 weeks TC: 3.81; HDL: 1.17; LDL: 1.85; TRI: 1.16	Tendency to ↓ BWG and FI ↓ TG, TC, and LDL ↑ HDL ↓ glucose and ↑ insulin
Fayek et al. (Fayek et al., 2017)	Baseline: Tangerine (alcoholic extract) TC: 2.00; TG: 0.78 Orange (alcoholic extract) TC: 3.25; TG: 0.94 Hybrid (alcoholic extract) TC: 3.95; TG: 0.85 Lime (alcoholic extract) TC: 5.47; TG: 0.51	Baseline: Diet TC: 3.92; TG: 2.66	Tendency to ↓ TC ↓ TG and glucose
Chou et al. (Chou et al., 2018)	Baseline: 11 weeks (1%) TC: 3.85; TG: 0.44	Baseline: 11 weeks (diet) TC: 4.68; TG: 0.85	Tendency to ↓ TC ↓ TG and insulin resistance
Feksa et al. (Feksa et al., 2018)	Baseline 45 days (50 mg/kg) TC: 2.12; TG: 2.84; HDL: 0.34; LDL: 0.61	Baseline: 45 days (diet): TC: 3.34; TG: 3.38; HDL: 0.47; LDL: 1.23	Tendency to ↓ TG, TC, and LDL
Mir et al. (Mir et al., 2019)	Baseline 4 weeks (1%)	Baseline: 4 weeks (diet)	Tendency to ↓ TG and TC

(Continued on following page)

TABLE 2 | (*Continued*) Outcomes of the preclinical studies included in this systematic review.

Reference	Experimental group (mmol/L)	Control group (mmol/L)	Summary of results
	TC: 3.8; TG: 0.9	TC: 5.9; TG: 1.8	
Sato et al. (Sato et al., 2019)	Baseline: 4 weeks (5%) TC: 3.31; TG: 0.28; HDL: 2.06	Baseline: 4 weeks (diet) TC: 4.39; TG: 0.41; HDL: 2.42	Tendency to ↓ TG and TC
Tamaru et al. (Hase-Tamaru et al., 2019)	Baseline: 4 weeks (2.5%) TC: 2.01; TG: 1.67 4 weeks (5%) TC: 2.22; TG: 1.63 4 weeks (10%) TC: 1.72; TG: 2.74	Baseline: 4 weeks (diet) TC: 2.27 TG: 2.00	Tendency to ↓ TG and TC ↓ free fatty acids, glucose, insulin, and leptin ↓ FAS, G6PDH in cytosol, and PAP in microsome
Lee et al. (Lee et al., 2020)	Baseline 8 weeks (CPEW 50 mg/kg): TC: 4.00; TG: 2.89; LDL: 2.58 8 weeks (CPEW 100 mg/kg): TC: 3.54; TG: 2.52; LDL: 2.27 8 weeks (CPEF 50 mg/kg): TC: 4.08; TG: 2.79; LDL: 2.56 8 weeks (CPEF 100 mg/kg): TC: 3.64; TG: 2.59; LDL: 2.37	Baseline: 8 weeks (diet): TC: 4.00; TG: 2.89; LDL: 2.58	Tendency to ↓ TG and TC
Ling et al. (Ling et al., 2020)	Baseline 4 weeks (25 mg/kg): TC: 32.00; TG: 10.20; HDL: 2.30; LDL: 11.41 4 weeks (50 mg/kg): TC: 22.30; TG: 5.30; HDL: 2.83; LDL: 9.83 4 weeks (100 mg/kg): TC: 21.70; TG: 5.30; HDL: 2.65; LDL: 8.67	Baseline: 4 weeks (diet) TC: 41.59; TG: 11.15; HDL: 4.95; LDL: 11.80	Tendency to ↓ TG, TC, and LDL-C
Ke et al. (Ke et al., 2020)	Baseline 4 weeks (0.2%): TC: 5.69; TG: 0.28; HDL: 4.10; LDL: 1.01 4 weeks (0.5%): TC: 5.04; TG: 0.28; HDL: 3.84; LDL: 0.81	Baseline: 4 weeks (diet) TC: 5.62; TG: 0.41; HDL: 4.20; LDL: 1.20	Tendency to ↓ TG, TC, and LDL-C

TC, total cholesterol; TG, triglycerides; LDL, low-density lipoprotein; HDL, high-density lipoprotein; VLDL, very low-density lipoprotein; BW, body weight; HMGR, 3-hydroxy-3-methylglutaryl-coenzyme A reductase; ACAT, acyl-CoA cholesterol acyltransferase; AI, atherogenic index; FI, food intake; BWG, body weight gain; PPARγ, peroxisome proliferator-activated receptor γ; FAS, fatty acid synthase; ACO, acyl-CoA oxidase; UCP2, uncoupling protein 2; CD36, cluster of differentiation 36; LXR, liver X receptor; ApoE, apolipoprotein E; CYP7A1, cholesterol 7α-hydroxylase; LPL, reducing lipoprotein lipase; ABCA1, ATP-binding cassette transporter A1; LDH, lactate dehydrogenase; GPT, glutamic-pyruvic transaminase; GOT, glutamic-oxaloacetic transaminase; AMPK, AMP-activated protein kinase; ACC, acetyl-CoA carboxylase; PKA; AMP-dependent protein kinase; HSL, hormone-sensitive lipase; PYY, pancreatic peptide YY; GLP-1, glucagon-like peptide-1; ABCG1, ATP-binding cassette transporter G1; ALP, alkaline phosphatase; CPT-1, carnitine palmitoyl transferase-1; G6PDH, glucose-6-phosphate dehydrogenase; PAP, phosphatidic acid phosphohydrolase in the microsome.

quantitative analyses, which were performed with patients with dyslipidemia and demonstrated the *Citrus* effects on the levels of total cholesterol [I^2 = 94.5% (87.3%; 97.6%)], triglycerides [I^2 = 95.6% (90.5%; 98.0%)], LDL [I^2 = 96.6% (93.0%; 98.4%)], and HDL [I^2 = 81.4% (42.2%; 94.0%)] (in both, n = 3; 100%).

The presentation of the forest graphs was distributed according to the results of the levels of total cholesterol, triglycerides, LDL, and HDL for preclinical and clinical studies. Through the global analysis of preclinical studies, a reduction of −1.08 mmol/L (95% CI: 1.23; −0.92; **Figure 4A**) was found in total cholesterol, equivalent to 41.76 mg/dL; a reduction of −0.50 mmol/L (95% CI: 0.69; −0.31; **Figure 4B**) was found in triglycerides, corresponding to 44.28 mg/dL; and a reduction of −0.71 mmol/L (95% CI: 0.97; −0.45; **Figure 4C**) was found in LDL, what represents 27.45 mg/dL. In addition, an increase of 0.11 mmol/L in the HDL levels was verified (95% CI: 0.05; 0.17; **Figure 4D**), equivalent to 4.25 mg/dL.

As illustrated in **Figure 5**, in the studies carried out on humans, the levels (mg/dL) of total cholesterol (MD = −42.03, 95% CI: 73.53; −10.52), triglycerides (MD = −62.41, 95% CI: 110.09; −14.73), and LDL (MD = −37.76, 95% CI: 69.45; −6.06) were reduced after treating patients with *Citrus* extracts. In addition, it was observed that these patients had increased HDL levels (MD = 5.85, 95% CI: 0.41; 11.28). Although a high heterogeneity has been observed (I^2 > 75%), the synthase of the results obtained with individual studies favors treatment to the control of serum lipids. After the analysis of subgroups, high heterogeneity was still verified and the sensitivity analysis did not change the result of the general analysis (data not shown).

DISCUSSION

This systematic review compiled data from 25 studies on the effects of *Citrus*-based products in the control of dyslipidemia. Based on the countries where the studies were carried out, most of them were developed in countries of Asia (such as Korea and China) and the European Union, in addition to United States and Egypt, which are among the biggest *Citrus* product makers in the world (FAS, 2018). In fact, countries that have greater production

TABLE 3 | Detailed description of the clinical studies of the effect of *Citrus* extract on hyperlipidemia included in the systematic review.

References/ country	Extract, plant part and species	Composition	Sample	Pathology	Parameters evaluated	Treatment protocol
Gorinstein et al., 2007 (Gorinstein et al., 2007) Israel	Fresh fruit peels of red grapefruit or blond grapefruit processed	Anthocyanins Red: 51.5 mg/100 g Blond: 49.3 mg/100 g Flavonoids (naringin) Red: 21.61 mg/100 g Blond: 19.53 mg/100 g Total fibers Red: 1.39 g/100 g Blond: 1.37 g/100 g	57 patients (39–72 years)	Hypertriglyceridemia and coronary disease	HR, BP, BW CT, LDL, HDL, TG, serum antioxidant activity by ABTS and TEAC	Daily supplementation with red or blond grapefruits associated with anti-atherosclerosis diet for 30 days (n = 19/group)
Mollace et al., 2011 (Mollace et al., 2011) Italy	Polyphenolic fraction of *C. bergamia* peeled-off fruits	Neoeriocitrin (77,700 ppm) Naringin (63,011 ppm) Neohesperidin (72,056 ppm) and melitidine (15,606 ppm) Brutieridine (33,202 ppm)	237 patients	Hyperlipemia associated or not with hyperglycaemia	TC, LDL, HDL, TG, reactive vasodilation	500 or 1,000 mg/day encapsulated with 50 mg ascorbic acid, for 30 days (n = 104–32/group)
Toth et al., 2016 (Toth et al., 2015) Italy	Bergavit® (Bergamot juice derived extract, *C. bergamia*)	150 mg of flavonoids 16% of neoeriocitrin 47% neohesperidin 37% naringin	80 individuals (42 men and 38 women)	Moderate hypercholesterolemia	TC, LDL, HDL, TG, VLDL, IDL, IMT, LDL size	150 mg/day for 6 months (n = 80)
Cai et al., 2017 (Cai et al., 2017) China	*C. bergamia* extract (CitriCholess®)	25% bioflavonoids, sterols and orange oil (820 mg/day), vitamin C (50 mg/day), vitamin B6 (20 mg/daily), B12 (2,000 μg/day), and folic acid (800 μg/day)	98 older people	Dyslipidemia and arterial hypertension and problems of glucose intolerance	TG, TC, LDL, HDL, glucose, BW, WC, HC, WHR, and BMI	500 mg/day for 12 weeks (n = 48–50/group)

Legend: TC, total cholesterol; TG, triglycerides; LDL, low-density lipoprotein; HDL, high-density lipoprotein; TEAC, Trolox-equivalent antioxidant capacity; HR, heart rate; BP, blood pressure; BW, body weight; IMT, carotid intima-media thickness; BW, body weight (kg); WC, waist circumference (cm); HC, hip circumference (cm); WHR, waist-to-hip ratio; BMI, body mass index.

of natural resources tend to explore their products more from a commercial and scientific point of view.

Through the scientific analyses compiled, we can also verify that species of the genus *Citrus* have the potential to reduce the serum levels of total cholesterol (TC), triglycerides (TGs), LDL, and VLDL and increase HDL. Consequently, *Citrus*-based products reduced the body weight, lipid accumulation, and atherosclerosis risk by the modulation of proteins and genes involved in the lipid metabolism. Recently, a study with a standardized extract containing *Citrus sinensis* L. Osbeck associated with *Citrus limon* (Chiechio et al., 2021) also demonstrated an effect in controlling the levels of total cholesterol and triglycerides as well as glycemia, possibly due to its composition rich in anthocyanins, flavonoids, and hydroxycinnamic acids, reinstating the high potential of *Citrus* species in lipid control.

These effects were studied mainly in the animal models of dyslipidemia induced by cholesterol- or high-fat diets. In these protocols, lipids ingested are initially degraded by intestinal lipase and, in enterocytes, TGs are resynthesized and associated with cholesterol and lipoproteins (ApoB-48, ApoE, and ApoC-II), forming chylomicrons. These distributed fatty acids between tissues and their remnants are metabolized in the liver. In this organ, fatty acid and glucose activate metabolic pathways for energy synthesis and storage, so that excess citrate is converted by citrate lyase (ACLY) into acetyl-CoA, which by the action of acetyl-CoA carboxylase (ACC) forms malonyl-CoA. This metabolic intermediate is used by the cell to produce fatty acid through the action of the enzymes Stearoyl-CoA Desaturase-1 (SCD1) and fatty acid synthase (FAS), in addition to downregulating CPT-1, an important transporter of Acil-Coa into the mitochondria which enables its β-oxidation. These fatty acids give rise to triglyceride molecules. In addition, acetyl-CoA can participate in the synthetic pathway of cholesterol, forming HMG-CoA which is converted into mevalonic acid by HMGR. This originates the free cholesterol molecule, which can be

TABLE 4 | Outcomes of the clinical studies included in this systematic review.

Reference	Experimental group (mg/dL)	Control group (mg/dL)	Summary of results
Gorinstein et al. (Gorinstein et al., 2007)	Baseline: Red TC: 258.70 LDL: 193.73 HDL: 52.59 TG: 149.68 Blond TC: 283.06 LDL: 217.32 HDL: 50.27 TG: 193.97	Baseline: TC: 306.26 LDL: 243.23 HDL: 46.20 TG: 205.49	Red: ↓ TC, LDL, and TG Blond: ↓ LDL only Both: ↑ serum antioxidant activity, without change in HR, BP, BW, HDL
Mollace et al. (Mollace et al., 2011)	Baseline (500 mg) TC: 286.00 LDL: 184.96 HDL: 34.55 TG: 266.87 Baseline (1,000 mg) TC: 279.40 LDL: 189.70 HDL: 32.78 TG: 270.11 After 30 days (500 mg) TC: 211.42 LDL: 132.79 HDL: 40.53 TG: 180.18 After 30 days (1,000 mg) TC: 201.99 LDL: 125.34 HDL: 46.00 TG: 157.48	Treated with capsules containing 500 mg of maltodextrin and 50 mg of ascorbic acid Baseline TC: 275.67 LDL: 186.31 HDL: 34.59 TG: 275.62 TC: 279.40 LDL: 185.64 HDL: 35.05 TG: 275.71	↓ TC, TG, and LDL ↑ HDL ↓ glucose ↑ reactive vasodilation
Toth et al. (Toth et al., 2015)	Baseline TC: 224.28 LDL: 143.07 HDL: 54.13 TG: 132.86	Baseline: TC: 255.22 LDL: 177.88 HDL: 50.27 TG: 159.43	↓ TC, LDL, TG, and IMT ↑ HDL, IDL, and LDL size without changing VLDL
Cai et al. (Cai et al., 2017)	Baseline TC: 211.13 LDL: 131.09 HDL: 49.88 TG: 192.20 500 mg TC: 198.76 LDL: 121.03 HDL: 50.27 TG: 162.09	Baseline TC: 217.32; LDL: 138.43; HDL: 51.81; TG: 170.94 TC: 210.36 LDL: 132.63 HDL: 52.20; TG: 172.71	↓ LDL ↓ BW, WC, WHR, and BMI without changing TG, TC, HDL, glucose, HC

Legend: TC, total cholesterol; TG, triglycerides; LDL, low-density lipoprotein; HDL, high-density lipoprotein; TEAC, Trolox-equivalent antioxidant capacity; HR, heart rate; BP, blood pressure; BW, body weight; IMT, carotid intima-media thickness; BW, body weight (kg); WC, waist circumference (cm); HC, hip circumference (cm); WHR, waist-to-hip ratio; BMI, body mass index.

esterified by acyl-CoA:cholesterol acyltransferase (ACAT) or converted into bile acids by CYP7A1. TG, free cholesterol, and cholesterol ester conjugate with lipoproteins (ApoE, ApoC-II, and ApoB-100) constituting the VLDL molecule (TGs > cholesterol). This lipoprotein distributes fatty acids to tissues by the action of lipoprotein lipase (LPL) and becomes IDL (TGs ≈ cholesterol, ApoB-100, ApoE) and later LDL (TGs, < cholesterol, ApoB-100). That way, high-lipid diets increase the plasmatic concentrations of TG, TC, VLDL, IDL, and LDL (DiNicolantonio and O'Keefe, 2018; Andreadou et al., 2020). These mechanisms can be observed in **Figure 6** (black lines).

Through this review, it was found that the effect of *Citrus*-based products on the release of adipocytokines and their signaling pathways has been studied. These molecules are produced by adipose tissue and control several metabolic pathways, in addition to affecting the state of hunger and

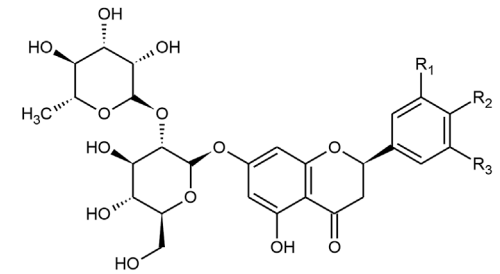

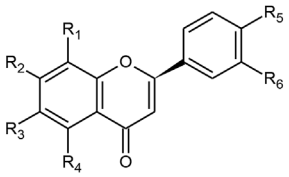

Naringin	R_1= H; R_2= OH; R_3= H	Nobiletin	R_1= OCH_3; R_2= OCH_3; R_3= OCH_3; R_4= OCH_3; R_5= OCH_3; R_6= OCH_3
Neohesperidin	R_1= H; R_2= OCH_3; R_3= OH	Tangeritin	R_1= OCH_3; R_2= OCH_3; R_3= OCH_3; R_4= OCH_3; R_5= OCH_3; R_6= H
Neoeriocitrin	R_1= OH; R_2= OH; R_3= H	Naringenin	R_1= H; R_2= OH; R_3= H; R_4= OH; R_5= OH; R_6= H

FIGURE 2 | Chemical structure of the main flavonoids found in *Citrus*.

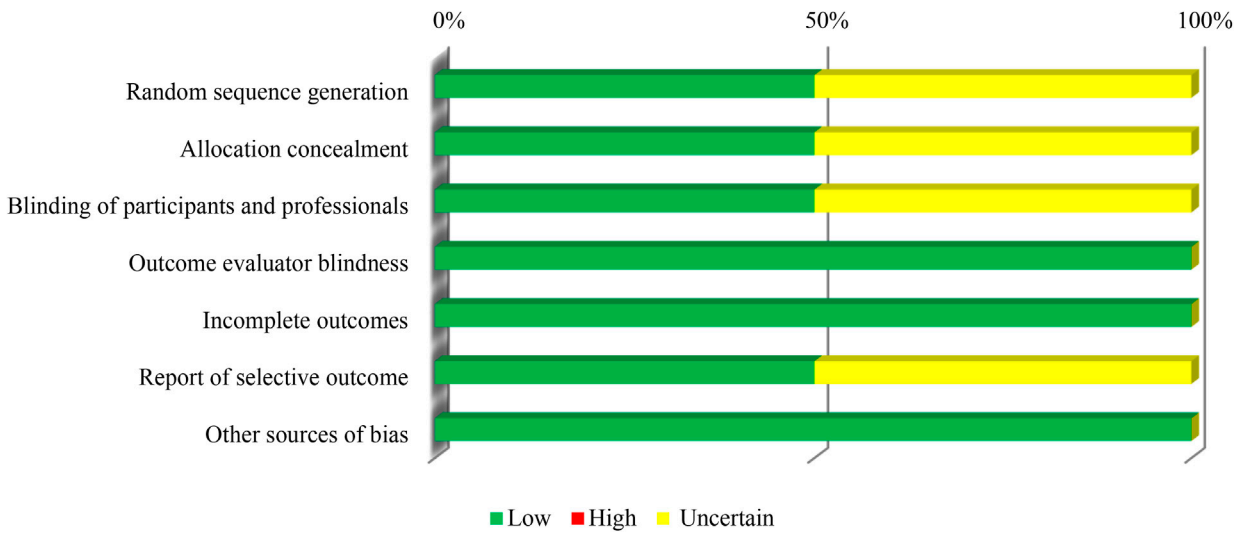

FIGURE 3 | Methodological quality of clinical trials included.

satiety and being related to the development of coronary diseases and metabolic disorders (Cao, 2014). *Citrus* products reduce adiponectin (Kang et al., 2012), whose action on specific receptors (AdipoR) increases the phosphorylation of LKB1 and AMPK (Kang et al., 2012; Shin et al., 2016). It negatively modulates ACC (Kang et al., 2012; Shin et al., 2016), reducing malonyl-Coa levels and, consequently, increasing CPT-1 (Shin et al., 2016); in addition, it decreases the HMGR activity (Bok et al., 1999; Shin et al., 2016) and modulates genes like LXR (Ding et al., 2012; Lu et al., 2013) and PPAR (Kim et al., 2013; Shin et al., 2016; Lu et al., 2018). Through these genes, *Citrus* regulates several protein targets involved in lipogenesis (FAS, aP2, ACC) (Ding et al., 2012; Lu et al., 2013; Shin et al., 2016), lipoprotein formation and metabolism (ApoE, LPL) (Ding et al., 2012; Lu et al., 2013), cholesterol metabolism (CYP7A1) (Ding et al., 2012), and cholesterol and lipid efflux (ABCG1 and ABCA1) (Ding et al., 2012; Lu et al., 2013). At the same time, its ability to stimulate the PKA-HSL pathway has also been observed (Kang et al., 2012), increasing the degradation of TG in glycerol and fatty acid, in addition to reducing the activity of ACAT (Bok et al., 1999), which contributes to the reduction of cholesterol ester levels. It is worth mentioning that bio-products based on *Citrus* help in glycemic control (Mollace et al., 2011; Ding et al., 2012; Kim et al., 2013; Lu et al., 2013; Raasmaja et al., 2013; Muhtadi et al., 2015; Dinesh and Hegde, 2016; Ashraf et al., 2017; Fayek et al., 2017), possibly by reducing resistin (Kim et al., 2013), an adipocytokine whose increase has been associated with insulin resistance, atherosclerosis, oxidative stress, and inflammation. All of these molecular events result in decreased lipogenesis and increased lipid oxidation, contributing to the control of the lipid profile (**Figure 6**).

However, some results seem contradictory, such as the effect of *Citrus* in reduction of the mRNA levels of PPARγ target genes, including ACO and UCP2 in the liver tissue (Ding et al., 2012).

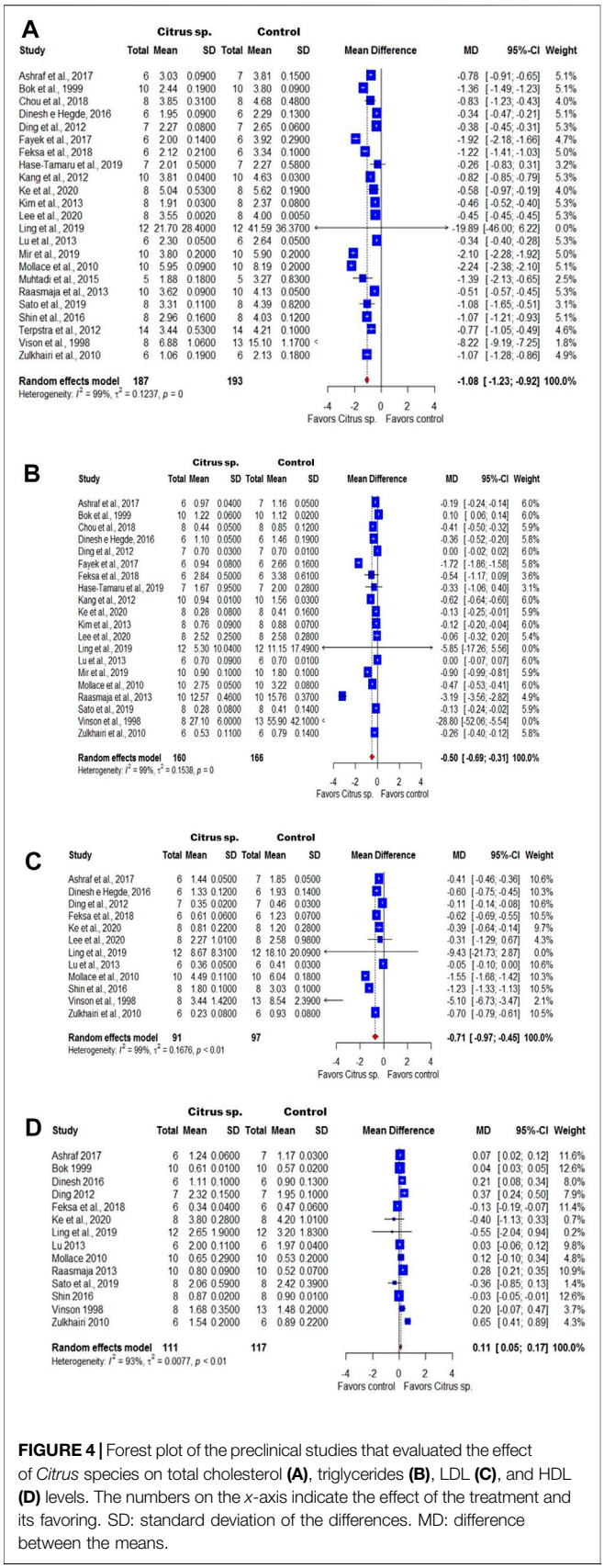

FIGURE 4 | Forest plot of the preclinical studies that evaluated the effect of *Citrus* species on total cholesterol **(A)**, triglycerides **(B)**, LDL **(C)**, and HDL **(D)** levels. The numbers on the *x*-axis indicate the effect of the treatment and its favoring. SD: standard deviation of the differences. MD: difference between the means.

ACO is the first enzyme of peroxisomal β-oxidation which will reduce the accumulation of lipids in the liver and promote its excretion (Ferdinandusse et al., 2007). On the other hand, UCP2 is an uncoupling protein which acts as a carrier of protons present in the inner membrane of mitochondria and contributes to thermogenesis, being a positive factor for the prevention of obesity (Brand and Esteves, 2005). Thus, upregulation of these mRNAs would contribute to the observed outcomes. However, the absence of baseline conditions for these targets makes it difficult to understand these data, so further studies are needed to elucidate this mechanism.

Similarly, *Citrus* seems to increase CD36 (Ding et al., 2012), the fatty acid translocase protein that facilitates the transport of fatty acids, the hepatic uptake of fatty acids, and the accumulation of fat and has a high affinity for binding with the oxidized LDL molecule, increasing the inflammatory activity and being a main condition for the development of atherosclerosis and thrombosis (Pepino et al., 2014). However, the correlation with the observed outcomes also needs to be further investigated, since the experimental conditions of the study do not allow a thorough analysis of this target in the experimental model used, as well as in the primary outcome studied.

It is also worth noting that some studies have shown that *Citrus* can help control hunger promoting the modulation of ghrelin. Known as "Hunger Hormone," this peptide is produced by endocrine cells present in the stomach and acts in the control of hunger, adiposity, and glucose- and energy-homeostasis, among other functions (Pradhan et al., 2013). More over, *Citrus* also downregulates leptin and GLP-1 levels, which are involved with satiety control. Leptin, a hormone produced by adipose tissue, plays an important role in the control of energy homeostasis, the excess and resistance of which are associated with obesity, leading to failures in the signaling mechanisms associated with decreased nutrition and body weight control (Pan and Myers, 2018). On the other hand, glucagon-like peptide 1 (GLP-1) is a gut hormone that promotes satiety; potentiates insulin release and suppression of glucagon release in response to nutrient intake; and decreases postprandial plasma levels of glucose (Andersen et al., 2018). Thus, the effects observed for *Citrus* in the reduction of GLP-1 may be related to overnight fasting or long-term regulation of eating and energy metabolism, requiring further investigation.

The notations are as follows: ABCA1: ATP-binding cassette transporter A1; ABCG1: ATP-binding cassette transporter G1; ACAT: acyl-CoA:cholesterol acyltransferase; ACC: acetyl-CoA carboxylase; ACLY: citrate lyase; ACO: acyl-CoA oxidase; AdipoR: adiponectin receptor; AMPK: AMP-activated protein kinase; aP2: adipocyte fatty-acid-binding protein; ApoB-100: apolipoprotein B-100; ApoC-II: apolipoprotein C2; ApoE: apolipoprotein E; CD36: cluster of differentiation 36; CPT-1: carnitine palmitoyl transferase-1; CYP7A1: cholesterol 7α-hydroxylase; FAS: fatty acid synthase; GLUT 4: glucose transporter 4; HMGR: 3-hydroxy-3-methylglutaryl-coenzyme A reductase; HSL:

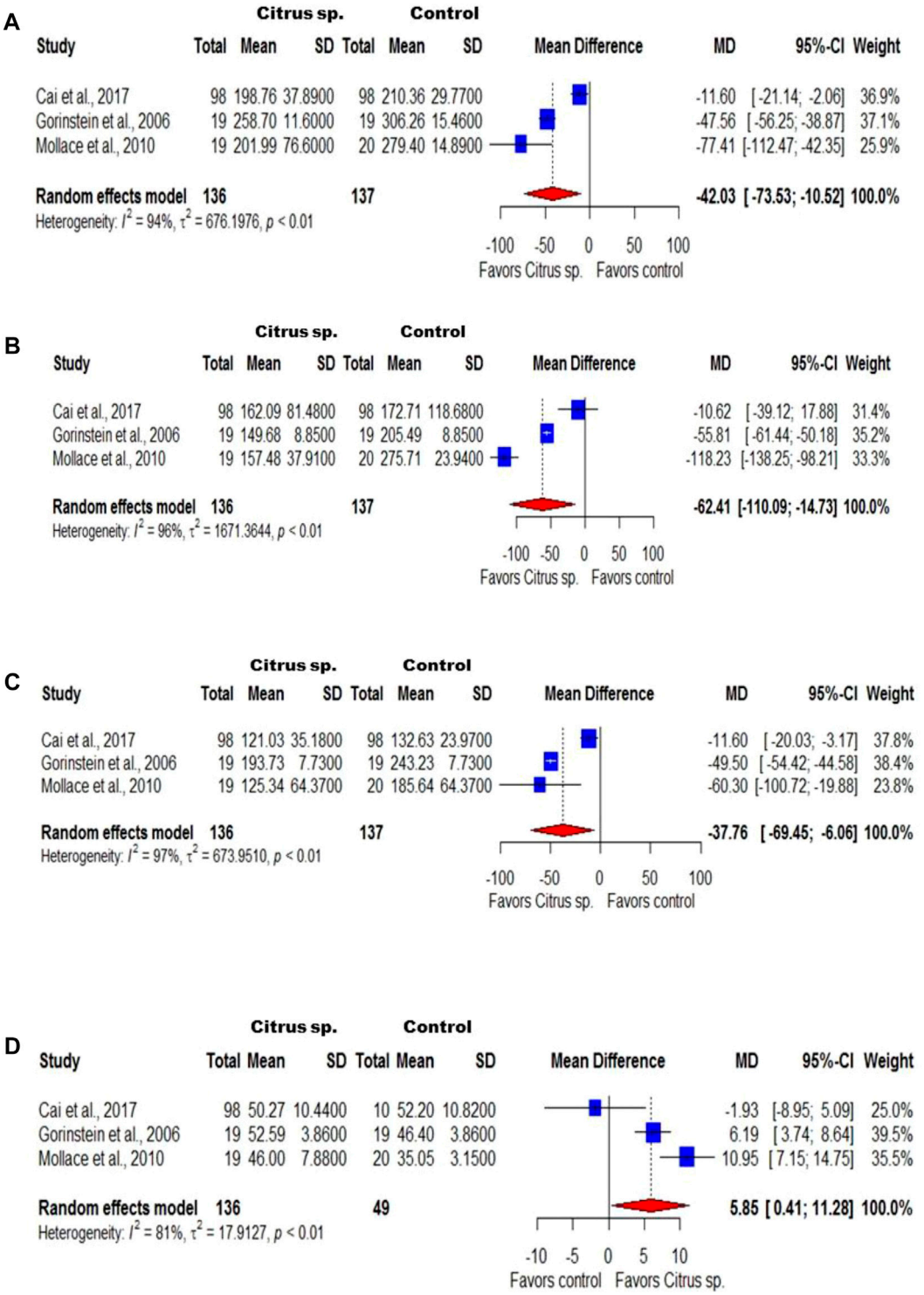

FIGURE 5 | Forest plot of the clinical studies that evaluated the effect of *Citrus* species on total cholesterol **(A)**, triglyceride **(B)**, LDL **(C)**, and HDL **(D)** levels. The numbers on the *x*-axis indicate the effect of the treatment and its favoring. SD: standard deviation of the differences. MD: difference between the means.

hormone-sensitive lipase; IDL: intermediate low-density lipoprotein; LDL: low-density lipoprotein; LKB1: liver kinase B1; LPL: lipoprotein lipase; LXR: liver X receptor; p-ACC: phosphorylated acetyl-CoA carboxylase; PKA: cAMP-dependent protein kinase; PPAR: peroxisome proliferator-activated receptor; SCD1: Stearoyl-CoA

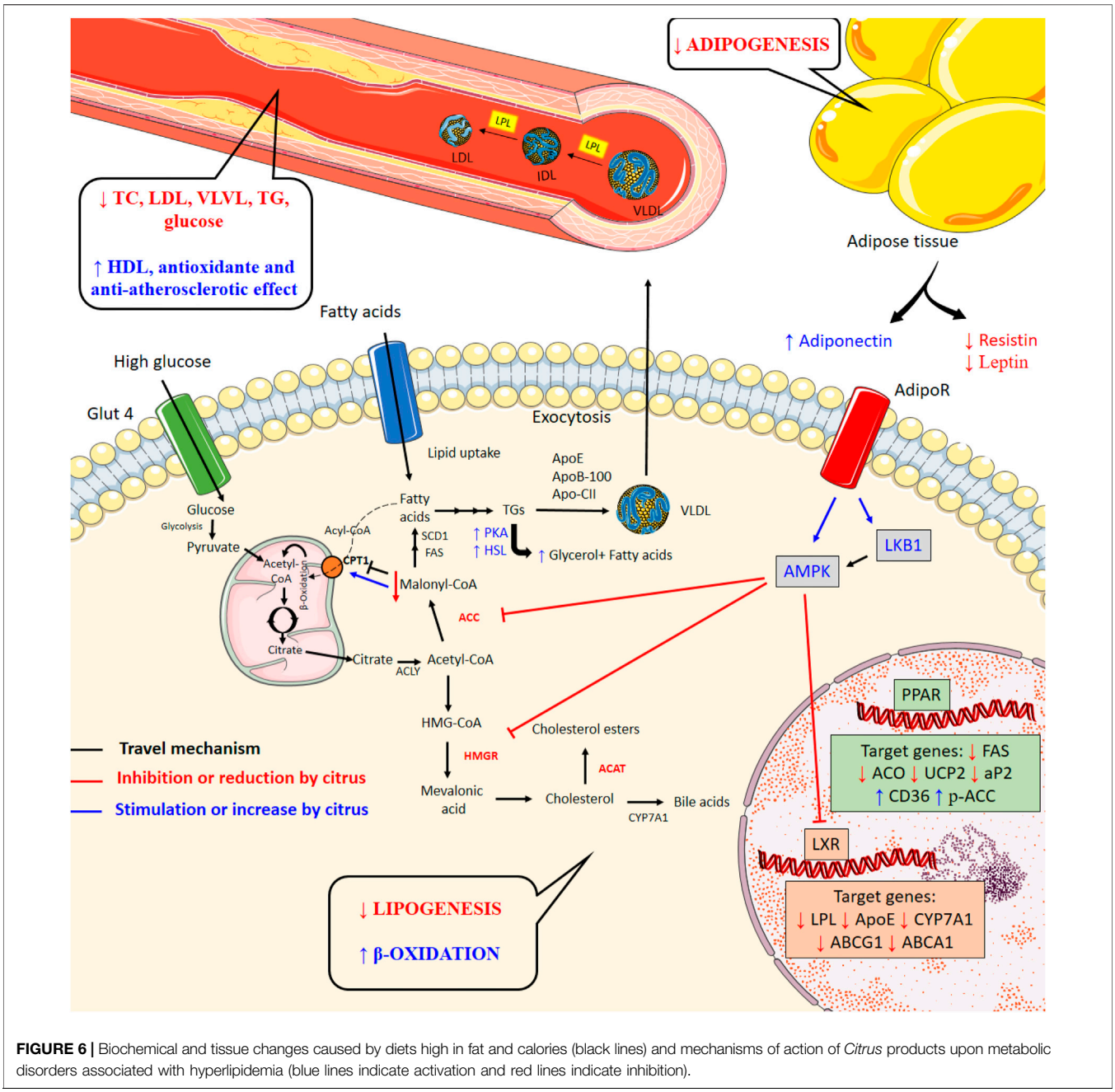

FIGURE 6 | Biochemical and tissue changes caused by diets high in fat and calories (black lines) and mechanisms of action of *Citrus* products upon metabolic disorders associated with hyperlipidemia (blue lines indicate activation and red lines indicate inhibition).

Desaturase-1; TC: total cholesterol; TGs: triglycerides; UCP2: uncoupling protein 2; VLDL: very low-density lipoprotein.

The effects of *Citrus* bioproducts on the lipid profile may be related to the presence of bioactive compounds, with emphasis on the flavonoids, such as naringin, hesperidin, neohesperidin, neoeriocitrin, nobiletin, tangeretin, and naringenin as compiled in this review. In fact, these compounds are believed to play a very significant role in reducing the levels of total cholesterol, triglycerides, and LDL (Mulvihill and Huff, 2012; Assini et al., 2013; Kou et al., 2017; Zeka et al., 2017). Several studies have shown that naringin reduces the HMGR activity more potently than does vitamin E (Choi et al., 2001; Lee et al., 2001), as well as decreasing the action of ACAT (Kim et al., 2006), which contributed to hypocholesterolemic action and higher excretion of fecal sterols (Jeon et al., 2004). Similarly, hesperidin reduces plasma cholesterol in hypercholesterolemic rats by decreasing ACAT and HMGR (Lee et al., 1999; Lee et al., 2012) besides changing the expressions of genes encoding PPARs and the LDL receptor (Akiyama et al., 2009). A recent study demonstrated that neohesperidin is also able to regulate the lipid metabolism *in vivo* and *in vitro via* FGF21 and AMPK/SIRT1/PGC-1α signaling axis (Wu et al., 2017). Furthermore, the non-glycoside *Citrus* flavonoid, naringenin, stimulates the hepatic fatty acid oxidation *via* PPARγ and prevents lipogenesis in both the liver and the muscle, reducing the serum lipid levels (Mulvihill et al., 2009).

In this review, we also observed that the *Citrus* products act by reducing the atherogenic index or tissue manifestations associated with atherosclerosis (Vinson et al., 1998; Bok et al., 1999; Zulkhairi et al., 2010). In fact, the polyphenolic compounds and flavonoids found in the *Citrus* species have antioxidant (Vinson et al., 1998; Gorinstein et al., 2007; Zulkhairi et al., 2010; Craft et al., 2012) and anti-inflammatory properties, in addition to their ability to decrease LDL levels, inhibiting the formation of atherosclerotic plaques (Tripoli et al., 2007; Assini et al., 2013; Onakpoya et al., 2017). Naringin, for example, reduces plaque progression once it decreases non-high-density lipoprotein cholesterol concentrations and biomarkers of endothelial dysfunction and inhibits the expression of ICAM-1 in endothelial cells, preventing immune cell adhesion and infiltration in the vascular wall (Choe et al., 2001; Chanet et al., 2012).

Confirming the results of the systematic review, the meta-analysis of preclinical studies indicated that *Citrus* products reduce the total cholesterol, triglycerides, and LDL levels by −41.76, −44.28, and −27.45 mg/dL, respectively, while increasing the HDL levels by 4.25 mg/dL. Similar results were observed in the clinical studies, in which the *Citrus* species induce a reduction in the total cholesterol, triglycerides, and LDL levels by −42.03, −62.41, and −37.76 mg/dL, respectively, whereas the HDL levels increased by an average of 5.85 mg/dL.

In the meta-analysis published by Onakpoyaa et al. (2015) (Onakpoya et al., 2017), performed with two clinical trials about the effect of grapefruits on the lipid profile, significant effects were observed only for the increase in HDL, without TC and LDL changes. More recently, a meta-analysis published by Kou et al. (2017) showed that the sizes of effect measures for LDL and total cholesterol presented significant results in the group of patients treated with *Citrus* juice, without considerable changes in HDL and TG levels. The divergence between the results presented in our meta-analysis compared to those previously published is justified by the broader scope of our question, as well as the inclusion of more recent studies, which have confirmed the contribution of *Citrus*-based products in the control of blood lipids.

Through the analysis of the risk of bias, it can be observed that the preclinical studies have a satisfactory average score, with some limitations in the methodological description of the studies and the results. Similarly, clinical studies had limitations in reporting or methodology in terms of blinding, allocation, randomization, and reporting of results. The use of tools to assess the risk of bias in the studies included in the systematic reviews has been widely well supported by groups such as SYRCLE (Hooijmans et al., 2014), ARRIVE (Kilkenny et al., 2010), and Cochrane (Cochrane Training, 2019), since the credibility of the results and the strength of the evidence depend on the methodological criteria of the studies (Busch et al., 2020).

Thus, although the results obtained are favorable to the treatment with *Citrus* extracts, the methodological limitations and high heterogeneity of the studies included in the meta-analysis weaken the evidence about the real benefits of this intervention. In addition, the studies do not provide information on effective dose, bioavailability, efficacy, and safety. These parameters are required to propel the use of these promising therapeutic agents into the clinical area. For this reason, further studies are needed to strengthen the evidence of the effects of *Citrus* on dyslipidemia.

This systematic review presents as limitations the low evidence found due to the high variability of the studies and variation of the methodological protocols of the articles. Among them, we can mention the differences in the induction of dyslipidemia, routes of administration, and types of extracts, besides the absence of baseline serum levels of lipids for comparison after the induction and inconclusive report. Finally, as in our review, of the 25 studies included in the meta-analysis, only 3 presented results in humans; we chose not to use the GRADE system. For this reason, we believe that further clinical studies are needed to provide sufficient scientific support to measure the effectiveness of *Citrus* effects on dyslipidemia.

CONCLUSION

From the compilations of the studies, one can suggest that the *Citrus* extract has a potential effect in dyslipidemia control, both in the preclinical studies and clinical trials. These effects can be associated with the presence of bioactive compounds, as flavonoids, which act synergistically through several pathways, causing inhibition of lipogenesis and activating β-oxidation. However, due to the high heterogeneity of the reposted findings, further studies are needed to increase the strength of clinical evidence of the action of *Citrus* extracts on the control of dyslipidemia and increase the strength of that evidence.

DATA AVAILABILITY STATEMENT

The original contributions presented in the study are included in the article/**Supplementary Material**; further inquiries can be directed to the corresponding author.

AUTHOR CONTRIBUTIONS

Ideation and preparation of the review: BC and AG; search and selection of studies: BC and LN; third evaluation for discrepancy analysis: AG; qualitative data extraction: BC, LN, and JN; quantitative data extraction: BC and VG; meta-analysis: BC, VG, and PZ; writing and finalizing the review: BC, DT, and AG.

FUNDING

The authors acknowledge grants from the Foundation for Support of Research and Technological Innovation of the State of Sergipe (*Fundação de Apoio à Pesquisa e Inovação Tecnológica do Estado de Sergipe: FAPITEC/SE*, EDITAL CAPES/FAPITEC/SE N° 10/2016 – PROMOB 1995/2017), National Council for Scientific and Technological Development (*Conselho Nacional de Desenvolvimento Científico e Tecnológico: CNPq*/Brazil), Coordination for the Improvement of Personnel Higher Education (*Coordenação de Aperfeiçoamento de Pessoal de Nível Superior: CAPES*/Brazil), and Federal University of Sergipe.

ACKNOWLEDGMENTS

We are grateful for the support given by Patrícia K. Ziegelmann in the elaboration of the meta-analysis and to teacher Abilio Borghi for the assistance with English language review.

SUPPLEMENTARY MATERIAL

The Supplementary Material for this article can be found online at: https://www.frontiersin.org/articles/10.3389/fphar.2022.822678/full#supplementary-material

REFERENCES

Abid, H., Abid, Z., and Abid, S. (2021). Atherogenic Indices in Clinical Practice and Biomedical Research: A Short Review. *Baghdad J. Biochem. Appl. Biol. Sci.* 2 (02), 60–70. doi:10.47419/bjbabs.v2i02.52

Adel Mehraban, M. S., Tabatabaei-Malazy, O., Rahimi, R., Daniali, M., Khashayar, P., and Larijani, B. (2021). Targeting Dyslipidemia by Herbal Medicines: A Systematic Review of Meta-Analyses. *J. Ethnopharmacology* 280, 114407. doi:10.1016/j.jep.2021.114407

Akiyama, S., Katsumata, S., Suzuki, K., Nakaya, Y., Ishimi, Y., and Uehara, M. (2009). Hypoglycemic and Hypolipidemic Effects of Hesperidin and Cyclodextrin-Clathrated Hesperetin in Goto-Kakizaki Rats with Type 2 Diabetes. *Biosci. Biotechnol. Biochem.* 73 (12), 2779–2782. doi:10.1271/bbb.90576

Alam, M., Kauter, K., and Brown, L. (2013). Naringin Improves Diet-Induced Cardiovascular Dysfunction and Obesity in High Carbohydrate, High Fat Diet-Fed Rats. *Nutrients* 5 (3), 637–650. doi:10.3390/nu5030637

Andersen, A., Lund, A., Knop, F. K., and Vilsbøll, T. (2018). Glucagon-like Peptide 1 in Health and Disease. *Nat. Rev. Endocrinol.* 14 (7), 390–403. doi:10.1038/s41574-018-0016-2

Andreadou, I., Schulz, R., Badimon, L., Adameová, A., Kleinbongard, P., Lecour, S., et al. (2020). Hyperlipidaemia and Cardioprotection: Animal Models for Translational Studies. *Br. J. Pharmacol.* 177 (23), 5287–5311. doi:10.1111/bph.14931

Ashraf, H., Butt, M. S., Iqbal, M. J., and Suleria, H. A. R. (2017). Citrus Peel Extract and Powder Attenuate Hypercholesterolemia and Hyperglycemia Using Rodent Experimental Modeling. *Asian Pac. J. Trop. Biomed.* 7 (10), 870–880. doi:10.1016/j.apjtb.2017.09.012

Assini, J. M., Mulvihill, E. E., and Huff, M. W. (2013). Citrus Flavonoids and Lipid Metabolism. *Curr. Opin. Lipidol.* 24 (1), 34–40. doi:10.1097/MOL.0b013e32835c07fd

Atmosudigdo, I. S., Lim, M. A., Radi, B., Henrina, J., Yonas, E., Vania, R., et al. (2021). Dyslipidemia Increases the Risk of Severe COVID-19: A Systematic Review, Meta-analysis, and Meta-regression. *Clin. Med. Insights*: Endocrinol. Diabetes 4, 1–7. doi:10.1177/1179551421990675

Ballard, C. R., Galvão, T. F., Cazarin, C. B. B., and Maróstica, M. R. (2019). Effects of Polyphenol-Rich Fruit Extracts on Diet-Induced Obesity in Rodents: Systematic Review and Meta-Analysis. *Curr. Pharm. Des.* 25 (32), 3484–3497. doi:10.2174/1381612824666190101701000

Bok, S. H., Lee, S. H., Park, Y. B., Bae, K. H., Son, K. H., Jeong, T. S., et al. (1999). Plasma and Hepatic Cholesterol and Hepatic Activities of 3-Hydroxy-3-Methyl-Glutaryl-CoA Reductase and Acyl CoA: Cholesterol Transferase Are Lower in Rats Fed Citrus Peel Extract or a Mixture of Citrus Bioflavonoids. *J. Nutr.* 129 (6), 1182–1185. doi:10.1093/jn/129.6.1182

Brand, M. D., and Esteves, T. C. (2005). Physiological Functions of the Mitochondrial Uncoupling Proteins UCP2 and UCP3. *Cell Metab* 2 (2), 85–93. doi:10.1016/j.cmet.2005.06.002

Busch, L. M., Sun, J., Cui, X., Eichacker, P. Q., and Torabi-Parizi, P. (2020). Checkpoint Inhibitor Therapy in Preclinical Sepsis Models: a Systematic Review and Meta-Analysis. *Intensive Care Med. Exp.* 8 (1), 7. doi:10.1186/s40635-019-0290-x

Cai, Y., Xing, G., Shen, T., Zhang, S., Rao, J., and Shi, R. (2017). Effects of 12-week Supplementation of Citrus Bergamia Extracts-Based Formulation CitriCholess on Cholesterol and Body Weight in Older Adults with Dyslipidemia: a Randomized, Double-Blind, Placebo-Controlled Trial. *Lipids Health Dis.* 16 (1), 251. doi:10.1186/s12944-017-0640-1

Cao, H. (2014). Adipocytokines in Obesity and Metabolic Disease. *J. Endocrinol.* 220 (2), T47–T59. doi:10.1530/JOE-13-0339

Chanet, A., Wizinska, P., Polakof, S., Mazur, A., Bennetau-Pelissero, C., Morand, C., et al. (2012). Naringin at a Nutritional Dose Modulates Expression of Genes Related to Lipid Metabolism and Inflammation in Liver of Mice Fed a High-Fat Diet. *Nutr. Aging* 1 (2), 113–123. doi:10.3233/nua-2012-0010

Chiechio, S., Zammataro, M., Barresi, M., Amenta, M., Ballistreri, G., Fabroni, S., et al. (2021). A Standardized Extract Prepared from Red Orange and Lemon Wastes Blocks High-Fat Diet-Induced Hyperglycemia and Hyperlipidemia in Mice. *Molecules* 26 (14), 4291. doi:10.3390/molecules26144291

Choe, S. C., Kim, H. S., Jeong, T. S., Bok, S. H., and Park, Y. B. (2001). Naringin Has an Antiatherogenic Effect with the Inhibition of Intercellular Adhesion Molecule-1 in Hypercholesterolemic Rabbits. *J. Cardiovasc. Pharmacol.* 38 (6), 947–955. doi:10.1097/00005344-200112000-00017

Choi, M. S., Do, K. M., Park, Y. S., Jeon, S. M., Jeong, T. S., Lee, Y. K., et al. (2001). Effect of Naringin Supplementation on Cholesterol Metabolism and Antioxidant Status in Rats Fed High Cholesterol with Different Levels of Vitamin E. *Ann. Nutr. Metab.* 45 (5), 193–201. doi:10.1159/000046729

Chou, Y. C., Ho, C. T., and Pan, M. H. (2018). Immature Citrus Reticulata Extract Promotes Browning of Beige Adipocytes in High-Fat Diet-Induced C57BL/6 Mice. *J. Agric. Food Chem.* 66 (37), 9697–9703. doi:10.1021/acs.jafc.8b02719

Cochrane Training (2019). *Cochrane Handbook for Systematic Reviews of Interventions*. Wiley Online Books. Available at: : https://onlinelibrary.wiley.com/doi/book/10.1002/9781119536604.

Craft, B. D., Kerrihard, A. L., Amarowicz, R., and Pegg, R. B. (2012). Phenol-Based Antioxidants and the *In Vitro* Methods Used for Their Assessment. *Compr. Rev. Food Sci. Food Saf.* 11 (2), 148–173. doi:10.1111/j.1541-4337.2011.00173.x

Dinesh, S. S., and Hegde, K. (2016). Antiobesity Activity of Ethanolic Extract ofCitrus Maximaleaves on Cafeteria Diet Induced and Drug Induced Obese Rats. *Rese. Jour. Pharm. Technol.* 9 (7), 907–912. doi:10.5958/0974-360x.2016.00173.6

Ding, X., Fan, S., Lu, Y., Zhang, Y., Gu, M., Zhang, L., et al. (2012). Citrus Ichangensis Peel Extract Exhibits Anti-metabolic Disorder Effects by the Inhibition of PPARγ and LXR Signaling in High-Fat Diet-Induced C57BL/6 Mouse. *Evid. Based Complement. Alternat Med.* 2012, 678592. doi:10.1155/2012/678592

DiNicolantonio, J. J., and O'Keefe, J. H. (2018). Effects of Dietary Fats on Blood Lipids: a Review of Direct Comparison Trials. *Open Heart* 5 (2), e000871. doi:10.1136/openhrt-2018-000871

FAS (2018). *Citrus: World Markets and Trade*. Washington: USDA Foreign Agricultural Service. Available at: https://www.fas.usda.gov/data/citrus-world-markets-and-trade.

Fayek, N. M., El-Shazly, A. H., Abdel-Monem, A. R., Moussa, M. Y., Abd-Elwahab, S. M., and El-Tanbouly, N. D. (2017). Comparative Study of the Hypocholesterolemic, Antidiabetic Effects of Four Agro-Waste Citrus Peels Cultivars and Their HPLC Standardization. *Revista Brasileira de Farmacognosia* 27 (4), 488–494. doi:10.1016/j.bjp.2017.01.010

Feksa, D. L., Coelho, R. P., Aparecida da Costa Güllich, A., Dal Ponte, E. S., da Costa Escobar Piccoli, J., and Manfredini, V. (2018). Extract of Citrus Maxima (Pummelo) Leaves Improve Hepatoprotective Activity in Wistar Rats Submitted to the Induction of Non-alcoholic Hepatic Steatosis. *Biomed. Pharmacother.* 98, 338–346. doi:10.1016/j.biopha.2017.12.070

Ferdinandusse, S., Denis, S., Hogenhout, E. M., Koster, J., van Roermund, C. W., IJlst, L., et al. (2007). Clinical, Biochemical, and Mutational Spectrum of Peroxisomal Acyl-Coenzyme A Oxidase Deficiency. *Hum. Mutat.* 28 (9), 904–912. doi:10.1002/humu.20535

Fruchart, J. C., Sacks, F. M., Hermans, M. P., Assmann, G., Brown, W. V., Ceska, R., et al. (2008). The Residual Risk Reduction Initiative: a Call to Action to Reduce Residual Vascular Risk in Dyslipidaemic Patient. *Diab Vasc. Dis. Res.* 5 (4), 319–335. doi:10.3132/dvdr.2008.046

Gattuso, G., Barreca, D., Gargiulli, C., Leuzzi, U., and Caristi, C. (2007). Flavonoid Composition of Citrus Juices. *Molecules* 12 (8), 1641–1673. doi:10.3390/12081641

Geleijnse, J. M., Launer, L. J., Hofman, A., Pols, H. A., and Witteman, J. C. (1999). Tea Flavonoids May Protect against Atherosclerosis: the Rotterdam Study. *Arch. Intern. Med.* 159 (18), 2170–2174. doi:10.1001/archinte.159.18.2170

Gorinstein, S., Leontowicz, H., Leontowicz, M., Krzeminski, R., Gralak, M., Jastrzebski, Z., et al. (2007). Effect of Hesperidin and Naringin on the Plasma Lipid Profile and Plasma Antioxidant Activity in Rats Fed a Cholesterol-Containing Diet. *J. Sci. Food Agric.* 87 (7), 1257–1262. doi:10.1002/jsfa.2834

Hase-Tamaru, S., Okushima, A., Miyata, Y., Nakayama, H., Aramaki, S., Miyata, Y., et al. (2019). Unripe and Discarded Satsuma Mandarin (Citrus Unshiu MARC.) Improves Lipid Metabolism in Rats. *Fstr* 25, 705–713. doi:10.3136/fstr.25.705

Higgins, J. P., and Thompson, S. G. (2002). Quantifying Heterogeneity in a Meta-Analysis. *Stat. Med.* 21 (11), 1539–1558. doi:10.1002/sim.1186

Hooijmans, C. R., Rovers, M. M., de Vries, R. B., Leenaars, M., Ritskes-Hoitinga, M., and Langendam, M. W. (2014). SYRCLE's Risk of Bias Tool for Animal Studies. *BMC Med. Res. Methodol.* 14, 43. doi:10.1186/1471-2288-14-43

Ingersgaard, M. V., Helms Andersen, T., Norgaard, O., Grabowski, D., and Olesen, K. (2020). Reasons for Nonadherence to Statins - A Systematic Review of Reviews. *Patient Prefer Adherence* 14, 675–691. doi:10.2147/PPA.S245365

Jeon, S. M., Park, Y. B., and Choi, M. S. (2004). Antihypercholesterolemic Property of Naringin Alters Plasma and Tissue Lipids, Cholesterol-Regulating Enzymes, Fecal Sterol and Tissue Morphology in Rabbits. *Clin. Nutr.* 23 (5), 1025–1034. doi:10.1016/j.clnu.2004.01.006

Kang, S. I., Shin, H. S., Kim, H. M., Hong, Y. S., Yoon, S. A., Kang, S. W., et al. (2012). Immature Citrus Sunki Peel Extract Exhibits Antiobesity Effects by β-oxidation and Lipolysis in High-Fat Diet-Induced Obese Mice. *Biol. Pharm. Bull.* 35 (2), 223–230. doi:10.1248/bpb.35.223

Ke, Z., Zhao, Y., Tan, S., Chen, H., Li, Y., Zhou, Z., et al. (2020). Citrus Reticulata Blanco Peel Extract Ameliorates Hepatic Steatosis, Oxidative Stress and Inflammation in HF and MCD Diet-Induced NASH C57BL/6 J Mice. *J. Nutr. Biochem.* 83, 108426. doi:10.1016/j.jnutbio.2020.108426

Khan, W., Augustine, D., Rao, R. S., Patil, S., Awan, K. H., Sowmya, S. V., et al. (2021). Lipid Metabolism in Cancer: A Systematic Review. *J. Carcinog* 20, 4. doi:10.4103/jcar.JCar_15_20

Kilkenny, C., Browne, W. J., Cuthill, I. C., Emerson, M., and Altman, D. G. (2010). Improving Bioscience Research Reporting: The ARRIVE Guidelines for Reporting Animal Research. *Plos Biol.* 8 (6), e1000412. doi:10.1371/journal.pbio.1000412

Kim, S. H., Hur, H. J., Yang, H. J., Kim, H. J., Kim, M. J., Park, J. H., et al. (2013). Citrus Junos Tanaka Peel Extract Exerts Antidiabetic Effects via AMPK and PPAR-γ Both *In Vitro* and *In Vivo* in Mice Fed a High-Fat Diet. *Evid. Based Complement. Alternat Med.* 2013, 921012. doi:10.1155/2013/921012

Kim, S. Y., Kim, H. J., Lee, M. K., Jeon, S. M., Do, G. M., Kwon, E. Y., et al. (2006). Naringin Time-Dependently Lowers Hepatic Cholesterol Biosynthesis and Plasma Cholesterol in Rats Fed High-Fat and High-Cholesterol Diet. *J. Med. Food* 9 (4), 582–586. doi:10.1089/jmf.2006.9.582

Kou, G., Zhao, Z., Dong, X., Zhang, Y., Guo, L., and Zhou, Z. (2017). Effects of Citrus Fruits on Blood Lipid Levels: A Systematic Review and Meta- Analysis. *Acta Med. Mediterr.* 33, 1143–1150. doi:10.19193/0393-6384_2017_6_179

Lamiquiz-Moneo, I., Giné-González, J., Alisente, S., Bea, A. M., Pérez-Calahorra, S., Marco-Benedí, V., et al. (2020). Effect of Bergamot on Lipid Profile in Humans: A Systematic Review. *Crit. Rev. Food Sci. Nutr.* 60 (18), 3133–3143. doi:10.1080/10408398.2019.1677554

Lee, C. H., Jeong, T. S., Choi, Y. K., Hyun, B. H., Oh, G. T., Kim, E. H., et al. (2001). Anti-atherogenic Effect of Citrus Flavonoids, Naringin and Naringenin, Associated with Hepatic ACAT and Aortic VCAM-1 and MCP-1 in High Cholesterol-Fed Rabbits. *Biochem. Biophys. Res. Commun.* 284 (3), 681–688. doi:10.1006/bbrc.2001.5001

Lee, G. H., Peng, C., Park, S. A., Hoang, T. H., Lee, H. Y., Kim, J., et al. (2020). Citrus Peel Extract Ameliorates High-Fat Diet-Induced NAFLD via Activation of AMPK Signaling. *Nutrients* 12 (3), 673. doi:10.3390/nu12030673

Lee, S.-H., Jeong, T.-S., Park, Y. B., Kwon, Y.-K., Choi, M.-S., and Bok, S.-H. (1999). Hypocholesterolemic Effect of Hesperetin Mediated by Inhibition of 3-Hydroxy-3-Methylgultaryl Coenzyme a Reductase and Acyl Coenzyme a: Cholesterol Acyltransferase in Rats Fed High-Cholesterol Diet. *Nutr. Res.* 19 (8), 1245–1258. doi:10.1016/s0271-5317(99)00085-8

Lee, Y. S., Huh, J. Y., Nam, S. H., Moon, S. K., and Lee, S. B. (2012). Enzymatic Bioconversion of Citrus Hesperidin by Aspergillus Sojae Naringinase: Enhanced Solubility of Hesperetin-7-O-Glucoside with *In Vitro* Inhibition of Human Intestinal Maltase, HMG-CoA Reductase, and Growth of Helicobacter pylori. *Food Chem.* 135 (4), 2253–2259. doi:10.1016/j.foodchem.2012.07.007

Ling, Y., Shi, Z., Yang, X., Cai, Z., Wang, L., Wu, X., et al. (2020). Hypolipidemic Effect of Pure Total Flavonoids from Peel of Citrus (PTFC) on Hamsters of Hyperlipidemia and its Potential Mechanism. *Exp. Gerontol.* 130, 110786. doi:10.1016/j.exger.2019.110786

Lu, M., Cao, Y., Xiao, J., Song, M., and Ho, C. T. (2018). Molecular Mechanisms of the Anti-obesity Effect of Bioactive Ingredients in Common Spices: a Review. *Food Funct.* 9 (9), 4569–4581. doi:10.1039/c8fo01349g

Lu, Y., Xi, W., Ding, X., Fan, S., Zhang, Y., Jiang, D., et al. (2013). Citrange Fruit Extracts Alleviate Obesity-Associated Metabolic Disorder in High-Fat Diet-Induced Obese C57BL/6 Mouse. *Ijms* 14 (12), 23736–23750. doi:10.3390/ijms141223736

Mach, F., Baigent, C., Catapano, A. L., Koskinas, K. C., Casula, M., Badimon, L., et al. (2020). 2019 ESC/EAS Guidelines for the Management of Dyslipidaemias: Lipid Modification to Reduce Cardiovascular Risk. *Eur. Heart J.* 41 (1), 111–188. doi:10.1093/eurheartj/ehz455

Mir, H., Krouf, D., Taleb-Dida, N., Berzou, S., Guenzet, A., and Khelladi, H. (2019). Effects of Citrus Latifolia Extract on Dyslipidemia and Tissues Redox Status in Rats Fed a High-Cholesterol Diet. *Nfs* 49 (6), 989–999. doi:10.1108/nfs-04-2018-0110

Mollace, V., Sacco, I., Janda, E., Malara, C., Ventrice, D., Colica, C., et al. (2011). Hypolipemic and Hypoglycaemic Activity of Bergamot Polyphenols: from Animal Models to Human Studies. *Fitoterapia* 82 (3), 309–316. doi:10.1016/j.fitote.2010.10.014

Muhtadi, M., Haryoto, H., Azizah, T., Suhendi, A., and Yen, K. (2015). Antidiabetic and Antihypercholesterolemic Activities of Citrus Sinensis Peel: *In Vivo* Study. *Natl. J. Physiol. Pharm. Pharmacol.* 5 (5), 382–385. doi:10.5455/njppp.2015.5.2807201561

Mulvihill, E. E., Allister, E. M., Sutherland, B. G., Telford, D. E., Sawyez, C. G., Edwards, J. Y., et al. (2009). Naringenin Prevents Dyslipidemia, Apolipoprotein B Overproduction, and Hyperinsulinemia in LDL Receptor-Null Mice with Diet-Induced Insulin Resistance. *Diabetes* 58 (10), 2198–2210. doi:10.2337/db09-0634

Mulvihill, E. E., and Huff, M. W. (2012). Protection from Metabolic Dysregulation, Obesity, and Atherosclerosis by Citrus Flavonoids: Activation of Hepatic PGC1α-Mediated Fatty Acid Oxidation. *PPAR Res.* 2012, 857142. doi:10.1155/2012/857142

Onakpoya, I., O'Sullivan, J., Heneghan, C., and Thompson, M. (2017). The Effect of Grapefruits (Citrus Paradisi) on Body Weight and Cardiovascular Risk Factors: A Systematic Review and Meta-Analysis of Randomized Clinical Trials. *Crit. Rev. Food Sci. Nutr.* 57 (3), 602–612. doi:10.1080/10408398.2014.901292

Page, M. J., McKenzie, J. E., Bossuyt, P. M., Boutron, I., Hoffmann, T. C., Mulrow, C. D., et al. (2021). The PRISMA 2020 Statement: an Updated Guideline for Reporting Systematic Reviews. *BMJ* 372, n71. doi:10.1136/bmj.n71

Pan, W. W., and Myers, M. G. (2018). Leptin and the Maintenance of Elevated Body Weight. *Nat. Rev. Neurosci.* 19 (2), 95–105. doi:10.1038/nrn.2017.168

Patil, V. C., Avhad, A. B., Kulkarni, A. R., and Pandere, K. A. (2020). High-Sensitive C-Reactive Protein in Patients with Coronary Artery Disease. *J. Nat. Sci. Biol. Med.* 11, 39–44. doi:10.4103/jnsbm.JNSBM_159_19

Pepino, M. Y., Kuda, O., Samovski, D., and Abumrad, N. A. (2014). Structure-Function of CD36 and Importance of Fatty Acid Signal Transduction in Fat Metabolism. *Annu. Rev. Nutr.* 34, 281–303. doi:10.1146/annurev-nutr-071812-161220

Pirillo, A., Casula, M., Olmastroni, E., Norata, G. D., and Catapano, A. L. (2021). Global Epidemiology of Dyslipidaemias. *Nat. Rev. Cardiol.* 18 (10), 689–700. doi:10.1038/s41569-021-00541-4

Pradhan, G., Samson, S. L., and Sun, Y. (2013). Ghrelin: Much More Than a Hunger Hormone. *Curr. Opin. Clin. Nutr. Metab. Care* 16 (6), 619–624. doi:10.1097/MCO.0b013e328365b9be

Raasmaja, A., Lecklin, A., Li, X. M., Zou, J., Zhu, G. G., Laakso, I., et al. (2013). A Water-Alcohol Extract of Citrus Grandis Whole Fruits Has Beneficial Metabolic Effects in the Obese Zucker Rats Fed with High Fat/high Cholesterol Diet. *Food Chem.* 138 (2–3), 1392–1399. doi:10.1016/j.foodchem.2012.09.140

Rafiq, S., Kaul, R., Sofi, S. A., Bashir, N., Nazir, F., and Ahmad Nayik, G. (2018). Citrus Peel as a Source of Functional Ingredient: A Review. *J. Saudi Soc. Agric. Sci.* 17, 351. Available at: http://www.sciencedirect.com/science/article/pii/S1658077X16300960.doi:10.1016/j.jssas.2016.07.006

Sahebkar, A. (2017). Effects of Quercetin Supplementation on Lipid Profile: A Systematic Review and Meta-Analysis of Randomized Controlled Trials. *Crit. Rev. Food Sci. Nutr.* 57 (4), 666–676. doi:10.1080/10408398.2014.948609

Sato, M., Goto, T., Inoue, E., Miyaguchi, Y., and Toyoda, A. (2019). Dietary Intake of Immature Citrus Tumida Hort. Ex Tanaka Peels Suppressed Body Weight Gain and Fat Accumulation in a Mouse Model of Acute Obesity. *J. Nutr. Sci. Vitaminol (Tokyo)* 65 (1), 19–23. doi:10.3177/jnsv.65.19

Schulz, I. (2006). Treatment of Dyslipidemia: How and when to Combine Lipid Lowering Drugs. *Arq Bras Endocrinol. Metabol* 50 (2), 344–359. doi:10.1590/s0004-27302006000200021

Shin, E. J., Park, J. H., Sung, M. J., Chung, M. Y., and Hwang, J. T. (2016). Citrus Junos Tanaka Peel Ameliorates Hepatic Lipid Accumulation in HepG2 Cells and in Mice Fed a High-Cholesterol Diet. *BMC Complement. Altern. Med.* 16 (1), 499. doi:10.1186/s12906-016-1460-y

Sowndarya, K., Joseph, J., Shenoy, A., and Hegde, A. (2021). Evaluation of Triglyceride/high-Density Lipoprotein Ratio as a Surrogate Marker for Insulin Resistance in Healthy Young Males. *J. Nat. Sci. Biol. Med.* 12 (2), 213–217. doi:10.4103/jnsbm.JNSBM-193-20

T Manuel, C Marco, and G Fred (Editors) (2020). 1st Edition. Available at: https://www.elsevier.com/books/the-genus-citrus/talon/978-0-12-812163-4.The Genus Citrus

Terpstra, A. H., Lapré, J. A., de Vries, H. T., and Beynen, A. C. (2002). The Hypocholesterolemic Effect of Lemon Peels, Lemon Pectin, and the Waste Stream Material of Lemon Peels in Hybrid F1B Hamsters. *Eur. J. Nutr.* 41 (1), 19–26. doi:10.1007/s003940200002

Toth, P. P., Patti, A. M., Nikolic, D., Giglio, R. V., Castellino, G., Biancucci, T., et al. (2015). Bergamot Reduces Plasma Lipids, Atherogenic Small Dense LDL, and Subclinical Atherosclerosis in Subjects with Moderate Hypercholesterolemia: A 6 Months Prospective Study. *Front. Pharmacol.* 6, 299. doi:10.3389/fphar.2015.00299

Tripoli, E., Guardia, M. L., Giammanco, S., Majo, D. D., and Giammanco, M. (2007). Citrus Flavonoids: Molecular Structure, Biological Activity and Nutritional Properties: A Review. *Food Chem.* 104 (2), 466–479. doi:10.1016/j.foodchem.2006.11.054

Vinson, J. A., Hu, S.-J., Jung, S., and Stanski, A. M. (1998). A Citrus Extract Plus Ascorbic Acid Decreases Lipids, Lipid Peroxides, Lipoprotein Oxidative Susceptibility, and Atherosclerosis in Hypercholesterolemic Hamsters. *J. Agric. Food Chem.* 46 (4), 1453–1459. doi:10.1021/jf970801u

Wiggins, B. S., Dixon, D., Bellone, J., Gasbarro, N., Marrs, J. C., and Tran, R. (2019). Key Articles and Guidelines in the Management of Dyslipidemia: 2019 Update. *J. Pharm. Pract.* 11, 0897190019868413. doi:10.1177/0897190019868413

Wu, H., Liu, Y., Chen, X., Zhu, D., Ma, J., Yan, Y., et al. (2017). Neohesperidin Exerts Lipid-Regulating Effects *In Vitro* and *In Vivo* via Fibroblast Growth Factor 21 and AMP-Activated Protein Kinase/Sirtuin Type 1/Peroxisome Proliferator-Activated Receptor Gamma Coactivator 1α Signaling Axis. *Pharmacology* 100 (3–4), 115–126. doi:10.1159/000452492

Zeka, K., Ruparelia, K., Arroo, R. R. J., Budriesi, R., and Micucci, M. (2017). Flavonoids and Their Metabolites: Prevention in Cardiovascular Diseases and Diabetes. *Diseases* 5 (3), 19. doi:10.3390/diseases5030019

Zhao, X., Wang, D., and Qin, L. (2021). Lipid Profile and Prognosis in Patients with Coronary Heart Disease: a Meta-Analysis of Prospective Cohort Studies. *BMC Cardiovasc. Disord.* 21 (1), 69. doi:10.1186/s12872-020-01835-0

Zulkhairi, H. A., Khairunnuur, A. F., Hafipah, M. R. N., Azrina, A., Rasadah, M. A., Kamilah, K. A. K., et al. (2010). An Aqueous Extract of Citrus Mitis Possesses Antioxidative Properties and Improves Plasma Lipid Profiles in Rat Induced with High Cholesterol Diet. *J. Med. Plant Res.* 4 (1), 49–57. doi:10.5897/JMPR09.385

Conflict of Interest: The authors declare that the research was conducted in the absence of any commercial or financial relationships that could be construed as a potential conflict of interest.

Publisher's Note: All claims expressed in this article are solely those of the authors and do not necessarily represent those of their affiliated organizations, or those of the publisher, the editors and the reviewers. Any product that may be evaluated in this article, or claim that may be made by its manufacturer, is not guaranteed or endorsed by the publisher.

frontiers in Pharmacology

ORIGINAL RESEARCH
published: 17 March 2022
doi: 10.3389/fphar.2022.778221

Rhein Protects Against Severe Acute Pancreatitis *In vitro* and *In vivo* by Regulating the JAK2/STAT3 Pathway

Xiaofang Yang†, Huan Geng†, Lijiao You, Lin Yuan, Jialei Meng, Yuhui Ma, Xuelian Gu and Ming Lei**

Department of Critical Care Medicine, Seventh People's Hospital Affiliated to Shanghai University of Traditional Chinese Medicine, Shanghai, China

OPEN ACCESS

Edited by:
Henrique Melo Coutinho, Regional University of Cariri, Brazil

Reviewed by:
Fabrício Souza Silva, Federal University of São Francisco Valley, Brazil
Luiz Jardelino de Lacerda Neto, Federal University of Campina Grande, Brazil
Andreza Ramos, Federal University of Campina Grande, Brazil

***Correspondence:**
Xuelian Gu
18930837717@163.com
Ming Lei
leiming6891@163.com

†These authors have contributed equally to this work

Specialty section:
This article was submitted to Gastrointestinal and Hepatic Pharmacology, a section of the journal Frontiers in Pharmacology

Received: *16 September 2021*
Accepted: *28 February 2022*
Published: *17 March 2022*

Citation:
Yang X, Geng H, You L, Yuan L, Meng J, Ma Y, Gu X and Lei M (2022) Rhein Protects Against Severe Acute Pancreatitis In vitro and In vivo by Regulating the JAK2/STAT3 Pathway. Front. Pharmacol. 13:778221. doi: 10.3389/fphar.2022.778221

Rhein is widely used in inflammation treatment in China, but its effects on severe acute pancreatitis (SAP) have not been studied closely. This study investigated rhein's protective effects against SAP using *in vitro* and *in vivo* models to determine whether its protective mechanism regulated the Janus kinase two and signal transducer and activator of transcription 3 (JAK2/STAT3) signalling pathway. Thirty-six male Sprague–Dawley rats were randomised into sham operation, SAP and rhein groups. The SAP model was induced by retrograde pancreatic bile duct injection of sodium taurocholate. Serum TNF-α and interleukin (IL)-6 levels were determined by ELISA, whereas serum amylase and lipase concentrations were measured using test kits. Western blot and/or immunohistochemistry quantified JAK2 and STAT3 expression. Furthermore, histopathological pancreatic changes were detected by haematoxylin and eosin staining. AR42J cells were randomly divided into the control, cerulein and rhein groups. Amylase activity was assessed using an amylase test kit; the tumour necrosis factor-α (TNF-α) expression was determined by enzyme-linked immunosorbent assay (ELISA). JAK2 and STAT3 protein expression were evaluated by western blot. SAP was concomitant with increased JAK2 and STAT3 expressions *in vivo*. Pre-treatment with rhein attenuated serum TNF–α and IL-6 levels effectively, and notably reduced p-JAK2, p-STAT3, JAK2 and STAT3 protein expression. Rhein significantly alleviated pancreatic histopathology. Compared to untreated groups, rhein significantly reduced amylase activity in supernatants of AR42J cells induced by cerulein *in vitro*. Furthermore, rhein altered JAK2 and STAT3 protein levels in AR42J cells after cerulein induction. Overall, rhein exerted protective effect on SAP *in vitro* and *in vivo*, possibly through the JAK2/STAT3 signalling pathway.

Keywords: rhein, severe acute pancreatitis, JAK2/STAT3, TNF-α, IL-6

INTRODUCTION

Acute pancreatitis is an acute inflammatory disease that severely affects health and threatens life, and about 30% of patients with acute pancreatitis progress to severe acute pancreatitis (SAP) (Lankisch and Lerch, 2006; Morel et al., 2006). About 15%–20% of SAP cases often develop multiple systemic complications, such as the liver, intestine, kidneys and lungs complications, and the therapeutic effects of current treatments are unsatisfactory (Zerem, 2014).

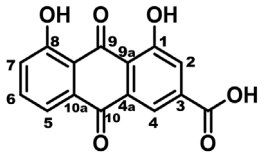

FIGURE 1 | The chemical structure of rhein.

Some studies propose that the effective inhibition of inflammation is key to preventing SAP progression (Gallmeier et al., 2005; Andersson et al., 2007; Ivanenkov et al., 2011). Therefore, cell signalling pathways related to inflammation in SAP have been the subject of increased research attention. The Janus kinase two and signal transducer and activator of transcription 3 (JAK2/STAT3) signalling pathway, one of the main cytokine signalling pathways, has become a hotspot of pancreatic research in recent years. The JAK2/STAT3 signalling pathway is widely involved in disease physiology and pathogenic development, including intracellular homeostasis, immune response, cell proliferation and apoptosis (O'shea, 2004). Tumour necrosis factor-α (TNF-α) and interleukin (IL)-6 are important transduction factors in the JAK2/STAT3 signalling pathway that can induce the inflammatory cascade, enhance the inflammatory effect and even lead to organ damage and multiple organ dysfunction syndrome in SAP (Zhu et al., 2017). Moreover, the JAK2/STAT3 signalling pathway amplifies the inflammatory response by initiating a series of inflammatory factor transmissions and related protein expression, thereby creating a waterfall effect. Several previous studies have shown that the JAK2/STAT3 pathway plays a key role in inflammatory diseases (Zhu et al., 2017; Xia et al., 2021). Thus, inhibiting this pathway may restrain the expansion of early cascading inflammatory response and prevent acute inflammatory injury to related tissues.

The current treatment protocol for SAP is a multi-targeted therapy based on the diagnostic and treatment guidelines for SAP, which focuses on pharmacological blockade of necrosis, inflammation and cellular damage in the pancreas. The multi-targeted action of natural drugs has attracted attention, compared to the single-targeted action of western drugs (Xue et al., 2006; Weng et al., 2012; Xia et al., 2012; Zhong, 2015). Rhein is also a natural molecule and is widely found in medicinal plants such as rhubarb, *Sennae folium*, *Semen cassiae*, and *Polygonum multiflorum*, and it is widely used in clinical practice (Xian et al., 2020). In China, approximately 10% (800) of more than 8,000 proprietary Chinese medicines contain rhubarb.

Rhein (the chemical structure is shown in **Figure 1**, the main rhubarb component, is reported to be widely used in inflammation treatment in China (Cheng et al., 2021). Rhein is also the major active component in Dachengqi Decoction with strong anti-inflammatory effects (Xu et al., 2008; Xu et al., 2010; Xu et al., 2010). Several studies have shown that Dachengqi Decoction can improve the inflammatory response in patients with SAP and reduce pathological pancreatic damage (Chen et al., 2010; Chen et al., 2015). In addition, the JAK2/STAT3 is predicted to be one of the targets of rhein according to network pharmacology. While rhein has been shown to play a prominent role as an inhibitor of the JAK2/STAT3 pathway in several experimental models and human diseases (Zhang et al., 2016; Yang et al., 2019). However, it is unclear whether rhein has a therapeutic effect on SAP by inhibiting JAK2/STAT3 pathway. Therefore, the present study was designed to investigate rhein's protective effects on SAP using *in vitro* and *in vivo* models.

MATERIALS AND METHODS

Drugs and Reagents

Purified rhein (Cat. No. 478-43-3) was purchased from the National Institute for Food and Drug Control (Beijing, China), the purity by authorization >98%. Sodium taurocholate (Cat. No. T4009), cerulein (Cat. No. C9026) and 5% carboxymethylcellulose sodium (CMCS) (CAS number:9004-32-4) were purchased from Sigma-Aldrich Merck KGaA (Darmstadt, Germany). Amylase kits (Cat. No. C016-1-1) were purchased from Nanjing Jiancheng Institute of Bioengineering (Jiangsu, China). Foetal bovine serum (Cat. No.10099-141), F12K medium (Cat. No. C11330500BT) and trypsin (Cat. No. 25200-056) were purchased from Gibco Ltd. (United States). PCR kits (Cat. No. RR820Q) were purchased from TaKaRa Corporation (Japan). GoScript Reverse Transcription Kits (Cat. No. A5001) were purchased from Promega (United States). Phosphatase inhibitors (Cat. No. P1081), SDS–PAGE gel preparation kits (Cat. No. P0012A) and ECL hypersensitive colour development kits (Cat. No. P0018AS) were purchased from Shanghai Biyuntian Biotechnology (Shanghai, China).

Cellular Model

Rat pancreatic acinar AR42J cells were obtained from the American Type Culture Collection and were cultured in F12K medium (Cat. No. C11330500BT, Gibco) supplemented with 20% Australian foetal bovine serum (Cat. No. 10099141C, Gibco), 100 U/ml penicillin and 100 mg/l streptomycin (Cat. No. 15140-122, Gibco) at 37°C and 5% CO_2. The AR42J cells were divided into three groups: control group, cerulein group (cerulein 10^{-8} mol/L) (Lee et al., 2003; Huang et al., 2012; Yu et al., 2003; Zhao et al., 2014; Chen et al., 2019) and rhein group (final concentration 0.25, 0.5 and 1 μg/ml). The AR42J cells density was 5×10^6/ml. In the cerulein group, cells and culture supernatants were collected at 0, 0.5, 1, 2, 4, 6, 12 and 24 h after the addition of cerulein.

Animal Model Thirty-six adult male Sprague–Dawley rats (8–10 weeks old, weighing 200–250 g) were obtained from the Shanghai SLAC Laboratory Animal Co., Ltd. SD rats were randomly divided into three groups: sham operation group (n = 12), SAP model group (n = 12), rhein (dissolved in 0.5% CMCS) treatment group (n = 12). All rats were maintained under standardised conditions on a 12 h light/dark cycle and allowed free access to food and water. The rats fasted for 12 h before the operation, however, drinking water was available ad libitum. The SAP model was induced via a standardised pressure-controlled infusion of 3.5% sodium taurocholate (1 ml/kg, 0.1 ml/min) into the bile–pancreatic duct, and the common hepatic duct was

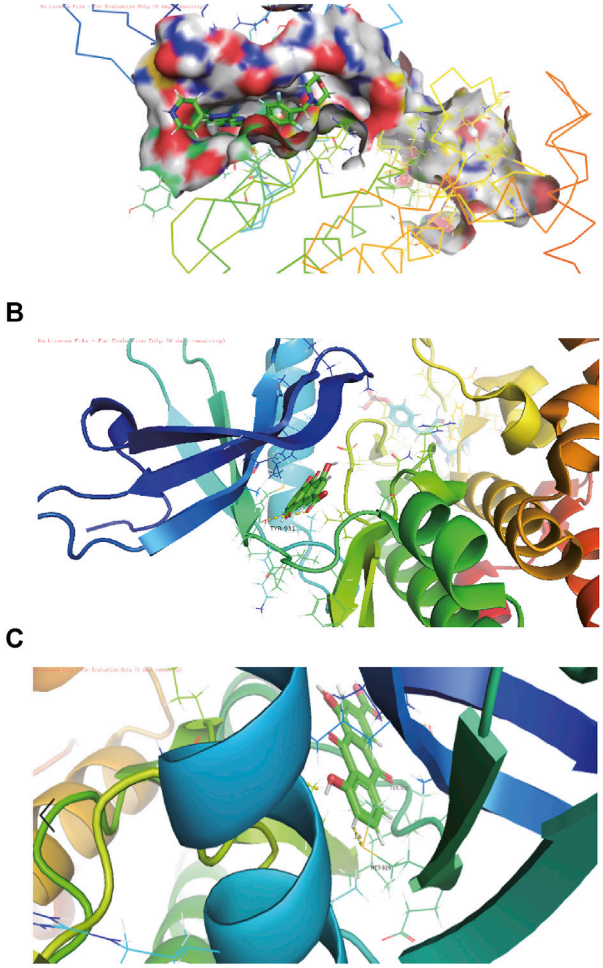

FIGURE 2 | The structure-activity relationships of rhein with JAK2 molecule. **(A)** Schematic diagram of the connection between jAk2 and 3kRR in the software pymol view, 3kRR is a compound structure that can already bind to JAK2. **(B)** Schematic diagram of docking with the pocket after rhein is replaced by 3KRR through molecular docking. **(C)** The residues in the pocket TYR-931 and MET-929 are the residues in the pocket, which they are stable binding sites for rhein.

closed with a small clamp for 5 min as previously described (Pérez et al., 2015). Subsequently, the clamp was removed, and the abdomen was closed. Rats in the sham control group underwent the same operative procedure with the injection of 0.9% saline in the pancreatic duct. In the rhein group, rats were given rhein by a gastric gavage (30 mg/kg, 0.5 ml/100 g) (Xian et al., 2020) once a day for 7 days prior to establishing the SAP model. Each group was orally administered with by gavage rhein (30 mg/kg) or saline for seven continuous days. All samples were collected 24 h after operation. All protocols and procedures were established in compliance with the US National Institute of Health Guidelines for the Care and Use of Laboratory Animals. They were approved by the Animal Care and Use Committee of Shanghai University of Traditional Chinese Medicine (Protocol number: PSHUTCM200103002).

Amylase, IL-6, TNF-α, lipase And myeloperoxidase Assays.

Amylase (Cat. No. C016-1-1), lipase (Cat. No. A054-2-1) and myeloperoxidase (Cat. No. A044-1-1) were purchased from Nanjing Jiancheng Institute of Bioengineering (Jiangsu, China). Serum amylase, lipase and myeloperoxidase concentrations were measured using test kits according to the manufacturer's instructions. The amounts of TNF-α (Cat. No. E-EL-M0049c) and IL-6 (Cat. No. E-EL-R0015c) were determined using ELISA kits (eBioscience Ltd., United States) according to the manufacturer's instructions.

Western Blot

RIPA lysis buffer was added to pancreatic tissues and centrifuged at 13,700× *g* at 4°C for 15 min. Supernatants were harvested, and the BCA protein kit was used to determine each protein sample's protein content. SDS–PAGE gels (10% separating gel, 3% concentrating gel) were prepared. After electrophoresis, the protein was transferred to a PVDF membrane, which was then sealed using 5% BSA for 2 h at room temperature. The following primary antibodies were added and incubated at 4°C overnight: JAK2 (Cat. No. 3230, 1:1,000, Cell Signaling Technology Inc.), STAT3 (Cat. No. 12640, 1:2000, Cell Signaling Technology Inc.), p-JAK2 (Cat. No. 3776, 1:1,000, Cell Signaling Technology Inc.), p-STAT3 (Cat. No. 9145, 1:1,000, Cell Signaling Technology Inc.) and GAPDH (Cat. No. 5174, 1:1,000, Cell Signaling Technology Inc). The membranes were then washed with Tris-Buffered Saline Tween buffer three times for 10 min and incubated with horseradish peroxidase (HRP)-labelled goat anti-rabbit IgG secondary antibody (Cat. No. 7074P2, 1:3,000, Cell Signaling Technology Inc.) for 2 h at room temperature. Afterwards, the membranes were washed with Tris-Buffered Saline Tween buffer three times for 10 min. Ultra-sensitive ECL luminescence solution was then added to detect the proteins, and a Fluorchem FC3 gel imager was used for detection. ImageJ 1.52a software was used to determine the gray value of the band. .

Pathological Changes in the Pancreas

The rat pancreatic tissues were fixed in 4% paraformaldehyde and embedded in paraffin wax for routine sections. The sample was cut into 5 μm thick sections. After staining with haematoxylin and eosin, the sections were photographed under the microscope (Nikon FCI IPSE NI, Nikon Corporation) at ×200 magnification for image processing and analysis. Pancreatic histopathology was scored by the double-blind method (Schmidt et al., 1992). The mean total score of each histopathological variable was subsequently calculated.

The methods of histological score of pancreatic injury were as follows: Edema: 0, absent; 1, focal expansion of the interlobar septa; and 2, diffuse expansion of the interlobar septa. vascular: 0, absent; 1, congestion; 2, congestion plus local interlobar or intralobar hemorrhage; 3, multifocal diffuse hemorrhage; and 4, vascular fibrinoid necrosis or thrombosis. Fat necrosis: 0, absent; 1, focal dissolution of the interlobular or peripancreatic fat; and 2, diffuse dissolution of the interlobular or peripancreatic fat. Acinar necrosis: 0, absent; 1, <10% patchy necrosis of the edges of the lobules; 2, 10–30% patchy, peripheral necrosis of the lobules; 3, <30% confluent lobules necrosis; 4, <50% confluent

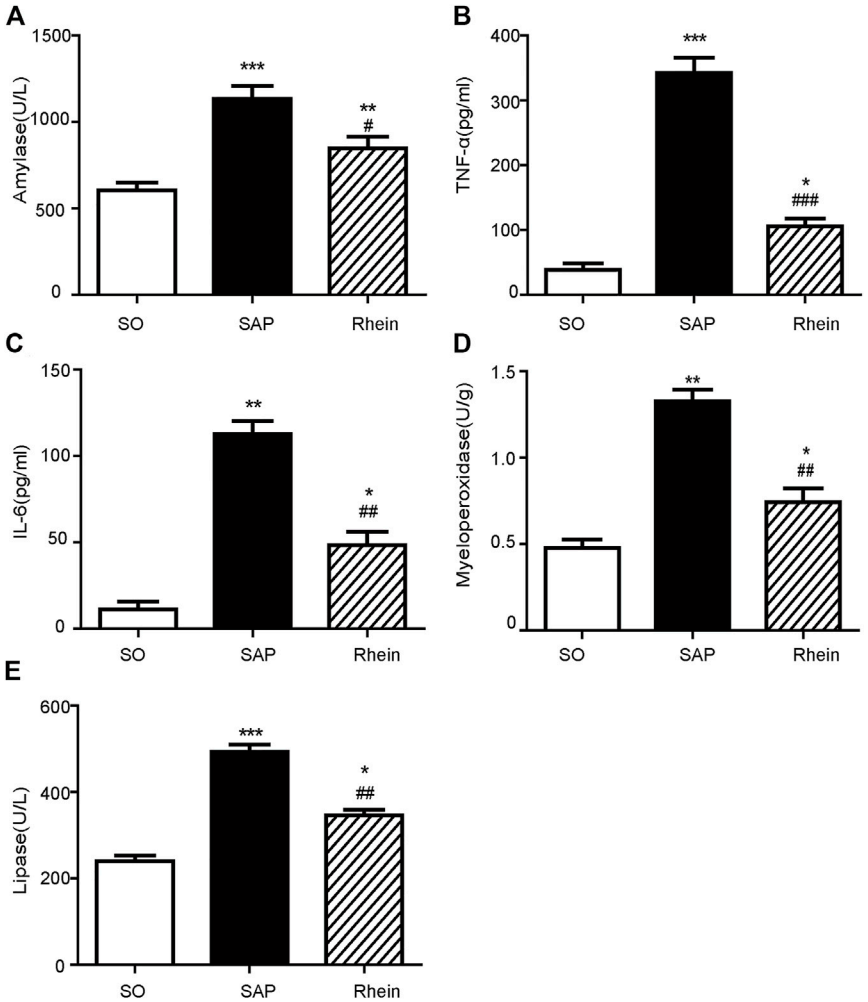

FIGURE 3 | Effects of rhein on the inflammatory cytokine levels in pancreatic tissue of the SAP rat model. **(A)** Serum amylase levels in the SO, SAP and rhein groups. **(B)** Serum TNF-α levels in the SO, SAP and rhein groups. **(C)** Serum IL-6 levels in the SO, SAP and rhein groups. **(D)** Myeloperoxidase levels in the SO, SAP and rhein groups. **(E)** Serum lipase levels in the SO, SAP and rhein groups. Data are expressed as mean ± SD ($n = 5$ per group). Significance between groups was evaluated by one way analysis of variance (ANOVA) followed by a Tukey post hoc test. $^{*}p < 0.05$, $^{**}p < 0.01$ and $^{***}p < 0.001$ compared with the SO group; $^{\#}p < 0.05$, $^{\#\#}p < 0.01$ and $^{\#\#\#}p < 0.001$ compared with the SAP group. SO, sham operation; SAP, severe acute pancreatitis; TNF-α, tumour necrosis factor-α; IL-6, interleukin-6.

lobular necrosis; and 5, formation of microabscesses. Calcification: 0, absent; 1, focal in fat or acinar necrosis; and 2, diffuse in fat or acinar necrosis.

Immunohistochemistry

The rat pancreatic tissues slices were dewaxed with xylene, dehydrated with an ethanol gradient, and then placed in a sodium citrate buffer solution for 15 min. The slices were cooled for 30 min and then treated with 3% hydrogen peroxide for 10 min at room temperature. After three washing with PBS (phosphate buffer saline), shook off the PBS before adding antibody to each slice. The following antibodies were added and incubated at 4°C overnight: p-JAK2 (Cat. No. ab32101, 1:50, Abacam Company), p-STAT3 (Cat. No. ab267373, 1:250, Abacam Company), After three washings with PBS, the HRP-labelled goat anti-rabbit IgG secondary antibody was added and incubated at room temperature for 1 h. The tissue sections were then covered with DAB solution. After colour development, the sections were rinsed with water. Hematoxylin stained for 1 min 20 s, then soaked in tap water, alcohol fractionated in 1% hydrochloric acid for 1 s, soaked in tap water and rinsed under running water for 7–8 min, dried at 65° for 30 min, then taken out and cooled to room temperature and sealed in neutral gum. Image processing and photography, two different observers calculated the positive areas.

Molecular Docking

Rhein was preprocessed by the Ligprep 3.6 program (Schrödinger, LLC, New York, NY, United States) applying OPLS_2005 force field before molecular docking, with Epik 3.4 (Schrödinger, LLC, New York, NY, United States) to generate the proper protonation states at pH 7.0 ± 2.0. A restrained

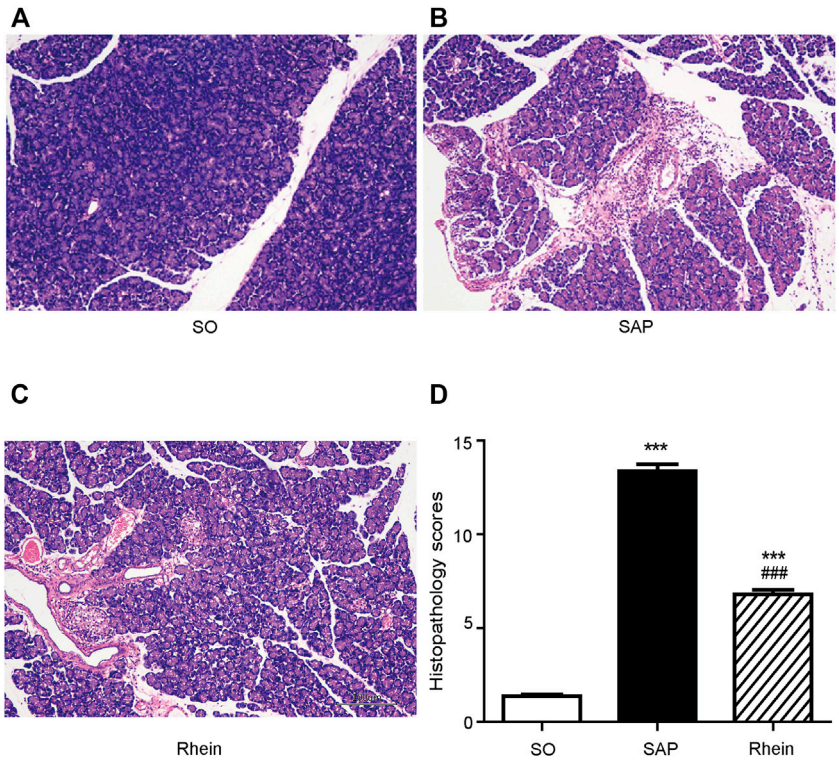

FIGURE 4 | Histological analysis of SAP. **(A–C)** Morphological analysis of H&E-stained sections; Scale bar: 100 μm. **(D)** Pathological scores of pancreatic tissue sections. Data are expressed as mean ± SD ($n = 3$ per group). Significance between groups was evaluated by one way analysis of variance (ANOVA) followed by a Tukey post hoc test. $^{*}p < 0.05$, $^{**}p < 0.01$ and $^{***}p < 0.001$ compared with the SO group; $^{\#}p < 0.05$, $^{\#\#}p < 0.01$ and $^{\#\#\#}p < 0.001$ compared with the SAP group. SO, sham operation; SAP, severe acute pancreatitis; H&E, haematoxylin and eosin.

minimization of the crystal structure was performed to reorient side-chain hydroxyl groups before further processing. The DQX pocket of 3KRR was selected to define and generate the receptor grid. In silico docking was performed by Glide 6.9 (Schrödinger, LLC, New York, NY, United States) in standard precision (SP) with default values for other parameters.

Statistical Analysis Statistical analyses of the obtained experimental data was carried out using SPSS version 21.0. ImageJ 1.52a software was used to calculate the greyscale value. Significance between groups was evaluated by one way analysis of variance (ANOVA) followed by a Tukey post hoc test. Data are expressed as mean ± SD, and $p < 0.05$ was considered statistically significant.

RESULTS

The network pharmacology results of rhein with JAK2 molecule.

3KRR is a Crystal Structure of JAK2 complexed with a potent quinoxaline ATP site inhibitor (**Figure 2A**). The pocket factor of 3KRR was mostly buried in the hydrophobic pocket of DQX, and its main body forms abundant hydrophobic interactions with surrounding residues, whereas its head forms hydrogen bonds with residues nearby the entrance and middle position of the pocket. The in silico docking models showed that the binding sites of the rhein was located near the entrance and middle part of the 3KRR pocket, find rhein partially overlapping with that of the pocket factor of Tyrosine 931 (TYR-931) and MET-929 (**Figure 2B**, **Figure 2C**), they may play an important role in the interaction of compounds with pockets, by preempting residue positions and thus achieving the ability to inhibit other compounds from binding to them.

The Effect of Rhein on Inflammatory Cytokines Levels in SAP Rats

Figure 3 shows the effect of rhein on the level of inflammatory cytokines in pancreatic tissue of SAP rat model. Compared with the control group, the levels of serum amylase, serum TNF-α, serum IL-6, myeloperoxidase and serum lipase were significantly increased in the SAP group ($p < 0.001$). After rhein treatment, the levels of serum amylase, serum TNF-α, serum IL-6, myeloperoxidase and serum lipase were significantly decreased in the rhein group compared with the SAP group ($p < 0.001$).

Effect of Rhein on Pathological Dmage in Pancreatic Tissue of SAP Rats

Figure 4 shows the protective effect of rhein on pancreatic injury. In the control group, typical normal acinar architecture were

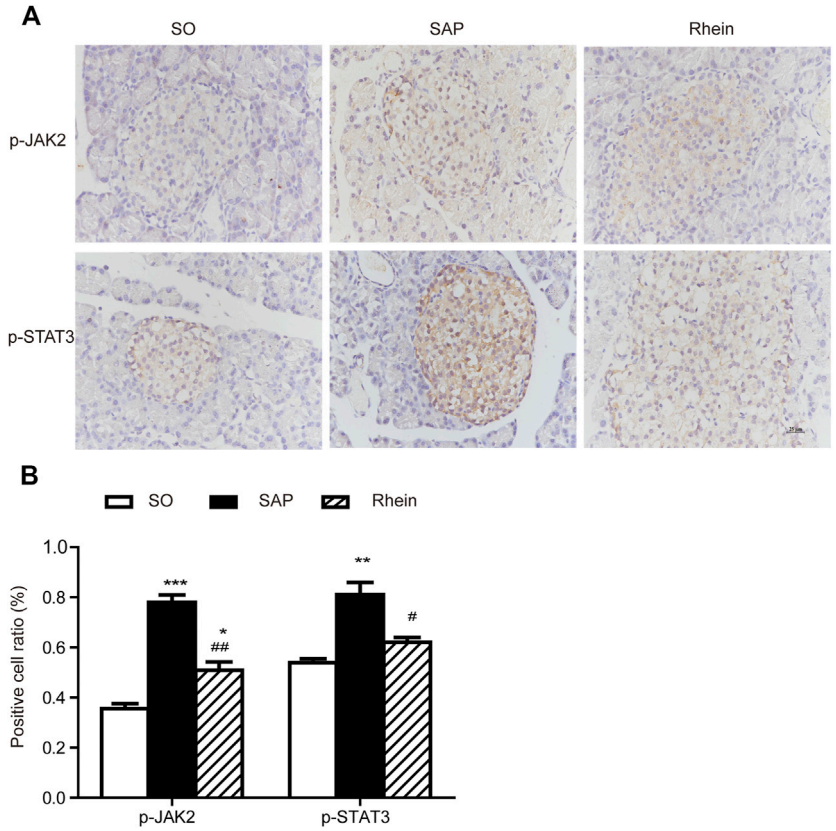

FIGURE 5 | Immunohistochemical analysis of p-JAK2 and p-STAT3 in pancreatic tissues. **(A)** Representative immunohistochemistry images of p-JAK2 and p-STAT3 in pancreatic tissues 24 h after the induction of SAP; Scale bar: 25 μm. **(B)** Positive cell ratio of pancreatic tissue sections. Data are expressed as mean ± SD (n = 3 per group). Significance between groups was evaluated by one way analysis of variance (ANOVA) followed by a Tukey post hoc test. $^{*}p < 0.05$, $^{**}p < 0.01$ and $^{***}p < 0.001$ compared with the SO group; $^{\#}p < 0.05$, $^{\#\#}p < 0.01$ and $^{\#\#\#}p < 0.001$ compared with the SAP group. JAK2, janus kinase two; STAT3, signal transducer and activator of transcription three; SO, sham operation; SAP, severe acute pancreatitis.

observed. Only minimal focal edema was detected, and no apparent inflammatory infiltration was found. Compared with the control group, edema, necrosis and inflammatory infiltration were observed in the acinar cells of pancreatic tissue in the SAP group. Compared with the SAP group, less infiltration of inflammatory cells was observed in the rhein group, Only fewer abnormal acinar cells were detected. **Figure 4D** reveals that the pathological scores were significantly increased in the SAP group compared with the control group ($p < 0.01$). Compared with the SAP group, the pathological scores were significantly decreased in the rhein group ($p < 0.05$).

Effects of Rhein on p-JAK2, p-STAT3, JAK2 and STAT3 Expression in Pancreatic Tissue of SAP Rats

Figure 5 indicates that p-JAK2 and p-STAT3 expression were significantly increased in the SAP group compared with the control group ($p < 0.001$). After rhein treatment, the activity of p-JAK2 and p-STAT3 were significantly decreased compared with the SAP group ($p < 0.001$). **Figure 6** shows that p-JAK2, JAK2, p-STAT3 and STAT3 proteins expression were significantly increased in the SAP group compared with the control group ($p < 0.001$). This increasing trend was significantly reversed by treatment with rhein ($p < 0.001$). These phenomena suggest that four proteins closely related to the JAK2/STAT3 signalling pathway are activated in the pancreatic tissue of SAP rats.

Establishment of AR42J Pancreatic Acinar Cell Injury Model Induced by Cerulein

We constructed an *in vitro* cell model mimicking SAP by treating the AR42J cells line with cerulein to stimulate pro-inflammatory cytokine expression. **Figure 7A** reveals that amylase activity increased significantly at 4 h, and then gradually increased at 6, 12 and 24 h. **Figures 7B–D** shows that JAK2, STAT3, p-JAK2 and p-STAT3 protein expression gradually increased and peaked at 4 h ($p < 0.001$), to gradually decrease at 6, 12 and 24 h. Therefore, we chose 4 h as the checkpoint for sample collection of cells in the succeeding experiments. These results suggested that the AR42J cell injury model was successfully established.

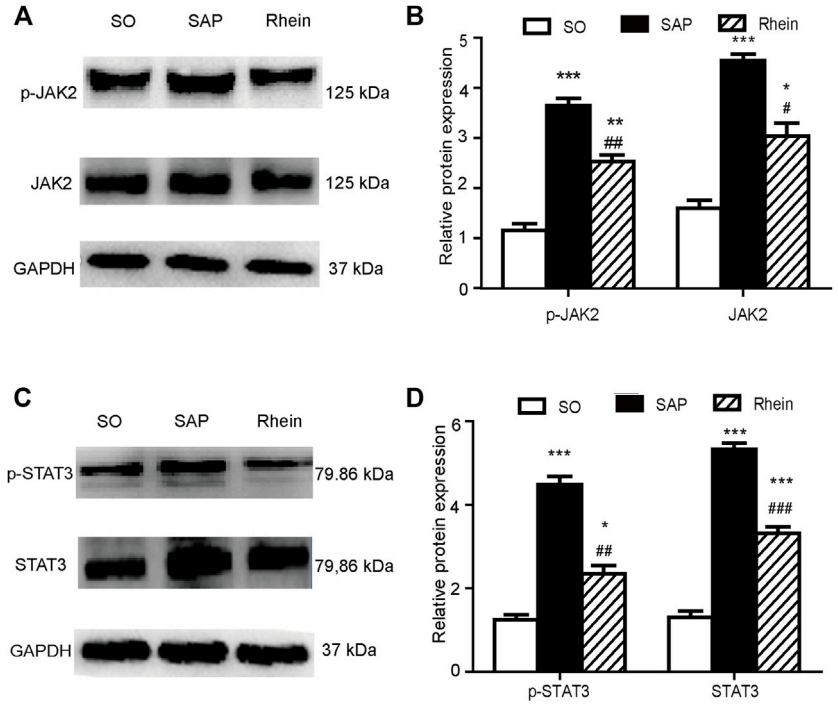

FIGURE 6 | Effects of rhein on p-JAK2, p-STAT3, JAK2 and STAT3 expression in pancreatic tissue of SAP rats. **(A,B)** p-JAK2 and JAK2 protein expression in the SO, SAP and rhein groups. **(C,D)** p-STAT3 and STAT3 protein expression in the SO, SAP and rhein groups. Data are expressed as mean ± SD (n = 5 per group). Significance between groups was evaluated by one way analysis of variance (ANOVA) followed by a Tukey post hoc test. $^{*}p < 0.05$, $^{**}p < 0.01$ and $^{***}p < 0.001$ compared with the SO group; $^{\#}p < 0.05$, $^{\#\#}p < 0.01$ and $^{\#\#\#}p < 0.001$ compared with the SAP group. JAK2, janus kinase two; STAT3, signal transducer and activator of transcription three; SO, sham operation; SAP, severe acute pancreatitis.

Figure 7E shows that the amylase activity in the cerulein group was significantly upregulated compared with the control group ($p < 0.001$). When rhein was added to the supernatants of cells at concentrations of 0.25, 0.5 and 1 μg/ml 20 min before adding cerulein, the amylase level downregulated in a concentration-dependent manner ($p < 0.001$). **Figure 7F** reveals that the TNF-α level in the cerulein group was significantly upregulated compared with the control group ($p < 0.001$). This increasing trend was significantly reversed by treatment with rhein in a concentration-dependent manner ($p < 0.001$). These results suggested that rhein protected the injured AR42J cells.

Effect of Rhein on the AR42J Cell Injury Model

Effect Of Rhein On JAK2 and STAT3 Expressions In The AR42J Cell Injury Model **Figure 8** shows that p-JAK2, JAK2, p-STAT3 and STAT3 proteins expression were significantly increased in the cerulein group compared with the control group ($p < 0.001$). After rhein treatment, the activity of p-JAK2, JAK2, p-STAT3 and STAT3 were significantly decreased compared with the cerulein group ($p < 0.001$). The expression of p-JAK2, JAK2, p-STAT3and STAT3 proteins at the middle and lower doses in the rhein group differed significantly from those at the high dose. These results suggest that rhein could inhibit the expression of protein p-JAK2, JAK2, p-STAT3and STAT3, which are important components in the JAK2/STAT3 signalling transduction pathway induced by cerulein in AR42J cells.

DISCUSSION

In the current study, we found that rhein significantly alleviated pancreatic histopathology, attenuated proinflammation factors, and inhibited JAK2/STAT3 signalling pathway in SAP rat model. In SAP cell model, rhein significantly decreased the expression of amylase and TNF-α induced by cerulein, and inhibited JAK2/STAT3 signalling pathway.

The pathogenesis of SAP seems to be related to multifaceted pathological processes, involving inflammation, parenchymal acinar cell death by necrosis, and cellular damage in the pancreas. We established SAP rat models by retrograde pancreatic bile duct injection of sodium taurocholate (Pereda et al., 2004; Wu et al., 2013; Pérez et al., 2015). However, under the action of sodium taurocholate, pancreatic acinar cells are damaged and the inflammatory response is enhanced, which may activate various disease-related signalling pathways, such as the JAK2/STAT3 signalling pathway (Booth et al., 2011; Husain et al., 2012; Lerch and Gorelick, 2013). Conversely, crosstalk between acinar cells and the immune system perpetuates the inflammatory response. These pathways amplify the production of proinflammatory cytokines,

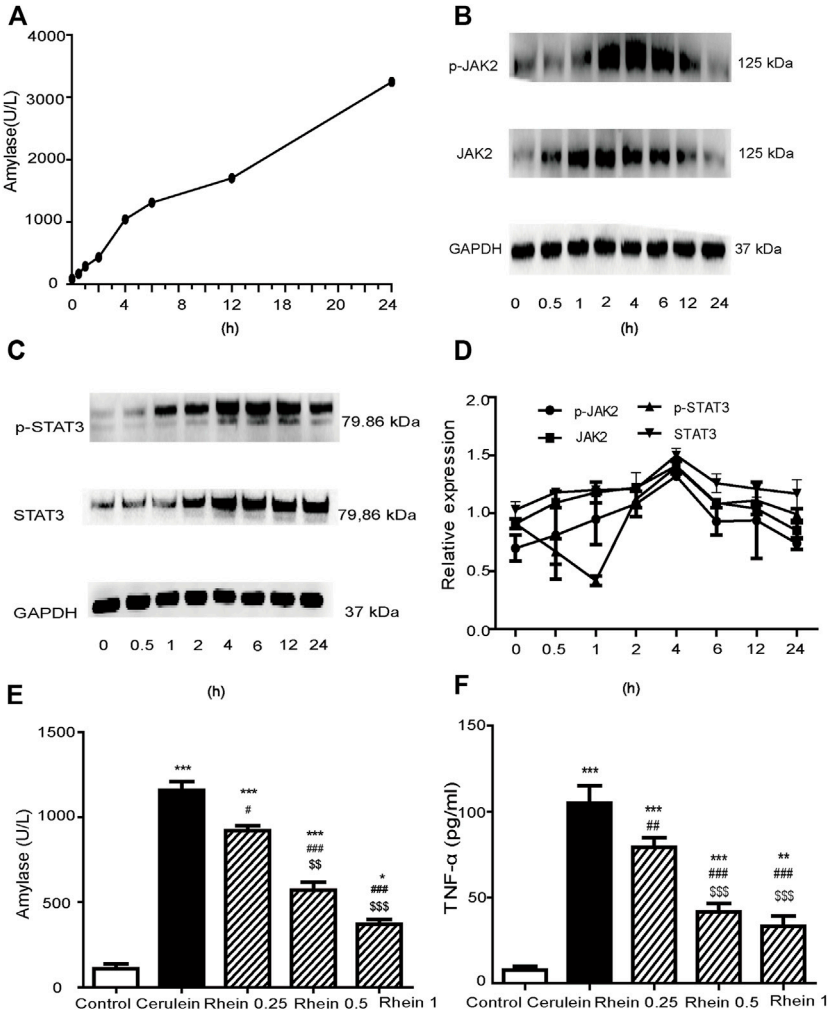

FIGURE 7 | AR42J cell injury model established by cerulein treatment. **(A)** The amylase activity was measured at different time points. **(B,C)** Western blot findings of p-JAK2, JAK2, p-STAT3 and STAT3 protein expression in AR42J cells treated with cerulein. **(D)** Peak of p-JAK2, JAK2, p-STAT3 and STAT3 proteins expression at different simultaneous phase sites. **(E)** amylase activity in the control, cerulein, rhein 0.25 μg/ml, rhein 0.5 μg/ml and rhein 1 μg/ml groups **(F)** The TNF-α levels in the control, cerulein, rhein 0.25 μg/ml, rhein 0.5 μg/ml and rhein 1 μg/ml groups. Data are expressed as mean ± SD (n = 5 per group). Significance between groups was evaluated by one way analysis of variance (ANOVA) followed by a Tukey post hoc test. JAK2, janus kinase two; STAT3, signal transducer and activator of transcription 3.

including TNF-α, IL-1 β, IL-6 and IL-18 (Lerch and Gorelick, 2013; Abu-El-Haija and Lowe, 2018; Lee and Papachristou, 2019). The SAP cell model was induced by cerulein. Pathological changes similar to those of human SAP were found during the induction (Yu et al., 2008; Lee et al., 2010). Because cerulein is a CCK analogue, it binds to CCK receptors to activate signal transduction in pancreatic acinar cells. The CCK2 receptor is a Gq protein-coupled receptor that mediates JAK2/STAT3 activation and promotes pancreatic tumour cell proliferation (Ferrand et al., 2005; Ferrand et al., 2006; Beales and Ogunwobi, 2009). Previous studies have shown that cerulein induces IL-1β expression in pancreatic acinar cells by activating the JAK2/STAT3 signalling pathway (Yu et al., 2006; Yu et al., 2007; Zhou et al., 2021). Therefore, relieving pancreatic inflammation and inhibiting activated JAK2/STAT3 should be included in new-generation of drugs for SAP.

Traditional Chinese medicine has rich experience in the prevention and treatment of SAP. At present, it has been reported that Dachengqi Decoction plays an important role in reducing the complications of SAP in patients (Zhang et al., 2008; Wan et al., 2011). In SAP rats treated with Dachengqi Decoction and rhubarb, the distribution characteristics of five main anthraquinone compounds of rhubarb (rhein, emodin methyl ether, rhubarb phenol, aloe-emodin and emodin) in pancreas were studied, rhein is the most abundant component of all anthraquinones detected in pancreatic tissue (Zhao et al., 2004; Gong et al., 2009). However, the research on the inhibitory effect of the above traditional Chinese medicine on SAP is often limited to the determination of inflammatory factors and pharmacodynamics, and there is a lack of in-depth research on its mechanism.

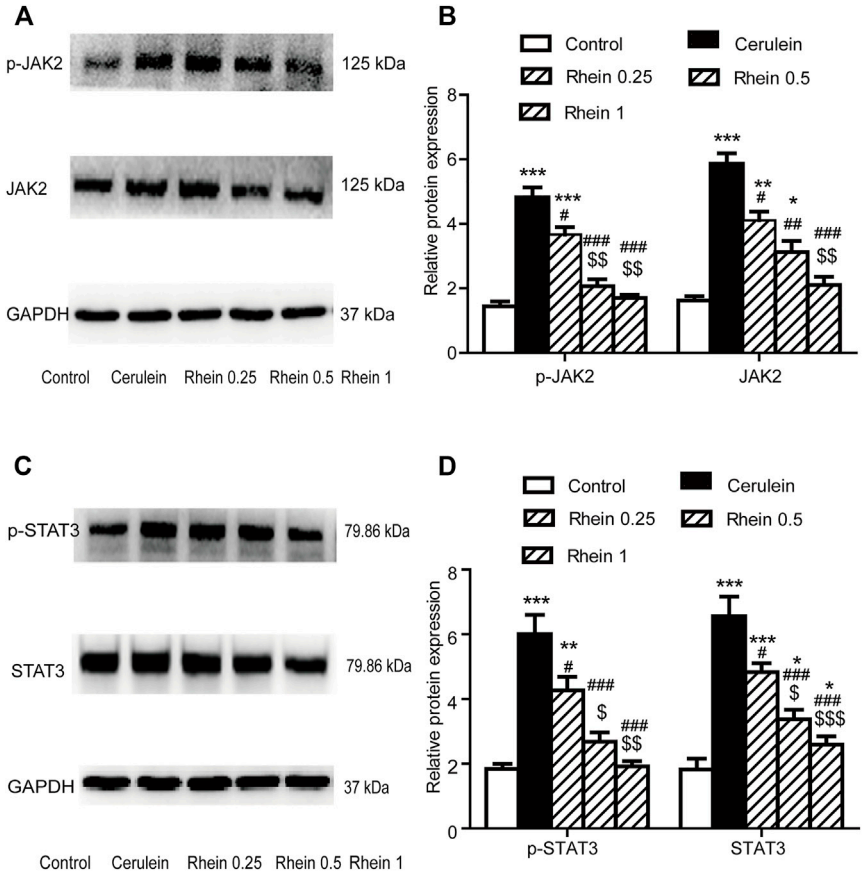

FIGURE 8 | The protein expression of p-JAK2, JAK2, p-STAT3 and STAT3 in the AR42J cell model was measured by western blot. **(A,B)** p-JAK2 and JAK2 protein expression in the control, cerulein, rhein 0.25 μg/ml, rhein 0.5 μg/ml and rhein 1 μg/ml groups. **(C,D)** p-STAT3 and STAT3 protein expression in the control, cerulein, rhein 0.25 μg/ml, rhein 0.5 μg/ml and rhein 1 μg/ml groups. Data are expressed as mean ± SD ($n = 5$ per group). Significance between groups was evaluated by one way analysis of variance (ANOVA) followed by a Tukey post hoc test. $^{*}p < 0.05$, $^{**}p < 0.01$ and $^{***}p < 0.001$ compared with the control group; $^{\#}p < 0.05$, $^{\#\#}p < 0.01$ and $^{\#\#\#}p < 0.001$ compared with the cerulein group; $^{\$}p < 0.05$, $^{\$\$}p < 0.01$ and $^{\$\$\$}p < 0.001$ compared with the rhein 0.25 μg/ml group. JAK2, janus kinase two; STAT3, signal transducer and activator of transcription 3.

At present, natural products with low side effects and efficacy have been considered for the treatment of SAP. In SAP model, huperzine II treatment was able to increase antioxidant, anti-inflammatory and anti-apoptotic activity (Piao et al., 2017), possibly by activating the farnesoid X receptor or affecting the JAK2/STAT3 signalling pathway to reduce oxidative, inflammatory and apoptotic levels (Li et al., 2020), thus providing protection for SAP. Another study also indicated that curcumin ameliorates acute renal injury in a rat model of SAP. The molecular mechanism of its effect may be associated with the suppression of the JAK2/STAT3 pathway to reduce TNF-α and IL-6 levels in SAP-induced acute renal injury. Rhein is a natural molecule and our results showed that it inhibited the JAK2/STAT3 signalling pathway, and caused a decrease in inflammatory factor levels, these results consistent with the predicted target results of network pharmacology. Besides, Rhein is widely found in medicinal plants such as rhubarb, *Sennae folium*, *Semen cassiae*, and *Polygonum multiflorum*, and it is widely used in clinical practice (Xian et al., 2020). These medical plants are broadly used all over the world. In China, approximately 10% (800) of more than 8,000 proprietary Chinese medicines contain rhubarb. So, rhein has extremely important value in the treatment of SAP.

Nowadays, rhein is widely used in inflammation treatment in China (Ji and Gu, 2021; Wang et al., 2020). In this study, in order to investigate whether rhein possessed anti-inflammatory effects in a rat model of SAP, we first established a rat model of SAP. In our current study, SAP model was established in rats by retrograde pancreatic bile duct injection of sodium taurocholate with a dose of 3.5% (Pereda et al., 2004; Wu et al., 2013; Pérez et al., 2015). Then the model was tested by pathological damage and inflammatory cytokines. For pancreatic injury, we tested it by HE staining. Edema, necrosis and inflammatory infiltration were observed in the acinar cells of pancreatic tissue. These alterations can be attributed to the action of sodium taurocholate. However, under the action of sodium taurocholate, pancreatic acinar cells are damaged and the inflammatory response is enhanced, which may activate various disease-related signalling

pathways, such as the JAK2/STAT3 signalling pathway (Booth et al., 2011; Husain et al., 2012; Lerch and Gorelick, 2013). Previous studies have reported that the JAK2/STAT3 pathway plays a key role in inflammatory diseases (Zhu et al., 2017; Xia et al., 2021). Therefore, the JAK2/STAT3 signalling pathway plays a crucial role in evaluating potential mechanism. In this work, p-JAK2, JAK2, p-STAT3 and STAT3 proteins expression were significantly increased in the SAP group compared with the control group. The above-mentioned findings indicated that a SAP rat model was successfully established.

After rhein treatment, inflammatory cytokines were decreased, and JAK2/STAT3 signalling pathway related proteins were also downregulated, suggesting that rhein plays an anti-inflammatory role by inhibiting JAK2/STAT3 signaling pathway. In addition, HE staining is another method frequently used in evaluation of pancreatic injury (Wang et al., 2020). In the current study, the protective effects of rhein were further validated by the significantly improved histological results. The histopathological changes were significantly restored by rhein treatment, and less infiltration of inflammatory cells was observed in the rhein group compared with the model group. These findings also provided convincing evidence that rhein exerted protective effects against sodium taurocholate-induced pancreatic injury.

According to published many literatures about rhein anti-inflammatory mechanism, such as the interactive relationships of rhein on multiple inflammatory signaling pathways and cellular processes (Wang et al., 2020; Ding et al., 2020) The SAP cell model was induced by cerulein in AR42J cells, which pathological changes similar to those of human SAP were found during the induction (Yu et al., 2008; Lee et al., 2010). AR42J cells were treated with 10^{-8} mol/L of cerulein for 24 h. Then the model was tested by inflammatory cytokines and JAK2/STAT3 signalling pathway related proteins at 4 h. These alterations can be attributed to the action of cerulein. In this work, amylase and TNF-α activity in the SAP group were significantly upregulated compared with the control group, and p-JAK2, JAK2, p-STAT3 and STAT3 proteins expression were significantly increased in the SAP group compared with the control group. The above-mentioned findings indicated that SAP cell model was successfully established. After rhein treatment, inflammatory cytokines were downregulated, and JAK2/STAT3 signalling pathway related proteins were also decreased, suggesting that rhein plays an anti-inflammatory role by regulating JAK2/STAT3 signaling pathway.

In summary, rhein not only inhibits the release of inflammatory factors but also alters the expression of JAK2/STAT3 signal pathway-related proteins in the SAP model *in vivo* and *in vitro*. Our findings indicate the potential therapeutic effects of rhein on SAP.

CONCLUSION

Taken together, our data provided evidence that rhein plays therapeutic role by inhibiting therelease of inflammatory factors in the SAP model *in vivo* and *in vitro*. This effect may be related to the regulation of JAK2/STAT3 signal pathway. This study will be helpful for the treatment of SAP.

DATA AVAILABILITY STATEMENT

The original contributions presented in the study are included in the article/Supplementary Material, further inquiries can be directed to the corresponding authors.

ETHICS STATEMENT

The present study was approved by the Animal Care and Use Committee of Shanghai University of Traditional Chinese Medicine. Written informed consent was obtained from the owners for the participation of their animals in this study.

AUTHOR CONTRIBUTIONS

XG and ML designed the study and revised the manuscript. XY, HG, LY, YM, LY, and JM performed the experiments, XY and HG conducted the data analysis and drafted the manuscript. All authors have read and approved the final manuscript.

FUNDING

This work was supported by the funded by Medical discipline Construction Project of Pudong Health Committee of Shanghai (Grant No.PWYgy2021-06), the National Natural Science Foundation of China (No.81973649), Emphasis Subspeciality of Shanghai Pudong (PWZy2020-07), the Leading Medical Talent Training Program of Pudong Health Bureau of Shanghai (PWR12019-02), the National Natural Science Foundation of China (No.8217141990), Shanghai University of Traditional Chinese Medicine "Postgraduate Innovation Training Special Project (Y2021022)", Shanghai Municipal Commission of Health and Wellness - Federation of Chinese and Western Medicine Burn Trauma Specialists (ZY(2021-2023)-0302).

REFERENCES

Abu-El-Haija, M., and Lowe, M. E. (2018). Pediatric Pancreatitis-Molecular Mechanisms and Management. *Gastroenterol. Clin. North. Am.* 47, 741–753. doi:10.1016/j.gtc.2018.07.003

Andersson, R., Andersson, B., Andersson, E., Axelsson, J., Eckerwall, G., and Tingstedt, B. (2007). Acute Pancreatitis-Ffrom Cellular Signalling to Complicated Clinical Course. *HPB (Oxford)* 9, 414–420. doi:10.1080/13651820701713766

Beales, I. L., and Ogunwobi, O. O. (2009). Glycine-extended Gastrin Inhibits Apoptosis in Barrett's Oesophageal and Oesophageal Adenocarcinoma Cells

through JAK2/STAT3 Activation. *J. Mol. Endocrinol.* 42, 305–318. doi:10.1677/JME-08-0096

Booth, D. M., Murphy, J. A., Mukherjee, R., Awais, M., Neoptolemos, J. P., Gerasimenko, O. V., et al. (2011). Reactive Oxygen Species Induced by Bile Acid Induce Apoptosis and Protect against Necrosis in Pancreatic Acinar Cells. *Gastroenterology* 140, 2116–2125. doi:10.1053/j.gastro.2011.02.054

Brands, M. W., Banes-Berceli, A. K., Inscho, E. W., Al-Azawi, H., Allen, A. J., and Labazi, H. (2010). Interleukin 6 Knockout Prevents Angiotensin II Hypertension: Role of Renal Vasoconstriction and Janus Kinase 2/signal Transducer and Activator of Transcription 3 Activation. *Hypertension* 56, 879–884. doi:10.1161/hypertensionaha.110.158071

Chen, H., Li, F., Jia, J. G., Diao, Y. P., Li, Z. X., and Sun, J. B. (2010). Effects of Traditional Chinese Medicine on Intestinal Mucosal Permeability in Early Phase of Severe Acute Pancreatitis. *Chin. Med. J. (Engl)* 123, 1537–1542. doi:10.3760/cma.j.issn.0366-6999.2010.12.011

Chen, Y., Xiang, W., Li, X., Wang, D., and Qian, C. (2019). Rosiglitazone Prevents Acute Pancreatitis through Inhibiting microRNA-26a Expression. *Exp. Ther. Med.* 18, 1246–1252. doi:10.3892/etm.2019.7711

Chen, Z., Chen, Y., Pan, L., Li, H., Tu, J., Liu, C., et al. (2015). Dachengqi Decoction Attenuates Inflammatory Response via Inhibiting HMGB1 Mediated NF-Kb and P38 MAPK Signaling Pathways in Severe Acute Pancreatitis. *Cell Physiol Biochem* 37, 1379–1389. doi:10.1159/000430403

Cheng, L., Chen, Q., Pi, R., and Chen, J. (2021). A Research Update on the Therapeutic Potential of Rhein and its Derivatives. *Eur. J. Pharmacol.* 899, 173908. doi:10.1016/j.ejphar.2021.173908

Ding, X., Wang, Y., Wen, C., Wang, S., Ruan, Q., Li, Z., et al. (2020). Anti-Inflammatory Efficacy of Fabricated Rhein Micelles. *J. Biomed. Nanotechnol* 16, 1463–1470. doi:10.1166/jbn10.1166/jbn.2020.2982

Ferrand, A., Kowalski-Chauvel, A., Bertrand, C., Escrieut, C., Mathieu, A., Portolan, G., et al. (2005). A Novel Mechanism for JAK2 Activation by a G Protein-Coupled Receptor, the CCK2R: Implication of This Signaling Pathway in Pancreatic Tumor Models. *J. Biol. Chem.* 280, 10710–10715. doi:10.1074/jbc.m413309200

Ferrand, A., Vatinel, S., Kowalski-Chauvel, A., Bertrand, C., Escrieut, C., Fourmy, D., et al. (2006). Mechanism for Src Activation by the CCK2 Receptor: Patho-Physiological Functions of This Receptor in Pancreas. *World J. Gastroenterol.* 12, 4498–4503. doi:10.1055/s-2006-92684410.3748/wjg.v12.i28.4498

Gallmeier, E., Schäfer, C., Moubarak, P., Tietz, A., Plössl, I., Huss, R., et al. (2005). JAK and STAT Proteins Are Expressed and Activated by IFN-Gamma in Rat Pancreatic Acinar Cells. *J. Cel Physiol* 203, 209–216. doi:10.1002/jcp.20216

Gjessing, J. (1972). Renal Failure in Acute Pancreatitis. *Br. Med. J.* 4, 359–360. doi:10.1136/bmj.4.5836.359-b

Gong, H. L., Tang, W. F., Yu, Q., Xiang, J., Xia, Q., Chen, G. Y., et al. (2009). Effect of Severe Acute Pancreatitis on Pharmacokinetics of Da-Cheng-Qi Decoction Components. *World J. Gastroenterol.* 15, 5992–5999. doi:10.3748/wjg.15.5992

Hanayama, R., Tanaka, M., Miwa, K., Shinohara, A., Iwamatsu, A., and Nagata, S. (2002). Identification of a Factor that Links Apoptotic Cells to Phagocytes. *Nature* 417, 182. doi:10.1038/417182a

He, Z. J., Matikainen, M. P., Alho, H., Harmoinen, A., Ahola, T., and Nordback, I. (1999). Extrapancreatic Organ Impairment in Caerulein Induced Pancreatitis. *Ann. Chir Gynaecol.* 88, 112–117. doi:10.1055/s-1999-7281

Hirano, T., and Manabe, T. (1993). A Possible Mechanism for Gallstone Pancreatitis: Repeated Short-Term Pancreaticobiliary Duct Obstruction with Exocrine Stimulation in Rats. *Proc. Soc. Exp. Biol. Med. Soc. Exp. Biol. Med.* 202, 246. doi:10.3181/00379727-202-43534

Horiguchi, A., Asano, T., Kuroda, K., Sato, A., Asakuma, J., Ito, K., et al. (2010). STAT3 Inhibitor WP1066 as a Novel Therapeutic Agent for Renal Cell Carcinoma. *Br. J. Cancer* 102, 1592–1599. doi:10.1038/sj.bjc.6605691

Huang, L. Y., Chen, P., Xu, L. X., Zhou, Y. F., Zhang, Y. P., and Yuan, Y. Z. (2012). SFractalkine Upregulates Inflammation Through CX3CR1 and the Jak-Stat Pathway in Severe Acute Pancreatitis rat Model. *Inflammation* 35, 1023–1030. doi:10.1007/s10753-011-9406-5

Husain, S. Z., Orabi, A. I., Muili, K. A., Luo, Y., Sarwar, S., Mahmood, S. M., et al. (2012). Ryanodine Receptors Contribute to Bile Acid-Induced Pathological Calcium Signaling and Pancreatitis in Mice. *Am. J. Physiol. Gastrointest. Liver Physiol.* 302, G1423–G1433. doi:10.1152/ajpgi.00546.2011

Ivanenkov, Y. A., Balakin, K. V., and Lavrovsky, Y. (2011). Small Molecule Inhibitors of NF-kB and JAK/STAT Signal Transduction Pathways as Promising Anti-inflammatory Therapeutics. *Mini Rev. Med. Chem.* 11, 55–78. doi:10.2174/138955711793564079

Ji, L., and Gu, H. (2021). The Anti-obesity Effects of Rhein on Improving Insulin Resistance (IR) and Blood Lipid Levels Are Involved in Endoplasmic Reticulum Stress (ERs), Inflammation, and Oxidative Stress *In Vivo* and Vitro. *Bioengineered* 12, 5797–5813. doi:10.1080/2165597910.1080/21655979.2021.1969196

Ju, K. D., Lim, J. W., Kim, K. H., and Kim, H. (2011). Potential Role of NADPH Oxidase-Mediated Activation of Jak2/Stat3 and Mitogen-Activated Protein Kinases and Expression of TGF-B1 in the Pathophysiology of Acute Pancreatitis. *Inflamm. Res.* 60, 791–800. doi:10.1007/s00011-011-0335-4

Lankisch, P. G., and Lerch, M. M. (2006). Pharmacological Prevention and Treatment of Acute Pancreatitis: where Are We Now? *Dig. Dis.* 24, 148–159. doi:10.1159/000090318

Lee, J., Seo, J., Kim, H., Chung, J. B., and Kim, K. H. (2003). Signal Transduction of Cerulein-Induced Cytokine Expression and Apoptosis in Pancreatic Acinar Cells. *Ann. N. Y Acad. Sci.* 1010, 104–108. doi:10.1196/annals.1299.017

Lee, J., Seo, J. H., Lim, J. W., and Kim, H. (2010). Membrane Proteome Analysis of Cerulein-Stimulated Pancreatic Acinar Cells: Implication for Early Event of Acute Pancreatitis. *Gut liver* 4, 84–93. doi:10.5009/gnl.2010.4.1.84

Lee, P. J., and Papachristou, G. I. (2019). New Insights into Acute Pancreatitis. *Nat. Rev. Gastroenterol. Hepatol.* 16, 479–496. doi:10.1038/s41575-019-0158-2

Lerch, M. M., and Gorelick, F. S. (2013). Models of Acute and Chronic Pancreatitis. *Gastroenterology* 144, 1180–1193. doi:10.1053/j.gastro.2012.12.043

Li, S., Xu, Z., Guo, J., Zheng, J., Sun, X., and Yu, J. (2020). Farnesoid X Receptor Activation Induces Antitumour Activity in Colorectal Cancer by Suppressing JAK2/STAT3 Signalling via Transactivation of SOCS3 gene. *J. Cell. Mol. Med.* 24, 14549–14560. doi:10.1111/jcmm.16083

Morel, D. R., Frossard, J. L., Cikirikcioglu, B., Tapponnier, M., and Pastor, C. M. (2006). Time Course of Lung Injury in Rat Acute Pancreatitis. *Intensive Care Med.* 32, 1872–1880. doi:10.1007/s00134-006-0264-9

Norman, J. (1998). The Role of Cytokines in the Pathogenesis of Acute Pancreatitis. *Am. J. Surg.* 175, 76. doi:10.1016/S0002-9610(97)00240-7

O'shea, J. J. (2004). Targeting the Jak/STAT Pathway for Immunosuppression. *Ann. Rheum. Dis.* 63 Suppl 2, ii67–ii71. doi:10.1136/ard.2004.028290

Pang, M., Ma, L., Gong, R., Tolbert, E., Mao, H., Ponnusamy, M., et al. (2010). A Novel STAT3 Inhibitor, S3I-201, Attenuates Renal Interstitial Fibroblast Activation and Interstitial Fibrosis in Obstructive Nephropathy. *Kidney Int.* 78, 257–268. doi:10.1038/ki.2010.154

Pereda, J., Sabater, L., Cassinello, N., Gómez-Cambronero, L., Closa, D., Folch-Puy, E., et al. (2004). Effect of Simultaneous Inhibition of TNF-Alpha Production and Xanthine Oxidase in Experimental Acute Pancreatitis: the Role of Mitogen Activated Protein Kinases. *Ann. Surg.* 240, 108–116. doi:10.1097/01.sla.0000129343.47774.89

Pérez, S., Pereda, J., Sabater, L., and Sastre, J. (2015). Pancreatic Ascites Hemoglobin Contributes to the Systemic Response in Acute Pancreatitis. *Free Radic. Biol. Med.* 81, 145–155. doi:10.1016/j.freeradbiomed.2014.08.008

Piao, X., Liu, B., Guo, L., Meng, F., and Guo, L. (2017). κPicroside II Shows Protective Functions for Severe Acute Pancreatitis in Rats by Preventing NF-B-Dependent Autophagy. *Oxid. Med. Cell. Longev.* 7085709. doi:10.1155/2017/7085709

Schmidt, J., Rattner, D. W., Lewandrowski, K., Compton, C. C., Mandavilli, U., Knoefel, W. T., et al. (1992). A Better Model of Acute Pancreatitis for Evaluating Therapy. *Ann. Surg.* 215, 44–56. doi:10.1097/00000658-199201000-00007

Vona-Davis, L. C., Frankenberry, K. A., Waheed, U., Peterson, E., and McFadden, D. W. (2005). Expression of STAT3 and SOCS3 in Pancreatic Acinar Cells. *J. Surg. Res.* 127, 14–20. doi:10.1016/j.jss.2005.03.019

Wan, M. H., Li, J., Gong, H. L., Xue, P., Zhu, L., Chen, G. Y., et al. (2011). Clinical Observation on the Effect of Dexamethasone and Chinese Herbal Decoction for Purgation in Severe Acute Pancreatitis Patients. *Chin. J. Integr. Med.* 17, 141–145. doi:10.1007/s11655-011-0630-5

Wang, H., Yang, D., Li, L., Yang, S., Du, G., and Lu, Y. (2020). Anti-inflammatory Effects and Mechanisms of Rhein, an Anthraquinone Compound, and its Applications in Treating Arthritis: A Review. *Nat. Prod. Bioprospect* 10, 445–452. doi:10.1007/s13659-020-00272-y

Weng, T. I., Wu, H. Y., Chen, B. L., and Liu, S. H. (2012). Honokiol Attenuates the Severity of Acute Pancreatitis and Associated Lung Injury via Acceleration of Acinar Cell Apoptosis. *Shock* 37, 478–484. doi:10.1097/SHK.0b013e31824653be

Wu, J., Hu, Y., Xiang, L., Li, S., Yuan, Y., Chen, X., et al. (2016). San-Huang-Xie-Xin-Tang Constituents Exert Drug-Drug Interaction of Mutual Reinforcement at Both Pharmacodynamics and Pharmacokinetic Level: A Review. *Front. Pharmacol.* 7, 448. doi:10.3389/fphar.2016.00448

Wu, L., Li, H., Zheng, S. Z., Liu, X., Cai, H., and Cai, B. C. (2013). Da-Huang-Fu-Zi-Tang Attenuates Liver Injury in Rats with Severe Acute Pancreatitis. *J. Ethnopharmacol* 150, 960–966. doi:10.1016/j.jep.2013.09.051

Xia, T., Gu, Y., Shen, J., Zheng, L., and Xu, C. (2021). Limonin Ameliorates Acute Pancreatitis by Suppressing JAK2/STAT3 Signaling Pathway. *Environ. Toxicol.* 36, 2392–2403. doi:10.1002/tox.23352

Xia, X. M., Li, B. K., Xing, S. M., and Ruan, H. L. (2012). Emodin Promoted Pancreatic Claudin-5 and Occludin Expression in Experimental Acute Pancreatitis Rats. *World J. Gastroenterol.* 18, 2132–2139. doi:10.3748/wjg.v18.i17.213210.3748/wjg.v18.i17.2132

Xian, Z., Tian, J., Wang, L., Zhang, Y., Han, J., Deng, N., et al. (2020). Effects of Rhein on Bile Acid Homeostasis in Rats. *Biomed. Res. Int.* 2020, 8827955. doi:10.1155/2020/8827955

Xu, F., Liu, Y., Song, R., Dong, H., and Zhang, Z. (2010). Constituents of Da-Cheng-Qi Decoction and its Parent Herbal Medicines Determined by LC-MS/MS. *Nat. Prod. Commun.* 5, 789–794. doi:10.1002/mnfr.20090024410.1177/1934578x1000500522

Xu, F., Liu, Y., Song, R., Dong, H., and Zhang, Z. (2010). HPLC/DAD Comparison of Sixteen Bioactive Components between Da-Cheng-Qi Decoction and its Parent Herbal Medicines. *Nat. Prod. Commun.* 5, 893–896. doi:10.1007/s00044-009-9208-6

Xu, F., Liu, Y., Zhang, Z., Song, R., Dong, H., and Tian, Y. (2008). Rapid Simultaneous Quantification of Five Active Constituents in Rat Plasma by High-Performance Liquid Chromatography/tandem Mass Spectrometry after Oral Administration of Da-Cheng-Qi Decoction. *J. Pharm. Biomed. Anal.* 47, 586–595. doi:10.1016/j.jpba.2008.02.005

Xue, D., Zhang, W., Zhang, Y., Wang, H., Zheng, B., and Shi, X. (2006). Adjusting Effects of Baicalin for Nuclear Factor-kappaB and Tumor Necrosis Factor-Alpha on Rats with Caerulein-Induced Acute Pancreatitis. *Mediators Inflamm.* 2006, 26295. doi:10.1155/mi/2006/26295

Yang, D. Y., Fushimi, H., Cai, S. Q., and Komatsu, K. (2004). Molecular Analysis of Rheum Species Used as Rhei Rhizoma Based on the Chloroplast Matk Gene Sequence and its Application for Identification. *Biol. Pharm. Bull.* 27, 375. doi:10.1248/bpb.27.375

Yang, L., Lin, S., Kang, Y., Xiang, Y., Xu, L., Li, J., et al. (2019). Rhein Sensitizes Human Pancreatic Cancer Cells to Egfr Inhibitors by Inhibiting Stat3 Pathway. *J. Exp. Clin. Cancer Res.* 38, 31. doi:10.1186/s13046-018-1015-9

Yang, S., Song, Y., Wang, Q., Liu, Y., Wu, Z., Duan, X., et al. (2021). Daphnetin Ameliorates Acute Lung Injury in Mice with Severe Acute Pancreatitis by Inhibiting the JAK2-STAT3 Pathway. *Sci. Rep.* 11, 11491. doi:10.1038/s41598-021-91008-6

Ye, J., Dai, H., Liu, Y., Yu, B., Yang, J., and Fei, A. (2020). Blockade of C3a/C3aR axis Alleviates Severe Acute Pancreatitis-Induced Intestinal Barrier Injury. *Am. J. Transl Res.* 12, 6290

Yu, J. H., Kim, K. H., and Kim, H. (2007). SOCS 3 and PPAR-Gamma Ligands Inhibit the Expression of IL-6 and TGF-Beta1 by Regulating JAK2/STAT3 Signaling in Pancreas. *Int. J. Biochem. Cel Biol* 40, 677–688. doi:10.1016/j.biocel.2007.10.007

Yu, J. H., Kim, K. H., and Kim, H. (2006). Suppression of IL-1beta Expression by the Jak 2 Inhibitor AG490 in Cerulein-Stimulated Pancreatic Acinar Cells. *Biochem. Pharmacol.* 72, 1555–1562. doi:10.1016/j.bcp.2006.07.008

Yu, J. H., Seo, J. Y., Kim, K. H., and Kim, H. (2008). Differentially Expressed Proteins in Cerulein-Stimulated Pancreatic Acinar Cells: Implication for Acute Pancreatitis. *Int. J. Biochem. Cel Biol* 40, 503–516. doi:10.1016/j.biocel.2007.09.001

Yu, J. H., Yun, S. Y., Lim, J. W., Kim, H., and Kim, K. H. (2003). Proteome Analysis of Rat Pancreatic Acinar Cells: Implication for Cerulein-Induced Acute Pancreatitis. *Proteomics* 3, 2446–2453. doi:10.1002/pmic.200300545

Zerem, E. (2014). Treatment of Severe Acute Pancreatitis and its Complications. *World J. Gastroenterol.* 20, 13879–13892. doi:10.3748/wjg.v20.i38.13879

Zhang, H. Y., and Chang, X. R. (2016). Astragaloside Ⅳ Inhibits Jak2/stat3 Signaling Pathway and Alleviates Severe Acute Pancreatitis-Associated Acute Liver Injury in Rats. *Chin. J. Pathophysiology*. doi:10.3969/j.issn.1000-4718.2016.06.004

Zhang, M. J., Zhang, G. L., Yuan, W. B., Ni, J., and Huang, L. F. (2008). Treatment of Abdominal Compartment Syndrome in Severe Acute Pancreatitis Patients with Traditional Chinese Medicine. *World J. Gastroenterol.* 14, 3574–3578. doi:10.3748/wjg.14.3574

Zhang, Y., Zhu, L., Wang, J., Zhao, J., Zhao, X., Guo, H., et al. (2016). Formula Compatibility Identification of Dachengqi Decoction Based on the Effects of Absorbed Components in Cerulein-Injured Pancreatic Ar42j Cells. *Evid. Based Complement. Alternat Med.* 2016, 3198549. doi:10.1155/2016/3198549

Zhao, J., Tang, W., Wang, J., Xiang, J., Gong, H., and Chen, G. (2013). Pharmacokinetic and Pharmacodynamic Studies of Four Major Phytochemical Components of Da-Cheng-Qi Decoction to Treat Acute Pancreatitis. *J. Pharmacol. Sci.* 122, 118–127. doi:10.1254/jphs.13037FP

Zhao, X., Li, J., Zhu, S., Liu, Y., Zhao, J., Wan, M., et al. (2014). Rhein Induces a Necrosis-Apoptosis Switch in Pancreatic Acinar Cells. *Evid. Based Complement. Alternat Med.* 2014, 404853. doi:10.1155/2014/404853

Zhao, Y. Q., Liu, X. H., Ito, T., and Qian, J. M. (2004). Protective Effects of Rhubarb on Experimental Severe Acute Pancreatitis. *World J. Gastroenterol.* 10, 1005–1009. doi:10.3748/wjg.v10.i7.1005

Zhong, K. (2015). Curcumin Mediates a Protective Effect via TLR-4/nf-Kb Signaling Pathway in Rat Model of Severe Acute Pancreatitis. *Cell Biochem. Biophys.* 73, 175–180. doi:10.1007/s12013-015-0664-y

Zhou, Z., Chen, Y., Dong, W., An, R., Liang, K., and Wang, X. (2021). Da Cheng Qi Decoction Alleviates Cerulein-Stimulated AR42J Pancreatic Acinar Cell Injury via the JAK2/STAT3 Signaling Pathway. *Evid Based. Complement. Altern. Med.* 2021, 1–13. doi:10.1155/2021/6657036

Zhu, S., Zhang, C., Weng, Q., and Ye, B. (2017). Curcumin Protects against Acute Renal Injury by Suppressing JAK2/STAT3 Pathway in Severe Acute Pancreatitis in Rats. *Exp. Ther. Med.* 14, 1669–1674. doi:10.3892/etm.2017.4647

Conflict of Interest: The authors declare that the research was conducted in the absence of any commercial or financial relationships that could be construed as a potential conflict of interest.

Publisher's Note: All claims expressed in this article are solely those of the authors and do not necessarily represent those of their affiliated organizations, or those of the publisher, the editors and the reviewers. Any product that may be evaluated in this article, or claim that may be made by its manufacturer, is not guaranteed or endorsed by the publisher.

frontiers | Frontiers in Pharmacology

ORIGINAL RESEARCH
published: 01 April 2022
doi: 10.3389/fphar.2022.857015

Kaempferol From *Penthorum chinense* Pursh Attenuates Hepatic Ischemia/Reperfusion Injury by Suppressing Oxidative Stress and Inflammation Through Activation of the Nrf2/HO-1 Signaling Pathway

Yifan Chen[1†], Tongxi Li[1†], Peng Tan[2], Hao Shi[1], Yonglang Cheng[1], Tianying Cai[1], Junjie Bai[1], Yichao Du[2] and Wenguang Fu[1,2*]*

[1]Department of General Surgery (Hepatopancreatobiliary Surgery), The Affiliated Hospital of Southwest Medical University, Luzhou, China, [2]Academician (Expert) Workstation of Sichuan Province, The Affiliated Hospital of Southwest Medical University, Luzhou, China

The purpose of this study is to investigate the protective effect of kaempferol (KAE), the main active monomer from *Penthorum chinense* Pursh, on hepatic ischemia/reperfusion injury (HI/RI) and its specific mechanism. HI/RI is a common complication closely related to the prognosis of liver surgery, and effective prevention and treatment methods are still unavailable. Ischemia/reperfusion (I/R) injury is caused by tissue damage during ischemia and sustained oxidative stress and inflammation during reperfusion. *Penthorum chinense* Pursh is a traditional Chinese medicine widely used to treat liver disease since ancient times. Kaempferol (KAE), a highly purified flavonoid active monomer isolated and extracted from *Penthorum chinense* Pursh, was investigated for its protective effect on HI/RI. Our study indicates that KAE pretreatment alleviated I/R-induced transaminase elevation and pathological changes. Further analysis revealed that KAE pretreatment attenuates I/R-induced oxidative stress (as measured by the content of MDA, SOD and GSH) *in vivo* and reduces hypoxia/reoxygenation (H/R) -induced reactive oxygen species (ROS) generation *in vitro*. Meanwhile, KAE inhibits activation of NF-κB/p65 and reduces the release of pro-inflammatory factors (TNF-α and IL-6) to protect the liver from I/R-induced inflammation. Nuclear erythroid 2-related factor 2 (Nrf2) is a crucial cytoprotection regulator because it induces anti-inflammatory, antioxidant, and cytoprotective genes. Therefore, we analyzed the protein levels of Nrf2 and its downstream heme oxygenase-1 (HO-1) in the liver of mice and hepatocytes of humankind, respectively, and discovered that KAE pretreatment activates the Nrf2/HO-1 signaling pathway. In summary, this study confirmed the hepatoprotective effect of KAE on HI/RI, which inhibits oxidative stress and inflammation by activating the Nrf2/HO-1 signaling pathway.

Keywords: kaempferol, ischemia/reperfusion, oxidative stress, inflammation, Nrf2/HO-1

OPEN ACCESS

Edited by:
Lucindo Quintans-Júnior, Federal University of Sergipe, Brazil

Reviewed by:
Maria Oliveira, State University of Ceará, Brazil
Andreza Ramos, Federal University of Campina Grande, Brazil

***Correspondence:**
Yichao Du
duyc@swmu.edu.cn
Wenguang Fu
fuwg@swmu.edu.cn

†These authors have contributed equally to this work and share first authorship

Specialty section:
This article was submitted to Gastrointestinal and Hepatic Pharmacology, a section of the journal Frontiers in Pharmacology

Received: *18 January 2022*
Accepted: *07 March 2022*
Published: *01 April 2022*

Citation:
Chen Y, Li T, Tan P, Shi H, Cheng Y, Cai T, Bai J, Du Y and Fu W (2022) Kaempferol From Penthorum chinense Pursh Attenuates Hepatic Ischemia/Reperfusion Injury by Suppressing Oxidative Stress and Inflammation Through Activation of the Nrf2/HO-1 Signaling Pathway. Front. Pharmacol. 13:857015. doi: 10.3389/fphar.2022.857015

INTRODUCTION

HI/RI is a pathological state characterized by initial restriction of blood flow to the organ followed by restoration of perfusion and concomitant reoxygenation. However, blood flow restoration and reoxygenation are frequently associated with worsening tissue damage and a severe inflammatory response (Eltzschig and Eckle, 2011). HI/RI is a severe and unavoidable complication of certain liver surgeries, particularly partial hepatectomy and liver transplantation. It can result in delayed recovery of liver function and nonfunctioning of the transplanted liver following surgery, compromising the prognosis of liver surgery (Jochmans et al., 2017). HI/RI is a biphasic pathophysiological process that consists of two phases; the ischemic phase and the reperfusion phase. During ischemia, activated Kupffer cells release ROS, TNF-α, and IL-1β, leading to subsequent leukocyte recruitment, hepatocyte death, and endothelial injury (Ju and Tacke, 2016; Abu-Amara et al., 2010). Meanwhile, reoxygenation during the reperfusion period will lead to acute ROS generation, and the rapid accumulation of ROS directly causes tissue damage and impairs mitochondrial function and antioxidant systems, further exacerbating the deleterious effects of ROS, leading to sterile inflammation, apoptosis, and organ failure (Elias-Miró et al., 2013).

Natural product-based drugs have been regarded as a novel therapeutic strategy for preventing and treating certain diseases in recent years. Previous studies have shown that herbal active monomers have tremendous therapeutic potential, with pharmacological effects, including anti-inflammatory, antioxidant, and anti-apoptotic (Subramanya et al., 2018). *Penthorum chinense* Pursh (also known as Ganhuangcao in traditional Chinese medicine) is a medicinal and edible herb native to Miao nationality in China that grows primarily in southwest China (especially in Gulin County, Luzhou, Sichuan). *Penthorum chinense* Pursh has been used to treat liver diseases and alleviate liver injury in acute and chronic hepatitis, liver fibrosis, and non-alcoholic fatty liver disease for thousands of years (Wang et al., 2015). The main active ingredients of *Penthorum chinense* Pursh include flavonoids, organic acids, sterols, lignans, and volatile oils (Guo et al., 2015).

In our previous study (Du et al., 2020), we isolated and extracted high purity KAE (purity >98%, based on High-performance liquid chromatography (HPLC) analysis) (**Figure 1**) from *Penthorum chinense* Pursh and demonstrated its significant anti-inflammatory, antioxidant, and anti-apoptotic effects using the acetaminophen (N-acetyl-p-aminophenol, APAP)-induced hepatotoxicity mice model. Furthermore, Rabha et al. (Rabha et al., 2018) demonstrated that in a mice model of sepsis-induced acute lung injury, KAE pretreatment reduced the levels of cytokines IL-6, IL-1β, and TNF-α in plasma and lung tissue and increases the antioxidant products, SOD and GSH, to attenuate inflammation and oxidative stress.

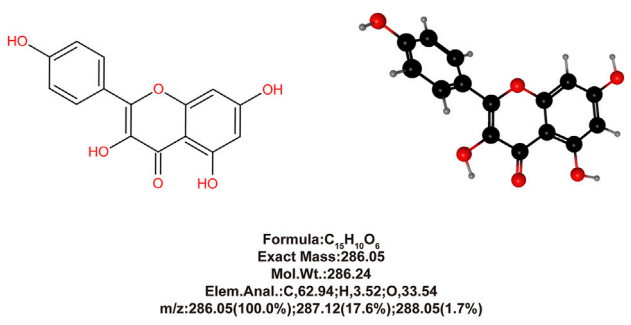

FIGURE 1 | Chemical and 3D structure of KAE and chemical properties.

Current studies widely indicate that oxidative stress and inflammation are critical mechanisms for the occurrence and progression of HI/RI, which is induced by the release of inflammatory factors (primarily TNF-α and IL-6, etc.) and the accumulation of ROS. Therefore, inhibiting oxidative stress and inflammation following liver surgery is a feasible therapeutic strategy for alleviating HI/RI (Pizzino et al., 2017; Nace et al., 2013). Based on the above background, this study examined the protective effect of KAE on I/R injury using the HI/RI model of mice and the H/R model of hepatocytes, and investigated the specific mechanism of the hepatoprotective effects of KAE.

MATERIALS AND METHODS

KAE Extraction and Isolation

The method for isolating and extracting KAE from *Penthorum chinense* Pursh is described in our previous study (Du et al., 2020), and the purity was confirmed to be >98% based on HPLC analysis (**Figure 1**).

Animals and Groups

We purchased 48 male C57BL/6 mice (8–10 weeks old, weighing 18–22 g) from Hua Fukang Bioscience (Beijing, China) and housed them under controlled light (12-h light/dark cycle) and temperature (22 ± 2°C) conditions with free access to food and water. After 1 week of adaptive feeding, the mice were randomly divided into the following groups (eight mice each): 1) Sham group (Sham); 2) KAE 60 mg/kg group (KAE60); 3) HI/RI group (HI/RI); 4) HI/RI + KAE 15 mg/kg (HI/RI + KAE15); 5) HI/RI + KAE 30 mg/kg (HI/RI + KAE30); 6) HI/RI + KAE 60 mg/kg (HI/RI + KAE60).

Mice in groups 2), 4), 5), and 6) were administered the above dose of KAE by gavage for 7 days, and HI/RI model was performed, with samples collected on day 8. All animal experiments in this study were reviewed and approved by the Animal Care and Use Committee and Ethics Committee of Southwest Medical University.

Mice HI/RI Model

According to Yuta Abe's method, nonlethal segmental (70%) liver ischemia was established. Briefly, all mice were anesthetized with sodium pentobarbital (40 mg/kg, i.p) before dissecting their abdomens along the midline. Then, using an atraumatic microvascular clamp, nonlethal segmental (70%) liver ischemia was induced by occlusion of the hepatic artery and portal vein of the left and median lobes. After 60 min of segmental liver

ischemia, the clamps were removed to initiate liver reperfusion. The mice were sacrificed with overdose sodium pentobarbital (90 mg/kg, i. p) after 6 h of reperfusion, and plasma and liver tissues were collected for analysis. Additionally, the mice belonging to the Sham group underwent a midline laparotomy incision without microvascular clamp placement.

Cell Culture and H/R Model of Hepatocytes

Normal human hepatocytes QSG-7701 were purchased from Beyotime Biotechnology (Shanghai, China) and cultured in Dulbecco's modified Eagle's medium (DMEM; Gibco; Thermo Fisher Scientific, United States) supplemented with 10% fetal bovine serum (Biological Industries, Beit Haemek, Israel) and 1% penicillin-streptomycin (Solarbio, Beijing, China) in a humidified incubator (Thermo Fisher Scientific, United States; 37°C, 5% CO_2). The H/R model of hepatocytes was established with some modifications to our previous study (Du et al., 2019). Briefly, experimental group hepatocytes were pretreated with various concentrations of KAE for 24 h before H/R procedure, while the control group was treated with the same volume of the KAE vehicle (DMSO; Solarbio, Beijing China) and maintained in the incubator. After that, all hepatocytes were washed twice with warm PBS and replaced with glucose-free and serum-free DMEM (Balanced with 1% O_2, 5% CO_2, and 94% N_2; Procell, Wuhan, China) 1 h before the hypoxia period. Experimental group cells were then cultured under hypoxic conditions (37°C, 1% O_2, 5% CO_2, and balanced N_2) in an Invivo$_2$ 400 hypoxic workstation (Baker Ruskinn, United Kingdom) for 6 h. Then, both groups of hepatocytes were replaced with fresh warm DMEM in the incubator (37°C, 5% CO_2) for a 4-h reoxygenation period.

Serum Aminotransferase Analyses

Mice serum samples were obtained by centrifuging (4°C, 5,000 rpm, 5 min) blood. An automatic biochemical analyzer (ADVIA 2400 Chemistry System, Siemens, Germany) was used to determine the serum activities of ALT and AST in mice.

Determination of Hepatic MDA, SOD and GSH Content

The supernatant was collected after the homogenization of the mice liver, and the content of MDA, SOD and GSH were measured according to the kit manufacturer's instructions (Beyotime, Shanghai, China).

Hematoxylin-Eosin and Immunohistochemistry Staining

Liver samples from each group of mice were collected immediately after the I/R procedure and fixed in a 4% paraformaldehyde solution for 24 h, followed by dehydration with gradient ethanol, paraffin embedding, and sectioning for H&E and IHC staining of HO-1 (1:500, Proteintech, Wuhan, China).

Terminal Deoxynucleotidyl Transferase-Mediated dUTP-Biotin Nick End Labeling Apoptosis Assay

TUNEL apoptosis assay for mice liver tissue sections was performed according to the kit manufacturer's instructions (Servicebio, Wuhan, China).

Cell Viability Assay

According to the manufacturer's instructions, cell viability was determined using the cell counting kit 8 (CCK-8; Beyotime, Shanghai, China). Briefly, hepatocytes (3×10^4/well) were inoculated in a 96-well plate, then 10 μl CCK-8 solution was added and cultured routinely. After 2 h, absorbance at 450 nm was measured using a Cytation5 Imaging Reader (BioTek, United States), and cell viability was calculated. Duplicate wells were used in the respective groups and repeated four times.

Detection of ROS Generation

For cellular ROS determination and fluorescence analysis, we loaded a dichlorofluorescein-diacetate (DCFH-DA) fluorescent probe according to the manufacturer's instructions (Beyotime, Shanghai, China). The area scan function (3 × 3 reads/well; excitation/emission = 488/525 nm) of the Gen5 software (Vision.3.08; Biotek, United States) was used to calculate the average fluorescence intensity of 6-well plates, and subsequent fluorescence images were captured using a fluorescence microscope (IX73; Olympus, Tokyo, Japan).

Western Blotting

According to the manufacturer's instructions, RIPA lysis buffer (Beyotime, Shanghai, China) was used to extract total protein from liver tissue and hepatocytes. Western blotting was performed as previously described (Lei et al., 2016). The membranes were incubated with primary antibodies against NF-κB/p65 (1:1,000; Proteintech, United States), phospho-NF-κB/p65 (p-p65; 1:1,000; Zen Bioscience, China), TNF-α (1:1,000; Proteintech; United States), IL-6 (1:1,000; Proteintech, United States), IL-10 (1:1,000; Wanleibio, China), Bax (1:2000; Proteintech, United States), Bcl-2 (1:1,000; Proteintech, United States), Nrf2 (1:1,000; Proteintech, United States), HO-1 (1:1,000; Proteintech, United States), β-actin (1:5,000; Proteintech, United States) and then incubated with horseradish peroxidase (HRP)-conjugated secondary antibodies (1:5,000; Proteintech, United States). The relative protein expression was analyzed using ImageJ software (NIH, Maryland, United States).

Statistical Analysis

All data analyses were performed using GraphPad Prism v.8.0 (GraphPad Software, San Diego, United States) and presented as mean ± standard deviation. All data were compared using one-way ANOVA and *t*-test, and a *p*-value less than 0.05 ($p < 0.05$) was considered to represent statistically significant results.

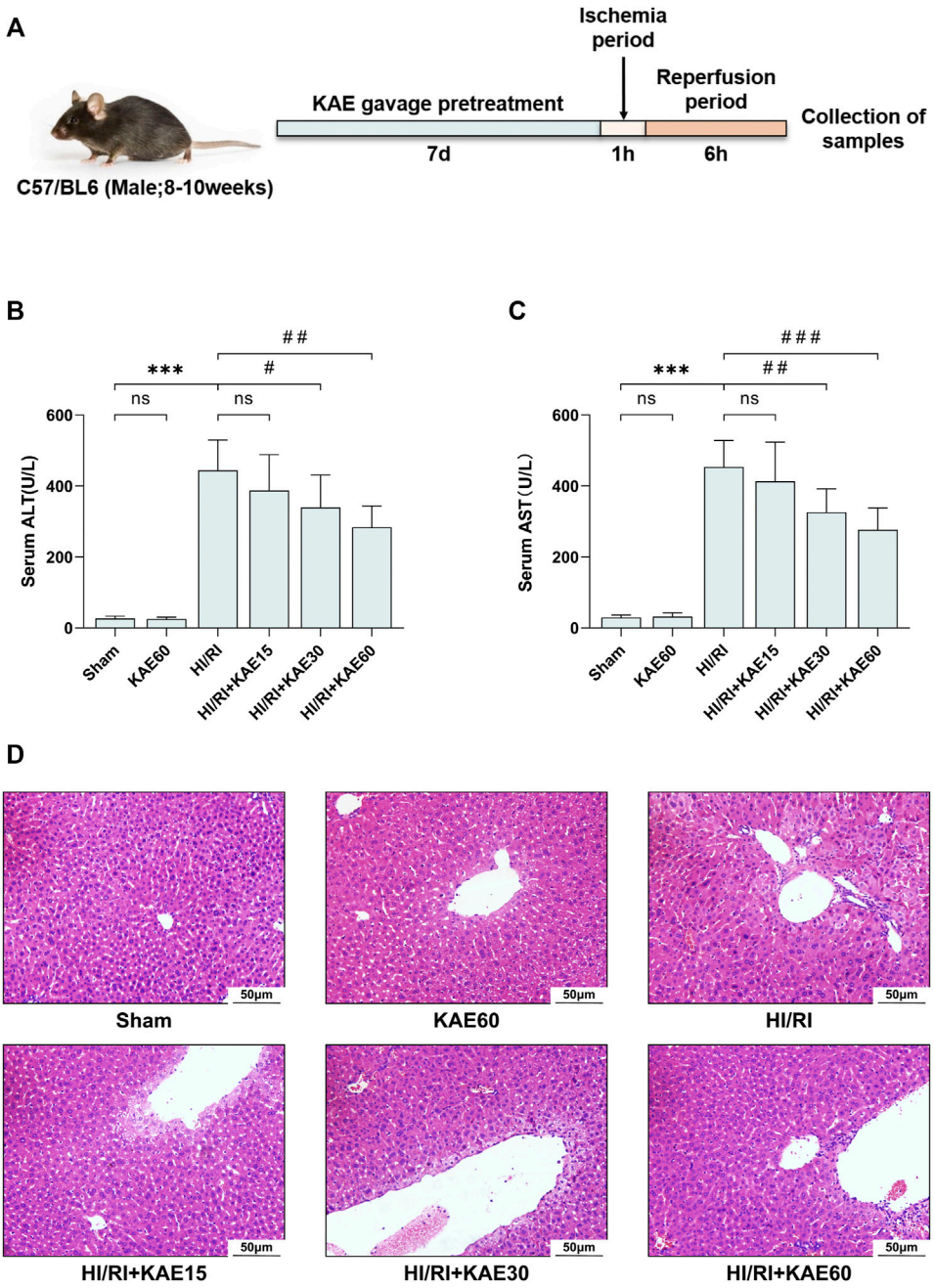

FIGURE 2 | KAE mitigates liver injury in mice HI/RI model. **(A)** KAE administration and HIRI model establishment in mice (n = 8/group); Effect of KAE pretreatment on serum of ALT **(B)** and AST **(C)**; **(D)** Pathological evaluation of liver tissue specimens by H&E staining (original magnification ×200). Data were expressed as mean ± standard deviation (SD) values. $^{*}p < 0.05$, $^{**}p < 0.01$, and $^{***}p < 0.001$ versus the sham group; $^{\#}p < 0.05$, $^{\#\#}p < 0.01$, and $^{\#\#\#}p < 0.001$ versus the HI/RI group; NS: no significance.

RESULTS

KAE Mitigates Liver Injury in Mice HI/RI Model

In this study, mice were pretreated with different doses of KAE gavage (15, 30, and 60 mg/kg) for 7 days before establishing HI/RI models, as previously described (**Figure 2A**). We first evaluated the effect of KAE on the liver of mice and observed no significant difference in liver function ($p > 0.05$) (**Figures 2B,C**) and tissue structure (**Figure 2D**) between the KAE60 and Sham groups of mice, confirming that the dose of KAE gavage was not significantly toxic to mice. While KAE pretreatment dose-dependently reduced I/R-induced transaminase elevation, with the most significant effect of KAE at 60 mg/kg (ALT, $p < 0.01$;

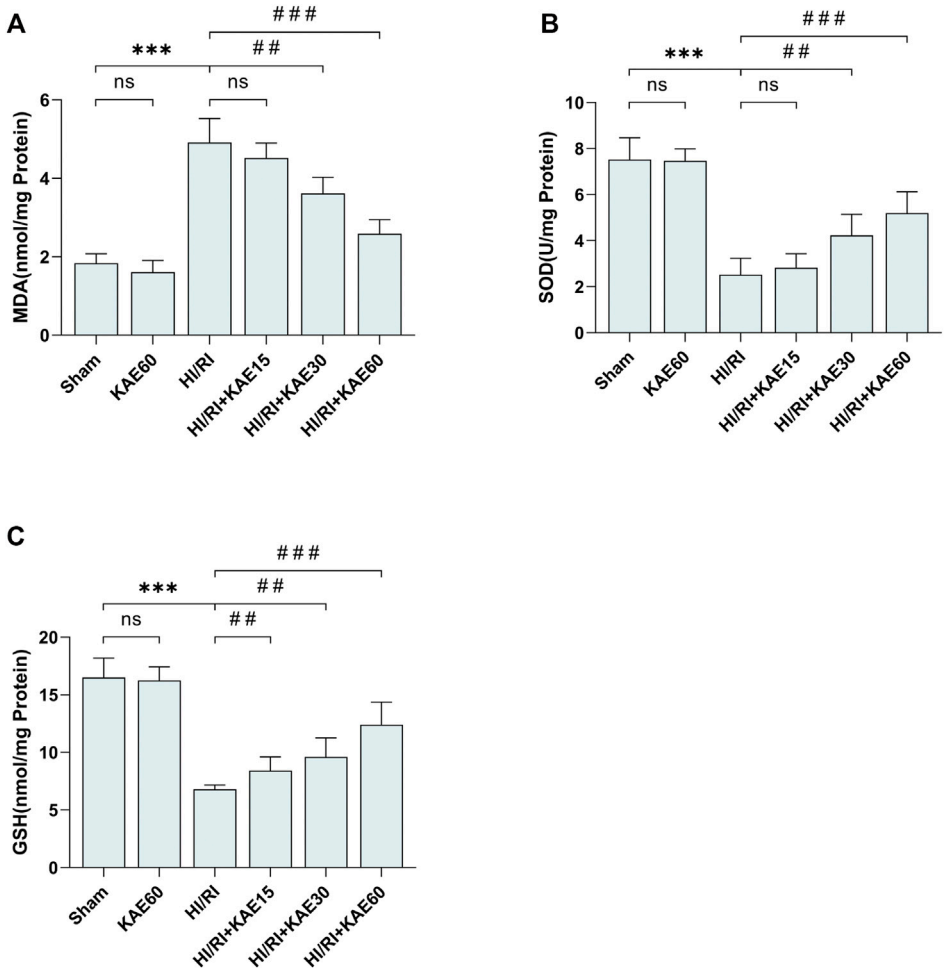

FIGURE 3 | KAE attenuates I/R-induced oxidative stress *in vivo*. Determination of MDA **(A)**, SOD **(B)** and GSH content **(C)** in mice liver tissue homogenates using the corresponding kits. Data were expressed as mean ± standard deviation (SD) values. $^{*}p < 0.05$, $^{**}p < 0.01$, and $^{***}p < 0.001$ versus the sham group; $^{\#}p < 0.05$, $^{\#\#}p < 0.01$, and $^{\#\#\#}p < 0.001$ versus the HI/RI group; NS: no significance.

AST, $p < 0.001$) (**Figures 2B,C**). The Sham and KAE60 groups had normal liver structure and intact liver lobules on morphological and histopathological inspection. In contrast, mice in the HI/RI group showed a larger area of necrosis in the liver, and KAE pretreatment reversed this result (**Figure 2D**). The area of I/R-induced necrosis was reduced in all KAE pretreatment groups, with the best effect in the KAE60 group. However, the improvement of I/R by KAE 15 mg/kg was less significant (**Figure 2D**), consistent with serological results ($p > 0.05$) (**Figures 2B,C**).

KAE Attenuates I/R-Induced Oxidative Stress *in vivo*

To assess the KAE effect on oxidative stress in the mice HI/RI model, we measured the content of MDA, SOD and GSH in the supernatant of mice liver tissue homogenates as markers of oxidative stress levels (**Figures 3A–C**). Compared with the Sham group, the MDA content in the liver of mice subjected to I/R injury significantly increased ($p < 0.001$) (**Figure 3A**), but the KAE pretreatment group was considerably lower than the HI/RI group, especially the HIRI + KAE60 group ($p < 0.001$) (**Figure 3A**). SOD and GSH, components of the antioxidant system in organisms, were significantly reduced by I/R-induced oxidative stress ($p < 0.001$) (**Figures 3B,C**), and KAE pretreatment dose-dependently reversed this result, with the best effect at a KAE dose of 60 mg/kg ($p < 0.001$) (**Figures 3B,C**). However, KAE pretreatment at 15 mg/kg had almost no effect on oxidative stress (**Figures 3A–C**).

KAE Suppresses I/R-Induced Inflammation *in vivo*

To investigate the protective effect of KAE against inflammation induced by I/R, we analyzed the protein expression of inflammatory factors and markers by western blotting. I/R-induced significant NF-κB/p65 phosphorylation and increased the expression of pro-inflammatory factors, including TNF-α and IL-6 ($p < 0.001$) (**Figures 4A–D**),

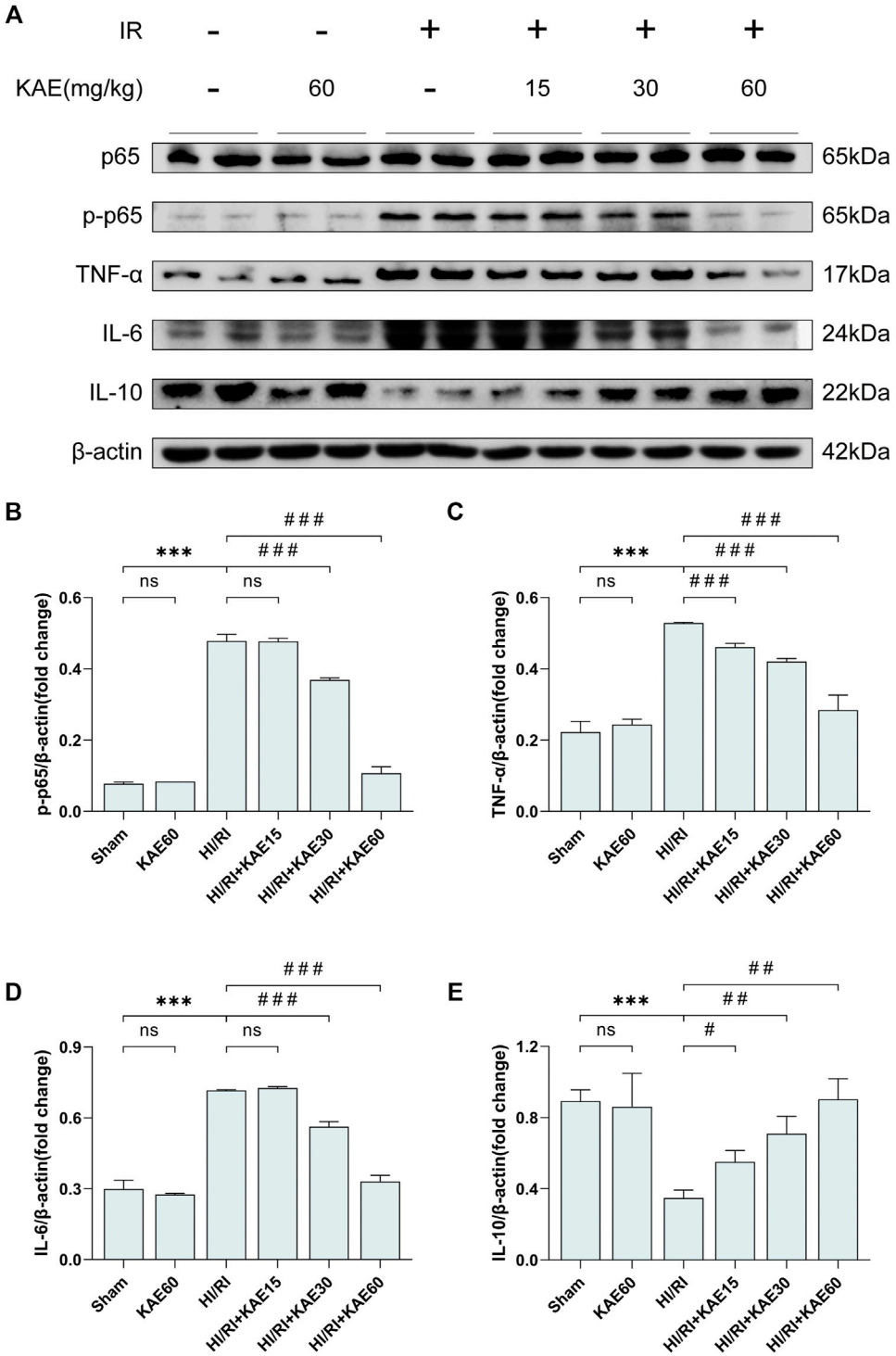

FIGURE 4 | KAE suppresses I/R-induced inflammation *in vivo*. **(A)** Protein expression in liver tissue were determined by western blotting for p65, p-p65, TNF-α, IL-6, IL-10 and β-actin. **(B–E)**Relative protein expression was semi-quantified by analyzing protein grayscale values. Data were expressed as mean ± standard deviation (SD) values. $^{*}p < 0.05$, $^{**}p < 0.01$, and $^{***}p < 0.001$ versus the sham group; $^{\#}p < 0.05$, $^{\#\#}p < 0.01$, and $^{\#\#\#}p < 0.001$ versus the HI/RI group; NS: no significance.

whereas KAE pretreatment dose-dependently reversed these effects, and the anti-inflammatory effect was most pronounced at a dose of 60 mg/kg ($p < 0.001$) (**Figures 4A–D**). In addition, the IL-10 involved in anti-inflammatory was significantly downregulated by I/R injury ($p < 0.001$) (**Figures 4A,E**), whereas KAE pretreatment dose-dependently restores some of

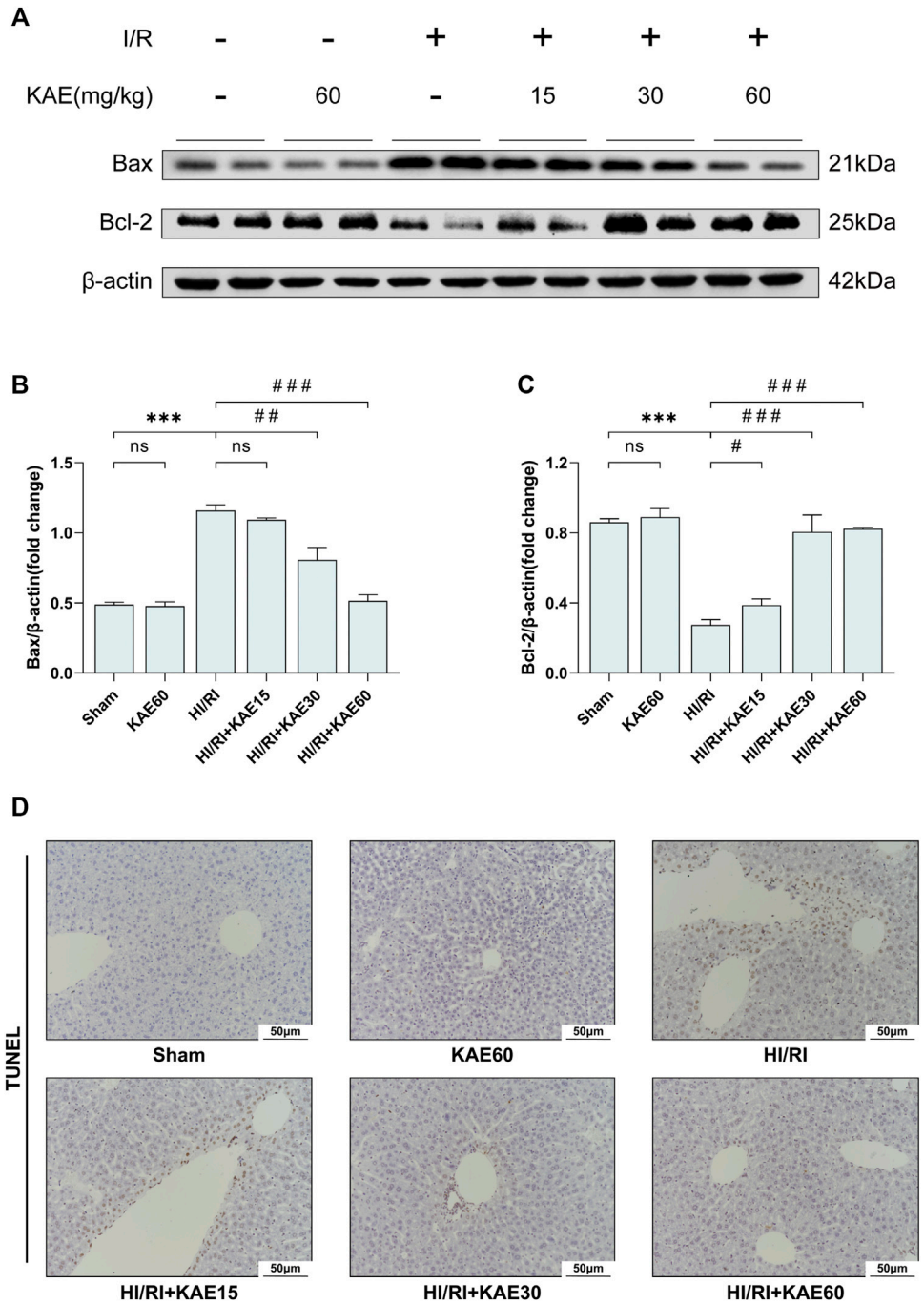

FIGURE 5 | KAE alleviates I/R-induced hepatocellular apoptosis *in vivo*. **(A)** Protein expression in liver tissue were determined by western blotting for Bax, BCL-2, and β-actin; **(B,C)** Relative protein expression was semi-quantified by analyzing protein grayscale values. **(D)** Analysis of hepatocellular apoptosis by TUNEL staining. Data were expressed as mean ± standard deviation (SD) values. $^{*}p < 0.05$, $^{**}p < 0.01$, and $^{***}p < 0.001$ versus the sham group; $^{\#}p < 0.05$, $^{\#\#}p < 0.01$, and $^{\#\#\#}p < 0.001$ versus the HI/RI group; NS: no significance.

the effects (**Figures 4A,E**). The above results indicate that KAE pretreatment inhibits I/R-induced pro-inflammatory factors release by suppressing NF-κB/p65 activation and increasing the expression of anti-inflammatory factors.

KAE Alleviates I/R-Induced Hepatocellular Apoptosis *in vivo*

To further assess the extent of I/R-induced injury *in vivo*, we analyzed the expression of related proteins by western blotting

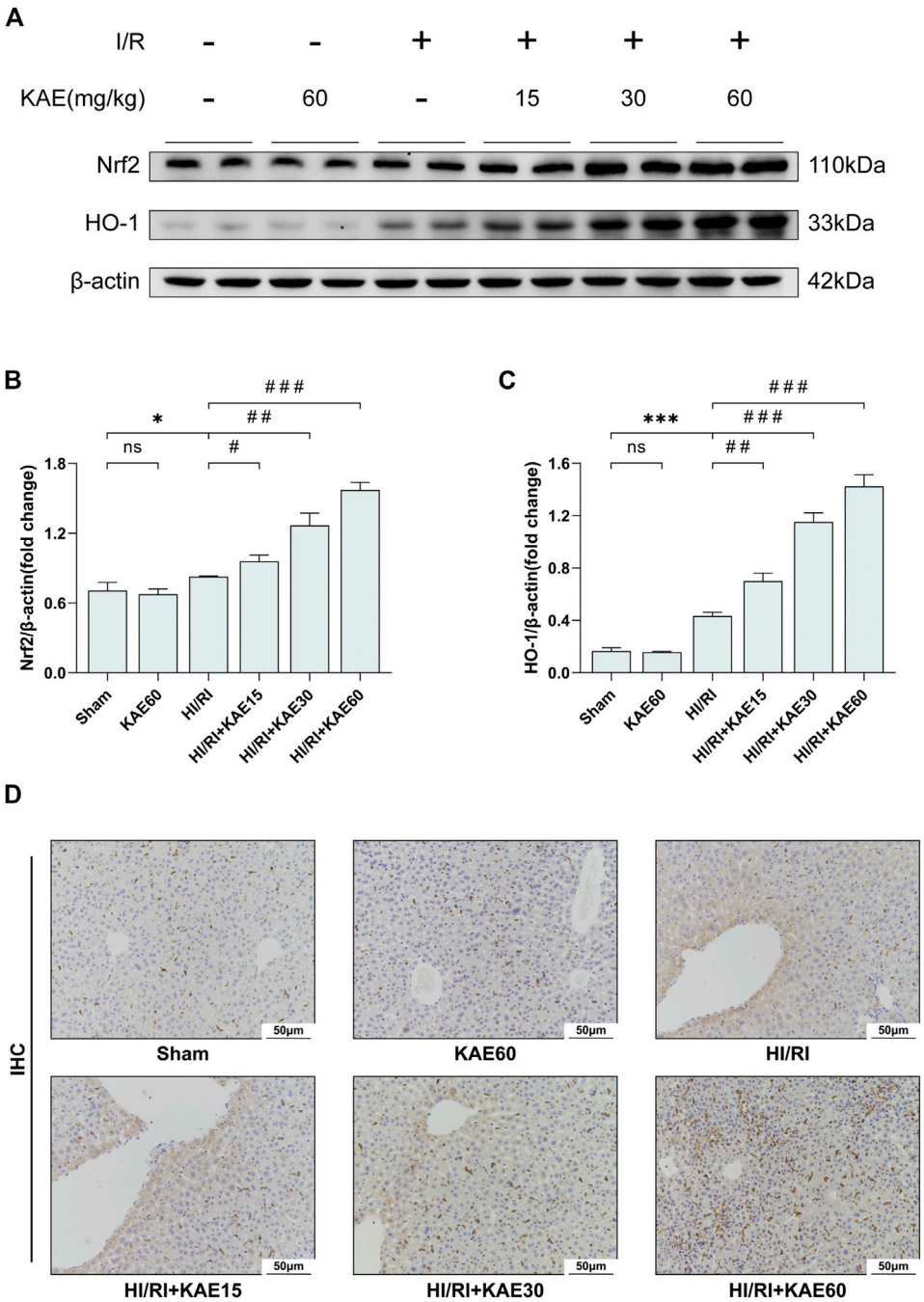

FIGURE 6 | KAE activates the Nrf2/HO-1 signaling pathway to attenuate I/R injury *in vivo*. **(A)** Protein expression in liver tissue were determined by western blotting for Nrf2, HO-1, and β-actin; **(B,C)** Relative protein expression was semi-quantified by analyzing protein grayscale values. **(D)** Analysis of HO-1 expression in mice liver tissues by IHC staining. Data were expressed as mean ± standard deviation (SD) values. $^{*}p < 0.05$, $^{**}p < 0.01$, and $^{***}p < 0.001$ versus the sham group; $^{\#}p < 0.05$, $^{\#\#}p < 0.01$, and $^{\#\#\#}p < 0.001$ versus the HI/RI group; NS: no significance.

and performed TUNEL staining on liver tissue sections. Western blotting of apoptosis-related protein expression revealed that I/R significantly upregulated the expression of the pro-apoptotic protein Bax while inhibiting the expression of the anti-apoptotic protein Bcl-2 ($p < 0.001$) (**Figures 5A–C**), which was reversed by KAE pretreatment at an optimal dose of 60 mg/kg ($p < 0.001$) (**Figures 5A–C**). TUNEL staining was the next section, and our results showed that a large number of TUNEL-positive cells were detected in the liver tissue of the HI/RI group compared with the Sham group (**Figure 5D**). However, apoptotic hepatocytes in the KAE pretreatment group were significantly lower than those in the HI/RI group, which was particularly significant in

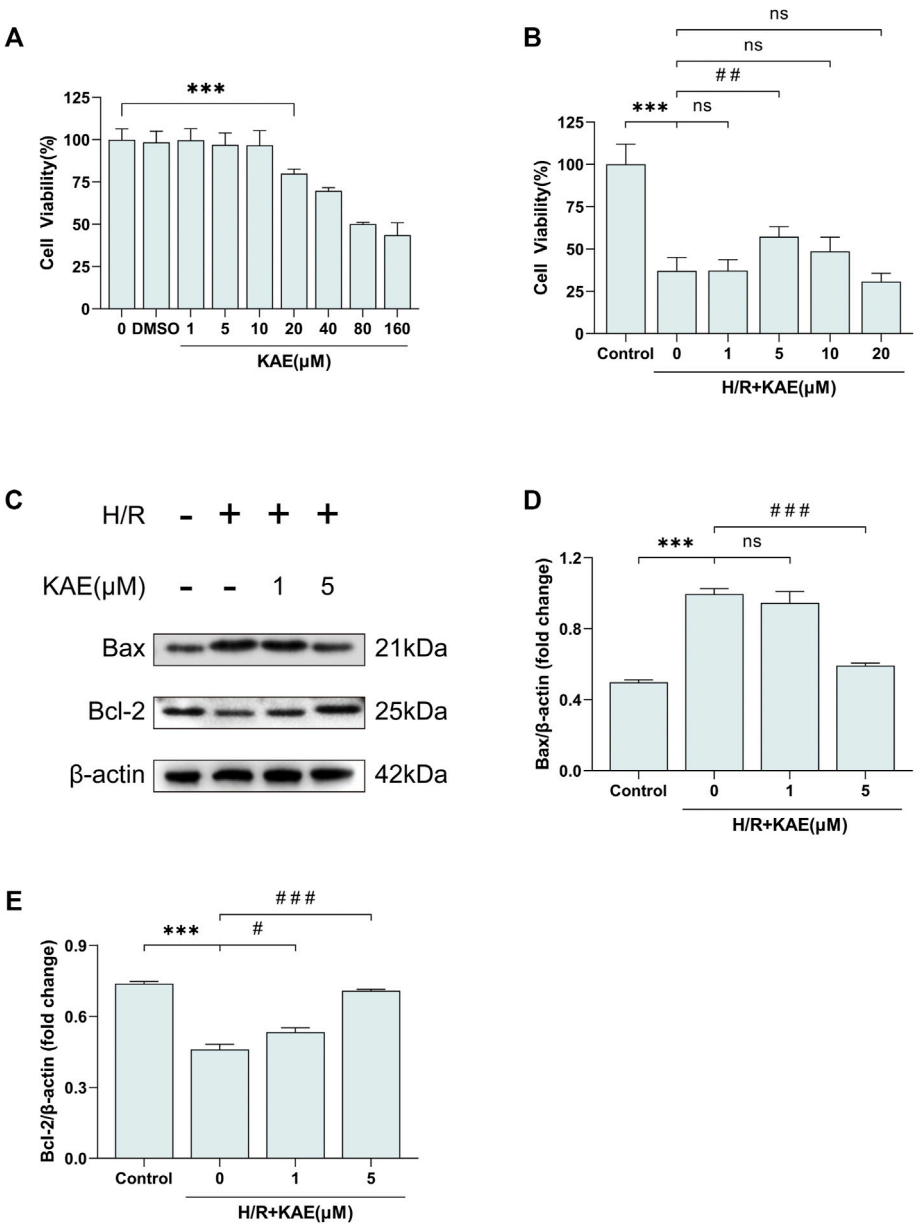

FIGURE 7 | KAE palliates H/R-induced hepatocellular apoptosis *in vitro*. **(A)** Assessment of cytotoxicity of KAE by cell viability assay; **(B)** Screening of optimal concentration of KAE pretreatment by cell viability assay. **(C)** Protein expression in liver tissue was determined by western blotting for Bax, BCL-2, and β-actin; **(D,E)** Relative protein expression was semi-quantified by analyzing protein grayscale values. Data were expressed as mean ± standard deviation (SD) values. $^{*}p < 0.05$, $^{**}p < 0.01$, and $^{***}p < 0.001$ versus the control group; $^{\#}p < 0.05$, $^{\#\#}p < 0.01$, and $^{\#\#\#}p < 0.001$ versus the H/R group; NS: no significance.

the HIRI + KAE60 group (**Figure 5D**), indicating that KAE pretreatment inhibits I/R-induced hepatocellular apoptosis by downregulating pro-apoptotic protein expression and upregulating anti-apoptotic protein expression.

KAE Activates the Nrf2/HO-1 Signaling Pathway to Attenuate I/R Injury *in vivo*

To investigate the role of KAE in the Nrf2/HO-1 signaling pathway, we analyzed the expression of Nrf2 and HO-1 in total protein extracts from the mice liver by western blotting. Our study showed that I/R injury mildly increased the expression of Nrf2 ($p < 0.05$) (**Figures 6A,B**) and dramatically increased the expression of HO-1 ($p < 0.001$) (**Figures 6A,C**) compared with the Sham group. Compared with the HI/RI group, expression of Nrf2 and HO-1 were further increased in the KAE pretreatment groups, and the extent of the increase correlated with the KAE dose, the effect was most pronounced when KAE pretreatment dose reached 60 mg/kg ($p < 0.001$) (**Figures 6A,C**). IHC staining of HO-1 showed similar results: a minor increase in HO-1-

positive cells in the HI/RI group compared with the Sham group, and a significant increase in HO-1-positive cells in the KAE pretreatment group (**Figure 6D**). These results indicate that Nrf2 was activated under stress conditions and upregulated HO-1 expression to counteract I/R injury, and KAE pretreatment further enhanced the effect.

KAE Palliates H/R-Induced Hepatocellular Apoptosis *in vitro*

At the cytological level, we started by pretreating the normal human hepatocyte line QSG-7701 with DMSO and different KAE concentrations for 24 h. Then, cell viability was measured to assess the cytotoxicity of KAE (**Figure 7A**). Hepatocyte proliferation was significantly inhibited at KAE concentrations up to 20 μM ($p < 0.001$) (**Figure 7A**), hence KAE concentrations below 20 μM will be used in subsequent experiments. H/R injury significantly inhibited the proliferation of hepatocytes ($p < 0.001$) (**Figure 7B**), and KAE pretreatment restored the injury, with 5 μM KAE being the optimal concentration ($p < 0.01$) (**Figure 7B**). Subsequently, western blotting was performed to detect the expression of pro-apoptotic factor Bax and anti-apoptotic factor Bcl-2 in each group of hepatocytes (**Figures 7C–E**). The results showed that H/R significantly upregulated Bax expression but downregulated the expression of Bcl-2, which was reversed by KAE with an optimal concentration of 5 μM ($p < 0.001$) (**Figures 7C–E**). These findings are similar to those obtained *in vivo*.

KAE Reduces ROS Generation and Activates the Nrf2/HO-1 Signaling Pathway to Relieve H/R Injury *in vitro*

To assess the level of H/R-induced oxidative stress *in vitro*, the DCFH-DA fluorescent probe was used to label ROS. DCFH-DA fluorescent probe was loaded on hepatocytes, and the fluorescence area was compared to measure ROS levels. Pretreatment with a 5 μM KAE concentration reversed H/R-induced fluorescent area increase, but increasing the KAE concentration to 20 μM may have caused more ROS generation ($p > 0.05$) (**Figure 8A**). The average fluorescence intensity measurement confirmed the above results ($p < 0.001$) (**Figure 8B**). Further, we investigated Nrf2 and HO-1 protein expression in hepatocytes under H/R conditions. Compared with the Sham group, H/R injury increased the expression of total Nrf2 and its downstream HO-1 ($p < 0.001$) (**Figures 8C–E**), which was further enhanced by KAE pretreatment, especially at KAE pretreatment concentration of 5 μM ($p < 0.001$) (**Figures 8C–E**). The above *in vitro* results were in good agreement with the *in vivo* experiments, confirming the validity of KAE pretreatment.

DISCUSSION

HI/RI is a common and severe complication in liver surgery, which constrains the development of hepatic surgery, but current therapeutic strategies are limited (Yang et al., 2019). KAE, a flavonoid isolated from *Penthorum chinense* Pursh, has been reported to exhibit significant anti-inflammatory and antioxidant effects (Suchal et al., 2016; Xu et al., 2019; Chen et al., 2020; Du et al., 2020). However, the effects of KAE on HI/RI are yet to be reported. Our study showed that KAE pretreatment significantly reduced I/R-induced impairment of liver function and tissue structure. We attempted to elucidate its possible mechanisms in three dimensions: inflammation, oxidative stress, and apoptosis.

HI/RI manifests as a direct result of hepatocyte injury during the ischemic phase, which induces an inflammatory response, and further cellular dysfunction and injury caused by inflammatory pathway activation (Nace et al., 2013). The anti-inflammatory effect of KAE has been demonstrated in several disease models (Devi et al., 2015), and our study showed that the anti-inflammatory effect of KAE is closely related to the inhibition of NF-κB phosphorylation. NF-κB/p65, as one of the primary regulators of classical inflammatory pathways, plays a vital role in the occurrence and progression of ischemia-reperfusion injury in multiple organs (Zhang et al., 2020). In addition, our study indicated that KAE downregulated the expression of pro-inflammatory factors (including TNF-α and IL-6) by inhibiting the activation of NF-κB/p65.

When it comes to oxidative stress, as mentioned previously, the occurrence and progression of HI/RI are closely related to oxidative stress, and ROS is a key link in it (Elias-Miró et al., 2013). Therefore, we measured the content of MDA, SOD, and GSH *in vivo* and the level of ROS *in vitro* to represent the degree of oxidative stress. Several existing studies have demonstrated the potential of KAE on scavenging ROS and mitigating oxidative stress (Saw et al., 2014; Zeka et al., 2020). In the present study, our data confirmed that KAE exerts antioxidant effects by activating the Nrf2/HO-1 signaling pathway.

Further investigation of the hepatoprotective effects of KAE revealed that KAE pretreatment attenuates inflammation and oxidative stress under stressful conditions *in vivo* and *in vitro* and remarkably alleviates hepatocyte apoptosis. It has long been demonstrated that Bcl-2 is a critical anti-apoptotic protein in organisms and promoting Bcl-2 expression significantly alleviates HI/RI (Selzner et al., 2002). Similarly, our results suggested that KAE downregulates the expression of apoptotic protein Bax and upregulates the expression of anti-apoptotic protein Bcl-2 in I/R and H/R-induced injury, thereby alleviating hepatocyte apoptosis. Also, TUNEL staining of liver sections supported the results of western blotting.

Our study on the mechanism of KAE revealed that the potent anti-inflammatory, antioxidant and anti-apoptotic effects of KAE might be attributed to the activation of the Nrf2/HO-1 signaling pathway by KAE. Previous studies have demonstrated that the Nrf2/HO-1 signaling pathway is one of the critical pathways for biological resistance to inflammation and oxidative stress, and the transcriptional response of Nrf2 is essential for maintaining homeostasis in the organism (Bardallo et al., 2021). Under physiological conditions, Nrf2 is anchored in the cytoplasm by binding to its inhibitor, Kelch-like ECH-associated protein-1 (Keap1). Various endogenous or exogenous stimuli dissociate

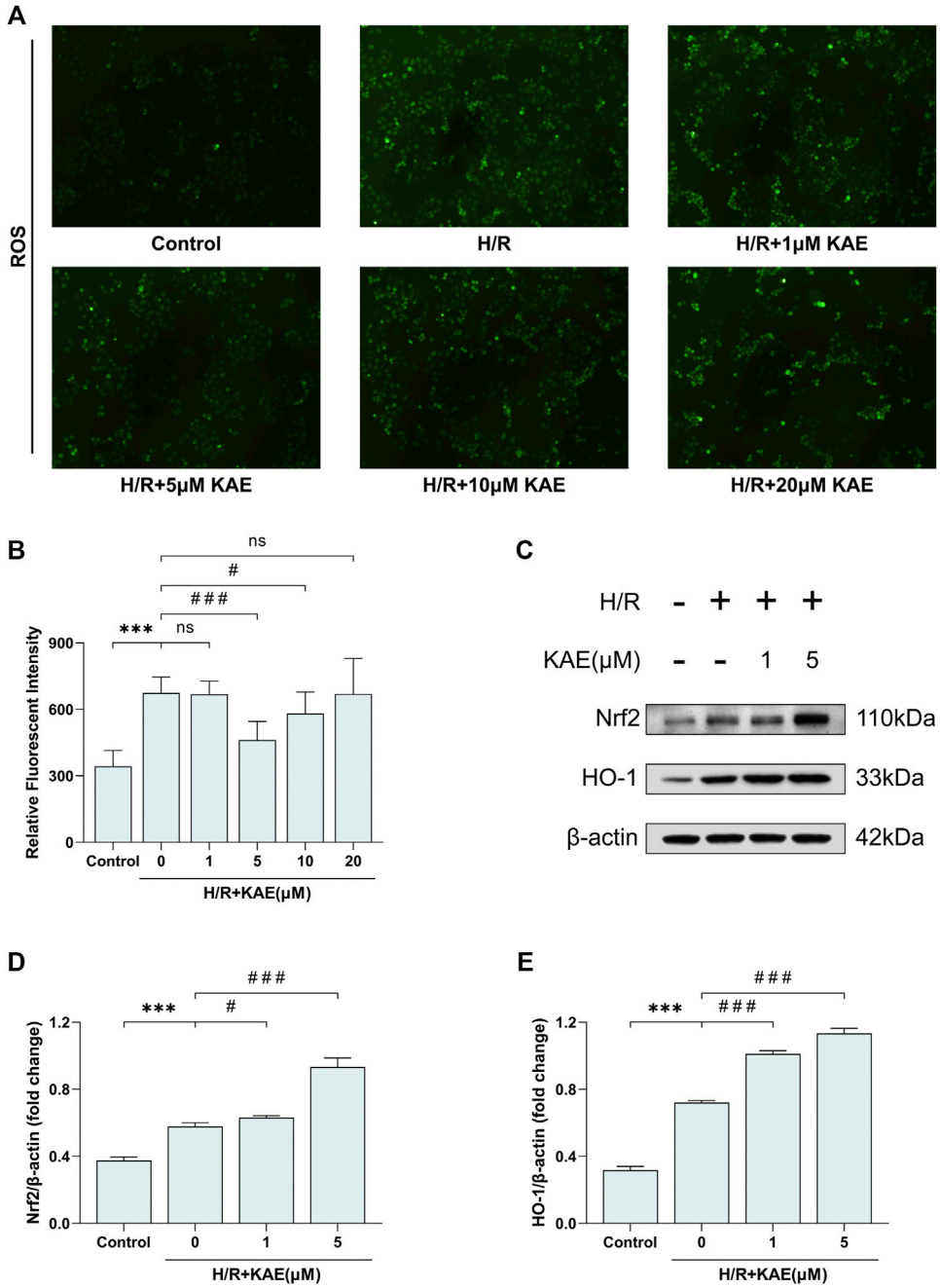

FIGURE 8 | KAE reduces ROS generation and activates the Nrf2/HO-1 signaling pathway to relieve H/R injury *in vitro*. **(A)** Assessment of hepatocellular ROS generation by DCFH-DA fluorescent probe; **(B)** Analysis of ROS relative fluorescence intensity by area scan (3 × 3 reads/well; excitation/emission = 488/525 nm); **(C)** Protein expression in liver tissue were determined by western blotting for Bax, BCL-2, and β-actin; **(D,E)** Relative protein expression was semi-quantified by analyzing protein grayscale values. Data were expressed as mean ± standard deviation (SD) values. $^{*}p < 0.05$, $^{**}p < 0.01$, and $^{***}p < 0.001$ versus the control group; $^{\#}p < 0.05$, $^{\#\#}p < 0.01$, and $^{\#\#\#}p < 0.001$ versus the H/R group; NS: no significance.

Nrf2 from Keap1, resulting in nuclear translocation of Nrf2, which in turn mediates transcriptional activation of antioxidant response element (ARE) regulatory genes, thereby reducing ROS levels, inflammation, and cell death (Bataille and Manautou, 2012; Galicia-Moreno et al., 2020; Jayasuriya et al., 2021). Among the genes downstream of ARE-mediated transcriptional activation, up-regulation of HO-1 may be one of the most critical cytoprotective mechanisms activated during cellular stress, such as inflammation, ischemia, hypoxia, hyperoxia, hyperthermia, or radiation (Brockmann et al., 2005). Moreover, HO-1 was thought to play a crucial role in maintaining antioxidant/oxidant balance during cellular injury

(Waltz et al., 2011), and its anti-inflammatory and anti-apoptotic effects have been validated in multiple disease models (McDaid et al., 2005).

Notably, studies showed that the expression of Nrf2 and HO-1 were downregulated under stress conditions (Yao et al., 2020; Yu et al., 2021). In addition, KAE was found to upregulate the expression of Nrf2 and HO-1 in WT mice and cells without any treatment (Yao et al., 2020). However, in contrast to earlier findings, our results demonstrate that KAE pretreatment has no significant effect under physiological conditions (Sham group versus KAE60 group *in vivo*). Meanwhile, Nrf2 and HO-1 expression was mildly elevated under stress conditions (Sham group versus HI/RI group *in vivo*; Control group versus H/R group *in vitro*), and the effect was dose-dependently enhanced by KAE pretreatment. Our results are similar to some studies that indicated that upregulation of Nrf2 and HO-1 expression was associated with anti-inflammatory and antioxidant functions initiated by hepatocytes during HI/RI (Li et al., 2021; Ma et al., 2021; Zhuang et al., 2021). Collectively, our results suggested that I/R injury upregulated Nrf2 and HO-1 to some extent to counteract stress and injury and that KAE pretreatment has a significant effect only when mice are subjected to I/R injury.

CONCLUSION

This study verified the protective effects of KAE pretreatment on the liver from both animal and cellular perspectives. Its potent anti-inflammatory and antioxidant effects were associated with inhibition of the NF-κB/p65 and activation of the Nrf2/HO-1 signaling pathway. Based on the existing studies, the current study further elaborated the specific mechanism of KAE to alleviate HI/RI. These results suggest promising drug candidates for preventing and treating HI/RI and laying the foundation for the development and application of *Penthorum chinense* Pursh.

DATA AVAILABILITY STATEMENT

The original contributions presented in the study are included in the article/Supplementary Material, further inquiries can be directed to the corresponding authors.

ETHICS STATEMENT

The animal study was reviewed and approved by Animal Care and Use Committee and Ethics Committee of Southwest Medical University.

AUTHOR CONTRIBUTIONS

WF and YD conceived and designed the experiments and revised the manuscript. YFC and TL performed the experiments, and YFC wrote the manuscript. HS, YLC, TC, and JB were involved in experimental analysis and data acquisition. All authors read and approved the final version of the manuscript. YFC and TL have contributed equally to this work and share first authorship.

FUNDING

This work was supported by the following project funding: The National Natural Science Foundation of China (No. 82170587), Luzhou Municipal People's Government-Southwest Medical University Science and Technology Strategic Cooperation Project (No. 2020LZXNYDZ07), Southwest Medical University New Academic Project (No. 2021ZKMS026), and Southwest Medical University-Luzhou Chinese Medicine Hospital Basic Project (No. 2019-LH015).

REFERENCES

Abu-Amara, M., Yang, S. Y., Tapuria, N., Fuller, B., Davidson, B., and Seifalian, A. (2010). Liver Ischemia/reperfusion Injury: Processes in Inflammatory Networks-Aa Review. *Liver Transpl.* 16, 1016–1032. doi:10.1002/lt.22117

Bardallo, R. G., Panisello-Roselló, A., Sanchez-Nuno, S., Alva, N., Roselló-Catafau, J., and Carbonell, T. (2021). Nrf2 and Oxidative Stress in Liver Ischemia/reperfusion Injury. *FEBS J.* [Epub ahead of print]. doi:10.1111/febs.16336

Bataille, A. M., and Manautou, J. E. (2012). Nrf2: a Potential Target for New Therapeutics in Liver Disease. *Clin. Pharmacol. Ther.* 92, 340–348. doi:10.1038/clpt.2012.110

Brockmann, J. G., August, C., Wolters, H. H., Hömme, R., Palmes, D., Baba, H., et al. (2005). Sequence of Reperfusion Influences Ischemia/reperfusion Injury and Primary Graft Function Following Porcine Liver Transplantation. *Liver Transpl.* 11, 1214–1222. doi:10.1002/lt.20480

Chen, J., Xuan, Y. H., Luo, M. X., Ni, X. G., Ling, L. Q., Hu, S. J., et al. (2020). Kaempferol Alleviates Acute Alcoholic Liver Injury in Mice by Regulating Intestinal Tight junction Proteins and Butyrate Receptors and Transporters. *Toxicology* 429, 152338. doi:10.1016/j.tox.2019.152338

Devi, K. P., Malar, D. S., Nabavi, S. F., Sureda, A., Xiao, J., Nabavi, S. M., et al. (2015). Kaempferol and Inflammation: From Chemistry to Medicine. *Pharmacol. Res.* 99, 1–10. doi:10.1016/j.phrs.2015.05.002

Du, Y. C., Lai, L., Zhang, H., Zhong, F. R., Cheng, H. L., Qian, B. L., et al. (2020). Kaempferol from Penthorum Chinense Pursh Suppresses HMGB1/TLR4/NF-Kb Signaling and NLRP3 Inflammasome Activation in Acetaminophen-Induced Hepatotoxicity. *Food Funct.* 11, 7925–7934. doi:10.1039/d0fo00724b

Elias-Miró, M., Jiménez-Castro, M. B., Rodés, J., and Peralta, C. (2013). Current Knowledge on Oxidative Stress in Hepatic Ischemia/reperfusion. *Free Radic. Res.* 47, 555–568. doi:10.3109/10715762.2013.811721

Eltzschig, H. K., and Eckle, T. (2011). Ischemia and Reperfusion-Ffrom Mechanism to Translation. *Nat. Med.* 17, 1391–1401. doi:10.1038/nm.2507

Galicia-Moreno, M., Lucano-Landeros, S., Monroy-Ramirez, H. C., Silva-Gomez, J., Gutierrez-Cuevas, J., Santos, A., et al. (2020). Roles of Nrf2 in Liver Diseases: Molecular, Pharmacological, and Epigenetic Aspects. *Antioxidants* 9, 980. doi:10.3390/antiox9100980

Guo, W., Jiang, Y., Chen, X., Yu, P., Wang, M., Wu, X., et al. (2015). Identification and Quantitation of Major Phenolic Compounds from Penthorum Chinense Pursh. By HPLC with Tandem Mass Spectrometry and HPLC with Diode Array Detection. *J. Sep. Sci.* 38, 2789–2796. doi:10.1002/jssc.201500303

Jayasuriya, R., Dhamodharan, U., Ali, D., Ganesan, K., Xu, B., and Ramkumar, K. M. (2021). Targeting Nrf2/Keap1 Signaling Pathway by Bioactive Natural Agents: Possible Therapeutic Strategy to Combat Liver Disease. *Phytomedicine* 92, 153755. doi:10.1016/j.phymed.2021.153755

Jochmans, I., Meurisse, N., Neyrinck, A., Verhaegen, M., Monbaliu, D., and Pirenne, J. (2017). Hepatic Ischemia/reperfusion Injury Associates with Acute Kidney Injury in Liver Transplantation: Prospective Cohort Study. *Liver Transpl.* 23, 634–644. doi:10.1002/lt.24728

Ju, C., and Tacke, F. (2016). Hepatic Macrophages in Homeostasis and Liver Diseases: from Pathogenesis to Novel Therapeutic Strategies. *Cell Mol Immunol* 13, 316–327. doi:10.1038/cmi.2015.104

Lei, X. F., Fu, W., Kim-Kaneyama, J. R., Omoto, T., Miyazaki, T., Li, B., et al. (2016). Hic-5 Deficiency Attenuates the Activation of Hepatic Stellate Cells and Liver Fibrosis through Upregulation of Smad7 in Mice. *J. Hepatol.* 64, 110–117. doi:10.1016/j.jhep.2015.08.026

Li, Z., Wang, Y., Zhang, Y., Wang, X., Gao, B., Li, Y., et al. (2021). Protective Effects of Fisetin on Hepatic Ischemia-Reperfusion Injury through Alleviation of Apoptosis and Oxidative Stress. *Arch. Med. Res.* 52, 163–173. doi:10.1016/j.arcmed.2020.10.009

Ma, H., Yang, B., Yu, L., Gao, Y., Ye, X., Liu, Y., et al. (2021). Sevoflurane Protects the Liver from Ischemia-Reperfusion Injury by Regulating Nrf2/HO-1 Pathway. *Eur. J. Pharmacol.* 898, 173932. doi:10.1016/j.ejphar.2021.173932

Mcdaid, J., Yamashita, K., Chora, A., Ollinger, R., Strom, T. B., Li, X. C., et al. (2005). Heme Oxygenase-1 Modulates the Allo-Immune Response by Promoting Activation-Induced Cell Death of T Cells. *Faseb j* 19, 458–460. doi:10.1096/fj.04-2217fje

Nace, G. W., Huang, H., Klune, J. R., Eid, R. E., Rosborough, B. R., Korff, S., et al. (2013). Cellular-specific Role of Toll-like Receptor 4 in Hepatic Ischemia-Reperfusion Injury in Mice. *Hepatology* 58, 374–387. doi:10.1002/hep.26346

Pizzino, G., Irrera, N., Cucinotta, M., Pallio, G., Mannino, F., Arcoraci, V., et al. (2017). Oxidative Stress: Harms and Benefits for Human Health, *Oxidative Med. Cell. longevity* 2017, 1–13. doi:10.1155/2017/8416763

Rabha, D. J., Singh, T. U., Rungsung, S., Kumar, T., Parida, S., Lingaraju, M. C., et al. (2018). Kaempferol Attenuates Acute Lung Injury in Caecal Ligation and Puncture Model of Sepsis in Mice. *Exp. Lung Res.* 44, 63–78. doi:10.1080/01902148.2017.1420271

Saw, C. L., Guo, Y., Yang, A. Y., Paredes-Gonzalez, X., Ramirez, C., Pung, D., et al. (2014). The berry Constituents Quercetin, Kaempferol, and Pterostilbene Synergistically Attenuate Reactive Oxygen Species: Involvement of the Nrf2-ARE Signaling Pathway. *Food Chem. Toxicol.* 72, 303–311. doi:10.1016/j.fct.2014.07.038

Selzner, M., Rüdiger, H. A., Selzner, N., Thomas, D. W., Sindram, D., and Clavien, P. A. (2002). Transgenic Mice Overexpressing Human Bcl-2 Are Resistant to Hepatic Ischemia and Reperfusion. *J. Hepatol.* 36, 218–225. doi:10.1016/s0168-8278(01)00259-810.1016/s0168-8278(01)00259-8

Subramanya, S. B., Venkataraman, B., Meeran, M. F. N., Goyal, S. N., Patil, C. R., and Ojha, S. (2018). Therapeutic Potential of Plants and Plant Derived Phytochemicals against Acetaminophen-Induced Liver Injury. *Int. J. Mol. Sci.* 19, 3776. doi:10.3390/ijms19123776

Suchal, K., Malik, S., Gamad, N., Malhotra, R. K., Goyal, S. N., Chaudhary, U., et al. (20162016). Kaempferol Attenuates Myocardial Ischemic Injury via Inhibition of MAPK Signaling Pathway in Experimental Model of Myocardial Ischemia-Reperfusion Injury. *Oxid Med. Cel Longev* 2016, 7580731. doi:10.1155/2016/7580731

Waltz, P., Carchman, E. H., Young, A. C., Rao, J., Rosengart, M. R., Kaczorowski, D., et al. (2011). Lipopolysaccaride Induces Autophagic Signaling in Macrophages via a TLR4, Heme Oxygenase-1 Dependent Pathway. *Autophagy* 7, 315–320. doi:10.4161/auto.7.3.14044

Wang, A., Lin, L., and Wang, Y. (2015). Traditional Chinese Herbal Medicine Penthorum Chinense Pursh: A Phytochemical and Pharmacological Review. *Am. J. Chin. Med.* 43, 601–620. doi:10.1142/s0192415x15500378

Xu, T., Huang, S., Huang, Q., Ming, Z., Wang, M., Li, R., et al. (2019). Kaempferol Attenuates Liver Fibrosis by Inhibiting Activin Receptor-like Kinase 5. *J. Cel Mol Med* 23, 6403–6410. doi:10.1111/jcmm.14528

Yang, L., Wang, W., Wang, X., Zhao, J., Xiao, L., Gui, W., et al. (2019). Creg in Hepatocytes Ameliorates Liver Ischemia/Reperfusion Injury in a TAK1-dependent Manner in Mice. *Hepatology* 69, 294–313. doi:10.1002/hep.30203

Yao, H., Sun, J., Wei, J., Zhang, X., Chen, B., and Lin, Y. (2020). Kaempferol Protects Blood Vessels from Damage Induced by Oxidative Stress and Inflammation in Association with the Nrf2/HO-1 Signaling Pathway. *Front. Pharmacol.* 11, 1118. doi:10.3389/fphar.2020.01118

Yu, Q., Chen, S., Tang, H., Zhang, X., Tao, R., Yan, Z., et al. (2021). Veratric Acid Alleviates Liver Ischemia/reperfusion Injury by Activating the Nrf2 Signaling Pathway. *Int. Immunopharmacol* 101, 108294. doi:10.1016/j.intimp.2021.108294

Zeka, K., Marrazzo, P., Micucci, M., Ruparelia, K. C., Arroo, R. R. J., Macchiarelli, G., et al. (2020). Activity of Antioxidants from Crocus Sativus L. Petals: Potential Preventive Effects towards Cardiovascular System. *Antioxidants (Basel)* 9. doi:10.3390/antiox9111102

Zhang, S., Feng, Z., Gao, W., Duan, Y., Fan, G., Geng, X., et al. (2020). Aucubin Attenuates Liver Ischemia-Reperfusion Injury by Inhibiting the HMGB1/TLR-4/nf-Kb Signaling Pathway, Oxidative Stress, and Apoptosis. *Front. Pharmacol.* 11, 544124. doi:10.3389/fphar.2020.544124

Zhuang, L., Ding, W., Zhang, Q., Ding, W., Xu, X., Yu, X., et al. (2021). TGR5 Attenuated Liver Ischemia-Reperfusion Injury by Activating the Keap1-Nrf2 Signaling Pathway in Mice. *Inflammation* 44, 859–872. doi:10.1007/s10753-020-01382-y

Conflict of Interest: The authors declare that the research was conducted in the absence of any commercial or financial relationships that could be construed as a potential conflict of interest.

Publisher's Note: All claims expressed in this article are solely those of the authors and do not necessarily represent those of their affiliated organizations, or those of the publisher, the editors and the reviewers. Any product that may be evaluated in this article, or claim that may be made by its manufacturer, is not guaranteed or endorsed by the publisher.

frontiers | Frontiers in Pharmacology

ORIGINAL RESEARCH
published: 02 May 2022
doi: 10.3389/fphar.2022.851267

Protective Effects of Tiaoganquzhi Decoction in Treating inflammatory Injury of Nonalcoholic Fatty liver Disease by Promoting CGI-58 and Inhibiting Expression of NLRP3 Inflammasome

Huicun Zhang[1,2]*, *Xiang Gao*[1], *Pengmin Chen*[3] and *Hongbing Wang*[1,4]

[1]Beijing Hospital of Traditional Chinese Medicine, Capital Medical University, Beijing, China, [2]Beijing Institute of Chinese Medicine, Beijing, China, [3]China-Japan Friendship Hospital, Beijing, China, [4]Beijing Hospital of Traditional Chinese Medicine Yanqing Hospital, Beijing, China

OPEN ACCESS

Edited by:
Jackson Almeida,
Federal University of São Francisco Valley, Brazil

Reviewed by:
Cicera Datiane De Morais Oliveira-Tintino,
Regional University of Cariri, Brazil
Maria Oliveira,
State University of Ceará, Brazil

***Correspondence:**
Huicun Zhang
zhanghuicun728@126.com

Specialty section:
This article was submitted to Gastrointestinal and Hepatic Pharmacology, a section of the journal Frontiers in Pharmacology

Received: 09 January 2022
Accepted: 08 April 2022
Published: 02 May 2022

Citation:
Zhang H, Gao X, Chen P and Wang H (2022) Protective Effects of Tiaoganquzhi Decoction in Treating inflammatory Injury of Nonalcoholic Fatty liver Disease by Promoting CGI-58 and Inhibiting Expression of NLRP3 Inflammasome. Front. Pharmacol. 13:851267. doi: 10.3389/fphar.2022.851267

Tiaoganquzhi Decoction (TGQZD) is a traditional Chinese herbal formulation demonstrated to be a clinically effective treatment for nonalcoholic fatty liver disease (NAFLD), although details concerning its clinical mechanism are poor. This study aimed to explore the mechanism of TGQZD on improvement of inflammatory damage and dyslipidemia caused by NAFLD through the CGI-58/ROS/NLRP3 inflammasome pathway. In our research, the *in vivo* protective effects of TGQZD on HFD-induced liver injury in rats and *in vitro* using lipopolysaccharide (LPS)+palmitate (PA)-stimulated HepG-2 cells model. Histological changes were evaluated by hematoxylin-eosin and Oil Red O staining. Inflammatory cytokines and protein expression were analyzed by ELISA, Real time PCR and western blotting. Liver function, blood lipids, free fatty acids (FFA), and reactive oxygen species (ROS) were determined by biochemical detection. Our results indicated that TGQZD exhibited anti-inflammatory activity, reduced the severity of NAFLD and ameliorated the pathological changes. Further, TGQZD improved liver function and lipid metabolism in NAFLD rats. TGQZD lowered serum aspartate aminotransferase, alanine aminotransferase, triglyceride, and total cholesterol levels. TGQZD suppressed the formulation of FFA and ROS. It also reduced the expression and release of the inflammatory cytokine interleukin-1β by promoting CGI-58 expression and inhibiting the expression of FFA, TNF-α, and the NLRP3 inflammasome induced by ROS. TGQZD exhibited anti-inflammatory effects via the CGI-58, ROS and NLRP3 inflammasome pathway *in vivo* and *in vitro*, respectively. Our findings demonstrated that TGQZD is a useful and effective therapeutic agent for treating NAFLD via promotion of CGI-58 to inhibit the expression of ROS-induced NLRP3 inflammasome.

Keywords: Tiaoganquzhi decoction, non-alcoholic fatty liver disease, CGI-58, ROS, NLRP3, IL-1β

INTRODUCTION

Nonalcoholic fatty liver disease (NAFLD) is the first cause of chronic liver disease, currently the prevalence of NAFLD in the world is 6.3–33% (Chalasani et al., 2012). NAFLD has become the most common chronic liver disease in the world. NAFLD is a clinicopathological syndrome that causes fatty degeneration of liver parenchyma cells due to excessive fat accumulation. NAFLD lesions generally develop from simple steatosis to steatohepatitis (NASH), liver fibrosis, cirrhosis and liver necrosis (Hasegawa et al., 2020), and may even transform into liver failure and liver cancer (Soresi et al., 2020). Therefore, it is of great significance to prevent and treat NAFLD.

NAFLD is a complex disease regulated by many factors and mechanisms, including environment, metabolism, gene, immunity and intestinal microecology, etc. Steatosis is a necessary condition for NAFLD. According to the classic theory of "second strike" in the pathogenesis of NAFLD, excessive accumulation of lipids in the cytoplasm of hepatic cell caused by various reasons are the first strike, which decreases the anti-strike ability of liver. The second attack is caused by the increase of reactive oxygen species (ROS), intestinal lipopolysaccharide (LPS), some cytokines secreted by immune system and adipose tissue, which triggered a series of cytotoxic events, leading to the inflammatory over reaction of liver (Day and James, 1998). The occurrence and progress of NAFLD mainly include fat accumulation in viscera, insulin and leptin resistance, oxygen stress, lipid peroxidation injury, inflammation of adipose tissue and liver tissue, etc. Inflammasome in liver cells may play an important role in the "second strike" response (Arab et al., 2018; Chen et al., 2020).

Comparative gene identification 58 (CGI-58) is named asα/βhydrolase domain-containing 5 (Abhd5) and expressed widely. Mutations CGI-58 in human will cause Chanarin-Dorfman syndrome (CDS) and it is a neutral lipid storage disease that the characterion is ichthyosis (thickened dry skin) and accumulation of triglyceride rich lipid droplets are found in most tissues and cell types (Lefevre et al., 2001). The role of CGI-58 in mediating intracellular fat hydrolysis is well established. CGI-58 has been shown to be involved in the intracellular fat hydrolysis (Lass et al., 2006; Brown et al., 2007; Brown et al., 2010; Zierler et al., 2013), but research concerning how CGI-58 is linked to inflammasome activation is limited.

The inflammatory corpuscle is a kind of multi protein complex which is involved in innate immune defense function and assembled by the cytoplasmic pattern recognition receptor (PRR), When cells are stimulated by external signals, specific inflammasome recruit and activate caspase-1, which processes and self activates and secretes cytokines IL-1β, IL-18 and TNF-αto enhance the inflammatory reaction of the body against internal and external stimuli (Lee et al., 2015; Sarkar et al., 2019). Nod-like receptor protein 3 (NLRP3) is the most well-known inflammasome. It is mainly composed of NLRP3, ASC (known as the apoptosis-associated speck-like granular protein with a CARD domain) and caspase-1 (a hydrolase containing hemitryptophan and hydrolysable aspartic acid protein). After receiving the activation signal, NLRP3 first combines with ASC, and ASC then recruits pro-caspase-1 to the multiprotein complex. The binding of multiple pro-caspase-1 clusters is unstable and is rapidly activated by via autocatalytic activity to produce active caspase-1 (Wan et al., 2016). Caspase-1 processes pro-IL-1β into IL-1β. IL-1β once released exerts effects outside the cell and activates a series of inflammatory chain reactions (Ajmera et al., 2017). NLRP3 inflammasome has been shown to be associated with a variety of immune diseases. At present, few studies have investigated the pathogenesis of NLRP3 inflammasome in NAFLD (Lee et al., 2015; Gao et al., 2016; Shao et al., 2018).

Specific CGI-58 knockout in mice can increase HFD-induced impaired glucose tolerance and insulin resistance (IR), which are associated with inflammation. CGI-58-deficiency leads to overproduction of ROS, which activates the NLRP3 inflammasome to secrete proinflammatory cytokines. CGI-58 as a suppressor inhibits the activation of the NLRP3 inflammasome in HFD-induced NAFLD mice (Miao et al., 2014).

Clinical studies have shown that the Tiaoganquzhi decoction (TGQZD) can improve the clinical symptoms of NAFLD patients, and has a certain role in regulating blood lipids and in reducing body weight. Compared with silibinin capsule, it has certain advantages in improving clinical symptoms, liver function and regulating blood lipids (Qi, 2012). However, there are few reports that TGQZD inhibited inflammatory damage of hepatocytes and improved the metabolism of lipid by regulated CGI-58 and the NLRP3 inflammasome. The aim of this study was to observe the effect of TGQZD on NAFLD rats and to explored whether its mechanism is related to the regulation of CGI-58 and NLRP3inflammasome expression, which will provide a reference for the treatment of NAFLD and deepen the therapeutic effect mechanism of TGQZD.

MATERIALS AND METHODS

Laboratory Animals

Male Sprague-Dawley (SD) rats, weighting 120 ± 20 g, were obtained from Beijing Weitong Lihua Research Center for Experimental Animals. Rats were maintained in a temperature-controlled room (25 ± 1 °C in 12–12 h light-dark cycles) and housed in the animal facilities at the Beijing Hospital of Traditional Chinese Medicine (Capital Medical University Beijing, China). The study was carried out under the established guidelines for animal experimentation and the protocol was approved by the Animal Studies Ethics Committee of Beijing Hospital of Traditional Chinese Medicine, Capital Medical University with code number 2019030201.

Preparation of TGQZD

TGQZD consists of the following 13 dried crude herbs: *Astragalus membranaceus* (Fisch.) Bge, *Bupleurum chinense* DC, *Atractylodes macrocephala* Koidz, *Curcuma wenyujin* Y. H. Chen et C. Ling, *Pinellia ternata* (Thunb.) Breit, *Artemisia scoparia* Waldst. etKit, *Alisma orientale* (Sam.) Juzep, *Cassia obtusifolia* L, *Salvia miltiorrhiza* Bge, *Angelica sinensis* (Oliv.) Diels, *Paeonia lactiflora* Pall, *Crataegus pinnatifida* Bge. var. Major N. E. Br and *Semen sinapis.* The ratio of the TGQZD formulation is 3:2:4:3:1:4:3:3:6:3:3:3:2 (**Table 1**). On the basis of standards specified in the Chinese Pharmacopoeia (2015 edition), Beijing Hospital of Traditional Chinese Medicine, Capital Medical University provided all the herbs for this preparation.

TABLE 1 | Different components in the formula of TGQZD.

Chinese name	Latin name	Used part	Traditional use	Voucher specimens
Huang qi	*Astragalus membranaceus* (Fisch.) Bge	root	Qi Reinforcing	TCM - 201101 - JPQCHSD01
Chai hu	*Bupleurum chinense* DC.	root	To relieve fever, to soothe the liver	TCM - 200926 - JPQCHSD02
Bai zhu	*Atractylodes macrocephala* Koidz	root	Qi-reinforcing	TCM - 200816 - JPQCHSD03
Yu jin	*Curcuma wenyujin* Y. H. Chen et C. Ling	tuberoid	Blood activating Stasis Removing	TCM - 201022 - JPQCHSD04
Ban xia	*Pinellia ternata* (Thunb.) Breit	tuber	Phlegresolving	TCM - 201007 - JPQCHSD05
Yin chen	*Artemisia scoparia* Waldst.etKit	aboveground part	Diuretic Dampness Excreting	TCM - 200901 - JPQCHSD06
Ze xie	*Alisma orientale* (Sam.) Juzep	tuber	Diuretic Dampness Excreting	TCM - 201019 - JPQCHSD07
Jue mingzi	*Cassia obtusifolia* L	ripe seed	Fire Purging	TCM - 201022 - JPQCHSD08
Danshen	*Salvia miltiorrhiza* Bge	root	Blood-activating and Stasis-removing	TCM - 200930 - JPQCHSD09
Dang gui	*Angelica sinensis* (Oliv.) Diels	root	Blood-Tonifying	TCM - 200903 - JPQCHSD10
Chi shao	*Paeonia lactiflora* Pall	root	Heat Clearing Blood Cooling	TCM - 201024 - JPQCHSD11
Shan zha	*Crataegus pinnatifida* Bge. var. Major N. E. Br	rosaceae	help digestion and Stasis-removing	TCM - 201009 - JPQCHSD12
Bai jiezi	*Semen sinapis*	ripe seed	removing the phlegm	TCM - 200526 - JPQCHSD13

The herbs were chopped into crude herbs and mixed. TGQZD was boiled in distilled water at 100°C for 2 h for extraction. Then the TGQZD solution was concentrated to the density of 2 g crude herb/ml and stored at −20 °C until further use.

Ultra-high-performance Liquid Chromatography-Tandem Mass Spectrometry (UPLC-MS/MS) Analysis of TGQZD

Then the components of the TGQZD were analyzed by liquid chromatography/mass spectrometry (LC/MS)/MS instrument (Thermo Fisher). Briefly, DIONEX Ultimate 3,000 (Thermo Fisher) ultrahigh-performance liquid chromatography and Thermo Hypersil Gold C18 column (1.7 μm × 2.1 mm × 100 mm) were used to analyze sample. The mobile phase consisted of A (water, 2 mmoL/L ammonium formate, and 0.1% formic acid, v/v) and B (acetonitrile) with gradient elution. The gradient conditions for C18 separation was as follows: 100% A and 0% B, initial; 70% A and 30% B, 2 min; 30% A and 70% B, 9 min; 5% A and 95% B, 11 min; 0% A and 100% B, 12 min; 0% A and 100% B, 14 min; 100% A and 0% B, 14.1 min, 14 min; 100% A and 0% B, 16 min. The flow rate was 300 μl/min and the injection volume was 1 μl. The column temperature was maintained at 45°C. Mass spectrometry analysis was performed by the Q Exactive mass spectrometer (Thermo Fisher). The voltage of positive and negative ion source were 3.7 and 3.5 kv, respectively, and the heated vaporizer temperature was maintained at 320°C. Data were collected and processed by the Xcalibur 2.2 SP1.48 software (Thermo Fisher).

In vivo Experimental Design

Eighteen 6-week-old male Sprague-Dawley rats were randomly divided into three groups of six rats each. One group (normal diet, ND, n = 6) of rats was fed with 11.4% kcal fat diet (Beijing Science and Cooperation Feed Technology Limited Company, Beijing, China; protein: 27.5%, carbohydrate: 65.8%, and fat: 11.4% kcal/g), and the other two groups (high-fat diet HFD, n = 6), or a high-fat diet along with TGQZD, HFD + TGQZD, n = 6) were fed with a 33.1% kcal fat diet (Beijing Science and Cooperation Feed Technology Limited Company, Beijing, China; protein: 19.6%, carbohydrate: 47.1%, and fat: 33.1% kcal/g). The high fat diet was administered for 8 weeks to establish the NAFLD rat model (Al-Shaaibi et al., 2016; Liu et al., 2016). From the ninth week rats were dosed by oral gavage once per day for 8 weeks with TGQZD 5 ml/kg per day. The rats were treated for 8 weeks.

Sample Collection

After 8 weeks of treatment, the rats were anesthetized by 10% pentobarbital sodium. After deep anesthesia abdominal blood samples from all rats were collected for serum biochemical assays. In order to minimize the time that rats suffered pain from experiment as much as possible, they were rapidly euthanized by cervical dislocation during deep anesthesia and then the liver was removed and washed in PBS before being placed in 4% paraformaldehyde. Liquid nitrogen was used to freeze the remaining liver tissue, which was stored at −80°C for subsequent analysis.

Histological Examination and Assessment

Sections of liver samples (4-μm thick) were stained with hematoxylin-eosin (H&E), while frozen liver tissues (5-μm thick) were dyed with Oil Red O stain. Liver samples were examined under a light microscope (Olympus Medical Systems Corp, Tokyo, Japan). Severity was assessed by the NAFLD score. The evaluation system consisted of the following: steatosis (on a scale of 0–3), lobular inflammation (on a scale of 0–3), and hepatocellular ballooning (on a scale of 0–2). Higher scores indicated more serious disease (Kleiner et al., 2005).

Serum Biochemical Parameter Analysis

The serum levels of alanine aminotransferase (ALT); aspartate aminotransferase dd (AST); blood triglyceride (TG), and total cholesterol (TC) were measured using the 7,160 Automatic Biochemical Analyzer (Hitachi, Japan) following the manufacturer's operating instructions.

Determination of FFA and ROS Levels in Liver

Liver tissues stored at −80 °C were then transferred to a homogenizer to obtain a tissue homogenate and then centrifuged at 3,500 rpm for

10 min to obtain the supernatant. The FFA and ROS levels in the supernatant were determined using the commercial kits (Nanjing Jiancheng Biochemical Co., Ltd. and Beijing Sino-Uk institute of Biological Technology, respectively).

Enzyme-Linked Immunosorbent Assay

The serum levels of IL-1β and TNF-α were detected by enzyme-linked immunosorbent assay (ELISA) according to the manufacturers' protocols (Beijing SINO-UK Institute of Biological Technology, cat. no. HY-10101, HY-H0019). Briefly, solid-phase antibodies are produced by microplates using purified biotin-based antibody packs, which are added to the colon tissue lysate and affinity labeled by 'spicy root peroxidase. After thorough washing, add 3, -3′, -5, -5′-tetamiphenyl benzene to develop color. The absorbance was measured at 450 nm and the sample concentration was calculated.

Cell Culture and Treatment

The human hepatocellular carcinoma cell line (HepG-2) was purchased from cell resource center of Shanghai Institutes for Biological Sciences Chinese Academy of Sciences. HepG-2 cells were cultured in DMEM containing 10% fetal bovine serum and maintained in 6-cm dishes under a humidified atmosphere with 5% CO_2 at 37°C in a cell culture incubator. When cells reached 60% confluence, the cells were divided into four groups: the Control, TGQZD, Lipopolysaccharide (LPS) + palmitate (PA), and LPS + PA + TGQZD groups. In the Control group, cells were treated with phosphate-buffered saline (PBS) in the culture medium; TGQZD group was treated with TGQZD in the culture medium; the LPS + PA group was treated with 10 μg/ml LPS+0.4 mM PA in the culture medium and the LPS + PA + TGQZD group was treated with 4 mg/ml TGQZD and 10 μg/ml LPS+0.4 mM PA in the culture medium, each group of cells was incubated at 37 °C with 5% CO_2. After 24 h of the co-culture, cells in each treatment group were collected and analyzed as described below.

The Institute of Traditional Chinese Medicine, Chinese Academy of Traditional Chinese Medicine provided TGQZD lyophilized powder. 100 mg TGQZD lyophilized powder were dissolved in 5 ml DMEM. The drug solution is sterilized after filtration through the filter membrane and stored at 4°C. TGQZD-dried powder solution was diluted to the required concentration prior to experimentation.

Cell Viability Assays

Cell viability was determined using MTT. HepG-2 cells were seeded at 1×10^4 cells/well in 96-well plates and then incubated with MTT for 4 h at 37°C. Absorbance was measured at 490 nm and the optical density (OD) values were compared to determine whether the TGQZD have an effect on cell viability.

Measurement of Lipid Accumulation and Intracellular ROS Formation

HepG-2 cells were seeded at 2×10^5 cells/well in a 6-well plate. When HepG-2 cells reached 70% confluence, cells were treated with 0, 4 mg/ml TGQZD and LPS + PA mixture for 24 h, respectively. The TG levels were measured using a commercial kit according to the manufacturer's instructions (Applygen Technologies Inc. Beijing, China). A fluorescence probe (DCF-DA) was used to detect the ROS levels of HepG-2 cells according to the manufacturer's instructions (Beijing Sino-Uk institute of Biological Technology).

RT-PCR

RNA was extracted from the liver tissue and HepG-2 cells were lysed in ice-cold samples preserved at −80 °C using a kit according to the manufacturer's protocol. The following PCR primers were synthesized. NLRP3-Human: forward, 5′-CCACAAGATCGTGAGAAAACCC-3′ and reverse, 5′-CGGTCCTATGTGCTCGTCA-3′; CGI-58-Human: forward,5′-CACATGGTGCCCTACGTCTAT-3′ and reverse, 5′-ACAGGTCTGTTGGTGCAAAGA-3′; ACTIN-Human:forward, 5′-CCTGGCACCCAGCACAAT-3′ and reverse, 5′-GGGCCGGAC TCGTCATAC-3′; NLRP3-Rat: forward, 5′-TGCATGCCGTATCTG GTTGT-3′ and reverse, 5′-AGCTGAGCAAGCTAAAGGCT; CGI-58-Rat: forward, 5′-CGGCAGTGATGAAAGCGATG-3′ and reverse, 5′-TAGACGTGGGACACCAGGTA; ACTIN-Rat:forward, 5′-TCC ACCCGCGAGTACAACC-3′ and reverse, 5′-CGACGAGCGCAG CGATA (Sangon Biotech, Shanghai, China). cDNA was synthesized using a RevertAid first-strand DNA synthesis kit (Tiangen Biotech). ABI-7500 Real-time quantitave PCR thermal cycl and a real-time PCR system kit (Tiangen Biotech) were used to detect Thermal cycler gene expression according to the manufacturer's instructions and cycle threshold (CT) values were calculated by normalizing CT to ACTIN expression to present target gene (2-ΔΔCT) expression. The SYBR Green real-time PCR cycling protocol used was as follows: DNA denaturation at 95°C for 3 min, followed by 40 cycles at 95°C for 5 s and 60°C for 33 s (Zhang et al., 2021).

Western Blot Analysis

The liver tissue and HepG-2 cells were lysed in ice-cold RIPA lysis buffer (Beyotime, Shanghai, China) for 30 min. Protein extracted were centrifuged at 20000r/min×10 min at 4 °C. BCA method (Beyotime Biotechnology, China) was used to determine the lysate protein concentration. The supernatant with buffer solution was then boiled at 100°C for 10 min and stored at −20 °C.

10% SDS gel electrophoresis (SDS-PAGE) was used to separate 60 μg liver and 30 μg HepG-2 cells denatured proteins solution. Then the protein in the gel was transferred to the nitrocellulose membrane. The membrane was sealed in TBST with 8% nonfat milk for 1 h at 37°C, then CGI-58 (sc-100468) antibody, NLRP3 antibody (AF2155) and anti-ACTIN (AA128) were added and incubated overnight at 4°C. After washing the membrane in TBST for three times for 10 min each, the secondary antibody was added and incubated at 37°C for 1 h. The film was washed in TBST for three times for 10 min each again, and was scaned by an Odyssey scanner (LI-COR). Then image was analyzed by ImageJ software.

Statistical Analysis

The statistical analyses was performed using statistical software package SPSS 17.0 and data were reported as means ± standard deviation. The normality test was performed by Shapiro-Wilk test, and then the differences among multiple groups were analyzed by one-way analysis of variance (ANOVA). ANOVA was followed by the least significant difference (LSD) post hoc test

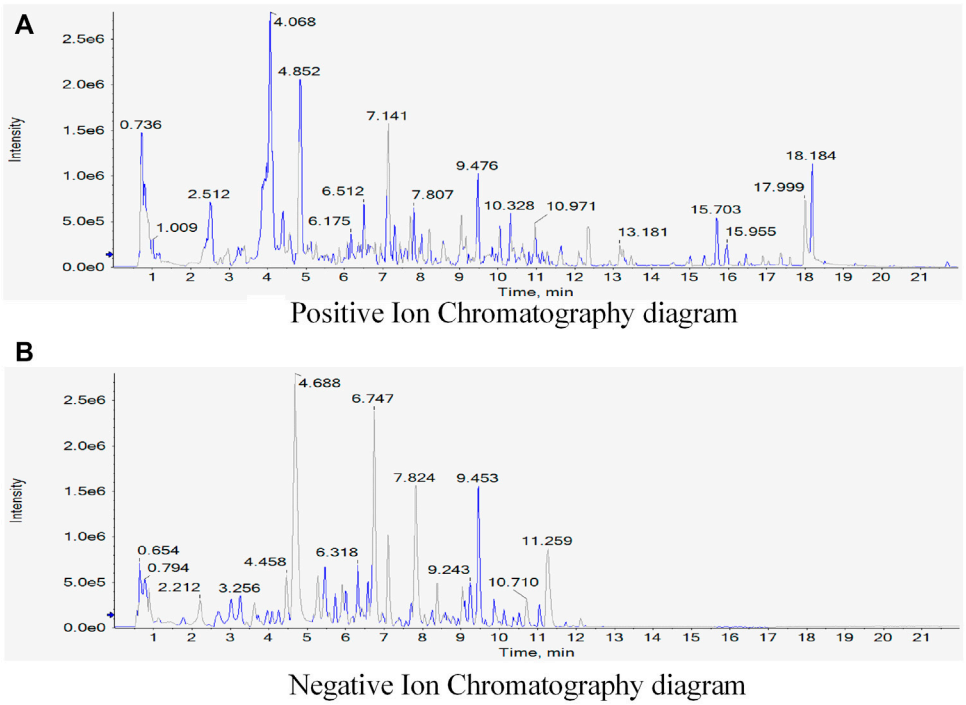

FIGURE 1 | Identification of components of Tiaoganquzhi Decoction(TGQZD) using UPLC-MS/MS. The positive **(A)** and negative **(B)** ion chromatograms of TGQZD were shown as indicated. The major component and their retention time were listed in the (**Table 2**).

for pairwise comparison. A p value less than 0.05 was considered statically significant.

RESULTS

Identification of the Components of the TGQZD Formula Using UPLC-MS/MS

The composition of TGQZD were analyzed by UPLC-MS/MS. The total ion chromatogram of the TGQZD is shown in **Figure 1**. According to the Chinese pharmacopeia (2015), the components identified in TGQZD were listed as follows: ferulic acid, salvigenin, saikosaponin A, bisdemethoxycurcumin, angelicoidenol, 1,2-dihydrotanshinone, astragaloside II, astragaloside I, galloylpaeoniflorin, paeonidaninol A, astraverrucin IV, paeonin A, saikosaponin C, salvianolic acid B, aurantio-obtusin, chrysophanol, atractylenolide I, and alisol B 23-acetate. They were eluted at 4.3, 6, 10.01, 10.3, 8.46, 12.24, 9.81, 10.32, 5.73, 8.03, 8.03, 8.26, 9.28, 6.76, 9.23, 12.33, 10.55 and 12.79 min, respectively (**Table 2**).

TABLE 2 | The components identified in TGQZD.

Compound	m.z	Retention.time.min
Ferulic acid	193.0504	4.3
Salvigenin	373.0929	6
Saikosaponin A	825.4658	10.01
Bisdemethoxycurcumin	307.0972	10.3
Angelicoidenol	215.1292	8.46
1,2-Dihydrotanshinone	277.087	12.24
Astragaloside II	871.4727	9.81
Astragaloside I	867.4766	10.32
Galloylpaeoniflorin	631.1676	5.73
Paeonidaninol A	629.1879	8.03
Astraverrucin IV	843.4763	8.03
Paeonin A	629.1882	8.26
Saikosaponin C	971.5254	9.28
Salvianolic acid B	717.148	6.76
Aurantio-Obtusin	329.0673	9.23
Chrysophanol	255.0651	12.33
Atractylenolide I	231.1379	10.55
Alisol B 23-acetate	515.3718	12.79

TGQZD Attenuates HFD-Induced TG Accumulation

H&E staining revealed that the morphology and structure of the liver tissue. There were limited red lipid droplets in the ND-treated group. In the HFD group, fatty degeneration appeared in the liver. Hepatocytes were swollen and round and their volume was significantly larger than that of the ND group. A large number of fat vacuoles and evidence of balloon degeneration was detected in the cytoplasm. Following treatment with TGQZD, the fatty vacuoles and balloon-like changes in the livers of NAFLD rats improved. Consistent with the H&E staining, the results of Oil Red O staining showed that a large

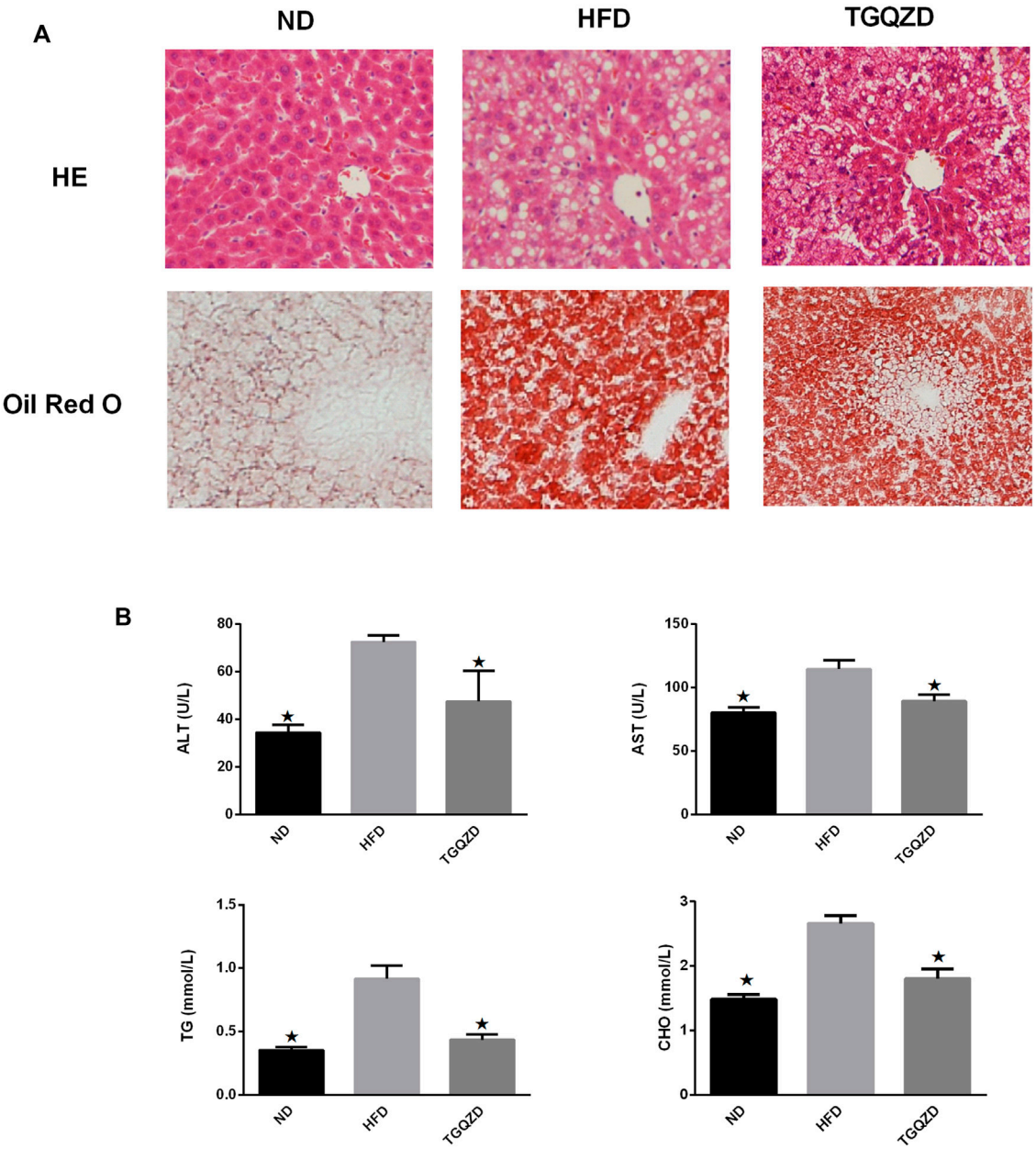

FIGURE 2 | (A) Effect of TGQZD on liver histomorphology of NAFLD rats. The HE staining showed that the morphology and structure of the liver tissue in the ND group were normal; In the HFD group, fatty degeneration appeared in the liver. Hepatocytes are swollen and round and their volume is significantly higher than that of ND group. There exist a large number of fat vacuoles and balloons in cytoplasm. After the treatment of TGQZD, the fatty vacuoles and balloon like changes in NAFLD rats' liver were improved. The results of oil red O staining showed that there was little red lipid drop in the liver tissue of the ND group and a large number of red lipid drops in the liver tissue of the HFD group, which showed that the lipid droplets infiltrated into the hepatocytes and fused into pieces. Red lipid droplets were also found in liver tissue of rats in TGQZD group, but the number and the fusion into pieces were less than that in HFD group (Figure 2). Histological examination showed that fatty degeneration, inflammation, and hepatocyte ballooning in TGQZD group were alleviated than HFD group (**Table 3**). **(B)** Effect of TGQZD on liver function and blood lipid of NAFLD rats. Compared with the ND group, the levels of ALT, AST, TG and TC in the HFD group were significantly higher ($p < 0.05$); compared with the HFD group, the levels of ALT, AST, TG and TC in the TGQZD group were significantly lower ($p < 0.05$). *$p <$ vs. HFD Group, alone.

number of red lipid droplets in the liver tissue of the HFD group. While lipid droplets in the TGQZD group were less than that in the HFD group (**Figure 2A**). Histological examination showed fatty degeneration, inflammation, and hepatocyte ballooning in the TGQZD group were alleviated compared with the HFD group (**Table 3**).

Compared with the ND group, the levels of ALT, AST, TG, and TC levels in the HFD group were significantly higher ($p <$

TABLE 3 | Average score of histopathological findings in livers ($\bar{x} \pm s, n = 6$).

Group	Steatosis	Inflammation	Ballooning
ND	0	0	0
HFD	2.00 ± 0.00*	2.46 ± 0.03*	2.00 ± 0.00*
TGQZD	1.33 ± 0.03**	1.23 ± 0.03**	1.30 ± 0.05**

*Quantitative data are expressed as mean ± SD., Statistical analysis of the data for multiple comparisons was performed by one-way ANOVA.*p<0.05, versus the ND, group, **p<0.05, versus the HFD, group.*

0.05); compared with the HFD group, the levels of ALT, AST, TG, and TC in the TGQZD group were significantly lower ($p < 0.05$) (**Figure 2B**).

TGQZD Lowered FFA and ROS Levels in Liver of NAFLD Rats

Compared with the ND group, FFA and ROS levels in the HFD group were significantly higher ($p < 0.05$), while Compared with the HFD group, TGQZD had significantly lowered levels of FFA and ROS in NAFLD rats ($p < 0.05$) (**Figure 3**).

TGQZD Decreased Serum IL-1β and TNF-α Content in NAFLD Rats

Compared with the ND group, the levels of serum IL-1β and TNF-α in HFD group increased significantly ($p < 0.05$). Compared with the HFD group, the levels of serum IL-1β and TNF-α in the TGQZD group decreased significantly ($p < 0.05$) (**Figure 4**).

TGQZD Improved the Viability of Hepatocytes-Stimulated With LPS + PA

After being stimulated with LPS + PA for 24 h, there was a significant difference in the rate of cell proliferation between in the LPS + PA and Control groups. Compared with the Control group, the cell proliferation of the LPS + PA group was markedly decreased. Compared with the LPS + PA group, TGQZD treatment resulted in a significant increase in cellular proliferation (**Figure 5**).

TGQZD Reduced Cellular TG and ROS Levels in HepG-2 Cells Exposed to LPS and PA

Following a 24 h treatment of HepG-2 cells with LPS + PA, the TG concentrations and ROS levels in the LPS + PA group were obviously higher than in control group. Meanwhile, TG and ROS production in the LPS + PA + TGQZD treatment group were markedly decreased compared with the LPS + PA group ($p < 0.05$). Compared with the control group, there were no significant TG and ROS change in the TGQZD alone group (**Figure 6**).

TGQZD Increased CGI-58 Expression and Reduced NLRP3 Inflammasome in HepG-2 Cells Stimulated With LPS and PA

Real time PCR and western blot analysis indicated, in HepG-2 cells stimulated with LPS + PA for 24 h, the expression of CGI-58 in the LPS + PA group was inhibited, while CGI-58 increased in the LPS + PA + TGQZD group. Compared with the control group, the expression of NLRP3 inflammasome in the LPS + PA group was overexpressed. TGQZD decreased the overexpression of NLRP3 inflammasome induced by LPS + PA. Compared with the control group, there were no significant CGI-58 and NLRP3 inflammasome change in the TGQZD alone group (**Figure 7**).

TGQZD Promoted CGI-58 Expression and Inhibited NLRP3 Inflammasome Formation in the Liver of NAFLD Rats

After TGQZD treatment, compared with the ND group, the hepatic levels of CGI-58 decreased, while NLRP3 inflammasome in the HFD group increased significantly ($p < 0.05$). Compared with those of the HFD group, TGQZD significantly promoted the formation of CGI-58 and inhibited the expression of NLRP3 inflammasome ($p < 0.05$) (**Figure 8**).

DISCUSSION

As with earlier research, SD rats fed by the high-fat diet were developed NAFLD asssocited with hepatic glycerol accumulation and hyperlipidaemia (Marchesini et al., 2003). In our study, the HFD fed rats have significant biochemical features of NAFLD, including significantly elevated liver enzymes and hyperlipidemia accompanied by an increase in the accumulation of triglyceride in the liver. The histological abnormalities in the HFD rats of this study were consistent with the findings of the previous literatures (Kim et al., 2017).

Researchers have widely used animal model of NAFLD induced by high-fat diet to identify the pathogenesis and explore its treatment for NAFLD (Barbuio et al., 2007).

The nonspecific clinical feature of NAFLD is elevated hepatic aminotransferase (ALT and AST) and they are positively correlated with most patients with NAFLD (Bacon et al., 1994). After Treatment with TGQZD, elevated hepatic aminotransferase were significantly reduced. The results of biochemical and histological analysis showed that TGQZD have a protective effect on HFD-induced liver damage.

The pathogenesis of NAFLD has not been clarified. Abnormal fat metabolism, oxygen stress, and lipid peroxidation, heredity, hormones, the microenvironment, and drugs may all play important roles in the excessive fat accumulation in the liver. Obesity and IR increases the levels of FFAs and promotes the accumulation of TGs in the liver as the first strike (Li et al., 2018) and changes the permeability of membrane. It promotes the release of inflammatory factors, swelling, inflammation, and necrosis. The second attack was mainly caused by the self-

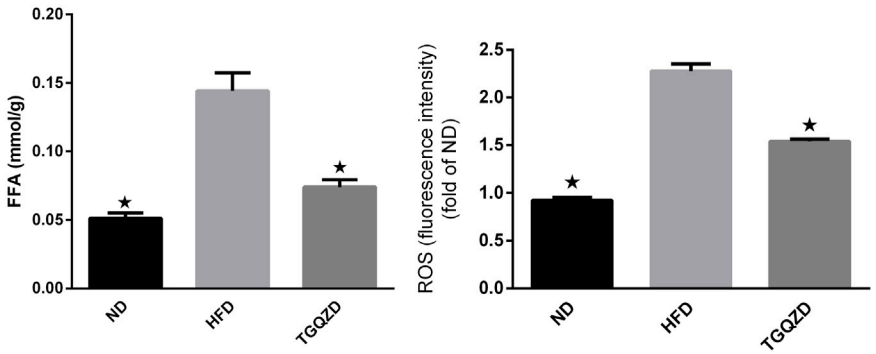

FIGURE 3 | Effect of TGQZD on FFA and ROS content in liver of NAFLD rats. Compared with the ND group, the content of FFA and ROS in the liver of NAFLD rats was significantly increased ($p < 0.05$), while compared with the HFD group, TGQZD significantly reduced the level of FFA and ROS in the liver of NAFLD rats ($p < 0.05$). *$p < 0.05$ vs. HFD Group, alone.

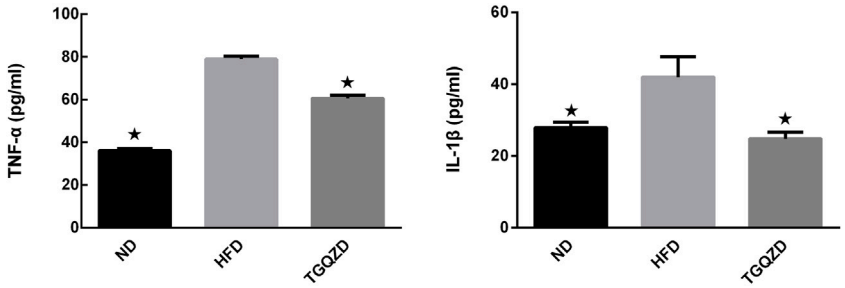

FIGURE 4 | Effect of TGQZD on serum IL-1 β content in NAFLD rats. After 8 weeks of treatment, compared with the ND group, the level of serum IL-1β in HFD group increased significantly ($p < 0.05$); while compared with the HFD group, the level of serum IL-1β in the TGQZD group decreased significantly ($p < 0.05$), indicating that TGQZD could effectively inhibit the formation of pro-inflammatory cytokines by reducing the increased level of IL-1 β in NAFLD rats. *$p < 0.05$ vs. HFD Group, alone.

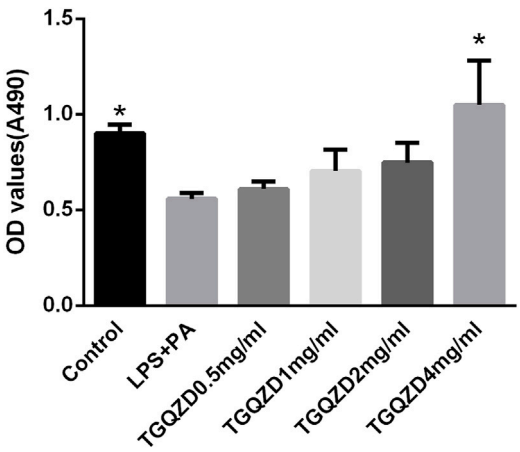

FIGURE 5 | Effects of TGQZD on the viability of HepG-2 cells. HepG-2 cells were treated with 10ug/ml LPS+0.4 mM palmitate and different concentrations of TGQZD for 24 h, and cell viability was measured using the MTT assay. Data are expressed as the mean ± SD (n = 3). *$p < 0.05$ vs. LPS + PA Group, alone.

injury of intracellular environmental factors including ROS, lipid peroxidation products, inflammasome, and inflammatory reactions caused by downstream inflammatory factors (Gao et al., 2020). Oxidative stress causes the peroxidation of membrane phospholipid and changes the permeability of the membrane. It promotes the release of inflammatory factors. Swelling, inflammation, and necrosis of hepatocytes lead to liver fibrosis, which can develop into cirrhosis (Canada et al., 2019). The liver is a key organ of fat metabolism. It is an important site of fat digestion, absorption, oxidation, decomposition, transformation, and maintenance of the balance of lipid metabolism in the body. If too much fat is ingested, the level of blood lipids is increased, thus the fat entering the liver exceeds the threshold of liver transformation, TG in hepatocytes are increased, apolipoproteins are insufficient, and the release of TGs from the liver is reduced, which leads to a large amount of TGs accumulating in the liver, eventually causing NAFLD (Grasselli et al., 2019). Clinically, NAFLD is often accompanied by damage in liver function and disorder in liver lipid metabolism. In the present study, compared with the HFD group, the levels of ALT,

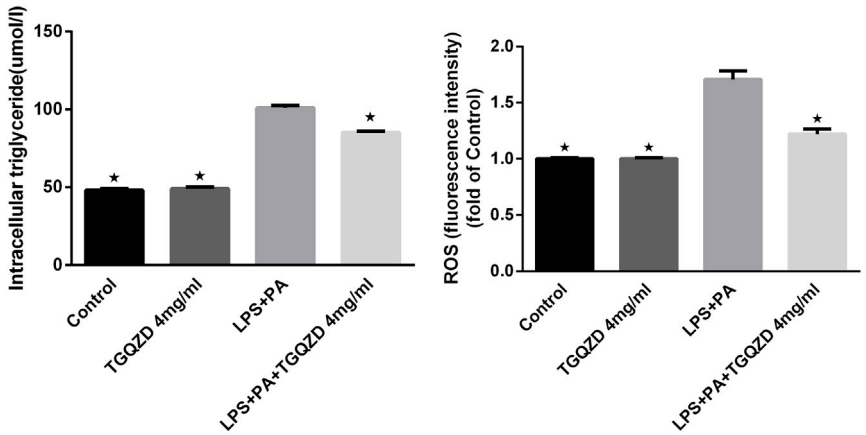

FIGURE 6 | Effect of water extract TGQZD on the formation of intracellular triglyceride (TG) and reactive oxygen species (ROS) in LPS + PA -treated HepG-2 cells. In the Control group, phosphate-buffered saline (PBS) in the culture medium; TGQZD group was treated with TGQZD in the culture medium; the LPS + PA group was treated with 10 μg/ml LPS + 0.4 mMPA in the culture medium and the LPS + PA + TGQZD group was treated with 4 mg/ml TGQZD and 10 μg/ml LPS + 0.4 mMPA in the culture medium, respectively. *$p < 0.05$ vs. LPS + PA Group, alone.

AST, TG, and TC in the TGQZD group were significantly lower ($p < 0.05$), which indicated that TGQZD could reduce the damage due to the presence of high fat levels in hepatocytes and improve the lipid metabolism of NAFLD rats. An analysis of the pathological sections also showed that TGQZD alleviated the liver damage, lipid deposition, and fatty degeneration of hepatocytes in NAFLD rats. Nonetheless, the abnormal fat metabolism, the inflammatory response by hepatocytes, the oxygen stress may play an important role in the formation and development of NAFLD (Yamada and Guo, 2018).

When the liver cell membrane is damaged, an inflammatory response is triggered, reducing various functions of liver, and causing excessive fatty accumulation in liver (Teimouri et al., 2020). The mitochondria are the main sites of fatty acid β-oxidation and trifusoic acid cycle. Lipid peroxidation leads to the formation of free radicals, which can directly damage the structure of cell membrane and brings about its functional disorder (Wang et al., 2020). Free radicals can react with the double bonds of fatty acyl lipids of the cell membrane to generate MDA. MDA affects mitochondrial activity and blocks fatty acid oxidation, which results in fat accumulation in the liver (Ji et al., 2019). Excessive lipid peroxide also can induce inflammatory cell infiltration, activate Kupffer's cell, and HSC, which can cause liver fibrosis (Liang et al., 2018). We showed that TGQZD effectively reduced the levels of FFA and ROS in NAFLD rats. This indicated that TGQZD could improve lipid metabolism and reduce the level of oxidative stress in NAFLD rats.

CGI-58 is a key regulator of TG conversion. CGI-58 regulates the mobilization of TG by stimulating adipose TG lipase (ATGL) enzyme activity. In neutral lipid storage disease patients, the presence of CGI-58 mutation is more strongly associated with the potential development of fatty liver disease and hepatomegaly than the ATGL mutation (Lord and Brown, 2012), which indicates that CGI-58 has an independent function of ATGL in the liver. CGI-58 gene knockout leads to hepatic steatosis, CGI-58 regulates the storage and secretion of liver neutral lipids in the absence of the ATGL gene. The regulation of hepatic triacylglycerol metabolism by CGI-58 does not require ATGL co-activation (Lord et al., 2016). CGI-58 is not only a lipolytic factor, but it is also an endogenous inhibitor of NLRP3 inflammasome activity. CGI-58 deficiency induced ROS accumulation and then activated NLRP3 inflammasome, which caused liver inflammatory injury induced by HFD in mice (Miao et al., 2014). In our study, TGQZD might promote the formation of CGI-58 and inhibit the expression of NLRP3 inflammasome, which can effectively improve the lipid metabolism disorder and inflammatory injury of hepatocytes induced by HFD.

ROS are key mediators in the activation of caspase-1 and the NLRP3 inflammasome (Dostert et al., 2008; Zhou et al., 2011). Studies have shown that mitochondrial dysfunction activates the NLRP3 inflammasome by inducing ROS accumulation (Wen et al., 2011). NLRP3 combines with ASC to activate caspase-1, and then activates IL-1β, which promotes the release of inflammatory factors, and thus aggravates the inflammatory response (Tilg et al., 2016). IL-1β could promote hepatocytes to take up fatty acids, synthesize TG, and aggravate the steatosis of liver. Under the condition of a high-fat diet, IL-1ra deficient mice exhibited a more severe fatty hepatitis than wild-type mice (Matsuki et al., 2003). These studies indicated that IL-1β could promote the accumulation of lipids and the development of inflammation in the liver (Stojsavljevic et al., 2014; Ajmera et al., 2017). The generation of ROS also led to the activation of the transcription factor NF-κB, which in turn leads to an increase in the production of TNF-α (Syn et al., 2009). TNF-α levels were found to be elevated in NASH patients (Wigg et al., 2001). Further, serum TNF-α levels have been associated with NAFLD and may be involved in hepatocellular inflammation and IR in NAFLD (Valenti et al., 2002). TGQZD could effectively inhibit the formation of pro-inflammatory

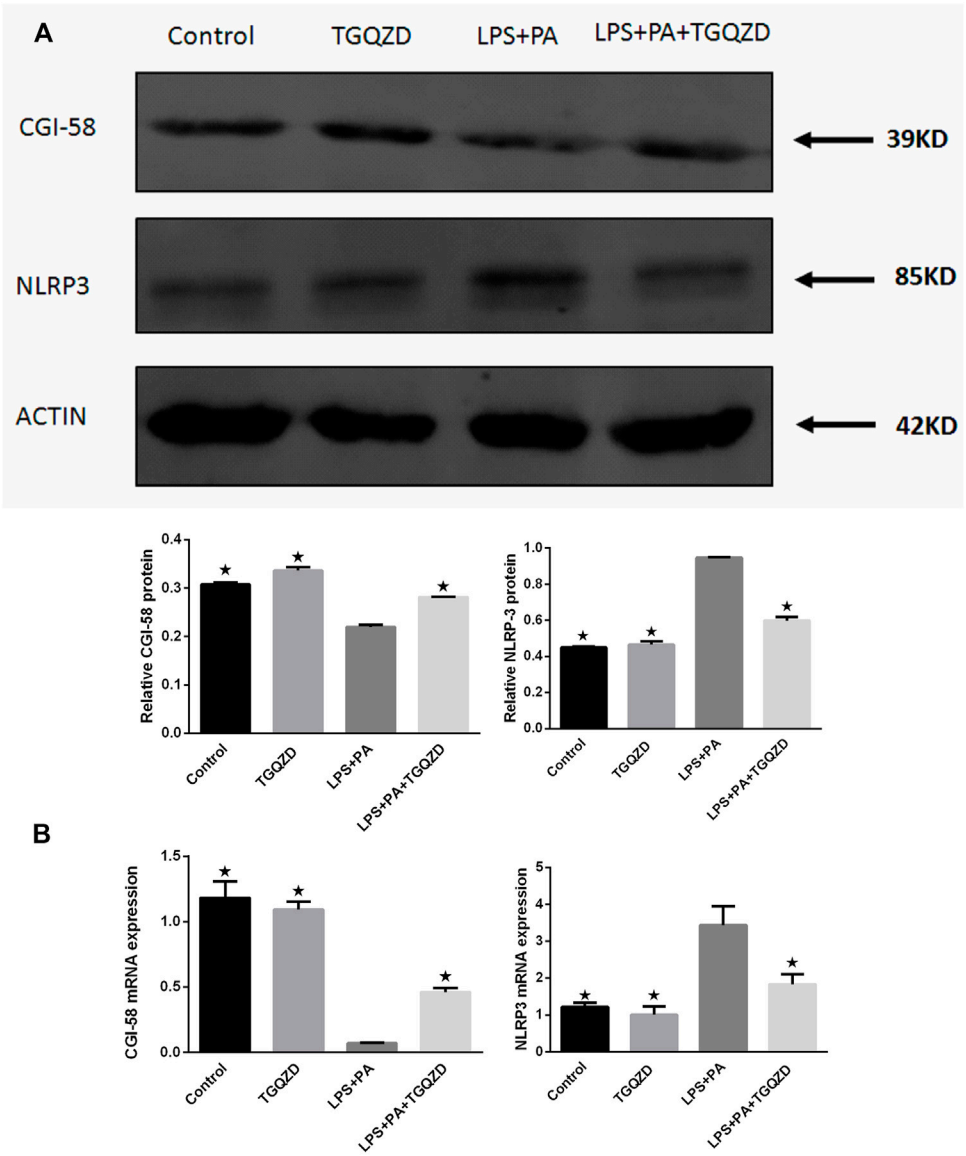

FIGURE 7 | Effect of TGQZD on CGI-58 and NLRP3 inflammasome of HepG-2 cells. **(A)** Representative images of Western blot showing CGI-58 and NLRP3 inflammasome protein expression in HepG-2 cells in the different groups. **(B)** Quantitation of CGI-58 and NLRP3 inflammasome mRNA expression in HepG-2 cells in different groups. ACTIN was used as a loading control. *$p < 0.05$ vs. LPS + PA Group, alone, ($n = 3$).

cytokines by reducing the upregulation of IL-1β and TNF-α levels in NAFLD rats. Thus, regulating CGI-58 and NLRP3 inflammasome are of great significance for the treatment of NAFLD in the future.

The "multiple parallel strikes" process emphasizes the parallel effects of different injury factors (Tilg and Moschen, 2010). The combined interaction of PA and LPS with toll-like receptors (TLRs) can increase NLRP3 inflammasome and pro-IL-1β expression (Wan et al., 2016). PA can be absorbed by the scavenger receptor CD36, which as a TLR activator and endophage agent, will promote the activation of NLRP3 inflammasome (Kagan and Horng, 2013). In order to study further mechanism of improving NAFLD fat metabolism *in vitro*, We applied PA and LPS as "parallel hits" to mimic NASH environment. HepG-2 cells, were incubated with LPS + PA and TGQZD. It is similar to the results of animal experiments, TGQZD decreased the NLRP3 inflammasome and ROS level while increased CGI-58 expression in HepG-2 cells induced by LPS + PA.

As discussed above, regulating CGI-58 and NLRP3 inflammasome will be of great significance for the treatment of NAFLD in the future. In this study we found that after the treatment with TGQZD, the CGI-58 levels increased significantly, while NLRP3 inflammasome protein, IL-1β, and TNF-α levels decreased

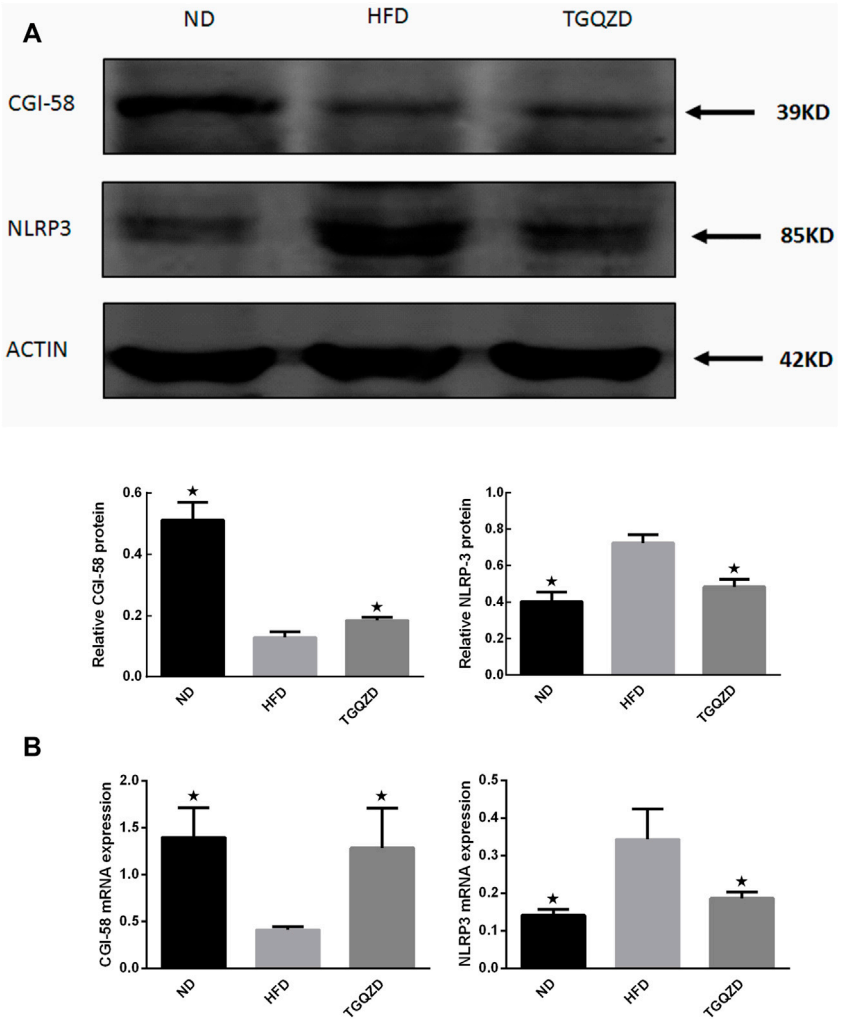

FIGURE 8 | Effect of TGQZD on CGI-58 and NLRP3 inflammasome of liver in NAFLD rats. **(A)** Representative images of Western blot showing CGI-58 and NLRP3 inflammasome protein expression in NAFLD rats in the different groups. **(B)** Quantitation of CGI-58 and NLRP3 inflammasome mRNA expression in NAFLD rats in different groups. ACTIN was used as a loading control. *$p < 0.05$ vs. HFD Group, alone, ($n = 3$).

significantly, which also suggested that TGQZD exerted certain protective effects on NAFLD-induced rats through the regulation of CGI-58 and NLRP3 inflammasome (**Figure 9**).

TGQZD significantly improved the liver function; blood lipids; the body weight of NAFLD patients (Qi, 2012). According to the dose conversion between rats and human (Nair and Jacob, 2016), we didn't design different doses of TGQZD in the experiment. TGQZD is prepared from the aqueous extracts of 13 medicinal herbs and thus may contain many different chemical compounds.

It has been reported that ferulic acid can ameliorate hepatic inflammation and modulate specific gut microbiota and genes involved in TG and TC metabolism (Ma et al., 2019; Wu et al., 2021). Salvigenin improve the metabolic syndrome symptoms by decreasing lipid levels and stimulating mitochondrial functionality and it also help cells to survive by inhibiting apoptosis and enhancing autophagy (Rafatian et al., 2012; Serino et al., 2021). Saikosaponin A, modulate glycerolipid metabolism role by regulating Lipe and Lipg and transcription factors peroxisome proliferator-activated receptor alpha (PPARa) (Li et al., 2021).

With the help of UPLC-MS/MS analysis of TGQZD, ferulic acid, salvigenin and saikosaponin A were also found in TGQZD. Combining previous research with our research data, TGQZD exerts its therapeutic effect may not only through regulation of CGI-58 and NLRP3 inflammasome, but also modulation the above targets and their related signal pathways, which needs to be confirmed in our follow-up study. It also refects that TGQZD posess the advantage of multi-target in the treatment of NAFLD.

Due to NAFLD belong to a complex systemic metabolic disease, it is not easy to design the ideal drugs for single target. Multi target therapy or combination therapy have

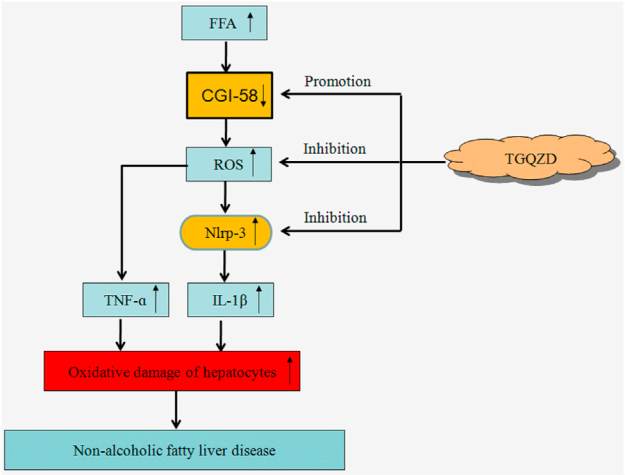

FIGURE 9 | The therapeutic effect of TGQZD on NAFLD rats. Based on the above, TGQZD can reduce the accumulation of lipid in liver by regulating the level of lipoproteins; improved hepatic function; inhibit FFA and promote CGI-58 expression to suppress activating the ROS-dependent NLRP3 inflammasome pathway, which reduce the liver inflammation injury.

recently become the main treatment to reduce the symptoms of NAFLD (Corey and Chalasani, 2011; Johnston et al., 2020), which is consistent with multi-target of TGQZD for treatment NAFLD.

To clarify the exact therapeutic effect of TGQZD in the treatment of NAFLD, we will perform a follow-up study to identify the main active ingredients of TGQZD that are responsible for the hepatic protective activities, which will be the focus of our future studies.

CONCLUSION

Our findings provide evidence that TGQZD can exert therapeutic effects on NAFLD and reduces the accumulation of lipids in the liver by regulating the level of lipoproteins; improving hepatic function, inhibiting FFA metabolism, and promoting CGI-58 expression to suppress the activation of the ROS-dependent NLRP3 inflammasome pathway, which ultimately reduces liver inflammatory injury. By inhibiting the formation of FFA and ROS formation, TGQZD induces CGI-58 expression, inhibits the formation of NLRP3 inflammasome, and TGQZD also could suppress the inflammatory response induced by IL-1 β and TNF-α.

DATA AVAILABILITY STATEMENT

The original contributions presented in the study are included in the article/Supplementary Material, further inquiries can be directed to the corresponding author.

ETHICS STATEMENT

The animal study was reviewed and approved by the Animal Studies Ethics Committee of Beijing Hospital of Traditional Chinese Medicine, Capital Medical University.

AUTHOR CONTRIBUTIONS

HZ designed the study, performed the experiments, analyzed the data and wrote the manuscript. XG weas responsible for collecting the data and performing the statistical analysis. PC and HW collected the data, performed the statistical analysis, and revised the manuscript.

FUNDING

This work was supported by the National Nature Science Foundation of China under Grant No. 81873244; and the Fund for Beijing Science & Technology Development of TCM No. JJ 2018-30.

REFERENCES

Ajmera, V., Perito, E. R., Bass, N. M., Terrault, N. A., Yates, K. P., Gill, R., et al. (2017). Novel Plasma Biomarkers Associated with Liver Disease Severity in Adults with Nonalcoholic Fatty Liver Disease. *Hepatology* 65, 65–77. doi:10.1002/hep.28776

Al-Shaaibi, S. N., Waly, M. I., Al-Subhi, L., Tageldin, M. H., Al-Balushi, N. M., and Rahman, M. S. (2016). Ameliorative Effects of Pomegranate Peel Extract against Dietary-Induced Nonalcoholic Fatty Liver in Rats. *Prev. Nutr. Food Sci.* 21, 14–23. doi:10.3746/pnf.2016.21.1.14

Arab, J. P., Arrese, M., and Trauner, M. (2018). Recent Insights into the Pathogenesis of Nonalcoholic Fatty Liver Disease. *Annu. Rev. Pathol.* 13, 321–350. doi:10.1146/annurev-pathol-020117-043617

Bacon, B. R., Farahvash, M. J., Janney, C. G., and Neuschwander-Tetri, B. A. (1994). Nonalcoholic Steatohepatitis: an Expanded Clinical Entity. *Gastroenterology* 107, 1103–1109. doi:10.1016/0016-5085(94)90235-6

Barbuio, R., Milanski, M., Bertolo, M. B., Saad, M. J., and Velloso, L. A. (2007). Infliximab Reverses Steatosis and Improves Insulin Signal Transduction in Liver of Rats Fed a High-Fat Diet. *J. Endocrinol.* 194, 539–550. doi:10.1677/JOE-07-0234

Brown, J. M., Betters, J. L., Lord, C., Ma, Y., Han, X., Yang, K., et al. (2010). CGI-58 Knockdown in Mice Causes Hepatic Steatosis but Prevents Diet-Induced Obesity and Glucose Intolerance. *J. Lipid Res.* 51, 3306–3315. doi:10.1194/jlr.M010256

Brown, J. M., Chung, S., Das, A., Shelness, G. S., Rudel, L. L., and Yu, L. (2007). CGI-58 Facilitates the Mobilization of Cytoplasmic Triglyceride for Lipoprotein Secretion in Hepatoma Cells. *J. Lipid Res.* 48, 2295–2305. doi:10.1194/jlr.M700279-JLR200

Canada, J. M., Abbate, A., Collen, R., Billingsley, H., Buckley, L. F., Carbone, S., et al. (2019). Relation of Hepatic Fibrosis in Nonalcoholic Fatty Liver Disease to Left Ventricular Diastolic Function and Exercise Tolerance. *Am. J. Cardiol.* 123, 466–473. doi:10.1016/j.amjcard.2018.10.027

Chalasani, N., Younossi, Z., Lavine, J. E., Diehl, A. M., Brunt, E. M., Cusi, K., et al. (2012). The Diagnosis and Management of Non-alcoholic Fatty Liver Disease: Practice Guideline by the American Gastroenterological Association, American Association for the Study of Liver Diseases, and American College of Gastroenterology. *Am. Assoc. Study LiverGastroenterology* 142, 1592–1609. doi:10.1053/j.gastro.2012.04.001

Chen, Z., Tian, R., She, Z., Cai, J., and Li, H. (2020). Role of Oxidative Stress in the Pathogenesis of Nonalcoholic Fatty Liver Disease. *Free Radic. Biol. Med.* 152, 116–141. doi:10.1016/j.freeradbiomed.2020.02.025

Corey, K. E., and Chalasani, N. (2011). Should Combination Therapy Be the Paradigm for Future Nonalcoholic Steatohepatitis Clinical Trials? *Hepatology* 54, 1503–1505. doi:10.1002/hep.24696

Day, C. P., and James, O. F. (1998). Steatohepatitis: a Tale of Two "hits"? *Gastroenterology* 114, 842–845. doi:10.1016/s0016-5085(98)70599-2

Dostert, C., Pétrilli, V., Van Bruggen, R., Steele, C., Mossman, B. T., and Tschopp, J. (2008). Innate Immune Activation through Nalp3 Inflammasome Sensing of Asbestos and Silica. *Science* 320, 674–677. doi:10.1126/science.1156995

Gao, H., Cao, Y., Xia, H., Zhu, X., and Jin, Y. (2020). CYP4A11 Is Involved in the Development of Nonalcoholic Fatty Liver Disease via ROS-induced Lipid Peroxidation and Inflammation. *Int. J. Mol. Med.* 45, 1121–1129. doi:10.3892/ijmm.2020.4479

Gao, X. J., Lin, S., and Zhu, Y. Y. (2016). NACHT-LRR-PYD-containing Proteins 3 Inflammasome and Nonalcoholic Fatty Liver Disease. *Zhonghua Gan Zang Bing Za Zhi* 24, 956–960. doi:10.3760/cma.j.issn.1007-3418.2016.12.019

Grasselli, E., Baldini, F., Vecchione, G., Oliveira, P. J., Sardão, V. A., Voci, A., et al. (2019). Excess Fructose and Fatty Acids Trigger a Model of Nonalcoholic Fatty Liver Disease Progression *In Vitro*: Protective Effect of the Flavonoid Silybin. *Int. J. Mol. Med.* 44, 705–712. doi:10.3892/ijmm.2019.4234

Hasegawa, T., Iino, C., Endo, T., Mikami, K., Kimura, M., Sawada, N., et al. (2020). Changed Amino Acids in NAFLD and Liver Fibrosis: A Large Cross-Sectional Study without Influence of Insulin Resistance. *Nutrients* 12, 1450. doi:10.3390/nu12051450

Ji, Y., Gao, Y., Chen, H., Yin, Y., and Zhang, W. (2019). Indole-3-Acetic Acid Alleviates Nonalcoholic Fatty Liver Disease in Mice via Attenuation of Hepatic Lipogenesis, and Oxidative and Inflammatory Stress. *Nutrients* 11, 2062. doi:10.3390/nu11092062

Johnston, M. P., Patel, J., and Byrne, C. D. (2020). Multi-drug Approaches to NASH: What's in the Development Pipeline? *Expert Opin. Investig. Drugs* 29, 143–150. doi:10.1080/13543784.2020.1668926

Kagan, J. C., and Horng, T. (2013). NLRP3 Inflammasome Activation: CD36 Serves Double Duty. *Nat. Immunol.* 14, 772–774. doi:10.1038/ni.2668

Kim, J. H., Suk, S., Jang, W. J., Lee, C. H., Kim, J. E., Park, J. K., et al. (2017). Salicornia Extract Ameliorates Salt-Induced Aggravation of Nonalcoholic Fatty Liver Disease in Obese Mice Fed a High-Fat Diet. *J. Food Sci.* 82, 1765–1774. doi:10.1111/1750-3841.13777

Kleiner, D. E., Brunt, E. M., Van Natta, M., Behling, C., Contos, M. J., Cummings, O. W., et al. (2005). Design and Validation of a Histological Scoring System for Nonalcoholic Fatty Liver Disease. *Hepatology* 41, 1313–1321. doi:10.1002/hep.20701

Lass, A., Zimmermann, R., Haemmerle, G., Riederer, M., Schoiswohl, G., Schweiger, M., et al. (2006). Adipose Triglyceride Lipase-Mediated Lipolysis of Cellular Fat Stores Is Activated by CGI-58 and Defective in Chanarin-Dorfman Syndrome. *Cell Metab* 3, 309–319. doi:10.1016/j.cmet.2006.03.005

Lee, H. J., Yeon, J. E., Ko, E. J., Yoon, E. L., Suh, S. J., Kang, K., et al. (2015). Peroxisome Proliferator-Activated Receptor-delta Agonist Ameliorated Inflammasome Activation in Nonalcoholic Fatty Liver Disease. *World J. Gastroenterol.* 21, 12787–12799. doi:10.3748/wjg.v21.i45.12787

Lefèvre, C., Jobard, F., Caux, F., Bouadjar, B., Karaduman, A., Heilig, R., et al. (2001). Mutations in CGI-58, the Gene Encoding a New Protein of the Esterase/lipase/thioesterase Subfamily, in Chanarin-Dorfman Syndrome. *Am. J. Hum. Genet.* 69, 1002–1012. doi:10.1086/324121

Li, D. J., Liu, J., Hua, X., Fu, H., Huang, F., Fei, Y. B., et al. (2018). Nicotinic Acetylcholine Receptor α7 Subunit Improves Energy Homeostasis and Inhibits Inflammation in Nonalcoholic Fatty Liver Disease. *Metabolism* 79, 52–63. doi:10.1016/j.metabol.2017.11.002

Li, X., Ge, J., Li, Y., Cai, Y., Zheng, Q., Huang, N., et al. (2021). Integrative Lipidomic and Transcriptomic Study Unravels the Therapeutic Effects of Saikosaponins A and D on Non-alcoholic Fatty Liver Disease. *Acta Pharm. Sin B* 11, 3527–3541. doi:10.1016/j.apsb.2021.03.018

Liang, D., Chen, H., Zhao, L., Zhang, W., Hu, J., Liu, Z., et al. (2018). Inhibition of EGFR Attenuates Fibrosis and Stellate Cell Activation in Diet-Induced Model of Nonalcoholic Fatty Liver Disease. *Biochim. Biophys. Acta Mol. Basis Dis.* 1864, 133–142. doi:10.1016/j.bbadis.2017.10.016

Liu, J., Han, L., Zhu, L., and Yu, Y. (2016). Free Fatty Acids, Not Triglycerides, Are Associated with Non-alcoholic Liver Injury Progression in High Fat Diet Induced Obese Rats. *Lipids Health Dis.* 15, 27. doi:10.1186/s12944-016-0194-7

Lord, C. C., and Brown, J. M. (2012). Distinct Roles for Alpha-Beta Hydrolase Domain 5 (ABHD5/CGI-58) and Adipose Triglyceride Lipase (ATGL/PNPLA2) in Lipid Metabolism and Signaling. *Adipocyte* 1, 123–131. doi:10.4161/adip.20035

Lord, C. C., Ferguson, D., Thomas, G., Brown, A. L., Schugar, R. C., Burrows, A., et al. (2016). Regulation of Hepatic Triacylglycerol Metabolism by CGI-58 Does Not Require ATGL Co-activation. *Cell Rep* 16, 939–949. doi:10.1016/j.celrep.2016.06.049

Ma, Y., Chen, K., Lv, L., Wu, S., and Guo, Z. (2019). Ferulic Acid Ameliorates Nonalcoholic Fatty Liver Disease and Modulates the Gut Microbiota Composition in High-Fat Diet Fed ApoE (-/-) Mice. *Biomed. Pharmacother.* 113, 108753. doi:10.1016/j.biopha.2019.108753

Marchesini, G., Bugianesi, E., Forlani, G., Cerrelli, F., Lenzi, M., Manini, R., et al. (2003). Nonalcoholic Fatty Liver, Steatohepatitis, and the Metabolic Syndrome. *Hepatology* 37, 917–923. doi:10.1053/jhep.2003.50161

Matsuki, T., Horai, R., Sudo, K., and Iwakura, Y. (2003). IL-1 Plays an Important Role in Lipid Metabolism by Regulating Insulin Levels under Physiological Conditions. *J. Exp. Med.* 198, 877–888. doi:10.1084/jem.20030299

Miao, H., Ou, J., Ma, Y., Guo, F., Yang, Z., Wiggins, M., et al. (2014). Macrophage CGI-58 Deficiency Activates ROS-Inflammasome Pathway to Promote Insulin Resistance in Mice. *Cel Rep* 7, 223–235. doi:10.1016/j.celrep.2014.02.047

Nair, A. B., and Jacob, S. (2016). A Simple Practice Guide for Dose Conversion between Animals and Human. *J. Basic Clin. Pharm.* 7, 27–31. doi:10.4103/0976-0105.177703

Qi, T. (2012). *Professor Wei Beihai's Academic Thought and Clinical Experience Summary and Clinical Research on the Treatment of Non-alcoholic Fatty Hepatitisdoctor Doctor*. Beijing: Beijing University of traditional Chinese Medicine.

Rafatian, G., Khodagholi, F., Farimani, M. M., Abraki, S. B., and Gardaneh, M. (2012). Increase of Autophagy and Attenuation of Apoptosis by Salvigenin Promote Survival of SH-Sy5y Cells Following Treatment with H_2O_2. *Mol. Cel Biochem* 371, 9–22. doi:10.1007/s11010-012-1416-6

Sarkar, S., Kimono, D., Albadrani, M., Seth, R. K., Busbee, P., Alghetaa, H., et al. (2019). Environmental Microcystin Targets the Microbiome and Increases the Risk of Intestinal Inflammatory Pathology via NOX2 in Underlying Murine Model of Nonalcoholic Fatty Liver Disease. *Sci. Rep.* 9, 8742. doi:10.1038/s41598-019-45009-1

Serino, E., Chahardoli, A., Badolati, N., Sirignano, C., Jalilian, F., Mojarrab, M., et al. (2021). Salvigenin, a Trimethoxylated Flavone from Achillea Wilhelmsii C. Koch, Exerts Combined Lipid-Lowering and Mitochondrial Stimulatory Effects. *Antioxidants (Basel)* 10, 1042. doi:10.3390/antiox10071042

Shao, N., Yu, X. Y., Ma, X. F., Lin, W. J., Hao, M., and Kuang, H. Y. (2018). Exenatide Delays the Progression of Nonalcoholic Fatty Liver Disease in C57BL/6 Mice, Which May Involve Inhibition of the NLRP3 Inflammasome through the Mitophagy Pathway. *Gastroenterol. Res. Pract.* 2018, 1864307. doi:10.1155/2018/1864307

Soresi, M., Cabibi, D., Giglio, R. V., Martorana, S., Guercio, G., Porcasi, R., et al. (2020). The Prevalence of NAFLD and Fibrosis in Bariatric Surgery Patients and the Reliability of Noninvasive Diagnostic Methods. *Biomed. Res. Int.* 2020, 5023157. doi:10.1155/2020/5023157

Stojsavljevic, S., Gomercic Palcic, M., Virovic Jukic, L., Smircic Duvnjak, L., and Duvnjak, M. (2014). Adipokines and Proinflammatory Cytokines, the Key Mediators in the Pathogenesis of Nonalcoholic Fatty Liver Disease. *World J. Gastroenterol.* 20, 18070–18091. doi:10.3748/wjg.v20.i48.18070

Syn, W. K., Choi, S. S., and Diehl, A. M. (2009). Apoptosis and Cytokines in Non-alcoholic Steatohepatitis. *Clin. Liver Dis.* 13, 565–580. doi:10.1016/j.cld.2009.07.003

Teimouri, M., Hosseini, H., Shabani, M., Koushki, M., Noorbakhsh, F., and Meshkani, R. (2020). Inhibiting miR-27a and miR-142-5p Attenuate Nonalcoholic Fatty Liver Disease by Regulating Nrf2 Signaling Pathway. *IUBMB Life* 72, 361–372. doi:10.1002/iub.2221

Tilg, H., and Moschen, A. R. (2010). Evolution of Inflammation in Nonalcoholic Fatty Liver Disease: the Multiple Parallel Hits Hypothesis. *Hepatology* 52, 1836–1846. doi:10.1002/hep.24001

Tilg, H., Moschen, A. R., and Szabo, G. (2016). Interleukin-1 and Inflammasomes in Alcoholic Liver Disease/acute Alcoholic Hepatitis and Nonalcoholic Fatty

Liver Disease/nonalcoholic Steatohepatitis. *Hepatology* 64, 955–965. doi:10.1002/hep.28456

Valenti, L., Fracanzani, A. L., Dongiovanni, P., Santorelli, G., Branchi, A., Taioli, E., et al. (2002). Tumor Necrosis Factor Alpha Promoter Polymorphisms and Insulin Resistance in Nonalcoholic Fatty Liver Disease. *Gastroenterology* 122, 274–280. doi:10.1053/gast.2002.31065

Wan, X., Xu, C., Yu, C., and Li, Y. (2016). Role of NLRP3 Inflammasome in the Progression of NAFLD to NASH. *Can. J. Gastroenterol. Hepatol.* 2016, 6489012. doi:10.1155/2016/6489012

Wang, J., He, W., Tsai, P. J., Chen, P. H., Ye, M., Guo, J., et al. (2020). Mutual Interaction between Endoplasmic Reticulum and Mitochondria in Nonalcoholic Fatty Liver Disease. *Lipids Health Dis.* 19, 72. doi:10.1186/s12944-020-01210-0

Wen, H., Gris, D., Lei, Y., Jha, S., Zhang, L., Huang, M. T., et al. (2011). Fatty Acid-Induced NLRP3-ASC Inflammasome Activation Interferes with Insulin Signaling. *Nat. Immunol.* 12, 408–415. doi:10.1038/ni.2022

Wigg, A. J., Roberts-Thomson, I. C., Dymock, R. B., Mccarthy, P. J., Grose, R. H., and Cummins, A. G. (2001). The Role of Small Intestinal Bacterial Overgrowth, Intestinal Permeability, Endotoxaemia, and Tumour Necrosis Factor Alpha in the Pathogenesis of Non-Alcoholic Steatohepatitis. *Gut* 48, 206–211. doi:10.1136/gut.48.2.206

Wu, J., Xue, X., Fan, G., Gu, Y., Zhou, F., Zheng, Q., et al. (2021). Ferulic Acid Ameliorates Hepatic Inflammation and Fibrotic Liver Injury by Inhibiting PTP1B Activity and Subsequent Promoting AMPK Phosphorylation. *Front. Pharmacol.* 12, 754976. doi:10.3389/fphar.2021.754976

Yamada, S., and Guo, X. (2018). Peroxiredoxin 4 (PRDX4): Its Critical *In Vivo* Roles in Animal Models of Metabolic Syndrome Ranging from Atherosclerosis to Nonalcoholic Fatty Liver Disease. *Pathol. Int.* 68, 91–101. doi:10.1111/pin.12634

Zhang, H., Ta, N., Shen, H., and Wang, H. (2021). Effects of Jian Pi Qing Chang Hua Shi Decoction on Mucosal Injuries in a 2,4,6-trinitrobenzene Sulphonic Acid-Induced Inflammatory Bowel Disease Rat Model. *Pharm. Biol.* 59, 683–695. doi:10.1080/13880209.2021.1928240

Zhou, R., Yazdi, A. S., Menu, P., and Tschopp, J. (2011). A Role for Mitochondria in NLRP3 Inflammasome Activation. *Nature* 469, 221–225. doi:10.1038/nature09663

Zierler, K. A., Jaeger, D., Pollak, N. M., Eder, S., Rechberger, G. N., Radner, F. P., et al. (2013). Functional Cardiac Lipolysis in Mice Critically Depends on Comparative Gene Identification-58. *J. Biol. Chem.* 288, 9892–9904. doi:10.1074/jbc.M112.420620

Conflict of Interest: The authors declare that the research was conducted in the absence of any commercial or financial relationships that could be construed as a potential conflict of interest.

Publisher's Note: All claims expressed in this article are solely those of the authors and do not necessarily represent those of their affiliated organizations, or those of the publisher, the editors and the reviewers. Any product that may be evaluated in this article, or claim that may be made by its manufacturer, is not guaranteed or endorsed by the publisher.

frontiers | Frontiers in Pharmacology

ORIGINAL RESEARCH
published: 19 May 2022
doi: 10.3389/fphar.2022.863797

Ferulic Acid Combined With Bone Marrow Mesenchymal Stem Cells Attenuates the Activation of Hepatic Stellate Cells and Alleviates Liver Fibrosis

Rui Zhang[1], *Wenhang Li*[1], *Xiaodan Jiang*[1], *Xinyi Cui*[1], *Hongjie You*[2], *Zuoqing Tang*[2] *and Wenlan Liu*[1]*

[1]School of Traditional Chinese Medicine, Capital Medical University, Beijing, China, [2]School of Basic Medical Sciences, Capital Medical University, Beijing, China

OPEN ACCESS

Edited by:
Jackson Almeida,
Federal University of São Francisco Valley, Brazil

Reviewed by:
Nada H. Eisa,
Mansoura University, Egypt
Jiannan Qiu,
The Affiliated Drum Tower Hospital of Nanjing University Medical School, China

***Correspondence:**
Wenlan Liu
wenlanliu1900@126.com

Specialty section:
This article was submitted to Gastrointestinal and Hepatic Pharmacology, a section of the journal Frontiers in Pharmacology

Received: 27 January 2022
Accepted: 13 April 2022
Published: 19 May 2022

Citation:
Zhang R, Li W, Jiang X, Cui X, You H, Tang Z and Liu W (2022) Ferulic Acid Combined With Bone Marrow Mesenchymal Stem Cells Attenuates the Activation of Hepatic Stellate Cells and Alleviates Liver Fibrosis. Front. Pharmacol. 13:863797. doi: 10.3389/fphar.2022.863797

Bone marrow mesenchymal stem cells (BMSCs) can effectively alleviate liver fibrosis, but the efficacy of cell therapy alone is insufficient. In recent years, a combination of traditional Chinese medicine (TCM) and cell therapy has been increasingly used to treat diseases in clinical trials. Ferulic acid (FA) is highly effective in treating liver fibrosis, and a combination of cells and drugs is being tested in clinical trials. Therefore, we combined BMSCs and Ferulic acid to treat CCl_4-induced fibrosis and determine whether this combination was more effective than single treatment. We used BMSCs and FA to treat CCl_4-induced fibrosis in rat models, observed their therapeutic effects, and investigated the specific mechanism of this combination therapy in liver fibrosis. We created a BMSC/hepatic stellate cell (HSC) coculture system and used FA to treat activated HSCs to verify the specific mechanism. Then, we used cytochalasin D and angiotensin II to investigate whether BMSCs and FA inactivate HSCs through cytoskeletal rearrangement. MiR-19b-3p was enriched in BMSCs and targeted TGF-β receptor II (TGF-βR2). We separately transfected miR-19b-3p into HSCs and BMSCs and detected hepatic stellate cell activation. We found that the expression of the profibrotic markers α-SMA and COL1-A1 was significantly decreased in the combination group of rats. α-SMA and COL1-A1 levels were also significantly decreased in the HSCs with the combination treatment. Cytoskeletal rearrangement of HSCs was inhibited in the combination group, and RhoA/ROCK pathway gene expression was decreased. Following angiotensin II treatment, COL1-A1 and α-SMA expression increased, while with cytochalasin D treatment, profibrotic gene expression decreased in HSCs. The expression of COL1-A1, α-SMA and RhoA/ROCK pathway genes was decreased in the activated HSCs treated with a miR-19b-3p mimic,

Abbreviations: SD rat, Sprague-Dawley rat; ANOVA, analysis of variance; DAPI, diamidinophenylindole; DMEM, Dulbecco's modified Eagle's medium; FA, ferulic acid; FBS, foetal bovine serum; PBS, phosphate-buffered saline; BMSCs, bone marrow mesenchymal stem cells; HE, haematoxylin and eosin; ROCK1, Rho-associated kinase 1; RhoA, Ras homologue family member A; SRF, serum response factor; LIMK1, LIM domain kinase 1; COL1-A1, collagen type I alpha 1 chain; α-SMA, alpha-smooth muscle actin; TGF-β1, transforming growth factor beta 1; TGF-βR2, transforming growth factor beta receptor 2; ECM, extracellular matrix; HSCs, hepatic stellate cells.

indicating that miR-19b-3p inactivated HSCs by suppressing RhoA/ROCK signalling. In contrast, profibrotic gene expression was significantly decreased in the BMSCs treated with the miR-19b-3p mimic and FA or a miR-19b-3p inhibitor and FA compared with the BMSCs treated with the miR-19b-3p mimic alone. In conclusion, the combination therapy had better effects than FA or BMSCs alone. BMSC and FA treatment attenuated HSC activation and liver fibrosis by inhibiting cytoskeletal rearrangement and delivering miR-19b-3p to activated HSCs, inactivating RhoA/ROCK signalling. FA-based combination therapy showed better inhibitory effects on HSC activation.

Keywords: liver fibrosis, BMSCs, ferulic acid, HSCs, miR-19b-3p

INTRODUCTION

Hepatic fibrosis is a repair response of the liver to chronic hepatocyte injury. Following persistent injury of the liver or stimulation by fibrotic factors, pathological changes in the extracellular matrix (ECM) occur in the liver tissue, and the balance between the production or degradation of ECM is disrupted, leading to excessive deposition of ECM in the liver tissue, fibrosis and eventually cirrhosis. (Bataller and Brenner 2005; M. Pinzani and Rombouts, 2004). Activated hepatic stellate cells (HSCs) are an important cause of liver fibrosis. Upon liver injury, Kupffer cells and endothelial cells in the liver release cytokines, such as transforming growth factor-β (TGF-β), to activate quiescent HSCs. Activated HSCs transdifferentiate into myofibroblastic HSCs (Virarkar et al., 2021). Then, the cytoskeleton in these HSCs undergoes rearrangement, the cell dynamics increase, and these cells migrate to the site of liver injury and produce substantial amounts of ECM components, such as α-smooth muscle actin (α-SMA) and collagens. Fired-Man proved that activated HSCs are the main source of extracellular collagen in the liver. Therefore, regulating HSC activation and migration could be an anticipated antifibrotic strategy.

Bone marrow mesenchymal stem cells (BMSCs) have become an emerging therapeutic agent for liver fibrosis in recent years due to their proliferative potential, low immunogenicity, abundant sources, tissue repair ability, and chemotactic and homing abilities (Alfaifi et al., 2018). The therapeutic effects of MSCs on liver fibrosis are related to their ability to undergo hepatocyte-like differentiation, participate in immunization activities and secrete paracrine factors (Yao et al., 2020). For example, hBMSC-derived exosomes protected against liver fibrosis by regulating the Wnt/β-catenin pathway, and antler stem cells were identified as a novel source to reduce liver fibrosis (Rong et al., 2019; Rong et al., 2020). In our previous study, BMSCs ameliorated CCl_4-induced liver damage and fibrosis in rats *via* the FGF2-Dlk1-Notch1 pathway (Li et al., 2017).

Although BMSCs can improve liver fibrosis, one of the major challenges of BMSCS therapy is the inefficiency of clinical treatment. BMSCs are commonly injected at 1×10^6 cells/kg. BMSC treatment can also lead to potential risks, such as *in vitro* cell amplification and adverse reactions caused by implanted BMSCs. In addition, several phase III clinical trials have failed due to the inefficiency of BMSCs. Therefore, identification of strategies to improve the therapeutic effects has become a key issue in BMSC therapy (Ankrum and Karp 2010; Liao et al., 2017). In recent studies, traditional Chinese medicine (TCM) combined with BMSC therapy has shown unique advantages and characteristics. Bie jia jian pill combined with BMSCs suppressed hepatocellular carcinoma (Jingjing et al., 2021). Saponins from *Rhizoma Panacis Majoris* combined with BMSCs could improve hepatic fibrosis (Tian 2016). Naringin combined with BMSCs and acellular dermal matrix affected cartilage injury (Ye Chao et al., 2021). Ferulic acid (FA), as an important ingredient in TCM, has therapeutic activity against a variety of diseases. The hepatoprotective effects of FA have been demonstrated in studies using CCl_4 to induce liver fibrosis (Jayamani et al., 2018; Ali et al., 2021; Li et al., 2021). Therefore, we proposed the combination of BMSCs and FA in the treatment of liver fibrosis and investigated the mechanisms underlying the antifibrotic effect in this study.

MATERIALS AND METHODS

Cell Culture

SD-BMSCs were isolated from the bone marrow of Sprague-Dawley (SD) rats aged 3–6 weeks and were cultured as previously described (Yuhui Lin et al., 2011). BMSCs were cultured in Dulbecco's modified Eagle's medium (DMEM; Gibco, MA, United States, CAT: C11995500BT) with 10% foetal bovine serum (FBS; AQ, Beijing, China, CAT: AQmv02200-500ml) and 1% penicillin/streptomycin (P/S; Gibco, CAT: 15140122) at 37°C in an incubator containing 5% CO_2. HSC-T6, a rat HSC cell line (purchased from Keygen Biotech, Nanjing, China, CAT: KG313), was cultured in DMEM-high (Gibco) with 10% FBS (AQ) and 1% P/S (Gibco) at 37°C in a humidified atmosphere containing 5% CO_2. SD-BMSCs and HSC-T6 cells were seeded in 25-cm^2 plates at 70% confluence.

Experimental Animal Models

Male SD rats were treated in the Experimental Animal Center of Capital Medical University in an environment without a specific pathogen barrier. All experiments were approved and supervised by the Animal Care and Use Committee of Capital Medical University (approval number: SCXK 2016-0006), and the animals were housed in a facility with a 12 h light/12 h dark cycle and allowed free access to food and water. Eight-week-old rats (n = 30) received 0.2 ml/kg

body weight of CCl_4 (RhawnSeal, Shanghai, China, CAT: R015578-500ml) dissolved in olive oil by intraperitoneal injection for 2 weeks, followed by 0.1 ml/kg body weight of CCl_4 for 2 weeks and finally 0.05 ml/kg body weight of CCl_4 for 2 weeks. As a normal control (NC group), rats were injected with an equal volume of olive oil (n = 6). All modelling injections were administered three times per week for a total of 6 weeks. After 6 weeks of modelling, 30 model rats were randomly divided into 5 groups (n = 6). We randomly chose rats in 2 CCl_4 groups (n = 6) by injection of 5×10^6 BMSCs into tail vein (stained with CFDA SE, Meilunbio, Dalian, China, CAT: MB2308-1) once a week for 2 weeks. Then, we established a CCl_4 group and a CCl_4+ BMSC group (LIU Wen-lan et al., 2014), and the animals were treated with FA (10 mg/kg) by intragastric administration (Solarbio, Beijing, China, CAT: F8330-5g). The rats in another CCl_4 group were treated with colchicine (0.1 mg/kg) (Aladdin, Shanghai, China, CAT: C106738-100mg) as a positive control (Mu et al., 2018). The animals in the other groups were treated with equal amounts of normal saline. All rats were gavaged once a day for 2 weeks. After treatment for 2 weeks, all rats were sacrificed, and the serum and liver tissues were obtained. The groups were as follows: normal control group (NC), model group (model), colchicine group (positive control), FA group (FA), BMSC group (BMSCs), and BMSC + FA group (FC).

Measurement of Aspartate Aminotransferase and Alanine Aminotransferase

We collected 1 ml of blood from each animal. After storage at room temperature for 4 h, the serum was separated by centrifugation (×1500 g, 10 min). Then, 200 μL serum samples were used for analysis. The activities of serum aspartate aminotransferase (AST) and alanine aminotransferase (ALT) were determined by commercial kits obtained from Konkahongyuan Co. (Beijing, China, CAT: KA4189) according to the manufacturer's instructions.

Histopathological Evaluation

Fresh liver tissue samples were fixed in 10% formaldehyde at 4°C overnight and embedded in paraffin wax for histological evaluation. Sections were stained with haematoxylin and eosin (HE), and the severity of the histological changes was evaluated. We obtained images by using a microscope equipped with a LI-COR Odyssey Infrared Imaging System (LI-COR, Inc., Lincoln, NE, United States).

Masson Trichrome Staining

For staining, 4–6 μm-thick sections were obtained from paraffin-embedded blocks and stained with Masson trichrome (MT) and FANCM. For MT staining, the Trichrome III Green Staining Kit (Solarbio, Beijing, China, CAT: G1340), a modified version of the MT stain, was used with Bouin's solution to intensify the final colouration.

Cell Coculture Experiments

HSCs were activated with TGF-β1 (10 ng/ml, PeproTech, United States, CAT: 100-21-10) for 24 h, and then, activated HSCs were cocultured with SD-BMSCs by using 6-well Transwell inserts (0.4 μm, Corning, NY, United States, CAT: 3412), which were permeable to the culture medium but not cells. All coculture experiments were performed with HSCs seeded in the bottom chambers and BMSCs seeded in the insert chambers. After coculture for 12 h, the cells were washed twice with PBS, randomly divided into 5 groups and incubated in fresh DMEM. One group with normal medium was set as the model group. The group with medium containing 6 μg/ml colchicine was used as a positive control. Another three groups with medium with three doses of FA (1 mg/ml, 0.5 mg/ml, 0.25 mg/ml) were set as the FA groups. In addition, inactivated HSCs cocultured with BMSCs were used as the normal group. After coculture for 24 h, we collected HSCs and medium for subsequent experiments.

Cell Migration Experiments

The cocultured cells were divided into 6 groups (NC, model, positive, FA-1 mg, FA-0.5 mg, and FA-0.25 mg). The specific cell coculture conditions were the same as those in the above experiments. When activated HSCs were treated with FA (1 mg/ml, 0.5 mg/ml, 0.25 mg/ml) and colchicine (6 μg/ml) for 24 h, we washed the cells with PBS twice, collected HSCs and seeded equal numbers of cells into 24-well Transwell inserts (8 μm, Corning, CAT: 3422), which allowed cell migration. After culture for 12 h, the cells were fixed with 4% paraformaldehyde for 20 min and washed twice with PBS, and the residual HSCs on the surface membranes were removed. Then, the cells were stained with crystal violet (Solarbio, CAT: C8470-25g) for 10 min and washed twice with PBS again. We removed the membranes from the inserts and counted the cells on the membrane by microscopy.

Cytoskeletal Inhibitor and Agonist Experiments

HSCs were activated with TGF-β1 (10 ng/ml) for 24 h, and then, activated HSCs and BMSCs were cocultured with 0.4 μm Transwell inserts for 12 h. When cells adhered to wells, the coculture system was divided into three groups, and we next added fresh medium. One group with 1 μM cytochalasin D (cytoskeleton inhibitor, purchased from Sigma, Germany, CAT: C2618) was set as the cytoskeletal inhibitor group, one with 10 μM angiotensin II (cytoskeleton agonist, purchased from Sigma, CAT: A9525) was set as the cytoskeletal agonist group, and the normal and model groups had blank medium. After 24 h of culture, we collected cells and medium for subsequent experiments.

Transfection of miR-19b-3p Mimics and a miR-19b-3p Negative Fragment Into Hepatic Stellate Cells

To detect the effect of miR-19b-3p on HSC activity, we designed miR-19b-3p mimics (5′-UGU GCA AAU CCA UGC AAA ACU GA-3′; KeyGEN, CAT:KGmiRNA) on the miR-19b-3p sequence and negative controls (NC-d). HSCs were activated in 10 ng/ml

TGF-β1 medium without FBS for 24 h, digested by trypsin, centrifuged and counted. The cells were randomly divided into a model group, mimic group and negative control group, and inactivated HSC-T6 cells were set as the normal group. Therefore, all cells were divided into 4 groups: normal, model, HSC + mimics (mimic), and HSC + mimics NC (NC-d). Transient transfection was performed at a concentration of 10 μg/ml, and the cells were mixed evenly with miRNAs. The mixtures were added to a 4 mm shock tube, and the volume was not more than 900 μL. Shock tubes were placed into the BTX tester, the preset conditions were selected, and the detected instrument had no short circuit. After transfection, the cell mixture was transferred to a 6-well plate and cultured for 24 h. Cells were observed and captured with inverted fluorescence microscope (Axio observer A1, Zeiss, Germany). We collected HSCs and medium for subsequent experiments. All mimic and inhibitor were tagged with Cy3 fluorescence markers based.

Transfection of miR-19b-3p Mimics, Inhibitors, and Negative Controls Into Bone Marrow Mesenchymal Stem Cells

To detect the effect of miR-19b-3p on SD-BMSCs, when BMSCs were digested, centrifuged and counted, we selected SD-BMSCs in good condition and randomly divided them into the model group, mimic group, inhibitor group, FA combined mimic group (FA + mimic group), FA combined inhibitor group (FA + inhibitor group), and negative control group (NC-d and NC-s). A total of 10 μg/ml miRNAs (miR-19b-3p mimic 5′-UGU GCA AAU CCA UGC AAA ACU GA-3′, KeyGEN; miR-19b-3p inhibitor 5′-UCA GUU UUG CAU GGA UUU GCA CA-3′, KeyGEN; miR-mimic NC-d, KeyGEN; miR-inhibitor NC-s KeyGEN) was used for transient transfection. The miRNAs all carried Cy3 markers. The cells and miRNAs were evenly mixed and placed into a 4 mm shock tube with a volume less than 900 μL. The shock tube was placed in the machine. After transfection, the cell mixture was transferred to inserts of 0.4 μm Transwell 6-well culture plates and cocultured with activated HSC-T6 cells for 24 h. After 24 h, we added fresh medium to each group. The medium of the mimic group and inhibitor group was exchanged with fresh DMEM containing 10% FBS. The mimic + FA and inhibitor + FA groups had fresh medium containing 1 mg/ml FA and 10% FBS. We also used normal BMSCs cocultured with resting HSCs or activated HSCs as a normal control or model and added normal fresh medium. Cells were divided into 8 groups: normal, model, BMSC + mimics (mimic), BMSC + inhibitors (inhibitor), BMSC + mimics + FA (mimic + FA), BMSC + inhibitors + FA (inhibitor + FA), BMSC + mimics NC (NC-d), and BMSC + inhibitor NC (NC-s). The coculture lasted for another 24 h. After coculture, we collected HSCs and medium for subsequent experiments.

Enzyme-Linked Immunosorbent Assay

We extracted the culture medium and centrifuged the medium (×10000g, 20 min) to remove the cell debris. Then, we detected the contents of COL1-A1 (Mlbio, Shanghai, China, CAT: ml058800) and α-SMA (Mlbio, CAT:ml038078) in the culture medium with enzyme-linked immunosorbent assay (ELISA) kits according to the manufacturer's protocol. The 20× washing solution was diluted to 1×, and an appropriate volume was prepared. Standard wells, sample wells and blank wells were used, and each group was assayed 3 times. We added 50 μL of the standard substance at different concentrations to each standard well, 50 μL of culture supernatant to the sample wells and 50 μL of sample dilution to the blank well. Next, we added 100 μL of horseradish peroxidase (HRP)-labelled detection antibody to each well, sealed the reaction well with a plate membrane, incubated it at 37°C for 60 min, discarded the liquid, washed it with 350 μL of washing solution 5 times, added 50 μL of substrates A and B to each well, incubated it at 37°C for 15 min in the dark, and added 50 μL of stop solution to each well. After 15 min, the OD value of each well was measured at a wavelength of 450 nm, and the sample well concentration was calculated. All data are presented as the mean ± SEM of values from at least three repeated experiments.

Cloning of Vector Constructs and Luciferase Reporter Assay

For cloning of vector constructs, Rat miR-19b-3p were predicted by database: http://mirwalk.umm.uni-heidelberg.de. The 3′ untranslated region (UTR) of rat TGF-βR2 from genomic DNA, containing binding sites for rat miR-19b-3p, was amplified by PCR. The primer sequences used for vector construction were as follows: forward, 5′-TTCTAGTTGTTTAAACGAGCTCGCTAGCCTCGA GCTTTTTCTGGGCAGGCTGGGCCAAGACTCCG-3′, reverse, 5′-GCAGCCGGATCAGCTTGCATGCCTGCAGGTCGACAA GTGCTAACGTTATGCCGAGCCCCTTCCGC-3'. The PCR product was purified using an AccuPrep PCR purification kit (Tiangen, CAT: DP204), cut by the restriction enzymes XhoI and SalI, and then cloned into the pmirGLO vector (Promega, WI, United States). The vector constructs with the 3′UTR of TGF-βR2 were transformed into *Escherichia coli*, and then, plasmid DNA was extracted from transformed, ampicillin-resistant *E. coli* using an AccuPrep Plasmid Mini Extraction Kit (Tiangen, Beijing, China, CAT: DP103). The sequences of the miR-19b-3p-binding sites of the 3′UTR of TGF-βR2 were confirmed by sequencing analysis (KeyGEN). Mutant vectors lacking the miR-19b-3p-binding site were manufactured by KeyGEN (KeyGEN, CAT: KGplasmid). For the luciferase reporter assay, HSC-T6 cells were seeded in 24-well culture plates in culture medium without P/S 1 day before transfection. The HSCs were divided into 3 groups: pmirGLO vector group, TGF-βR2-WT group, and TGF-βR2-MUT group. Either 10 μg miR-19b-3p mimic (KeyGEN) or scrambled miRNA (NC-d; KeyGEN) was added to each group. The cell mixture was placed into a 4 mm shock tube with a volume less than 900 μL. The shock tube was placed in the machine. After transfection, the cell mixture was cultured in 6-well plates for 48 h. After transfection, the cells were collected and tested with the Dual-Luciferase reporter assay system (Beyotime, Shanghai, China, CAT:RG028). Then, 100 μL of lysate was added to each well. After the cells were fully lysed, centrifugation was performed at ×10000 g–×15000 g for 5 min, and the supernatant was taken for analysis. Firefly luciferase detection reagent and sea kidney luciferase detection buffer were dissolved, an appropriate amount of sea kidney luciferase detection buffer was taken according to the amount of 100 μL for each sample,

and sea kidney luciferase detection substrate (100×) at 1:100 was added to prepare sea kidney luciferase detection working solution. According to the operating instructions of the instrument, we used a multifunctional microplate detector with a chemiluminescence detection function and set the determination interval to 2 s and the detection time to 10 s. For each sample, 50 μL was taken, 100 μL of firefly luciferase detection reagent was added, and the RLU was determined after blowing and mixing with a gun. The reporter lysate was used as a blank control. After completing the above steps for the determination of firefly luciferase activity, 100 μL of luciferase detection solution was added, the sample was blown and mixed, and the RLU was determined. With sea cucumber luciferase as an internal reference, the RLU value for firefly luciferase was divided by the RLU value for sea cucumber luciferase, and the activation degree of the target reporter gene in each sample was compared according to the obtained ratio. All firefly luciferase activity data were normalized to Renilla luciferase activity and are presented as the mean ± SEM of values from at least three repeated experiments.

Quantitative Real-Time PCR Analysis

We took 20 mg frozen animal tissues/cell samples, added 400 μL of TRIzol, homogenized them twice for 5 s each time, fully ground them, and homogenized them at room temperature for 5–10 min. Next, we added 80 μL of chloroform, mixed the sample for 15 s, incubated the sample at room temperature for 10–15 min, and then centrifuged it at 4°C and ×12000 g for 15 min at high speed. After centrifugation, the solution was divided into 3 layers, and RNA was in the supernatant. The supernatant was carefully transferred to a new 1.5-ml centrifuge tube without RNA enzyme, isopropyl alcohol was added to an equal volume and mixed evenly, and the sample was incubated at room temperature for 10 min. The mixture was centrifuged again at ×25000 g and 4°C for 15 min. The supernatant was carefully removed, precipitated with 1.5 ml of 75% ethanol to remove the organic solvent, and incubated until the precipitate floated. The samples were centrifuged at ×25000 g at 4°C for 10 min. Ethanol was discarded, and the precipitate was dried at room temperature for 3 min. The precipitate was dissolved in 20 μL of RNA-free water. After mixing, the RNA concentration and quality were detected, and reverse transcription was conducted. After the isolated RNA was reverse transcribed into cDNA by using a reverse transcription kit (Tiangen Biotech, Beijing, China, CAT: KR201), we used quantitative PCR (qRT-PCR) with a SYBR Green Taq kit (KAPA Biotechnology, CAT: KK4601) on a 7500HT Fast real-time PCR system to assay target gene expression. The primers were designed using Primer 5 (**Table 1**). The PCR conditions were as follows: 1) 95°C for 30 s and 2) 40 cycles of 95°C for 20 s, 60°C for 20 s, and 72°C for 20 s. The experiment was repeated three times.

Cytoskeleton Staining

HSCs were treated with TGFβ1 and then cocultured with BMSCs. After the coculture period, the cells were washed twice with PBS, fixed with 4% paraformaldehyde for 20 min, and permeabilized with 0.1% Triton X-100 in PBS for 2–3 min at room temperature. After the cells were washed with PBS twice, they were stained with phalloidin (1:200) (Keygen, CAT: KGMP001) for 30 min. After phalloidin staining, the cell nuclei were stained with DAPI (1: 100) (Solarbio, CAT: C0060) for 10 min. The cells were observed and captured using a confocal laser scanning microscope (Zeiss SP8, Germany). We observed the cytoskeleton in the FITC channel (wavelength = 498 nm) and miR-19b-3p markers in the Cy3 channel (wavelength = 550 nm).

Western Blot Analysis

Cells and liver tissues were lysed in RIPA buffer (Lablead, Beijing, China, CAT: P0013B) and fully ground for 20 min, and total protein was extracted. The protein concentration was measured using a BCA protein assay kit (Beyotime, Nanjing, China, CAT: P0012). Protein detection by Western blot analysis was performed routinely. Equal amounts of total protein were separated by 8% or 10% SDS-PAGE and transferred onto polyvinylidene fluoride (PVDF) membranes (0.45/0.22 μm, Milipore, United States, CAT: IPVH00010). The membranes were incubated with primary antibodies against α-SMA (1:1000; Sigma, CAT: A2547), Col1α1 (1:1000; Abcam, United States, CAT: ab260043), GAPDH (1:1000; Cell Signaling Technology, Boston, United States), ROCK (1:1000; CST, CAT: 4035S), RhoA (1:1000; CST, CAT: 2117T), LIMK1 (1:1000, CST, CAT: 3842S), SRF (1:1000, CST, CAT: 5147S), and TGF-βR2 (1: 1000, CST, CAT: 79424T) overnight at 4°C. Then, an HRP-conjugated goat anti-rabbit IgG (1:10000; Jackson ImmunoResearch, United States, CAT: 312-005-003) secondary antibody was incubated at 37°C for 1 h. The immunobands were visualized using a chemiluminescent HRP substrate (NCM, Beijing, China, CAT: P10200). Finally, the immunoreactive protein bands were detected and imaged by the Image Lab system (Bio-Rad ChemiDoc XRS, United States; Fusion FX, Vilber, France). Protein expression was standardized to that of GAPDH and quantified using Gel-Pro Analyzer software (Media Cybernetics, Rockville, MD, United States).

Statistical Analysis

The results are expressed as the mean ± SEM. Statistical differences were determined by one-way ANOVA and two-way ANOVA (SPSS 20.0, Chicago, IL, United States). p values < 0.05 were considered statistically significant.

RESULTS

Ferulic Acid Promotes the Ability of Bone Marrow Mesenchymal Stem Cells to Decrease Serum Aspartate Aminotransferase and Alanine Aminotransferase Levels in Liver Fibrosis Models

As shown in **Figure 1A**, the liver was dark red, the liver surface was rough, and adhesions appeared between the liver lobes in the CCl_4-treated group compared to the normal group. In contrast, following BMSC and FA treatment, the liver changed substantially. The colour of the liver returned to light red, the liver surface was smooth, and adhesions were reduced in the BMSC + FA group compared to the model group. Rat weight also showed differences among the groups.

TABLE 1 | Primer sequences.

Primer name	Sequences 5′-3′
GAPDH-F	CTGGAGAAACCTGCCAAGTATG
GAPDH-R	GGTGGAAGAATGGGAGTTGCT
ROCK1-F	CAAAAATGATCAGTGGGCTTGG
ROCK1-R	CCTACAAAAGGTAGCTGATTGCC
LIMK1-F	CACAGTCACCCTCGTGTCTATCC
LIMK1-R	TCTCGTCCAGCGGCACATT
RhoA-F	GATGGAGCTTGTGGTAAGACATGC
RhoA-R	GGCTGTCGATGGAAAAACACATC
SRF-F	GCGGCGTTACACGACCTTC
SRF-R	TCTGAATCAGCGCCTTGCC
COL1-A1-F	CACCTACAGCACGCTTGTGG
COL1-A1-R	GATTGGGATGGAGGGAGTTTAC
α-SMA-F	ACCCAGGCATTGCTGACAG
α-SMA-R	AGAAGCATTTGCGGTGGAC
U6-F	CTCGCTTCGGCAGCACA
U6-R	AACGCTTCACGAATTTGCGT
miR-19b-F	CTCAACTGGTGTCGTGGAGTCGGCAATTCAGTTGAG TCAGTTTT
miR-19b-R	ACACTCCAGCTGGGTGTGCAAATCCATGCAA
Universal primer -A	TGGTGTCGTGGAGTCG
miR-29b-3p-F	CTCAACTGGTGTCGTGGAGTCGGCAATTCAGTTGAG ACTGATTT
miR-29b-3p-R	ACACTCCAGCTGGGTAGCACCATTTGAA
miR-183-5p-F	CTCAACTGGTGTCGTGGAGTCGGCAATTCAGTTGAGCAGTGAAT
miR-183-5p-R	ACACTCCAGCTGGGTATGGCACTGGTAGAAT

Compared to that of the normal control rats, the weight of the model rats was significantly decreased ($p < 0.001$). The weight was significantly increased with FA and BMSC treatment ($p < 0.001$, vs. the model group), and there were no significant differences among the three treatment groups (**Figure 1B**). The serum ALT and AST levels in the model rats were significantly increased ($p < 0.05$, vs. control group), indicating successful establishment of the rat liver fibrosis model. FA, BMSC or FA&BMSC administration significantly decreased the serum AST and ALT levels ($p < 0.05$, vs. the model group) and there were no significant differences among the three treatment groups (**Figures 1C,D**).

Histopathological Assessment of Liver Damage

To further confirm the antifibrotic effects of BMSCs, FA and their combination in an *in vivo* rat liver fibrosis model, we performed HE and Masson staining. As shown in **Figures 1E,F**, inflammatory cell infiltration, fragmented hepatic nuclei, and collagenous fibre formation were observed in the model group. Damage caused by CCl_4 was significantly attenuated by BMSCs, FA, and the combination. In addition, the combination treatment achieved better reductions in collagenous fibres than the FA and BMSC single treatments.

Ferulic Acid Promotes the Ability of Bone Marrow Mesenchymal Stem Cells to Improve Liver Fibrosis *via* the RhoA/ROCK Pathway

We found that FA could promote the ability of BMSCs to reduce liver fibrosis via the RhoA/ROCK pathway. Compared with that of the normal group, the protein expression of the model group showed significant increases in the profibrotic markers α-SMA and COL1-A1, while in the FA and BMSC-treated groups, their expression levels were decreased. In addition, FA combined with BMSCs showed better effects than the other two treatments on reducing COL1-A1 expression ($p < 0.05$). The expression patterns of RhoA and ROCK showed the same trends (**Figures 2A,B**).

QRT-PCR assays confirmed the protein data, showing reductions in α-SMA, COL1-A1, RhoA and ROCK expression in the FA, BMSC and FA&BMSC (FC) groups. These results clearly indicated that BMSCs combined with FA could be a novel treatment for liver fibrosis (**Figure 2C**).

Ferulic Acid Promotes the Ability of Bone Marrow Mesenchymal Stem Cells to Inhibit Cytoskeletal Rearrangement in Hepatic Stellate Cells

The activation of HSCs is an important factor in the formation of liver fibrosis. When stellate cells are activated, the cytoskeleton rearranges and promotes the migration of stellate cells. The RhoA/ROCK pathway is not only associated with the formation of fibrosis but also closely associated with cytoskeletal rearrangement. Therefore, we focused on whether FA promotes BMSC-mediated inhibition of cytoskeletal rearrangement in HSCs. Cocultured HSCs were evaluated by fluorescence and confocal microscopy and showed successful uptake. Compared to those in the normal group, activated HSCs exhibited F-actin remodelling to form a large number of thick stress fibres across the whole cell. In the FA-treated group, F-actin was observed in lamellipodia or filopodia in each cell, and a few fine stress fibres were found in these cells (**Figure 3**).

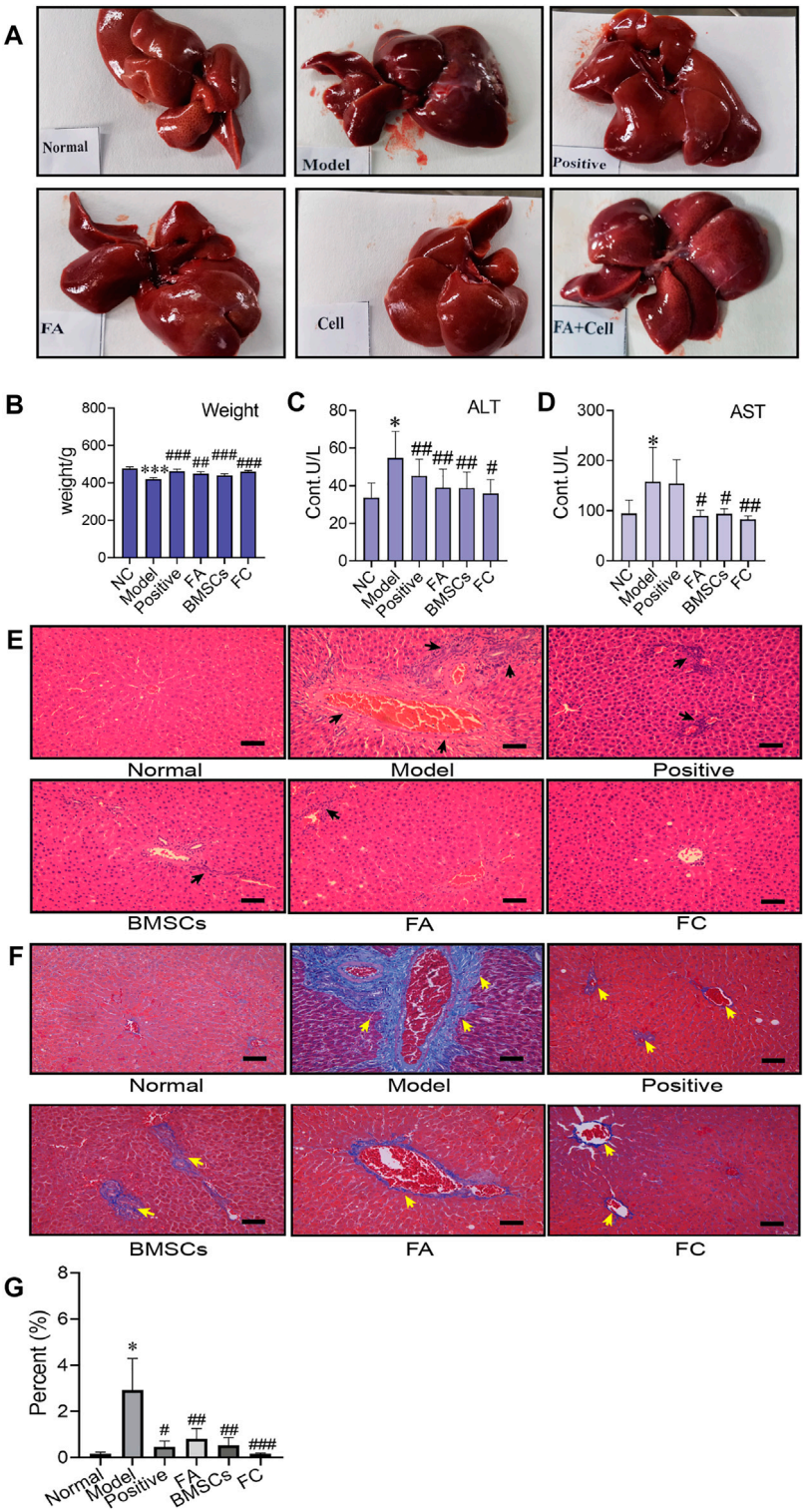

FIGURE 1 | Administration of BMSCs combined with FA ameliorates CCl_4-induced liver injury in rats. **(A)** The liver appearance of each group (normal, model, positive, BMSC, FA, and FC groups). **(B)** Comparison of body weight among the groups (Two-way ANOVA; *$p < 0.05$, **$p < 0.01$, ***$p < 0.001$ versus the normal group; #$p < 0.05$, ##$p < 0.01$, ###$p < 0.001$ versus the model group). **(C,D)** Serum levels of AST and ALT in each group ($n = 6$). Data are presented as the mean ± SEM (Two-way ANOVA; *$p < 0.05$ versus the normal group; #$p < 0.05$, ##$p < 0.01$ versus the model group). **(E)** Images of HE-stained liver sections from representative animals in the normal, model, positive, BMSC, FA, and FC groups (original magnification, ×10; scale bars, 100 μm, $n = 6$). **(F)** Masson stained liver sections from representative animals in the normal, model, positive, BMSC, FA, and BMSC&FA groups (original magnification, ×10; scale bars, 100 μm). The yellow squares indicate collagen. **(G)** The percentage of collagen area of Masson staining in each group ($n = 6$). Data are presented as the mean ± SEM (Two-way ANOVA; *$p < 0.05$ versus the normal group; #$p < 0.05$, ##$p < 0.01$, ###$p < 0.001$ versus the model group).

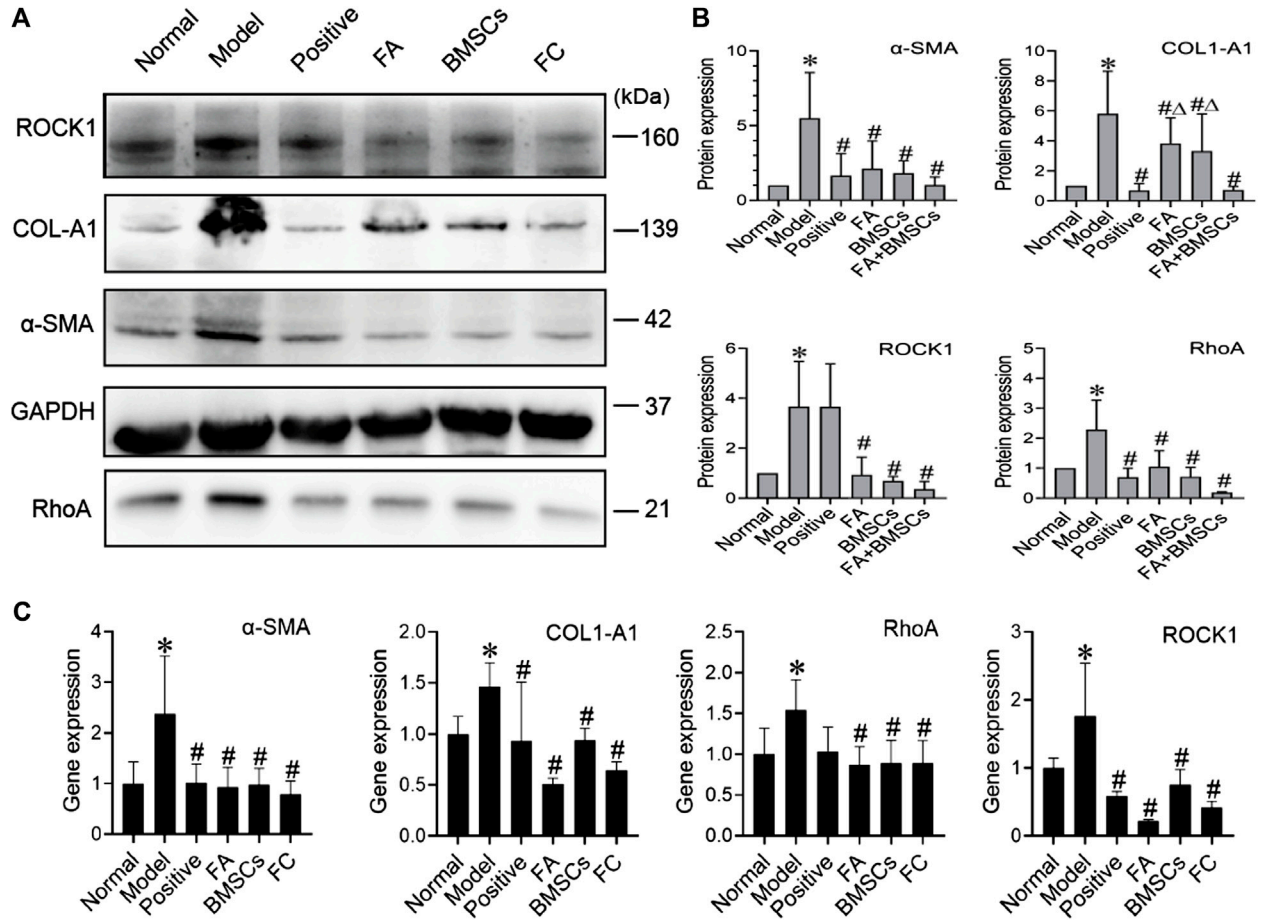

FIGURE 2 | (A,B) Western blot and cumulative densitometric analyses of ROCK1 (160 kDa), COL1-A1 (139 kDa), α-SMA (42 kDa), GAPDH (37 kDa), and RhoA (21 kDa) in livers from each group (normal, model, positive, FA, BMSCs, FC). Data are presented as the mean ± SEM ($n = 3$ independent experiments, Two-way ANOVA; *$p < 0.05$ versus the normal group; #$p < 0.05$, versus the model group; Δp<0.05, versus the FC group); **(C)** qRT-PCR analysis for α-SMA, COL1-A1, ROCK1, and RhoA in rat livers. Data are presented as the mean ± SEM ($n = 3$ independent experiments, Two-way ANOVA; *$p < 0.05$ versus the normal group; #$p < 0.05$ versus the model group).

Ferulic Acid Promotes Bone Marrow Mesenchymal Stem Cell-Mediated Inhibition of the Activation of Hepatic Stellate Cells *via* the RhoA/ROCK/SRF and RhoA/ROCK/LIMK1 Pathways

To investigate the promotive effect of FA on BMSC-mediated inhibition of HSC activation, we cultured activated HSC-T6 cells with an equal proportion of BMSCs as the model group, and activated HSC-T6 cells cocultured with BMSCs and treated with different doses of FA (1 mg/ml, 0.5 mg/ml, or 0.25 mg/ml FA) were used as the treatment groups. Inactivated HSCs cocultured with BMSCs in normal medium were used for the normal control group (NC group). We first detected the migration of HSCs. The activated HSC has great migration ability, the more active cells are, the more cells migrate in same period of time. The number of migration cell respects migration ability. HSC migration was significantly increased in the model group ($p < 0.05$, vs. the control group), but after FA treatment, HSC migration was significantly decreased ($p < 0.05$, vs. the model group), and 1 mg/ml FA showed a strong inhibitory effect (**Figures 4A,B**).

Western blot analysis confirmed that FA could promote BMSC-mediated inhibition of HSC activation, as indicated by assessment of HSC activation markers, including α-SMA and collagen type 1 a 1 chain (COL1-A1). The protein levels of α-SMA and COL1-A1 in the model group were significantly increased ($p < 0.05$, vs. the NC group). However, the expression of α-SMA and COL1-A1 was significantly decreased after FA treatment, and 1 mg/ml FA showed better and stable effects ($p < 0.05$, vs. the model group). We also detected α-SMA and COL1-A1 in extracellular medium by ELISA kits and found that their levels were decreased (**Figures 4C,D**). After confirming the effect of FA on HSC inactivation, we further assessed the direct pathway between BMSCs and HSCs. The cytoskeleton changed when HSCs were activated. We investigated the RhoA/ROCK/SRF and RhoA/ROCK/LIMK1 pathways. The protein levels of RhoA, ROCK, SRF, and LIMK1 were significantly increased in the model group compared to the NC group ($p < 0.05$), and after

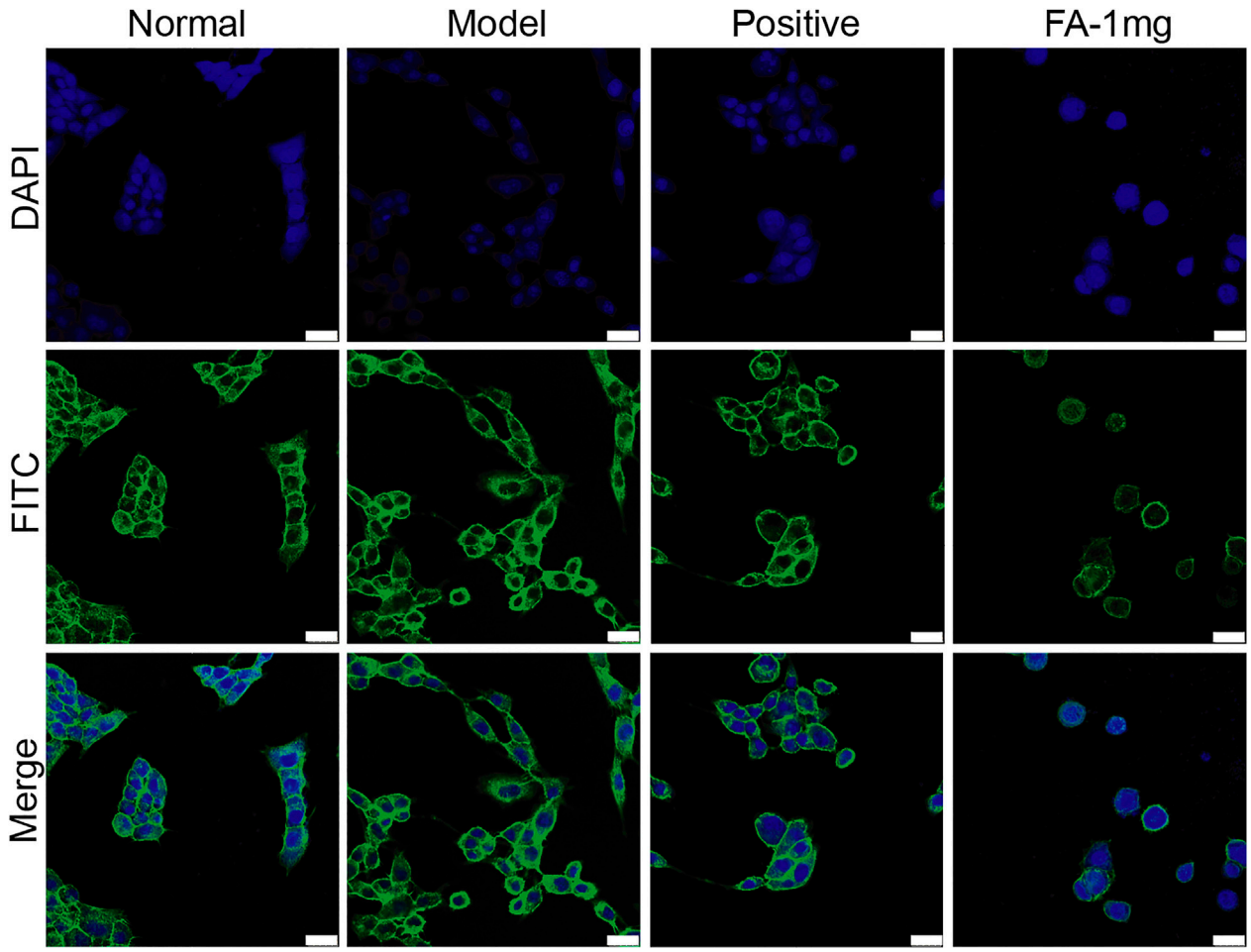

FIGURE 3 | Representative images of the cytoskeleton (green) in the HSCs treated with BMSCs or BMSC&FA (1 mg/ml). DAPI was used to stain cell nuclei (original magnification, ×40; scale bars: 25 μm).

1 mg/ml FA treatment, the expression of RhoA, ROCK, SRF, and LIMK1 was significantly decreased. Three dose groups showed no differences among them. The content of COL1-A1 and α-SMA in the ECM also decreased with 1 mg/ml FA treatment (**Figures 4F,G**). The mRNA levels showed the same trends (**Figure 4E**).

Bone Marrow Mesenchymal Stem Cells Regulate the Activation of Hepatic Stellate Cells by Inhibiting Cytoskeletal Rearrangement

To further prove that the cytoskeleton pathway is directly involved in BMSC inhibition of HSC activation, we added a cytoskeleton inhibitor (cytochalasin D) or cytoskeleton agonist (angiotensin II) when BMSCs were cocultured with activated HSCs. Compared to the model group, the agonist group showed significantly increased protein expression of COL1-A1, α-SMA, RhoA, ROCK, SRF, and LIMK1 ($p < 0.05$), while the expression levels of these proteins were significantly decreased in the inhibitor group ($p < 0.05$) (**Figures 5A,B**). The content of COL1-A1 and α-SMA in the ECM also decreased with cytochalasin D treatment (**Figures 5D,E**). The RNA levels of COL1-A1, α-SMA, RhoA, ROCK, SRF, and LIMK1 were reduced in the cytochalasin D groups (**Figure 5C**). These results indicate that FA promotes the ability of BMSCs to influence HSC activation. The cytoskeleton-related RhoA/ROCK pathway directly interacts with BMSCs and HSCs.

MiR-19b-3p Derived From Bone Marrow Mesenchymal Stem Cells Inactivates Hepatic Stellate Cells by Suppressing the Expression of its Target TGF-β Receptor II

MiRNAs are found in BMSCs, and miRNAs transferred into target cells can impact cell behaviours by regulating the expression of target genes. MiRNAs derived from BMSCs influenced HSC activation, we investigated which miRNAs contained in BMSCs regulated HSC activation. Three candidate miRNAs, miR-29b-3p, miR-19b-3p, and miR-183-5p, were selected because they were potentially linked to

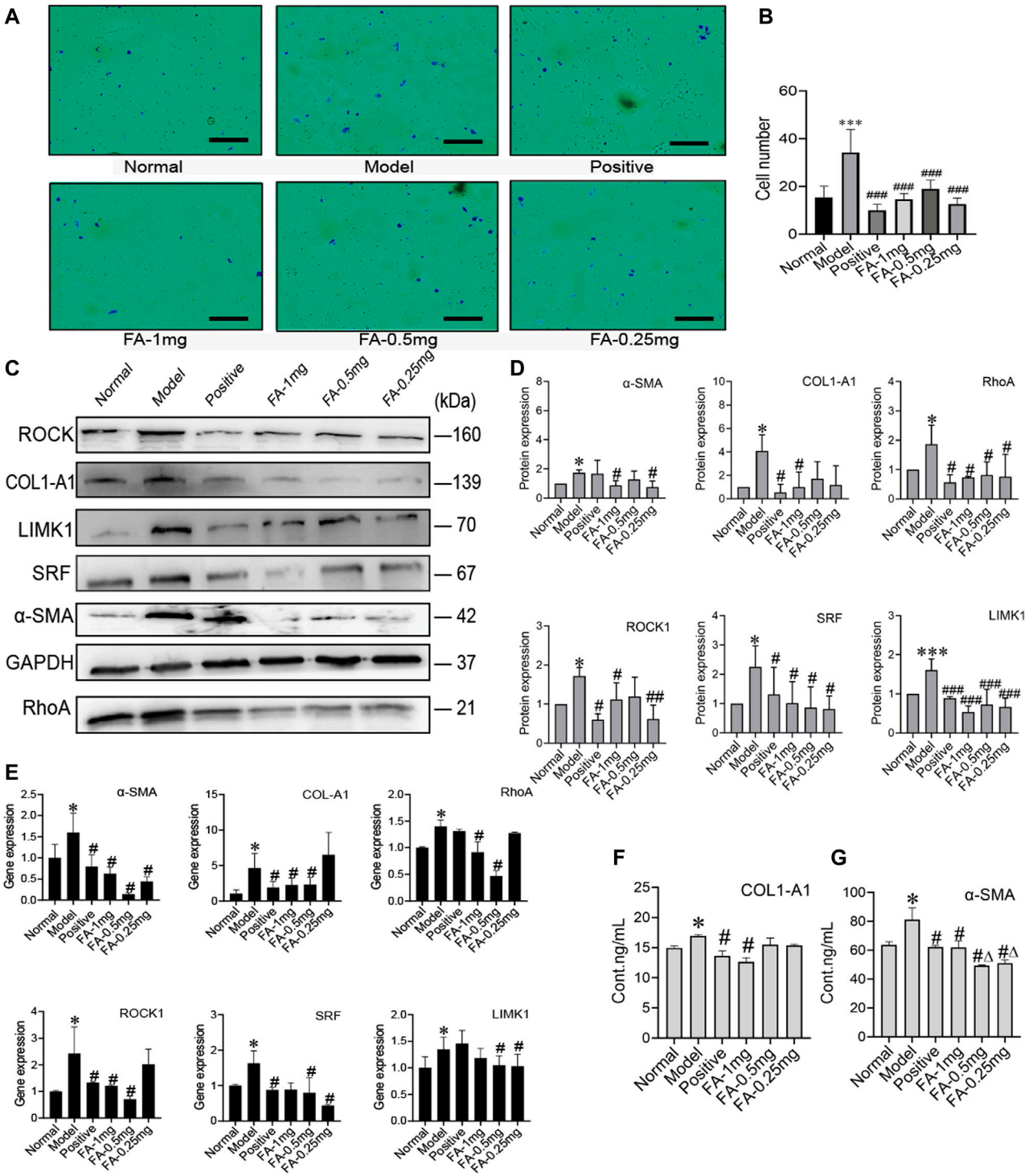

FIGURE 4 | FA promotes BMSC-mediated inhibition of the activation of HSCs. **(A)** Migration of HSCs (original magnification, ×10; scale bars, 100 μm). **(B)** The number of migrating HSCs. (n = 3 independent experiments, Two-way ANOVA; ***p < 0.001 versus the normal group; ###p < 0.001, versus the model group); **(C,D)** Western blot bands and cumulative densitometric analyses of each group (normal, model, positive, FA-1 mg, FA-0.5 mg, FA-0.25 mg). (n = 3 independent experiments, Two-way ANOVA; *p < 0.05, ***p < 0.001, versus the normal group; #p < 0.05, ###p < 0.001, versus the model group); **(E)** qRT-PCR analysis for α-SMA, COL1-A1, ROCK1, RhoA, SRF, and LIMK1 in HSCs. (n = 3 independent experiments, Two-way ANOVA; *p < 0.05 versus the normal group; #p < 0.05 versus the model group); **(F,G)** The protein content of α-SMA and COL1-A1 in extracellular medium. n = 3 independent experiments, Two-way ANOVA; *p < 0.05 versus the normal group; #p < 0.05 versus the model group; Δp<0.05 versus the 1 mg FA group.

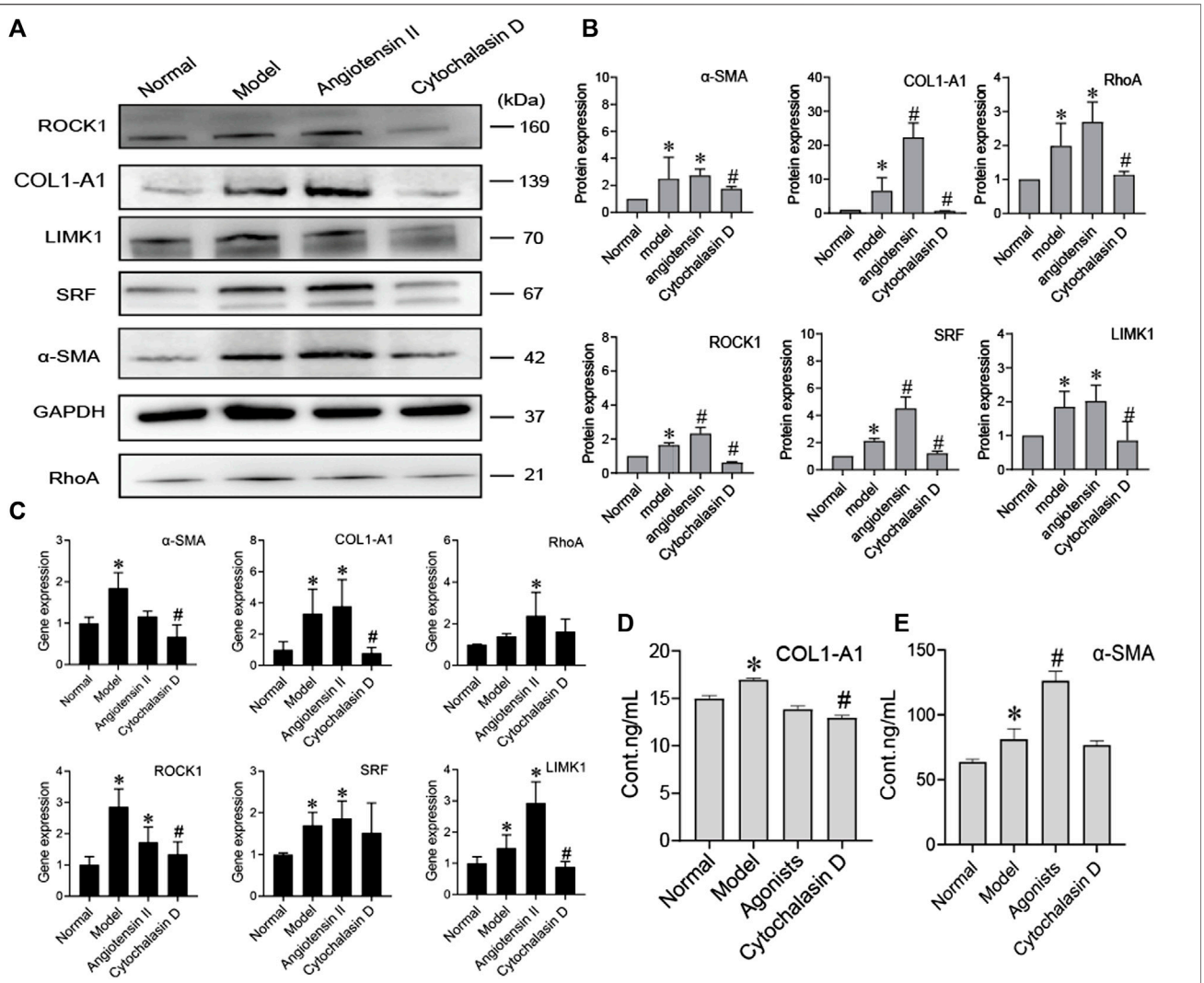

FIGURE 5 | BMSCs regulate the activation of HSCs by inhibiting cytoskeletal rearrangement. **(A,B)** Western blot bands and cumulative densitometric analyses of each group (normal, model, angiotensin II, cytochalasin D). Data are presented as the mean ± SEM ($n = 3$ independent experiments, one-way ANOVA; *$p < 0.05$, versus the normal group; #$p < 0.05$, versus the model group); **(C)** qRT-PCR analysis for α-SMA, COL1-A1, ROCK1, RhoA, SRF, and LIMK1 in HSCs. ($n = 3$ independent experiments, one-way ANOVA; *$p < 0.05$ versus normal; #$p < 0.05$ versus model); **(D,E)** The protein content of α-SMA and COL1-A1 in extracellular medium. $n = 3$ independent experiments, one-way ANOVA; *$p < 0.05$ versus the normal group; #$p < 0.05$ versus the model group.

fibrosis in previous reports, including a microarray analysis (GEO: GSE168712) and small RNA sequencing analysis, as these three miRNAs are abundantly expressed in BMSCs. The levels of miR-29b-3p, miR-19b-3p, and miR-183-5p were higher in BMSCs than in HSCs or normal rat liver tissues, and among them, miR-19b-3p was significantly enriched in BMSCs, suggesting that miR-19b-3p might be involved in modulating HSC activation. Bioinformatic analysis using TargetScan and miRWalk predicted TGF-βR2, a receptor for TGF-β1, as a putative target of miR-19b-3p, and a luciferase reporter assay revealed that miR-19b-3p directly bound to the 3′UTR of the TGF-βR2 mRNA transcript (**Figures 6A,B**).

To determine whether miR-19b-3p affects HSC activation, we transfected HSCs with a miR-19b-3p mimic and a meaningless fragment (negative control). Additionally, we chose inactivated HSCs and activated HSCs as the normal and model controls, respectively. Although miR-19b-3p was rarely expressed in activated HSCs, its expression was strongly elevated in the miR-19b-3p-transfected HSCs (**Figure 6C**). In addition, the profibrotic markers α-SMA, COL1-A1, RhoA, and ROCK1 had downregulated expression in the HSCs transfected with the miR-19b-3p mimics compared with those in the model and negative control groups ($p < 0.05$) (**Figures 6D,E**). The content of α-SMA and COL1-A1 in the ECM did not show a decreasing trend in the mimic group (**Figures 6F,G**). Western blot assays confirmed the RNA data, showing reductions in TGF-βR2 and profibrotic marker expression in the HSCs transfected with miR-19b-3p. These results suggest that miR-19b-3p inhibits HSC activation by directly targeting TGF-βR2.

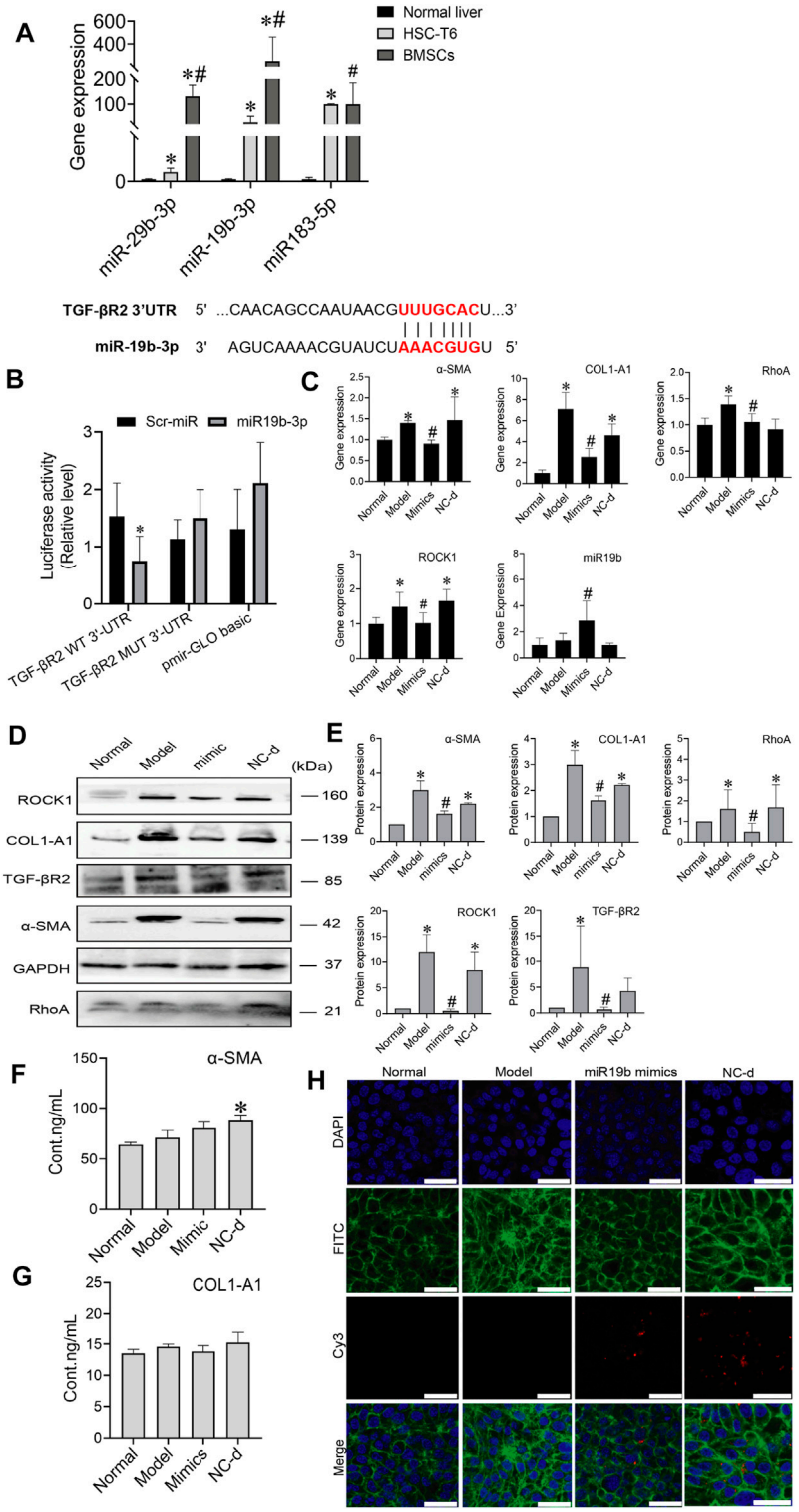

FIGURE 6 | MiR-19b-3p derived from BMSCs inactivates HSCs by suppressing the expression of its target TGF-βR2. **(A)** The potential binding site (red fonts) of miR-19b-3p was predicted in the 3′UTR of TGF-βR2 mRNA in rats. The dashed line represents complementary base pairs between miR-19b-3p and TGF-βR2 mRNA. **(B)** A dual-luciferase assay was performed to verify the binding interaction between miR-19b-3p and TGF-βR2 mRNA. Cells cotransfected with pmirGLO basic vector containing either wild-type (WT) or mutant (mut) target sites plus either the miR-19b-3p mimic or scrambled (Scr-) miR (control); **(C)** qRT-PCR analysis for α-SMA, COL1-A1, ROCK1, and RhoA in HSCs. $n = 3$ independent experiments, one-way ANOVA; *$p < 0.05$ versus the normal group; #$p < 0.05$ versus the model group; **(D,E)** Western blot bands and cumulative densitometric analyses of each group (normal, model, mimic, NC-d). Data are presented as the mean ± SEM ($n = 3$ independent

(*Continued*)

FIGURE 6 | experiments, one-way ANOVA; *$p < 0.05$, versus the normal group; #$p < 0.05$, versus the model group). **(F,G)** The protein content of α-SMA and COL1-A1 in extracellular medium. $n = 3$ independent experiments, one-way ANOVA; *$p < 0.05$ versus the normal group; #$p < 0.05$ versus the model group. **(H)** Representative images of the cytoskeleton (green) in the HSCs treated with miR19b-3p mimics or NC-d. DAPI was used to stain cell nuclei (original magnification, ×40; scale bars: 25 μm).

We also transfected the miR-19b-3p mimic, or negative control with the fluorescent Cy3 gene into activated HSCs. With confocal scanning microscopy, we observed red fluorescence in the miR-19b-3p mimic and negative control groups. Compared to the model group, the group transfected with the miR-19b-3p mimics showed F-actin mainly distributed in peripheral cells, and a few fine stress fibres were found in these cells. The cytoskeleton of cells in the negative control groups was similar to that of the cells in the model group (**Figure 6H**).

Ferulic Acid Induces Bone Marrow Mesenchymal Stem Cells to Release More miR-19b-3p to Hepatic Stellate Cells and Inhibit the Activation of Hepatic Stellate Cells

To determine whether BMSCs transfer miR-19b-3p to HSCs, we transfected the miR-19b-3p mimic or miR-19b-3p inhibitor with the fluorescent Cy3 gene into BMSCs and cocultured the transfected cells with activated HSCs. With confocal scanning microscopy, we observed red fluorescence in the miR-19b-3p mimic group, and F-actin was mainly distributed in peripheral cells. A few fine stress fibres were found in these cells compared to those in the model group. In addition, in the miR-19b-3p inhibitor group, the cell shape was similar to that in the model group, and F-actin in activated HSCs was remodelled to form a large number of thick stress fibres across the whole cell. With FA treatment, we found more red fluorescence in the miR-19b-3p mimic groups (**Figure 7A**).

To assess protein levels, we divided the BMSC/HSC coculture system into 8 groups: the normal, model, mimic, inhibitor, mimic + FA, inhibitor + FA, and negative control groups. We detected α-SMA, COL1-A1, RhoA, ROCK1 SRF, and found that their expression was significantly downregulated in the mimic + FA, and inhibitor + FA groups compared to the model group, while mimic + FA, and inhibitor + FA groups also showed significance respectively compared to mimics/inhibitor group on COL1-A1 expression. The mimic group showed the decreased trends (**Figures 7B,C**). The content of α-SMA and COL1-A1 in the ECM also showed a decreasing trend in the mimic, inhibitor&FA, mimic&FA group (**Figures 7D,E**). The mRNA levels showed the same trends (**Figure 7F**).

These results suggest that miR-19b-3p plays a critical role in regulating the effect of BMSCs against liver fibrosis. In conclusion, these results suggest that FA combined with BMSC treatment can induce greater release of miR-19b-3p, which inhibits the activation of HSCs by suppressing the RhoA/ROCK1/SRF and RhoA/ROCK1/LIMK1 pathways, contributing to alleviation of liver fibrosis.

DISCUSSION

In this study, we showed that FA combined with BMSCs was more effective in treating liver fibrosis than single treatment. We used BMSCs, FA or combination therapy to treat rats with hepatic fibrosis. By evaluating the AST, ALT, HE, and Masson staining results, we observed that liver fibrosis was decreased to different degrees and that the combination therapy showed better effects than FA or BMSC monotherapy. In addition, we detected the protein expression of COL1-A1, α-SMA, ROCK1 and RhoA, and the results for the combination therapy showed better effects. Therefore, these results suggest that FA can promote the ability of BMSCs to improve liver fibrosis by targeting the RhoA/ROCK pathway.

The RhoA/ROCK signalling pathway is related to intracellular cytosis, colonization, migration, apoptosis, gene expression and other behaviours (Xu et al., 2018; Yaqoob et al., 2020). The RhoA/ROCK pathway also affects the formation of fibrosis. This axis promotes collagen and ECM production in fibroblasts and increases the transformation of fibroblasts into myofibroblasts expressing α-SMA and other activated factors (Deng et al., 2019; Sloniecka and Danielson 2019). RhoA/ROCK is a classic fibrosis pathway, which has quantities of related studies have been carried out as a preliminary basis, and ROCK1 is also associated with cytoskeleton and cytodynamics. Therefore, we choose RhoA/ROCK pathway to study.

To verify the mechanism of BMSC and FA combination therapy, we established a BMSC/HSC-T6 coculture system. Activated HSCs were cocultured with an equal amount of BMSCs. We observed the cellular structure of HSC-T6 cells and found that with FA treatment, the deformed cell structure was restored, F-actin was mainly distributed in peripheral cells, and a few fine stress fibres were found in these cells. In addition to assessing cellular structure, we detected the migration of HSCs. The number of migrating cells was significantly decreased with FA and BMSC treatment. The protein expression of RhoA, ROCK, SRF, LIMK1, COL1-A1, and α-SMA was significantly decreased. These results all proved that FA promoted the ability of BMSCs to decrease HSC migration while inhibiting activation.

The RhoA/ROCK pathway is related to both development of fibrosis and cytoskeletal rearrangement. RhoA/ROCK/SRF directly influences collagen and α-SMA production, while RhoA/ROCK/LIMK1 influences cytoskeletal rearrangement, indirectly affecting HSC migration. Activated HSCs migrate to sites of damage and release collagen. Therefore, inhibiting cytoskeletal rearrangement is also an effective strategy for reducing fibrosis (Ni et al., 2013; Wu et al., 2019).

To verify the mechanism by which BMSCs inhibit HSC activation, we established a BMSC/HSC coculture system with angiotensin II and cytochalasin D used as agonists and inhibitors, respectively. The decreased protein expression of RhoA, ROCK,

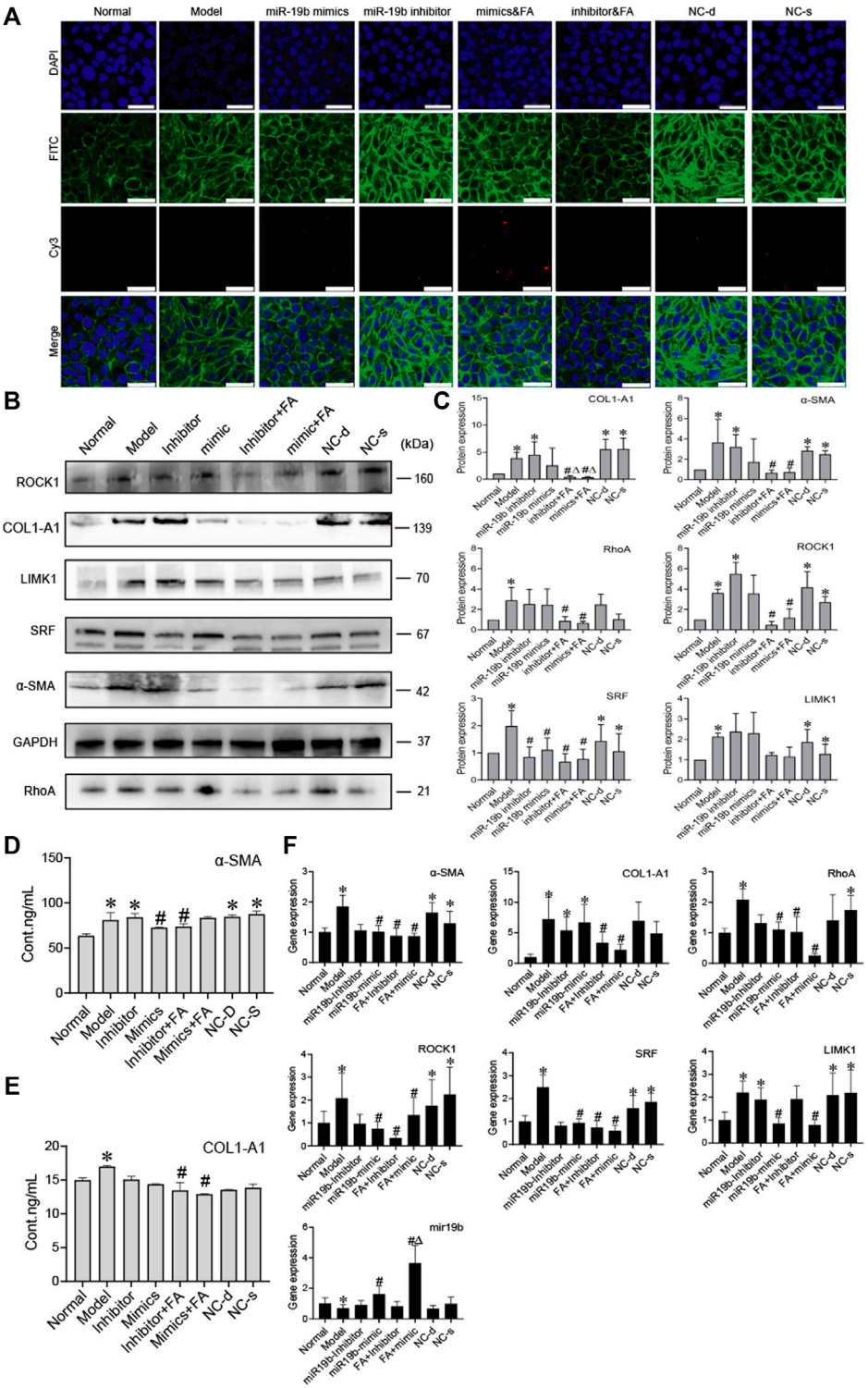

FIGURE 7 | FA induces BMSCs to release more miR-19b-3p to HSCs and inhibit the activation of HSCs. **(A)** Representative images of the cytoskeleton (green) in the HSCs treated with miR19b-3p mimics, inhibitor, or NC-d and NC-s. DAPI was used to stain cell nuclei (original magnification, ×40; scale bars: 25 μm). **(B,C)** Western blot bands and cumulative densitometric analyses of each group (normal, model, inhibitor, mimic, inhibitor&FA, mimic&FA, NC-d, NC-s). Data are presented as the mean ± SEM ($n = 3$ independent experiments, Two-way ANOVA; $^*p < 0.05$, versus the normal group; $\#p < 0.05$, versus the model group; $\Delta p < 0.05$, versus the inhibitor/mimic group). **(D,E)** The protein content of α-SMA and COL1-A1 in extracellular medium. $n = 3$ independent experiments, Two-way ANOVA; $^*p < 0.05$ versus the normal group; $\#p < 0.05$ versus the model group; **(F)** qRT-PCR analysis for α-SMA, COL1-A1, ROCK1, RhoA, SRF, and LIMK1 in HSCs. $n = 3$ independent experiments, Two-way ANOVA; $^*p < 0.05$ versus the normal group; $\#p < 0.05$ versus the model group; $\Delta p < 0.05$ versus the miR19b mimic group.

SRF, LIMK1, COL1-A1, and α-SMA also indicated that BMSCs could reduce HSC activation by inhibiting cytoskeletal rearrangement.

Many studies have proven that BMSCs can produce miRNAs (Cetin et al., 2021). Feng et al. demonstrated that MSC-derived miRNAs reduced infarct size and cardiac fibrosis by inhibiting apoptosis in mice with myocardial infarction. Exosomes derived from chorionic plate-derived MSCs (CP-MSCs) containing miR-125b could ameliorate hepatic fibrosis by regulating hedgehog (Hh) signalling, which is an essential regulator in liver fibrosis (Feng et al., 2014; Hyun et al., 2015). These findings suggest that miRNAs play important roles in MSC-mediated tissue repair and regeneration. In a recent study, BMSCs were found to release miRNAs, targeting specific proteins to reduce fibrosis (Chen et al., 2018; BI Hui-yang 2019). The results for the BMSC genomic sequence showed that BMSCs contain a variety of miRNAs (Lindoso et al., 2014; Zhao et al., 2017). Among them, miR-19b-3p was shown to be related to inhibition of fibrosis (Zou et al., 2016; Chen et al., 2019; Duan et al., 2019; Wang et al., 2021). We used the TargetScan website to predict the target genes of miR-19b-3p and found TGF-βR2 was a putative target. The luciferase reporter assay revealed that miR-19b-3p directly bound to TGF-βR2 in HSCs.

To determine whether miR-19b-3p can inhibit HSC activation, we transfected miR-19b-3p mimics or inhibitors with the Cy3 gene into HSCs and BMSCs. We observed the cytoskeleton of the HSCs transfected with miR-19b-3p mimics or inhibitors. With miR-19b-3p mimic transfection, the cytoskeleton of activated HSCs was not substantially changed, while with miR-19b-3p inhibitor transfection, the cytoskeleton of activated HSCs was still rearranged. The decreased expression of RhoA, ROCK, SRF, LIMK1, COL1-A1 and α-SMA showed that miR-19b-3p could affect HSC activation.

We also observed that the BMSCs transfected with the mimics released more miR-19b-3p to HSCs and that the cytoskeleton was similar to that of inactivated HSCs; the BMSCs transfected with the inhibitors released less miR-19b-3p to HSCs, and the cytoskeleton was similar to that of activated HSCs. The protein expression of RhoA, ROCK, SRF, LIMK1, COL1-A1, and α-SMA showed that BMSCs could release miR-19b-3p to inhibit HSC activation, and BMSCs combined with FA treatment resulted in better HSC inhibition. These results indicate that combining BMSCs with FA could be a promising therapeutic strategy for the treatment of liver disease.

Bone marrow is the most widely used source of BMSCs. However, due to the instability of BMSCs, the use of these cells in clinical applications is limited (Alsulami and Abdel-Gaber 2021; Muslimah Alsulami, 2021; Yang et al., 2021). FA is a derivative of cinnamic acid and has therapeutic activity against a variety of diseases. This molecule is also an effective ingredient in some TCMs, such as *Angelica sinensis*. In addition, FA may protect against fibrotic deterioration in rats with hepatic fibrosis (Mu et al., 2018). Therefore, we chose FA combined with BMSCs to treat hepatic fibrosis in rats and found that their combination showed better treatment effects.

CONCLUSION

Collectively, we demonstrated that FA promoted the ability of BMSCs to suppress HSC activation and liver fibrosis. MiR-19b-3p derived from BMSCs inactivated HSCs by suppressing the RhoA/ROCK/SRF and RhoA/ROCK/LIMK1 signalling pathways. Therefore, our findings suggest that BMSCs combined with a TCM have potential as an effective antifibrotic drug for chronic liver diseases.

DATA AVAILABILITY STATEMENT

The original contributions presented in the study are included in the article/**Supplementary Material**, further inquiries can be directed to the corresponding author.

ETHICS STATEMENT

The animal study was reviewed and approved by Animal Care and Use Committee of Capital Medical University.

AUTHOR CONTRIBUTIONS

RZ as principal author was responsible processing experiments, collecting, and analyzing data, finally independent wrote this manuscript. WLL performed design of study and reviewed manuscript, and acted as corresponding author. WHL, XJ, and XC contributed to complete experiments. HY and ZT contributed to data interpretation.

FUNDING

This work was supported by grants from the National Natural Science Foundation of China (to WLL) (Grant No. 81573879) and the Natural Science Foundation of Beijing (to WLL) (Grant No. 7182021).

SUPPLEMENTARY MATERIAL

The Supplementary Material for this article can be found online at: https://www.frontiersin.org/articles/10.3389/fphar.2022.863797/full#supplementary-material

REFERENCES

Alfaifi, M., Eom, Y. W., Newsome, P. N., and Baik, S. K. (2018). Mesenchymal Stromal Cell Therapy for Liver Diseases. *J. Hepatol.* 68 (6), 1272–1285. doi:10.1016/j.jhep.2018.01.030

Ali, S. A., Saifi, M. A., Pulivendala, G., Godugu, C., and Talla, V. (2021). Ferulic Acid Ameliorates the Progression of Pulmonary Fibrosis via Inhibition of TGF-B/smad Signalling. *Food Chem. Toxicol.* 149, 111980. doi:10.1016/j.fct.2021.111980

Alsulami, M., and Abdel-Gaber, R. (2021). Cell Therapy as a New Approach on Hepatic Fibrosis of Murine Model of Schistosoma Mansoni-Infection. *Acta Parasitol.* 66 (1), 136–145. doi:10.1007/s11686-020-00267-2

Alsulami, M., and Abdel-Gaber, R. (2021). Cell Therapy as a New Approach on Hepatic Fibrosis of Murine Model of Schistosoma Mansoni-Infection. *Acta Parasit.* 66, 136–145. doi:10.1007/s11686-020-00267-2

Ankrum, J., and Karp, J. M. (2010). Mesenchymal Stem Cell Therapy: Two Steps Forward, One Step Back. *Trends Mol. Med.* 16 (5), 203–209. doi:10.1016/j.molmed.2010.02.005

Bataller, R., and Brenner, D. A. (2005). Liver Fibrosis. *J. Clin. Invest.* 115 (2), 209–218. doi:10.1172/jci20052428210.1172/JCI24282

Bi Hui-yang, G. J-l. (2019) Research Progress of miRNA Related to Bone Marrow Mesenchymal Stem Cells. World Latest Medicine Information (Electronic Version) 19 (52), 68–69. doi:doi:10.19613/j.cnki.1671-3141.2019.52.035

Cetin, Z., Saygili, E. I., Görgisen, G., and Sokullu, E. (2021). Preclinical Experimental Applications of miRNA Loaded BMSC Extracellular Vesicles. *Stem Cel Rev Rep* 17 (2), 471–501. doi:10.1007/s12015-020-10082-x

Chen, L., Lu, F. B., Chen, D. Z., Wu, J. L., Hu, E. D., Xu, L. M., et al. (2018). BMSCs-Derived miR-223-Containing Exosomes Contribute to Liver protection in Experimental Autoimmune Hepatitis. *Mol. Immunol.* 93, 38–46. doi:10.1016/j.molimm.2017.11.008

Chen, W., Zhou, Z. Q., Ren, Y. Q., Zhang, L., Sun, L. N., Man, Y. L., et al. (2019). Effects of Long Non-coding RNA LINC00667 on Renal Tubular Epithelial Cell Proliferation, Apoptosis and Renal Fibrosis via the miR-19b-3p/LINC00667/CTGF Signaling Pathway in Chronic Renal Failure. *Cell Signal* 54, 102–114. doi:10.1016/j.cellsig.2018.10.016

Deng, Z., Jia, Y., Liu, H., He, M., Yang, Y., Li, Y., et al. (2019). RhoA/ROCK Pathway: Implication in Osteoarthritis and Therapeutic Targets. *Am. J. Transl Res.* 11 (9), 5324–5331.

Duan, L., Duan, D., Wei, W., Sun, Z., Xu, H., Guo, L., et al. (2019). MiR-19b-3p Attenuates IL-1β Induced Extracellular Matrix Degradation and Inflammatory Injury in Chondrocytes by Targeting GRK6. *Mol. Cel Biochem* 459 (1-2), 205–214. doi:10.1007/s11010-019-03563-2

Feng, Y., Huang, W., Wani, M., Yu, X., and Ashraf, M. (2014). Ischemic Preconditioning Potentiates the Protective Effect of Stem Cells through Secretion of Exosomes by Targeting Mecp2 via miR-22. *PLoS One* 9 (2), e88685–8. doi:10.1371/journal.pone.0088685

Hyun, J., Wang, S., Kim, J., Kim, G. J., and Jung, Y. (2015). MicroRNA125b-mediated Hedgehog Signaling Influences Liver Regeneration by Chorionic Plate-Derived Mesenchymal Stem Cells. *Sci. Rep.* 5, 14135. doi:10.1038/srep14135

Jayamani, J., Naisini, A., Madhan, B., and Shanmugam, G. (2018). Ferulic Acid, a Natural Phenolic Compound, as a Potential Inhibitor for Collagen Fibril Formation and its Propagation. *Int. J. Biol. Macromol* 113, 277–284. doi:10.1016/j.ijbiomac.2018.01.225

Jingjing, H., Hongna, H., Wenfu, Z., Jianlin, L., Guochu, H., Yuanjia, L., et al. (2021). Bie Jia Jian Pill Combined with Bone Mesenchymal Stem Cells Regulates microRNA-140 to Suppress Hepatocellular Carcinoma Stem Cells. *Int. J. Stem Cell* 14 (3), 275–285. doi:10.15283/ijsc20157

Li, D., Rui, Y. X., Guo, S. D., Luan, F., Liu, R., and Zeng, N. (2021). Ferulic Acid: A Review of its Pharmacology, Pharmacokinetics and Derivatives. *Life Sci.* 284, 119921. doi:10.1016/j.lfs.2021.119921

Li, R., Luo, X., Zhu, Y., Zhao, L., Li, L., Peng, Q., et al. (2017). ATM Signals to AMPK to Promote Autophagy and Positively Regulate DNA Damage in Response to Cadmium-Induced ROS in Mouse Spermatocytes. *Environ. Pollut.* 231 (Pt 2), 1560–1568. doi:10.1016/j.envpol.2017.09.044

Liao, L., Shi, B., Chang, H., Su, X., Zhang, L., Bi, C., et al. (2017). Heparin Improves BMSC Cell Therapy: Anticoagulant Treatment by Heparin Improves the Safety and Therapeutic Effect of Bone Marrow-Derived Mesenchymal Stem Cell Cytotherapy. *Theranostics* 7 (1), 106–116. doi:10.7150/thno.16911

Lindoso, R. S., Collino, F., Bruno, S., Araujo, D. S., Sant'Anna, J. F., Tetta, C., et al. (2014). Extracellular Vesicles Released from Mesenchymal Stromal Cells Modulate miRNA in Renal Tubular Cells and Inhibit ATP Depletion Injury. *Stem Cell Dev* 23 (15), 1809–1819. doi:10.1089/scd.2013.0618

Mu, M., Zuo, S., Wu, R. M., Deng, K. S., Lu, S., Zhu, J. J., et al. (2018). Ferulic Acid Attenuates Liver Fibrosis and Hepatic Stellate Cell Activation via Inhibition of TGF-β/Smad Signaling Pathway. *Drug Des. Devel Ther.* 12, 4107–4115. doi:10.2147/DDDT.S186726

Ni, J., Dong, Z., Han, W., Kondrikov, D., and Su, Y. (2013). The Role of RhoA and Cytoskeleton in Myofibroblast Transformation in Hyperoxic Lung Fibrosis. *Free Radic. Biol. Med.* 61, 26–39. doi:10.1016/j.freeradbiomed.2013.03.012

Pinzani, M., and Rombouts, K. (2004). Liver Fibrosis: from the Bench to Clinical Targets. *Dig. Liver Dis.* 36, 231–242. doi:10.1016/j.dld.2004.06.00110.1016/j.dld.2004.01.003

Rong, X., Liu, J., Yao, X., Jiang, T., Wang, Y., and Xie, F. (2019). Human Bone Marrow Mesenchymal Stem Cells-Derived Exosomes Alleviate Liver Fibrosis through the Wnt/β-Catenin Pathway. *Stem Cel Res Ther* 10 (1), 98. doi:10.1186/s13287-019-1204-2

Rong, X., Yang, Y., Zhang, G., Zhang, H., Li, C., and Wang, Y. (2020). Antler Stem Cells as a Novel Stem Cell Source for Reducing Liver Fibrosis. *Cell Tissue Res* 379 (1), 195–206. doi:10.1007/s00441-019-03081-z

Słoniecka, M., and Danielson, P. (2019). Substance P Induces Fibrotic Changes through Activation of the RhoA/ROCK Pathway in an *In Vitro* Human Corneal Fibrosis Model. *J. Mol. Med.* 97 (10), 1477–1489. doi:10.1007/s00109-019-01827-4

Tian, J. Z. H. W. M. S. L. X. J. Z. Y. T. L. T. H. L. P. (2016). Therapeutical Effect of Saponins fromRhizoma Panacis Majoris Combined with BMSCs on Hepatic Fibrosis Induced by CCl_4 in Rats. *J. China Three gorges Univ. (Natural Science)* 38 (3), 104–108. doi:10.13393/j.cnki.issn.1672-948X.2016.03.023

Virarkar, M., Morani, A. C., Taggart, M. W., and Bhosale, P. (2021). Liver Fibrosis Assessment. *Semin. Ultrasound CT MR* 42 (4), 381–389. doi:10.1053/j.sult.2021.03.003

Wang, Y., Wang, L., Guo, J., Zuo, S., Wang, Z., and Hua, S. (2021). MYPT1, Regulated by miR-19b-3p Inhibits the Progression of Non-small Cell Lung Cancer via Inhibiting the Activation of Wnt/β-Catenin Signaling. *Life Sci.* 278, 1–10. doi:10.1016/j.lfs.2021.119573

Wu, Y., Li, Z., Wang, S., Xiu, A., and Zhang, C. (2019). Carvedilol Inhibits Angiotensin II-Induced Proliferation and Contraction in Hepatic Stellate Cells through the RhoA/Rho-Kinase Pathway. *Biomed. Res. Int.* 2019, 1–15. doi:10.1155/2019/7932046

Xu, A., Li, Y., Zhao, W., Hou, F., Li, X., Sun, L., et al. (2018). PHP14 Regulates Hepatic Stellate Cells Migration in Liver Fibrosis via Mediating TGF-B1 Signaling to PI3Kγ/AKT/Rac1 Pathway. *J. Mol. Med. (Berl)* 96 (2), 119–133. doi:10.1007/s00109-017-1605-6

Yang, X., Chen, Z., Chen, C., Han, C., Zhou, Y., Li, X., et al. (2021). Bleomycin Induces Fibrotic Transformation of Bone Marrow Stromal Cells to Treat Height Loss of Intervertebral Disc through the TGFβR1/Smad2/3 Pathway. *Stem Cel Res Ther* 12 (1), 34. doi:10.1186/s13287-020-02093-9

Yao, X., Wang, J., Zhu, J., and Rong, X. (2020). The Anti-fibrotic Effect of Human Fetal Skin-Derived Stem Cell Secretome on the Liver Fibrosis. *Stem Cel Res Ther* 11 (1), 379. doi:10.21203/rs.3.rs-39850/v110.1186/s13287-020-01891-5

Yaqoob, U., Luo, F., Greuter, T., Jalan Sakrikar, N., Sehrawat, T. S., Lu, J., et al. (2020). GIPC-regulated IGFBP-3 Promotes HSC Migration In Vitro and Portal Hypertension In Vivo through a β1-Integrin Pathway. *Cell Mol Gastroenterol Hepatol* 10 (3), 545–559. doi:10.1016/j.jcmgh.2020.05.005

Ye Chao, W. Q., Chen, J., Zheng, Y., Qu, Y. I., Wang, J., Wang, F., et al. (2021). Repair Effect and Mechanism of Naringin Combined with Bone Marrow Mesenchymal Stem Cells and Acellular Dermal Matrix on Cartilage Injury. *Mod. J. Integrated Traditional Chin. West. Med.* 30 (4), 375–380.

Yuhui Lin, X. H., Xiaobin, N., Ning, H., Qi, D., Cheng feng, L., Shi ming, L., et al. (2011). Transfection of Rat Bone Marrow Mesenchymal Stem Cells with

Adenovirus Vector Carrying hBcl -2 and hVEGF165 Genes. *Guangdong Med. J.* 32 (5). doi:10.13820/j.cnki.gdyx.2011.05.004

Zhao, X. K., Yu, L., Cheng, M. L., Che, P., Lu, Y. Y., Zhang, Q., et al. (2017). Focal Adhesion Kinase Regulates Hepatic Stellate Cell Activation and Liver Fibrosis. *Sci. Rep.* 7 (1), 4032. doi:10.1038/s41598-017-04317-0

Zou, M., Wang, F., Gao, R., Wu, J., Ou, Y., Chen, X., et al. (2016). Autophagy Inhibition of Hsa-miR-19a-3p/19b-3p by Targeting TGF-β R II during TGF-B1-Induced Fibrogenesis in Human Cardiac Fibroblasts. *Sci. Rep.* 6, 24747. doi:10.1038/srep24747

Conflict of Interest: The authors declare that the research was conducted in the absence of any commercial or financial relationships that could be construed as a potential conflict of interest.

Publisher's Note: All claims expressed in this article are solely those of the authors and do not necessarily represent those of their affiliated organizations, or those of the publisher, the editors and the reviewers. Any product that may be evaluated in this article, or claim that may be made by its manufacturer, is not guaranteed or endorsed by the publisher.

Frontiers in Pharmacology

Explores the interactions between chemicals and living beings

The most cited journal in its field, which advances access to pharmacological discoveries to prevent and treat human disease.

Discover the latest Research Topics

See more →

Frontiers

Avenue du Tribunal-Fédéral 34
1005 Lausanne, Switzerland
frontiersin.org

Contact us

+41 (0)21 510 17 00
frontiersin.org/about/contact